DOCTOR OF PHILOSOPHY

Identification Methods for Fractional Order Nonlinear Models

Allafi, Walid

Award date:
2015

Awarding institution:
Coventry University

Identification Methods for Fractional Order Nonlinear Models

By

Walid Allafi

October 2015

The work contained within this document has been submitted by the student in partial fulfilment of the requirement of their course and award

Identification Methods for Fractional Order Nonlinear Models

By

Walid Allafi

October 2015

Control Theory and Applications Center

Coventry University

A thesis submitted in partial fulfilment of the University's requirements

for the Degree of Doctor of Philosophy

ABSTRACT

This thesis considers the development of novel parameter estimation and system identification methods for fractional-order continuous-time nonlinear systems from sampled input-output signals. It is recognised that there is no universal model parameter estimation method which would be suitable for all types of nonlinear system models. In this work, two parameter estimation methods, targeting specific nonlinear model structures, have been developed.

The first proposed parameter estimation method is based on an extension of the simplified and refined instrumental variable method for identification of integer-order continuous-time linear transfer function models. The proposed extended method is able to estimate parameters of fractional-order continuous-time Hammerstein–Wiener (HWFC) models, where the case of estimation of linear, Hammerstein (HFC), and Wiener (WFC) models is considered as a special case. It is also possible to estimate the classical integer-order model counterparts as a special case. Subsequently, the proposed extension to the simplified and refined instrumental variable methods for HWFC model estimation is abbreviated to HWSRIVCF and HWRIVCF, respectively. The refined version, HWRIVCF, considers the noise model to be of Box-Jenkins type, while the simplified version, HWRIVCF, assumes an output error measurement noise scenario. The advantage of this novel extension, compared to published methods, is that the output static nonlinearity of the Wiener model part does not need to be invertible.

The second proposed fractional-order parameter estimation method is based on an existing delayed integer-order state variable filtering technique. In general, the developed method is able to estimate parameters of continuous-time fractional-order nonlinear models, when formulated in input-output form. The individual elements of the input-output equation (regression model) comprises of higher order time derivatives, signal powers, and products between the input and output signals and their powers. In this thesis, the focus is on a special model subclass, namely, a class of bilinear system models due mainly to its previous use in control engineering applications.

A comprehensive case study, presenting the full system identification cycle, is also given. In this study, fractional-order continuous-time transfer function model of a 1D linear solid a diffusion process has been identified from sampled input-output data. The data was generated from a governing diffusion equation solved by the finite volume method.

ACKNOWLEDGEMENTS

Undertaking this Ph.D. has been a truly life-changing experience for me, and it would not have been possible to progress without the support and guidance that I received from these people.

First and foremost I would like to express my special appreciation and thanks to my director of the studies, Professor Prof. Keith Burnham, he has been a tremendous mentor for me. I would like to thank him for the continuous support of my Ph.D. study and related research, for his patience, motivation, and immense knowledge. I could not have imagined having a better director and mentor for my Ph.D. study.

Besides my director, I would like to express my sincere thanks to my supervisor, Dr Ivan Zajıc for his insightful comments, encouragement and advice throughout my Ph.D.

Lastly, I am also grateful to the following colleagues whose suggestions and collaboration were invaluable throughout my Ph.D. study: Ionut Gheorghe and Zhonghua Shen.

TABLE OF CONTENTS

LIST OF TABLES

LIST OF FIGURES

LIST OF ABBREVIATIONS

ARMA	Autoregressive moving average
BJ	Box-Jenkins
CVs	Control volumes
ERR	Error reduction ratio
ETFE	Empirical transfer function estimation
FVM	Finite volume method
GA	Genetic Algorithm
HFC	Fractional-order continuous-time Hammerstein model
HRIVCF/HSRIVCF	Refined/simplified refined instrumental variable for fractional-order Hammerstein model
HWFC	Fractional-order continuous-time Hammerstein-Wiener model
HWRIVCF/HWSRIVCF	Refined/simplified refined instrumental variable for fractional-order Hammerstein-Wiener model
IAE	Integral of the absolute error
MC	Monte Carlo

RIVCF	Refined instrumental variable method for fractional-order transfer function model
SNR	Signal to noise ratio
SPA	Spectral analysis
SRIVCF	Simplified refined instrumental variable method for fractional-order transfer function model
std	Standard deviation
WFC	Fractional-order continuous-time Wiener model
WRIVCF/WSRIVCF	Refined/simplified refined instrumental variable for fractional-order Wiener model

Chapter 1: Introduction, Motivation and Outline

1.1 Motivation

When considering the adoption of linear system models for describing real-world processes, as opposed to the use of nonlinear system models, a trade-off between model complexity and model accuracy is often made. Commonly, linear system models are used in control engineering and relevant disciplines, for the relative simplicity these models offer and the simplicity of the associated system identification methods. To close the gap between linear and purely nonlinear modelling approaches, adoption of mildly nonlinear models have been considered in the past (Mohler 1973, Dunoyer, Burnham, and McAlpine 1996 and Zajic 2013). Examples of such nonlinear model structures are classes of bilinear, Hammerstein, Wiener, Hammerstein-Wiener models and their combinations. Bilinear systems are linear with respect to the input and state, but nonlinear when jointly considered (Mohler 1973). The Hammerstein-Wiener model structure consists of a linear dynamic model, between two static nonlinear functions. Numerous nonlinear phenomena have been modelled by bilinear models, see (Mohler 1973, Dunoyer, Burnham, and McAlpine 1996 and Zajic 2013), and Hammerstein-Wiener models, see (Bai et al. 2009, and Taringou et al. 2010). When considering these nonlinear models, which relate closely

to linear model structures, it is often the case that the linear system identification approaches are still applicable. It is the increased modelling fidelity yet relative simplicity of these nonlinear models which has historically attracted the attention of researchers in the past, and contributes to do so today.

To date, the aforementioned nonlinear system models have only been considered with integer-order time derivatives of the input-output signals. To further increase the modelling flexibility of these models yet retain the relative simplicity of the adopted system identification methods, it is proposed in this thesis to extend the integer-order models to a class of fractional-order nonlinear system models.

Fractional-order systems can be approximated by ordinary integer-order systems with an infinite order, or approximated by finite integer-order systems by considering a selected frequency range, but with decreased accuracy outside this frequency range. In order to highlight the difference between integer-order and fractional-order systems, consider the following system, described by

$$\frac{d^n y^m(t)}{dt^n} = u(t) \tag{1.1}$$

When the system order *n=1* and parameter *m=1*, the system is said to be an integer-order linear system. If $u(t)=\cos(t)$ and $y(0)=0$, the time domain solution of the differential equation in (1.1) is $y(t)=\sin(t)$. It implies that the system lags the input by $\frac{\pi}{2}$. However, if there is a need to lag the function $\cos(t)$ by a fraction, denoted α, of $\frac{\pi}{2}$, then the integer-order linear system would have to be of infinite order to lag the phase shift by $\frac{\alpha\pi}{2}, \alpha \in \mathbb{R}^+$, or finite order with less accuracy. The fractional-order phase lag can be achieved by considering a fractional-order model of $n=\alpha$ in the above system. The system in (1.1) is then described by the fractional-order system with much fewer parameters which, in return, enhances the clarity of such a model and its use in control engineering. As a result,

fractional-order systems have been employed in different fields of engineering and science, e.g. system identification of thermal systems (Gabano, Poinot, and Kanoun 2011), modelling of heat conduction (Žecová, and Terpák 2015), and edge detection in image processing (Mathieu et al. 2003).

In the case where the parameters of the exemplary system in (1.1) are $\alpha = 2$ and $m = 2$, the system is said to be a fractional-order nonlinear system. For simplicity, this fractional-order nonlinear system can be modelled by a fractional-order linear model, but this may lead to loss of accuracy over a wide operating range. This accuracy might be increased by considering $n = \alpha$ a bilinear fractional-order or Hammerstein-Wiener model. Therefore, the use of fractional-order bilinear and Hammerstein-Wiener system models may be the preferred option. Thus, the next step would be to consider bilinear fractional-order, Hammerstein-Wiener or even input-output nonlinear system models.

In this thesis, the gap between existing, commonly used, fractional-order linear models and simple nonlinear models is closed by proposal of classes of fractional-order nonlinear system models. Furthermore, a collection of parameter estimation methods and system identification approaches is also proposed, creating a complete set of modelling tools. In particular, two complementary parameter estimation methods are proposed, which are named: the delayed fractional-order state variable identification approach, and the refined instrumental variable method for fractional-order Hammerstein-Wiener models, respectively.

1.2 Aims and Objectives

The primary goal of this thesis is to design state variable filter based system identification approaches for nonlinear dynamic fractional-order systems using sampled input-output data. To the best knowledge of the author, there is no single system identification approach, which would be applicable to all types of nonlinear systems. Prompted by this

deficiency, this research focuses on selected nonlinear fractional-order system model structures. These structures are, namely, Hammerstein-Wiener system models and a class of bilinear system models these being a subclass of a wider nonlinear system models, which can be represented in an input-output model form.

The main aim of the thesis is divided into following objectives/deliverables:

I. Introduce a mathematical definition of fractional-order Hammerstein-Wiener, bilinear, and input-output nonlinear models used throughout this thesis.
II. Extend the refined instrumental variable method to encompass the fractional-order Hammerstein-Wiener and bilinear model structures. The newly defined refined instrumental method shall estimate the parameters of the Hammerstein-Wiener models for the case of non-invertible output static nonlinearity.
III. Design a fractional-order delayed state variable filter to generate filtered fractional-order time derivative terms of sampled input-output signals. The filtered signals are then used in the proposed system identification methods for identifying a class of nonlinear input-output models, including bilinear system models as a special case.
IV. Use an example of a diffusion equation in order to illustrate the advantages of adopting the fractional-order system identification methods in practice.

1.3 Thesis outline

The logical flow of the research work reported within the thesis has a top-down structure, where the developments presented in one chapter directly depend on the developments carried out in the previous chapter (and chapters) as illustrated in

Figure 1-1. The outline of the presented research work is given chapter by chapter in the order as they appear in the thesis.

Chapter 2: This chapter provides the essential background and literature review. Only the necessary background is provided here. Such background includes fractional-order Laplace transform and the selected numerical approximation methods for simulating linear and nonlinear fractional-order systems. The rest of the chapter covers the literature review and explains the need for fractional-order systems, refined instrumental variable methods in continuous-time domain, advantages of Hammerstein-Wiener and bilinear system models. Part of this chapter is presented in (Allafi, and Burnham 2013).

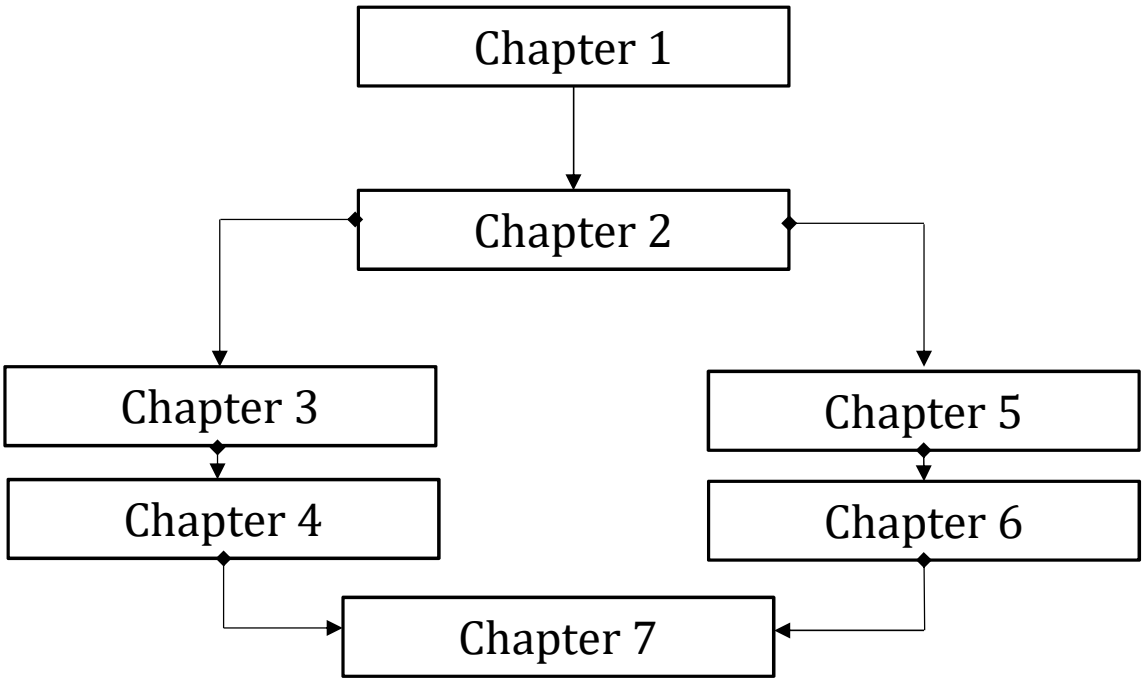

Figure 1-1: Schematic diagram of the logical flow of chapter's dependency in the thesis.

Chapter 3: In this chapter, the use of the introduced parameter estimation and system identification methods is demonstrated on a modelling example of 1D diffusion process, which can be found in Lithium Ion cells. The diffusion process is described by a linear partial differential equation, which is numerically solved by making use of a finite volume approach. The input and output signals of the diffusion equation (process) are stored and used for identification purposes. Firstly, the model structure is detected using the estimated Bode plot (commonly used approach). Subsequently, the model parameters are

estimated using a (simplified) refined instrumental variable method. This chapter refers to (Allafi, Zajic, and Burnham 2015b and Allafi, and Burnham 2014)

Chapter 4: This chapter introduces the refined instrumental variable parameter estimation method and the proposed extension to encompass a class of fractional-order continuous-time Hammerstein-Wiener system models subject to auto-regressive moving average measurement noise. Numerical examples are implemented to evaluate the two proposed parameter estimation methods.

Chapter 5: In this chapter, a delayed fractional-order state variable filter is proposed and presented. The filter comprises of two sub-filters, namely, a Butterworth filter and an all-pass filter. Three different formulations of a fractional-order Butterworth filter are proposed and evaluated; these are the fractional-order Butterworth filter of base-order $\alpha = 0.5$ design, the square root base design for base-order $\alpha = 1/2^n$ where $n \in \mathbb{Z}$ and the compartmental fractional-order Butterworth filter design. The fractional-order Butterworth filter is equalised by an all-pass filter to achieve the required (or demanded) group-delay, which results in the proposed delayed fractional-order state variable filter. Numerical implementation of the proposed filter is presented together with potential drawbacks. The recommended input selection is also discussed together with a detailed guideline on using the proposed filter for parameter estimation of nonlinear fractional-order input-output system models. Finally, a numerical example and conclusions are provided. Part of this chapter was presented in (Allafi, Zajic, and Burnham 2015a).

Chapter 6: In this chapter, a class of bilinear fractional-order system models is introduced and studied. This chapter also presents how the filtered input-output signals, obtained by the proposed delayed fractional-order state variable filter, can be used for bilinear model structure detection. The method uses a so-called error reduction ratio approach. The numerical implementation of bilinear fractional-order system models in MATLAB and Simulink is explained. Subsequently, two numerical benchmark examples are used to

evaluate the proposed parameter estimation method, namely, the delayed fractional-order state variable identification approach. These numerical examples are also used to assess the performance of the error reduction ratio approach for model structure detection.

Chapter 7: Conclusions are highlighted and directions for the potential areas for further research are suggested.

1.4 Contributions

This section provides a list of findings and contributions in order of their appearance in the thesis:

I. Chapter 3: A full system identification cycle of a 1D diffusion process within a Lithium Ion cell is developed. This includes input-output signal generation, model structure detection and model parameter estimation. The resulting system is described by a fractional-order continuous-time linear transfer function.

II. Chapters 4/6: Two new model structures, termed the fractional-order Hammerstein-Wiener and bilinear fractional-order models, are developed. The proposed models are a result of promoting a class of classical bilinear and Hammerstein-Wiener models by the fractional-order calculus.

III. Chapter 4: Extension of the simplified and refined instrumental variable methods for parameter estimation of integer-order models to encompass a class of fractional-order continuous-time Hammerstein, Wiener, and Hammerstein-Wiener models. The introduced approaches use sampled input-output data and do not require the output static nonlinearity of the Wiener system model to be invertible.

IV. Chapter 5: Development of a novel delayed fractional-order state variable filter. The proposed filter is designed to generate delayed input-output signals

and their higher order fractional-order time derivatives, within a selected frequency range.

V. Chapter 5: Development of a fractional-order Butterworth filter for providing a maximally flat frequency response gain. The proposed fractional-order Butterworth filter is part of the proposed delayed fractional-order state variable filter where all arbitrary fractional-order signal time derivatives are generated and collected. Three different approaches are proposed for designing the fractional-order Butterworth filter, namely fractional-order Butterworth filter of base-order $\alpha = 0.5$ design, the square root base design for base-order $\alpha = 1/2^n$ and the compartmental fractional-order Butterworth filter design.

VI. Chapters 5/6: Proposal of a novel parameter estimation method based on a delayed fractional-order state variable filtering approach. The method is capable of estimating the parameters of a general single-input single-output fractional-order nonlinear ordinary differential equation. This approach is applied to estimate the parameters of a class of bilinear fractional-order system models, which can be written in a form of the fractional-order input-output nonlinear equation.

VII. Chapter 6: Development of an error reduction ratio approach for model structure detection of input-output fractional-order nonlinear ordinary differential equations. This method is used in conjunction with the proposed delayed fractional-order state variable filtering method for model parameter estimation.

Chapter 2: Background and Literature Review

The chapter consists of two essential sections, namely background and literature review. In the first section, most of the prior knowledge required for understanding the proposed methods is stated. Furthermore, it provides the essential background of the fractional-order model and numerical methods for simulation of the fractional-order system in MATLAB and Simulink based on fractional-order system toolboxes.

The literature review aims to demonstrate arguments, supporting the selection of the nonlinear structure according to fractional-order or integer-order, continuous-time or discrete-time, Hammerstein and Wiener model and nonlinear input-output model in particular (bilinear fractional-order systems). It then illustrates the linear and nonlinear identification approaches, already extended to the fractional-order case. It is followed by stating the reasons why the proposed methods are selected to be extended to fractional-order. The existing context of using the fractional-order system to describe the physical system is presented. It is expected from this literature review to answer the following questions:

I. *Why fractional-order?*

II. *Why continuous-time?*

III. *Why input-output representation and the Hammerstein and Wiener model?*

IV. *Why refined instrumental variable method and delay state variable identification approaches?*

2.1 Introduction

An increasingly significant subject in the literature of engineering, science, and applied mathematics is that of fractional-order calculus and fractional-order differential equations. It is attractive to use fractional-order calculus in modelling phenomena and many physical processes that depend on both the current state and the overall time history. In modelling, it has been experienced in charging and discharging of the lossy capacitor and lossy coil the inherent fractional-order differentiation behaviour as presented in (Schäfer, and Krüger 2008 and Das, and Pam 2011). Furthermore, Randle's equivalent circuit, which has Warburg impedance representing the fractional-order element, has been used to model electrochemical process, for more details see (Yuan et al. 2003). A major challenge for the fractional-order modelling was the numerical implementation. One of the numerical implementation approaches was built on RC-networks and operational amplifiers, representing the fractional-order transfer function (Ichise, Nagayanagi, and Kojima 1971).

The common need for accurate and efficient control of today's industrial process applications has driven the system identification field to face the constant challenge of providing better models of physical phenomena. Although there is a massive demand for the nonlinear fractional-order continuous-time systems, there is only a limited amount of literature dealing with nonlinear fractional-order continuous-time system identification compared to fractional-order continuous-time linear system identification.

This chapter is organised as follows: it is divided into three main sections, namely Section 2.2 Background to fractional-order systems, 2.3 Literature review and 2.4 Conclusions. The background to fractional-order systems section outlines some basic fractional-order theory for understanding the rest of the thesis. These are Subsections 2.2.1, 2.2.2, 2.2.3, 2.2.4 and 2.2.5 for fractional-order calculus, linear fractional-order model, fractional-order transfer function and state-space representation, fractional-order frequency response and numerical implementation of fractional-order systems, respectively. The literature review is divided into Subsection 2.3.1 Motivations of fractional-order continuous-time identification, Subsection 2.3.2 Nonlinear fractional-order continuous-time models, Subsection 2.3.3 System identification, Subsection 2.3.4 Linear parameter estimation of linear fractional-order continuous-time systems, Subsection 2.3.5 Parameter estimation of nonlinear systems, Subsection 2.3.6 Model structuring of fractional-order continuous-time systems. Finally, the chapter is completed with Conclusions in Section 2.4.

2.2 Background to fractional-order systems

In the literature, three different expressions, non-integer, fractional and fractional-order, refer to the same class of system whose order is an arbitrary real number. Non-integer gives a meaning of excluding the integer-order. Fractional and fractional-order terms cover both integer and non-integer. In this thesis, only the fractional-order term is used. This section introduces the fundamental theory upon which this thesis is based, the theory of fractional-order derivatives and integrals. It covers a demonstration of a linear fractional-order time invariant systems and transfer functions as well as their numerical implementation. Furthermore, a brief overview of frequency-domain responses and fractional-order simulation methods are presented.

2.2.1 Fractional-order Calculus

Fractional-order integral and derivative terms are generalised by the fractional-order calculus. The term denoted by ${}_aD_t^\alpha$ is defined as:

$$ {}_a\mathcal{D}_t^\alpha = \begin{cases} \dfrac{d^\alpha}{dt^\alpha} & \alpha > 0 \\ 1 & \alpha = 0 \\ {}_a^t\mathcal{I}^{-\alpha} = \displaystyle\int_a^t dt^{-\alpha} & \alpha < 0 \end{cases} \tag{2.1} $$

The operator $\mathcal{D}$ and the real number order α together represent the fractional-order term whether it is derivative or integral. When the real number α is positive, it represents fractional-order derivative and when α is negative, it represents fractional-order integral. In this thesis, for retaining moderate complexity, the order α is considered to be a real number and always positive $\alpha \in \mathbb{R}^+$. Thus, in this thesis, the terms for describing the fractional-order derivative and integral are $\mathcal{D}^\alpha$ and $\mathcal{I}^\alpha$, respectively.

2.2.1.1 Fractional-order integral

In this section, concentration is only on the Riemann–Liouville's conceptions while more definitions are presented in Appendix A. The Riemann–Liouville's definition is selected because it is used later for Laplace transform derivation. The Riemann–Liouville's definition is based on a consequence of Cauchy's formula for iterated integrals (Oldham, and Spanier 1974).

$$ {}_a^t\mathcal{I}^\alpha f(t) = \frac{1}{\Gamma(\alpha)} \int_a^t (t-\tau)^{\alpha-1} f(\tau)\, d\tau \ , \ \alpha \in \mathbb{R}^+ \tag{2.2} $$

where the Euler function is defined as:

$$ \Gamma(x) = \int_0^\infty t^{x-1} e^{-t}\, dt \qquad x \in \mathbb{R} \tag{2.3} $$

If $a = 0$, it can be noted that the integral in (2.2) is a convolution of two signals $t^{\alpha-1}$ and $f(t)$. Therefore, (2.2) can be expressed as:

$$I^{\alpha} f(t) = \frac{1}{\Gamma(\alpha)} \left[t^{\alpha-1} * f(t) \right] \tag{2.4}$$

2.2.1.2 Fractional-order derivative

One of the numerical simulations of fractional-order systems, used in this thesis, is based on the difference equation and was derived from the Grünwald–Letnikov definition. Therefore, this section focuses on the Grünwald–Letnikov definition and more fractional-order derivative definitions are stated in Appendix A. A discrete-time definition of the concept of fractional-order differentiation was defined by Grünwald–Letnikov based on the generalisation of the backward difference (Das 2011):

$$\mathcal{D}^{\alpha} f(t)\Big|_{t=KT_s} = \lim_{T_s \to 0} \frac{1}{T_s^{\alpha}} \sum_{k=0}^{K} (-1)^k \binom{\alpha}{k} f\left((K-k)T_s\right) \tag{2.5}$$

where $\binom{\alpha}{k}$ is the Newton's binomial function and T_s is the sampling interval. It is generalised using the Euler's Gamma function, and extended to fractional-order as:

$$\binom{\alpha}{k} = \frac{\Gamma(\alpha+1)}{\Gamma(k+1)\Gamma(\alpha-k+1)} \tag{2.6}$$

It can be noted from (2.6) that the fractional-order derivative depends on all past data unless $\alpha \in \mathbb{Z}$. This is why the fractional-order derivative is known as long memory.

2.2.2 Linear fractional-order model

A fractional-order differential equation can describe the linear time invariant fractional-order model in the following manner:

$$\begin{aligned} &a_0 \mathcal{D}^{\alpha_n} y(t) + a_1 \mathcal{D}^{\alpha_{n-1}} y(t) + \ldots + a_n \mathcal{D}^{\alpha_0} y(t) = \\ &b_0 \mathcal{D}^{\beta_m} u(t) + b_1 \mathcal{D}^{\beta_{m-1}} u(t) + \ldots + b_m \mathcal{D}^{\beta_0} u(t) \end{aligned} \tag{2.7}$$

where $u(t)$ and $y(t)$ are the input and output of the model, respectively. $\mathcal{D}^{\alpha}x(t)=\frac{d^{\alpha}x(t)}{dt^{\alpha}}$, $a_j\,(j=0,1,\ldots n)$ and $b_j\,(j=0,1,\ldots m)$ are constants, $\left(\alpha_j\,(j=n,n-1,\ldots 0),\beta_j\,(j=m,m-1,\ldots 0)\right)\in\mathbb{R}^{+}$, $\alpha_n>\alpha_{n-1}\ldots>\alpha_0$, $\beta_m>\beta_{m-1}\ldots>\beta_0$ and $\alpha_n\geq\beta_m$ for physical feasibility.

2.2.3 Fractional-order transfer function and state-space representation

One of the most significant theories in, for instance, control engineering, is the Laplace transform of the linear fractional-order model. The Laplace transform of the fractional-order integral term can be derived from Riemann-Liouville theory. The Laplace transform of the convolution in (2.4) can be expressed as:

$$\mathcal{L}\left(I^{\alpha}f(t)\right)=\mathcal{L}\left(\frac{t^{\alpha-1}}{\Gamma(\alpha)}\right)\mathcal{L}\left(f(t)\right),\qquad \alpha>0 \tag{2.8}$$

$$\mathcal{L}\left(I^{\alpha}f(t)\right)=\frac{F(s)}{s^{\alpha}} \tag{2.9}$$

where $\mathcal{L}\left(\frac{t^{\alpha-1}}{\Gamma(\alpha)}\right)=s^{\alpha}$, see (Schiff 1999:210).

The Laplace transform of the fractional-order derivative of $f(t)$ can be obtained by (Podlubny 1998:105):

$$\mathcal{L}\left(D^{\alpha}f(t)\right)=s^{\alpha}F(s)-\sum_{k=0}^{n-1}\left[s^{k}\,\frac{d^{\alpha-1-k}f(t)}{dt^{\alpha-1-k}}\right]_{t=0} \tag{2.10}$$

where $\alpha\geq 0$ and $n\leq\alpha<n+1$. For simplicity, zero initial conditions are considered. Applying this property to (2.7) yields the fractional-order transfer function:

$$G(s)=\frac{Y(s)}{U(s)}=\frac{b_0s^{\beta_m}+b_1s^{\beta_{m-1}}+\ldots+b_ms^{\beta_0}}{a_0s^{\alpha_n}+a_1s^{\alpha_{n-1}}+\ldots+a_ns^{\alpha_0}} \tag{2.11}$$

where $y(t)$ and $u(t)$ are relaxed i.e. $y(t)=u(t)=0$ at $t=0$.

The fractional-order transfer function is termed commensurate if the orders of the Laplace variable in (2.11) are integer multiples of a base-order, denoted α. Therefore, the commensurate form of the transfer function in (2.7) becomes:

$$G(s)=\frac{\sum_{k=0}^{m} b_{m-k} s^{k\alpha}}{\sum_{k=0}^{n} a_{n-k} s^{k\alpha}} \tag{2.12}$$

where $n > m$.

A fractional-order state-space representation is obtained by converting the fractional-order transfer function only if the fractional-order transfer function is commensurate (Podlubny 1998). In this case, the conversion from the fractional-order transfer function to state-space representation is similar to the conversion in the integer-order case. Therefore, the obtained fractional-order state-space representation becomes (Podlubny 1998):

$$\begin{aligned} s^{\alpha} X(s) &= AX(s)+BU(s) \\ Y(s) &= CX(s)+DU(s) \end{aligned} \tag{2.13}$$

where $X(s)$ is the state variable vector and A, B, C and D are system, input, output and feedforward through matrices , respectively. A, B, C and D are obtained in a similar way to the integer-order case.

2.2.4 Fractional-order frequency response

The fractional-order frequency response can be achieved by replacing s with $j\omega$. For instance, for deriving the frequency response of $G(s)=s^{\alpha}$:

$$G(j\omega)=(j\omega)^{\alpha}=\omega^{\alpha} j^{\alpha} \tag{2.14}$$

Considering $j^{\alpha}=\cos\left(\alpha\frac{\pi}{2}\right)+j\sin\left(\alpha\frac{\pi}{2}\right)=e^{j\alpha\frac{\pi}{2}}$, this leads to re-express (2.14) as:

$$G(j\omega) = \omega^{\alpha} e^{j\alpha\frac{\pi}{2}} \tag{2.15}$$

Therefore, the magnitude (in logarithm form) and phase are:

$$20\log_{10}\left|G(j\omega)\right| = \alpha 20\log_{10}(\omega) \tag{2.16}$$

$$\angle G(j\omega) = \alpha\frac{\pi}{2} \tag{2.17}$$

Furthermore, the frequency response of $G(s) = s^{\alpha} + 1$ can be obtained as follows:

$$G(j\omega) = (j\omega)^{\alpha} + 1 = \omega^{\alpha}\cos\left(\alpha\frac{\pi}{2}\right) + \omega^{\alpha} j\sin\left(\alpha\frac{\pi}{2}\right) + 1 \tag{2.18}$$

$$\begin{aligned}\left|G(j\omega)\right| &= \sqrt{\left(\omega^{\alpha}\cos\left(\alpha\frac{\pi}{2}\right)+1\right)^{2} + \left(\omega^{\alpha}\sin\left(\alpha\frac{\pi}{2}\right)\right)^{2}} \\ &= \sqrt{\omega^{2\alpha} + 2\omega^{\alpha}\cos\left(\alpha\frac{\pi}{2}\right)+1}\end{aligned} \tag{2.19}$$

$$\angle G(j\omega) = \tan^{-1}\left(\frac{\omega^{\alpha}\ \sin\left(\alpha\frac{\pi}{2}\right)}{1+\omega^{\alpha}\ \cos\left(\alpha\frac{\pi}{2}\right)}\right) \tag{2.20}$$

For more details, see (Manabe 1961 and Jifeng, and Yuankai 2005).

2.2.5 Numerical implementation of fractional-order systems

A major issue in fractional-order calculus was the real time simulation. However, the improvement in technology during the last three decades has given rise to a massive development in numerical algorithms for approximating fractional-order systems. There are different approaches for simulating the fractional-order derivative and integral which can then be used for simulating the linear and nonlinear fractional-order systems in Simulink. If the fractional-order transfer function is commensurate with base-order α, by applying partial fraction expansion on the fractional-order transfer function, leads to the fractional-order transfer function being expressed as a sum of eigenmodes, whose orders are α in the case of real roots or 2α in the case of complex roots. In the case all roots are

real, the fractional-order transfer function, whose order is αm, can be expressed in eigenmodes as:

$$G(s)=\sum_{i=1}^{m}\frac{A_i}{s^{\alpha}+\lambda_i} \tag{2.21}$$

Considering zero initial condition, each eigenmode can be individually simulated in the time-domain as shown in Figure 2-1. Therefore, if it is possible to approximate s^{α} or $s^{-\alpha}$, it leads to the overall fractional-order transfer function, being approximated, as illustrated in Figure 2-2, and even more complex nonlinear fractional-order systems as seen later.

Figure 2-1: Schema of one eigenmode (Aoun 2003).

There are several approaches to approximate the fractional-order derivative and integral terms and the selected approaches can be classified as a time-domain base and a complex representation base.

2.2.5.1 The time-domain base approach

It is categorised as a direct approach because the fractional-order derivative operator is directly replaced by its numerical approximation. The Grünwald–Letnikov definition in

(2.5) is used for deducing a numerical approximation of the fractional-order derivatives as:

Figure 2-2: Fractional-order system in eigenmode form (Aoun 2003).

$$\mathcal{D}^{\alpha}x(t) \approx \Delta_{T_s}^{\alpha}x(t)$$

$$\Delta_{T_s}^{\alpha}x(t)\Big|_{t=KT_s} = \frac{1}{T_s^{\alpha}}\sum_{k=0}^{K}\omega_k^{\alpha}x\big((K-k)T_s\big) \tag{2.22}$$

where $\omega_k^{\alpha} = (-1)^k \binom{\alpha}{k}$ and T_s is the sampling interval, so that $t = KT_s$. It can be noted from (2.22) that as time t increases, there is a need to increasingly add more and more to the summation for computing the solution. However, it is observed that for large t the coefficients of the Grünwald–Letnikov definition have much greater influence on the more recent values than the older ones. Hence, the numerical solution can be approximated by using only the recent values. This leads to a memory length, denoted L, (Podlubny 1997)

such that $\mathcal{D}^{\alpha}x(t) \approx_{t-L} \Delta^{\alpha}x(t)$ for $t > L$. One approach for selecting L is given in (Podlubny 1999) where the approximation error, denoted $\varepsilon(t)$ and generated during approximation, for $|x(t)| \le M, (0 < t < t_1)$ is bounded by

$$\varepsilon(t) = \left|\mathcal{D}^{\alpha}x(t) -_{t-L} \Delta^{\alpha}x(t)\right| \le \frac{ML^{-\alpha}}{\left|\Gamma(\alpha-1)\right|}, (0 < t < t_1) \tag{2.23}$$

(2.23) can be used to obtain the necessary L by considering a certain error bound, as

$$\varepsilon(t) < \epsilon, L \le t \le t_1 \Rightarrow L \ge \left(\frac{M}{\epsilon\left|\Gamma(1-\alpha)\right|}\right)^{1/\alpha} \tag{2.24}$$

This approach is used in the numerical examples in Chapter 3.

2.2.5.1.1 The complex representation base approach

The complex representation base of the fractional-order derivative and integral approximation comes from the complex Laplace transform variable. The frequency response of the Laplace transform of the fractional-order derivative and integral terms is approximated by higher integer-order transfer functions. According to (Vinagre et al. 2000), the direct method (continuous-time approach) can be categorised into continued fraction expansions and frequency response curve fitting. Some examples of methods, designed based on continued fraction expansions, are Carlson's method and Matsuda's method, introduced in (Carlson, and Halijak 1964 and Matsuda 1993), respectively. The methods, designed based on frequency response curve fitting and used in Chapters 4, 5 and 6, are known as Oustaloup's and modified Oustaloup's methods. This section considers these two methods. In these approaches, the approximation is based on fitting the frequency response curve of an integer-order function to the fractional-order function frequency response curve. This approximation is restricted with limited frequency. This might be achieved by minimising the cost function of the integrated square error (Vinagre et al. 2000):

$$J(j\omega)=\int W(j\omega)\left|G(j\omega)-\hat{G}(j\omega)\right|^2 d\omega \tag{2.25}$$

where $G(j\omega)$ is the frequency response of the fractional-order function, $\hat{G}(j\omega)$ is the frequency response of an estimated integer-order transfer function and $W(j\omega)$ is a weighting function.

2.2.5.1.1.1 Oustaloup's method

Oustaloup's recursive filter fits the fractional-order Laplace variable s^{α} very well within a selected frequency range (ω_b,ω_h). This is the most widely used approximation approach in the field of fractional-order calculus. The general form of the Oustaloup filter can be expressed as:

$$G_f(s)=s^{\alpha}=K\prod_{k=-N}^{N}\frac{s+\omega_k^{'}}{s+\omega_k} \tag{2.26}$$

where it is assumed that the fitting frequency range is within (ω_b,ω_h) . The poles, zeros and gain of the filter in (2.26) might be calculated by $\omega_k=\omega_u\left(\frac{\omega_h}{\omega_b}\right)^{\frac{k+N+\frac{1}{2}(1+\alpha)}{2N+1}}$, $\omega_k^{'}=\omega_u\left(\frac{\omega_h}{\omega_b}\right)^{\frac{k+N+\frac{1}{2}(1-\alpha)}{2N+1}}$, $\omega_u=\sqrt{\omega_h/\omega_b}$ and $K=\omega_h^{\alpha}$, respectively, according to (Vinagre et al. 2000 and Das, and Pan 2011:29).

2.2.5.1.1.2 Modified Oustaloup's method

For better fitting of the fractional-order derivative within a selected frequency range, the Oustaloup filter is extended to improve the frequency convergence. The modified Oustaloup filter is expressed as (Vinagre et al. 2000). :

$$s^{\alpha}=\left(\frac{d\omega_h}{b}\right)^{\alpha}\left(\frac{ds^2+b\omega_h s}{d(1-\alpha)s^2+b\omega_h s+d\alpha}\right)\prod_{k=-N}^{N}\frac{s+\omega_k^{'}}{s+\omega_k} \tag{2.27}$$

where the poles, zeros, and gain of the filter can be evaluated as in Oustaloup's method. The modified filter gives a good approximation when $b=10$ and $d=9$.

A question arises when considering these two methods: Why there is a need to consider a fractional-order system if it can be then described by an integer-order system. This section considers this argument through modelling and control perspectives. From a modelling perspective, the fractional-order transfer function is the original model which can be then approximated according to the required accuracy and efficiency. For example, consider a system is described by a fractional-order transfer function and expressed as:

$$H(s^{\alpha})=\frac{a}{s^{\alpha}+a} \tag{2.28}$$

The approximated integer-order transfer function of (2.28), using the modified Oustaloup's method, is:

$$\hat{H}(s)=\frac{a}{\left(\frac{d\omega_h}{b}\right)^{\alpha}\left(\frac{ds^2+b\omega_h s}{d(1-\alpha)s^2+b\omega_h s+d\alpha}\right)\prod_{k=-N}^{N}\frac{s+\omega_k'}{s+\omega_k}+a} \tag{2.29}$$

It can be noted that (2.29) depends on coefficients $d,b,\omega_h,\omega_k,\omega_k'$ and generates different poles and zeros as different values of these coefficients are selected while there is only one form of the fractional-order transfer function (2.28). Additionally, (2.28) can be directly numerically solved using (2.22) without expressing as an approximate through the integer-order systems.

From control perspective, the stability of the system must be considered for designing a reliable control algorithm. The original fractional-order system (2.28) gives the actual stability while the approximated integer-order transfer function approximates the stability within the selected frequency range. Furthermore, any control design requires the original model to produce a better design. For example, the pole placement design needs to know the pole locations. In the case of the system in (2.28) there is only one root

(which is equivalent to the term pole in the integer-order systems) while the number of poles and zeros in (2.29) are set according to N.

2.2.5.2 Nonlinear fractional-order system simulation

One of the significant stages in nonlinear system identification and control design is system simulation. In this thesis, the nonlinear fractional-order differential equations are simulated using Simulink and the FOMCON toolbox which can be downloaded and installed in Simulink, for more details see (Tepljakov, Petlenkov, and Belikov 2011). This is achieved by representing the nonlinear fractional-order system in a fractional-order state-space representation which can be then implemented in the equivalent block diagram, using fractional-order integral blocks. The fractional-order integral blocks are provided by the FOMCON toolbox and both (2.26) and (2.27) can also be found in the Simulink block in the FOMCON toolbox. For an illustrative example see (Xue, Chen, and Atherton 2007:297).

2.3 Literature review

The main goal of this section is to illustrate how and why model structures and identification methods are selected.

2.3.1 Motivations of fractional-order continuous-time identification

2.3.1.1 Continuous-time system identification

There has been a significant switch towards the discrete-time identification for almost four decades because of simplicity in the discrete-time identification and the increase in digital technology availability (Garnier, and Wang 2008). However, it is important to realise that the continuous-time identification directly from measured data has greater advantages than the discrete-time identification in many aspects which are presented in this section. The continuous-time parameter estimation approaches can be classified as

indirect and direct approaches. In the indirect approaches, the estimation of the continuous-time model parameters is achieved by two steps: (1) estimate the discrete-time model of auxiliary parameters and (2) transform the estimated discrete-time model to continuous-time model. On the other hand, the direct approach involves only one step to directly estimate the continuous-time model. The main idea of the direct method is that the actual continuous-time parameters are estimated directly without the intermediate step to obtain the additional discrete-time auxiliary parameters. In the last decade Garnier, Unbehauen and Rao have studied the continuous-time versus discrete-time representations of systems and came up with recommendations for applying the identification techniques directly to estimate the parameters of the continuous-time system from sampled data. The following references cover the finding of using the continuous-time model and direct continuous-time model identification (Garnier 2015, Garnier, and Wang 2008, and Rao, and Unbehauen 2006). To illustrate these findings, a second order stiff system is used as a benchmark. The meaning of stiff in the context is where the modes differ significantly. It is expressed in both continuous-time transfer function and discrete-time transfer function, the later using a zero-order hold with sampling interval of $T_s = 1,\ 10^{-1},\ 10^{-2}$ and 10^{-3} s :

$$H(s) = \frac{1}{(s+1)(s+100)} \tag{2.30}$$

$$\begin{aligned} H_{T_s=1}(z) &= \frac{0.006284(z+0.0059)}{(z)(z-0.3679)} \\ H_{T_s=10^{-1}}(z) &= \frac{0.8602(z+0.1062)}{(z-0.9048)(z-4.54\times10^{-5})} \\ H_{T_s=10^{-3}}(z) &= \frac{4.836\times10^{-7}(z+0.9669)}{(z-0.9990)(z-0.9048)} \end{aligned} \tag{2.31}$$

I. Continuous–time domain interprets most physical phenomena, most scientific laws (Newton's, Faraday's, etc.) and the majority of classical theories in signal processing, systems and control. The physical systems are reformulated in

differential equations whose parameters are directly connected to the physical properties of the system, such as mass. This increases the confidence in the analysis and design of the physical systems. On the other hand, the parameters of the discrete representation of the model are related to the sampling time (Garnier, and Wang 2008).

II. Continuous-time models conserve a *priori* knowledge of the physical system. This can be observed in different continuous-time representations. For example, the order of the ordinary differential equations, the number of poles in the transfer function or the number of states in state-space representation equals to the number of independent energy-storage elements in mechanical systems, see (Nise 2011). Transforming the continuous-time transfer function with *m* zeros and *n* poles to discrete-time transfer function, considering a zero-order hold, generates the discrete-time transfer function with *n-1* zeros and *n* poles. So *n-m-1* zeros make the model lose the properties of the original transfer function and this can be seen in (2.30) and (2.31).

III. In the general approach to system identification, explicit filtering strategies are suggested. This statistically increases the efficiency of the parameter estimates. Moreover, the filtering approach which is inherent in continuous-time is not inherent in discrete-time, for more details see (Garnier, Wang, and; Young 2008:13).

IV. Selection of the sampling rate is generally critical and challenging for discrete-time systems. Too slow and insufficient sampling rate compared to the time constant of each mode might generate aliasing. On the other hand, the changes in the sampling rate affects the poles of the discrete-time model representation, which leads to a potential increase of the undesirable sensitivity problem. This can be explicitly noted in the three different sampling intervals used in the example given in (2.31). This leads the

estimates to become statistically ill-defined. However, it is enough to consider that the sampling rate of data collection is sufficiently fast to allow the identification of a continuous-time model from sampled data.

V. The continuous-time systems and system identification do not require a uniform sampling rate since it is fast enough. But it might not be possible to perform discrete-time identification in the case of irregular sampling. In fact, discrete-time system identification can be applied only to uniformly sampled data.

VI. The issue of selecting the sampling rate appears again in the case of stiff systems. The stiff systems have both slow and fast dynamics as in the case of the system described in (2.30). In (2.30), there are two time constants. One is fast $0.01s$, and the other is slow $1s$. Therefore, the selection cannot be achieved without some compromise by losing some dynamic information of the fast dynamics and increasing the sensitivity of the slow dynamics.

2.3.1.2 Fractional-order system motivations

Although the topic of fractional-order systems subject is not new, for a relatively long time the researchers have only focused on the integer-order systems. This is due in part to the absence of numerically efficient solution methods for fractional-order differential equations. Since the 1980's when the technology provided the required tools to implement complex problems, there has been a significant shift of emphasis in the development of approximation methods of fractional-order integral and derivative representations. This allows applying the fractional-order systems to describe natural phenomena, such as diffusion in the electrochemical processes (Allafi, Zajic, and Burnham 2015b). Advantages of applying fractional-order representations against the integer-order representations and presenting numerical implementation capabilities of fractional-order systems are summarised as follows:

i. Wider performance range in modelling aspects: According to the derivative definition and approximation in (2.5) and (2.22), respectively, the fractional-order systems have both short and long memories (Monje et al. 2011). Moreover, the integer-order representation is intuitively a subset of the fractional-order representation. therefore, the fractional-order model gives a much wider range of different performances than the integer-order model. This can be observed in the gain and phase of the derivative term. For example, in (2.16) and (2.17) the gain and phase are gained by α in the fractional-order systems and $\alpha \in \mathbb{R}$ while in the integer-order $\alpha \in \mathbb{Z}$.

ii. Better robust control: The most popular controller in industrial field is, without a doubt, the proportional integral derivative (PID) controller. The transfer function of the PID may be expressed as:

$$C(s) = K_p + \frac{K_i}{s} + K_d s \tag{2.32}$$

where K_p, K_i, K_d are the proportional, integral and derivative gains. These gains can be selected to modify the position, smoothness, and minimum value of the magnitude curve and the slope of the phase but not change the slope of the magnitude curve and the phase at low and high frequencies. These findings appear in Figure 2-3 and Figure 2-4 when gains in (2.32) are selected to be $K_p = K_i = K_d = 1$ and $K_p = 1,\ K_i = 0.5,\ K_d = 1$.

The fractional-order proportional integral and derivative (FPID) controller was first proposed as a complete PID by Podlubny (1999) and expressed as a $PI^{\lambda} D^{\mu}$. The transfer function of FPID is expressed as:

$$C(s) = K_p + \frac{K_i}{s^{\lambda}} + K_d s^{\mu} \tag{2.33}$$

where K_p, K_i, K_d are the proportional, integral and derivative gains, respectively, and have the same influence in the classical PID while λ, μ are the fractional-

orders of the integral and derivative terms, respectively. Apart from noting that the classical PID is a subset of the FPID when $\lambda = \mu = 1$, the fractional-orders of the integral and derivative terms involve modifying the slope of the magnitude and the phase at low and frequencies. Figure 2-5 and Figure 2-6 show the magnitude and phase of (2.32) and (2.33) when the gains in (2.32) and (2.33) are set to unity $K_p = K_i = K_d = 1$ and fractional-orders of the integral and derivative terms are selected to be half-order $\lambda = \mu = 0.5$. The slope of the magnitude decreased from 20dB/decade, in the case of the classical PID $\lambda = \mu = 1$, to 10dB/decade in the case of FPID $\lambda = \mu = 0.5$ as shown in Figure 2-5. Moreover, the effect of switching from classical PID to FPID on the phase is that the phase at low frequencies increases by half, from around $-\lambda 90^\circ$ to $-\lambda 45^\circ$ while decreases at high frequencies from around $\lambda 90^\circ$ to $\lambda 45^\circ$. Therefore, it can be said, the FPID gives more robust control than the classical PID. Due to the higher flexibility of fractional-order theory, a new controller was introduced by Oustaloup and denoted by the CRONE controller which is an abbreviation of the French expression (Commande Robuste d'Ordre Non Entier). It has been developed in three different generations given in (Sabatier et al. 2015).

Figure 2-3: Magnitude of the frequency response of the classical PID controller in grey line when $K_p = K_i = K_d = 1$ and black line when $K_p = K_d = 1$ and $K_i = 0.5$ (Monje et al. 2011).

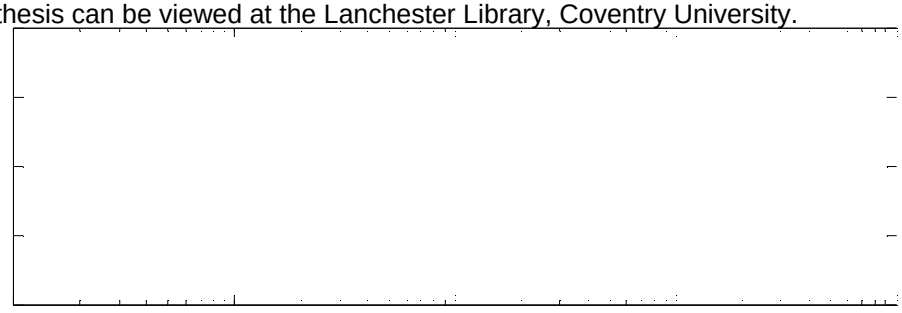

Figure 2-4: Phase of the frequency response of the classical PID controller in grey line when $K_p = K_i = K_d = 1$ and black line when $K_p = K_d = 1$ and $K_i = 0.5$ (Monje et al. 2011).

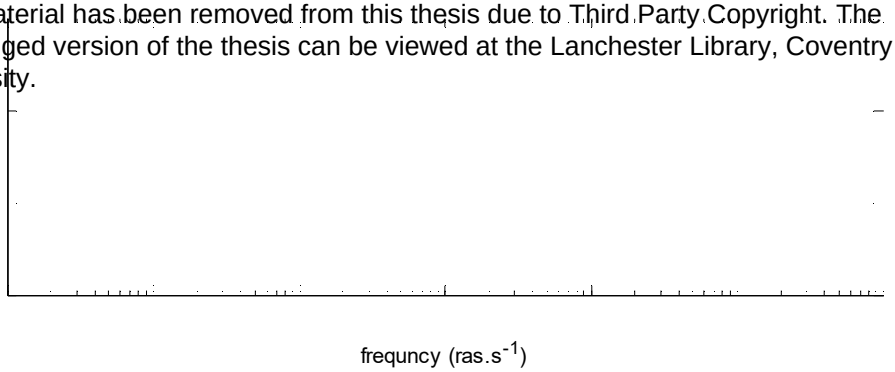

Figure 2-5: Magnitude of the frequency response of the classical PID controller in grey line when $K_p = K_i = K_d = 1$ and FPID in black line when $K_p = K_i = K_d = 1$ and $\lambda = \mu = 0.5$.

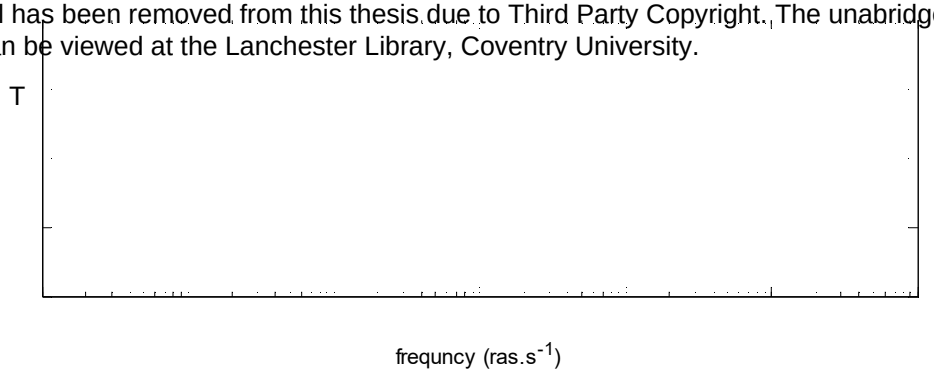

Figure 2-6: Phase of the frequency response of the classical PID controller in grey line when Kp = Ki = Kd = 1 and FPID in black line when Kp = Ki = Kd = 1 and λ= μ=0.5.

iii. Other supportive promotions: Before the 1980s of the last century, there was no toolboxes and not enough literature of classical theories for fractional-order control, fractional-order signal processing and fractional-order systems, such as fractional-order Laplace, and Fourier transforms. For example, if a researcher wanted to achieve any task in fractional-order systems, this would lead to face undiscovered theories and knowledge, associated with a lack of numerical

solutions. However, at the current time, there is a significant increase raise in fractional-order development and the fractional-order library is rich with many classical theories, such as fractional-order Laplace transforms of well-known functions and ordinary differential equations (Podlubny 1998), fractional-order Fourier transform (Almeida 1994), discrete fractional-order Fourier transform presented in (Candan, Kutay, and Ozaktas 2000), stability analysis for fractional-order linear time-invariant systems (Matignon 1998) and nonlinear systems (Momani, and Hadid 2004). This is associated with the introduction of reliable MATLAB toolboxes, e.g. the CRONE toolbox (Lanusse, Malti, and Melchior 2013), Ninteger toolbox (Valerio 2005) and FOMCON toolbox (Tepljakov, Petlenkov, and Belikov 2011). In this thesis, the FOMCON toolbox has been used because it provides all the required functions, methods, and algorithms for achieving all the tasks required this thesis.

2.3.2 Nonlinear continuous-time models

Although a significant number of literature items covers linear models, the majority of real processes are described by nonlinear models. This larger attention to the linear models stems from the simplicity and generalizability. The complexity of nonlinear systems is always the challenging issue but there is not deny a deficiency of nonlinear models to describe complex phenomena. However, there are the nonlinear models which can be considered to be relatively simple and holds more efficiency than the linear model. These model structures are (i) block-oriented models and (ii) bilinear models. One of the goals of this thesis is to identify a subclass of the block-oriented models and bilinear models, which are a Hammerstein and Wiener subclass and bilinear models which can be represented by input-output nonlinear ordinary differential equations.

The work here is not limited to considering nonlinear integer-order continuous-time models but rather extended to include fractional-order continuous-time nonlinear models.

This is because the nonlinear integer-order continuous-time models are in fact a subset of the fractional-order continuous-time nonlinear model. Therefore, these classes are selected to be extended to the fractional-order case and implemented in simulation. Following on from this, an illustration is presented of how the proposed identification method can be used to solve the identification problem of these selected models.

2.3.2.1 Bilinear models

The bilinear models, initially defined in a continuous-time state-space, represent a significant class of nonlinear model with the nonlinearity arising as a product between the input and state (Mohler 1973).

Due to the fact the bilinear system is a 'nearly-linear' system, it increases the opportunities to extend the algorithms and techniques, used in the linear systems, to cope with bilinear systems by making use of quase-linear time-step approaches. Furthermore, bilinear system models retains the required information about the system such as time constant and the process gain where the system input can be involved to calculate these quantities. (Zajic 2013). The bilinear models offer a wider performance range and are more controllable than linear models (Mohler 1973).

It has been shown that bilinear systems arise in biology, engineering and socioeconomics (Mohler 1973). From a practical perspective, the practical nonlinear industrial plant might be controlled and characterised as a bilinear model, stated in (Dunoyer et al. 1996). Furthermore, a general heating, ventilation, and air conditioning system is structured as a Hammerstein-bilinear model in (Zajic, 2013). The bilinear model offered improved modelling capabilities and retained a close link to well-understood linear models. The extension of the integer-order case of the bilinear model to the fractional-order case may assist in describing the higher order bilinear integer-order system more accurately. This is because the fractional-order systems have been used to describe much larger integer-order systems more efficiently and the integer-order modelling is a special case of

fractional-order modelling. Therefore, the bilinear fractional-order model gives a larger range of behaviours whilst preserving the simplicity offered by the properties of the bilinear models. This potential advantage further increases the motivation to investigate the problem of bilinear fractional-order identification.

2.3.2.2 Hammerstein and Wiener models

Hammerstein and Wiener continuous-time models are a class of block-oriented nonlinear systems. They are structured by input and output static nonlinear functions representing the Hammerstein and Wiener models, respectively, with an intermediate block being a continuous-time linear model. Both non-linear functions might be described by a sum of a *priori* known basis functions.

The advantages of the Hammerstein-Wiener models are (i) the dynamics of systems are mainly generated by the linear subsystem so that algorithms and techniques, used in the linear systems, might be adopted for the Hammerstein-Wiener model case and (ii) if the static nonlinearity has an inverse function, then it may allow a cancellation with the static nonlinearity and linear control algorithms could then be applied.

Several practical applications confirmed that Hammerstein and Wiener models can be utilised to model significant nonlinear systems, for instance, magnetospheric and ionospheric system (Palanthandalam-Madapusi, Ridley, and Bernstein 2005), radio frequency transmitter and power amplifier (Taringou et al. 2010) and electrical muscle stimulation in (Bai et al. 2009). Due to above advantages of the fractional-order continuous-time linear models and Hammerstein and Wiener models, this introduces a motivation to investigate fractional-order continuous-time Hammerstein and Wiener models. These introduced models are denoted fractional-order Hammerstein and Wiener models. They might be considered as a class of fractional-order block-oriented nonlinear systems. The linear part of both Hammerstein and Wiener continuous-time models is extended to fractional-order continuous-time linear time-invariant. Furthermore, both

fractional-order continuous-time Hammerstein and Wiener models are coupled within one model denoted as a fractional-order continuous-time Hammerstein-Wiener (HWFC) model.

2.3.3 System identification

The previous sections has covered the bilinear and Hammerstein-Wiener models while this section presents a review of the identification approaches for the linear, nonlinear, bilinear and Hammerstein-Wiener models. The term system identification refers to extraction of information about the mathematical model directly from the experimental data (Kerschen et al. 2006). Indeed, most of the principles applied for identification might fit under one of the three steps, namely structure detection or selection, parameter estimation and model validation. The term nonlinear model identification in this thesis refers to the identification of a nonlinear system model whether with linear or nonlinear estimators.

2.3.4 Parameter estimation of linear fractional-order continuous-time systems

The aim of this section is to bring to highlight the fractional-order linear system identification to illustrate the reasons why the selected method is used to deal with fractional-order continuous-time Hammerstein-Wiener systems and bilinear systems. The majority of the existing methods can be classified under an orthonormal basis class and filter base class.

An integer-order orthonormal basis concept has been extended to a fractional-order orthonormal basis, for example by synthesising fractional-order Kautz-like basis (Malti, Aoun, and Oustaloup 2004), extrapolating Laguerre functions to any fractional-order derivative in (Aoun et al. 2007 and Stanisławski et al. 2013). Furthermore, both a

fractional-order Legendre basis and Kautz- like basis have been generalised in (Akçay 2008) and a recent approach is the fractional-order Legendre basis, presented in (Ghanbari, and Haeri 2010). The orthogonal basis method approximates the system by a sum of orthogonal bases but not the original form. Therefore, in this thesis, a major attention is directed to the filter base approaches which retain the structure of the system.

By different approaches, the majority of integer-order linear filter methods have been extended to fractional-order as the cases of fractional-order state variable filter and fractional-order Poisson filter criteria, introduced in (Cois et al. 2001). Another integer-order linear filter, named simplified refined instrumental variable method (SRIV), has been extended to estimate the parameters of a fractional-order continuous-time model and abbreviated to the SRIVCF method.

In this thesis, the SRIVCF is extended to cope with fractional-order continuous-time Hammerstein and Wiener models. The selection of this filter based approach is due to its significant advantages. The main benefits of the SRIVCF method over the well known the fractional-order state variable filter and the fractional-order Poisson filter approaches (Cois et al. 2001) are that (i) the SRIVCF method does not need to design the filter and (ii) an iterative estimation is implemented in order to update the filter parameters and this then ensures that the estimates convergence and the estimates have statistically optimum properties (Young 2002).

In the case of direct identification of the integer-order continuous-time linear system, Young and Jakeman in 1980 firstly applied the refined instrumental method for identifying a linear integer-order continuous-time stochastic model (Young, and Jakeman 1980). The convergence of this approach was studied in (Liu, Wang, and Zheng 2011). In the linear system case, this thesis presents the refined instrumental variable (RIVCF) and simplified refined instrumental variable methods for estimating the parameters of a fractional-order continuous-time system, corrupted by white and coloured noise, respectively. The SRIVCF

method had already been extended by Malti see (Malti et al. 2008) to cope with stochastic fractional-order continuous-time linear and time-invariant systems in the case of white noise. Moreover, the RIVCF method was extended for considering the coloured noise in (Victor et al. 2011 and Allafi, and Burnham 2014). The linear model is a hybrid of a fractional-order continuous-time linear transfer function and an integer-order discrete-time linear transfer function. The output of the fractional-order continuous-time linear transfer function represents the noise-free output and the noise process is described by an integer-order discrete-time autoregressive moving average (ARMA) model. The sufficient estimated parameters of a fractional-order continuous-time transfer function of a hybrid fractional-order continuous-time Box-Jenkins model is obtained by applying the SRIVCF method. However, the RIVCF method statistically offers a more efficient estimation process, see (Young, Garnier, and Gilson 2006). Therefore, the SRIVCF and RIVCF methods are extended to estimate the parameters of the fractional-order continuous-time Hammerstein and Wiener models.

2.3.5 Parameter estimation of nonlinear systems

This section presents the state of the art of fractional-order continuous-time nonlinear system identification and illustrates the findings of the majority of the nonlinear fractional-order continuous-time identification approaches. This analysis identifies the knowledge gaps as well as limitations in the study approaches applied for nonlinear identification.

Differential evolution has been used as an algorithm for optimisation purposes and belongs to the class of genetic algorithms and has been considered as an suitable objective function for identifying the orders and parameters of the commensurate fractional-order chaotic system. The main findings of this approach are as follows: (i) it has the capability to find the actual global minimum, regardless of parameter initialisation accuracy; (ii) it has the ability of fast convergence with less control parameters. The differential evolution

algorithm is applied to perform the chaotic system (Tang et al. 2012). However, the drawbacks of the differential evolution are (i) it is designed for a chaotic system and requires to be redesigned for coping with a different system and (ii) the convergence is not guaranteed in the case where noise is present.

A different approach based on Volterra series was extended in (Maachou et al. 2010) where the nonlinear fractional-order differentiation model describes the nonlinear characteristics. Moreover, Volterra kernel functions are generated by the fractional-order orthogonal bases. The use of these can be explained by two main reasons: (i) separation of the contribution of the linear and the nonlinear quantities due to decomposition of a nonlinear model and (ii) the Volterra series can be considered as a generalised linear model (Maachou 2010). In (Maachou et al. 2010) and (Maachou et al. 2014), nonlinear parameters and linear coefficients are estimated by using linear and nonlinear programming, respectively. This approach has the Volterra series structure which can model nonlinear systems more efficiently than the linear model as shown in (Maachou et al. 2010) for describing a nonlinear thermal system. However, it may model the fractional-order Hammerstein-Weiner system and the bilinear fractional-order system but it leads to different model structures and parameters.

Fractional-order multimodels or fractional-order Takagi-Sugeno multimodels method was first proposed in (Malti et al. 2003). It is applied to the modelling of a fractional-order nonlinear system. The basis of the fractional-order multimodels is to represent the system as an interpolation of a set of simple fractional-order submodels. Each submodel describes the dynamics of the system within an operating range. The weighting function specifies the local validity of the submodel. This approach requires restructuring of the original model to a sum of nonlinear base functions, which is not preferable for identifying the fractional-order Hammerstein-Weiner and bilinear fractional-order systems.

Applying the aforementioned methods can lead to unpreferred consequences such as describing the nonlinear system with higher fractional-order model or using indirect optimisation techniques associated with intensive computation time. The main aim is to retain the original structure of the fractional-order Hammerstein-Weiner and bilinear fractional-order systems which the aforementioned methods do not offer.

However, different time-domain approaches have been applied for integer-order continuous-time nonlinear model identification and these have not yet been extended to cope with fractional-order systems. Although there are considerable advantages in taking into account the nonlinear continuous-time systems, there is a lack of literature related to the direct methods to identify the parameters of the nonlinear ordinary differential equation in input-output representations which is the general case for bilinear systems.

The issue rests on when the nonlinear derivative term is required to be identified from measured data associated with measurement noise. Several methods directly approximate the derivative terms. The derivative term approximation is achieved after smoothing the measured data by, for instance, using a polynomial nonlinear auto-regressive smoother combined with the wavelet threshold techniques (Zhang, and Billings 2015). These are employed for the noise reduction of the measured data, see (Zhang, and Billings 2015). The efficiency of the noise reduction is still a challenge in this approach.

The delayed state variable filter is used for identifying the nonlinear integer-order differential equation and developed by Kohr (1963) and Tsang and Billing (1994). The main idea consists in the unique choice of the delay or transport lag filters. The consequence of passing a signal through a nonlinear function and then passing this resulting signal through a transport delay filter is the same when the nonlinear function and the lag transport filter are interchanged. This property allows collecting all the required data for identification directly from the filter possible while retaining the original structure of the nonlinear integer-order differential equation. The delayed state variable

filter identification approach is capable of identifying the bilinear model which can be described by the nonlinear integer-order differential equation. Therefore, in this thesis, the delayed state variable filter is extended to the delayed fractional-order state variable filter, which is to be used for generating the delayed fractional-order higher derivatives from the sampled data. The delayed state variable filter is fundamentally a Butterworth filter, equalised by all-pass filters for achieving a constant group-delay.

2.3.5.1 Bilinear system identification

The previous section considers identification of the nonlinear integer-order differential equation and recognises that the bilinear model is a subclass of the nonlinear integer-order differential equation. This section is concerned with selecting the delayed state variable filter identification approach for identifying the bilinear fractional-order system. Bilinear system identification emerged after the introduction of the bilinear system by using the Walsh function (Karanam, Frick, and Mohler 1978). In this approach, the properties of a linear combination of orthogonal functions are used to avoid the derivative terms by producing integral terms. Different functions and polynomials have been applied similarly based on orthogonal bases and functions. For example, block-pulse functions (Cheng, and Hsu 1982), Chebyshev polynomials (Liu, and Shih 1984), shifted Legendre polynomials (Hwang, and Chen 1986), Haar wavelets (Hsiao, and Wang 2000) and generalised orthogonal polynomials (Wang, Chang, and Yang 1987) have been applied. Moreover, modulation approaches have also been used for bilinear system identification, for example, the Hartley-based modulating functions (Daniel-Berhe, and Unbehauen 1998). All these methods can be considered as the function series, which contains the drawback of the need for running multiple experiments with the system at rest to obtain enough equations for bilinear system determination. According to (Juang 2012), implementing the multiple experiment method in the real-time case is quite complicated.

Recently, the ordinary simplified refined instrumental variable for the continuous-time linear model has been extended to identify the bilinear continuous-time model directly from measured data based on special observation where the input must hold special properties and it is assumed that the system be linear time-invariant (Zajic 2013).

Another approach considers multiple experiments for generating a combination of pulses for identifying state-space matrices. This method was firstly introduced for noise-free data of bilinear continuous-time systems in (Juang 2005) and a simpler computational approach has then been achieved in (Majji, Juang, and Junkins 2009). More extensions and improvements can be found in (Juang 2009, Juang, and Lee 2010 and Lee, and Juang 2012). All these approaches have the same disadvantage of not considering stochastic data.

2.3.5.2 Hammerstein and Wiener system identification

The Hammerstein and Wiener model identification can be classified as parametric and nonparametric methods. The nonparametric approach is based on different concepts and frequently does not need *a priori* knowledge of nonlinearity. The most basic concept is the cross-correlation analysis which is applied to decouple linear and nonlinear submodels with the assistance of white Gaussian input (Billings, and Fakhouri 1978). Furthermore, a kernel algorithm is used to recover the nonlinearity of the Hammerstein and Wiener model with a random input (Mzyk 2010, and Mzyk 2014) and other nonparametric methods can be found in (Greblicki, and Pawlak, 2008).

On the other hand, the parametric methods can be categorised as iterative and non-iterative methods. This literature focuses only on the iterative methods. In the discrete-time-domain, the iterative algorithm proposed in (Vörös 2004) is based on accessing the internal signals by using the key term separation principle as decomposition techniques and this algorithm was extend for the case of multi-inputs, see (Vörös 2007). This approach expresses Hammerstein and Wiener models linearly in parameters. The key

term separation principle and estimated linear outputs are used in the case of the Wiener model, (Zhou, Li, and Pan 2013). The drawbacks of this approach are that it is not a direct identification method and the convergence is not guaranteed. Other approaches for discrete iterative methods can be found in (Wang, and Ding 2011, Chen, Hwang, and Chang 2009). For the continuous-time domain, the refined instrumental variable method is used to identify the Hammerstein-Wiener continuous-time model with the assumption of an invertible static nonlinear function for the Wiener part. The parameters are obtained by applying singular value decomposition to the estimated multiple-inputs single-output linear model which represents the whole nonlinear model (Ni, Gilson, and Garnier2013).

In this thesis, the SRIVC and RIVC methods are extended to SRIVCF and RIVCF methods to work with HFC and WFC models and fractional-order continuous-time Hammerstein and Wiener models without the invertible output static nonlinearity assumption. The SRIVCF and RIVCF methods for identifying the HFC models are similar to SRIV and RIV in the case of the integer-order continuous-time models, proposed in (Laurain et al. 2008). In the case of the WFC model, the approach presented in (Ni, Gilson, and Garnier 2013) is extended to the fractional-order continuous-time case and improved by using the estimated linear output for approximating the output static nonlinearity.

2.3.6 Model structuring of fractional-order continuous-time systems

Most of the parameter estimation methods make the assumption that the model structure is known, however, in reality, every model structure is a challenging task and should be considered carefully. A significant number of research publications shows different approaches to detect the model structure of integer-order continuous-time systems. The classical approach of order detection for fractional-order continuous-time systems is to search for the optimal order by designing an approach based on optimisation techniques. This might be achieved by an identification algorithm based on a Genetic Algorithm (GA) in the time-domain with the weighted value of output error for fractional-order systems.

An associated with a drawback of a GA approach is that it may be difficult to find the appropriate input signal with specific conditions, as mentioned in (Zhou, Cao, and Chen 2013). Furthermore, a GA has been integrated with a particle swarm optimisation for fractional-order continuous-time linear identification in (Wang et al. 2015), and nonlinear identification in (Huang et al. 2015).

Aiming to achieve a more robust convergence, the Marquardt algorithm has been applied for estimating the order of a fractional-order model (Sabatier et al. 2006). Gauss–Newton optimisation has been coupled with least squares and iterative least squares algorithms based on fractional-order third-order in (Chetoui et al. 2013). Finally, all aforementioned methods are for order detection of each term, not for structure detection and not for fractional-order continuous-time nonlinear systems, apart from the method proposed in (Huang et al. 2015).

Some other methods are based on the linear model analysis in the frequency-domain, such as (Ghanbari and, Haeri 2011). The structure detection is based on fitting a piecewise linear approximating function to the estimated Bode diagram. The Bode diagram of the system could be obtained from the collected input-output data by either spectral analysis or an empirical transfer function. The weakness is that if the measured signals are corrupted by noise, the Bode plot estimation may not be achievable by using either spectral analysis or an empirical transfer function. There are other approaches considering the model structure as a linear combination of fractional-order orthogonal basis functions (Aoun et al. 2007). More details can be found in a critical survey of integer-order continuous-time model structures in (Zhu et al. 2015 and Hosseini, Johansen, and Fatehi 2015).

A more direct method uses the sum of error reduction ratios. This approach ranks the candidate terms according to the contribution of these terms to the output variance. In this approach, the targeted system must be described by the input-output representation

of a nonlinear ordinary differential equation, such as a bilinear system. This method was firstly proposed by Billings (1994) for the integer-order discrete system and later it was extended to identify the structure of the nonlinear continuous-time system (Tsang, Billings 1994). In this thesis, the error reduction ratios method is extended to assist in the selection of the structure of the nonlinear fractional-order systems.

2.4 Conclusions

This chapter has highlighted the background for fractional-order continuous-time systems needed for handling the remainder of this thesis. It has provided an introduction to the fundamental theory of fractional-order calculus. The selected methods for modelling and simulating the fractional-order linear and nonlinear systems have been presented. The selected fractional-order simulation is based on time-domain, by approximating the fractional-order derivative operator directly by performing Grünwald–Letnikov definition, and complex representation, named the Oustaloup's method, of fractional-order derivative and integral terms. Based on these two approaches, both linear and nonlinear fractional-order systems can be simulated by use of modelling and simulation environment in Simulink.

This chapter has summarised the major methods and approaches used in the system identification. Two filter base methods, namely the SRIVCF and RIVCF methods and the delayed fractional-order state variable identification approach, are selected to be extended to estimate the parameters of the Hammerstein and Wiener fractional-order continuous-time model and input-output representation of a nonlinear ordinary differential equation, for instance, a bilinear fractional-order system. For nonlinear structure detection, the error reduction ratios approach has been selected to cope with the nonlinear fractional-order systems.

Chapter 3: Preliminary Studies and Extension of Fractional-order Approach: Application to Diffusion Model

In this chapter, the simplified refined instrumental variable (SRIVCF) method for fractional-order transfer function model identification is applied to a simulated diffusion system of concentration of the lithium ions in a battery cell. The diffusion process is represented by a 1D spherical diffusion partial differential equation of concentration and is solved numerically by finite volume method (FVM) in spatial and temporal domains. The fractional-order transfer function model order is selected, and model parameters are identified based on sampled input-output data. The main advantage of using fractional-order transfer function model for simulation purposes is the increased accuracy, as compared to FVM while retaining simulation simplicity of having a reduced order model.

Furthermore, the refined instrumental variable method is applied to a fractional-order continuous-time model while the associated additive noise model could be a fractional-order continuous-time autoregressive or discrete-time autoregressive or autoregressive moving average process. This method is abbreviated as RIVCF. Monte Carlo simulation analysis is

applied for illustrating the performance of the refined instrumental variable method to estimate the parameters of the fractional-order continuous-time hybrid Box-Jenkins model as addressed in (Walid, and Burnham 2014).

3.1 Introduction

Mathematical modelling of Li-ion and Ni/MH batteries, including solid-phase processes, has gained considerable attention in the literature (Thomas et al. 2002 and Doyle. Fuller, and Newman 1993). The charging and discharging process of the battery consist of de-intercalation of lithium from the positive and negative electrode, respectively. Subsequently, the diffusion of lithium ions through the electrolyte occurs, which is followed by the intercalation of lithium back into the negative and positive electrodes. Consequently, the battery model is commonly derived in terms of the concentration of a solution using the porous electrode theory (Newman, and Thomas-Alyea 2012). Expressing the lithium intercalation in the electrode as a solid diffusion and solving the resulting spherical diffusion equation is a commonly adopted modelling approach (Nagarajan, Van Zee, and Spotnitz 1998). In this approach, the pseudo 2D model is constructed, where one of the dimensions is spread between two collectors while the other dimension extends into the solid particle. In this regard, (Doyle 2010) derived an extended one-dimensional model of Li+ battery, which is also adopted in this work. In this model, the one-dimensional concentration as well as the distribution of the electric potential are governed by the boundary-value-problems.

The development of a mathematical model of the Li+ battery consists of establishing the governing equations for the dependent variables, such as the concentration of lithium ions. Additionally, the initial, as well as the boundary conditions, must be stated and a suitable numerical solver technique must be selected. A detailed review of the governing equations, which can be applied to the porous electrode case, can be found in (Botte,

Subramanian, and White 2000). The overall energy balance equations for the battery systems can be found in (Bernardi, Pawlikowski, and Newman 1985).

There are several studies in electrochemistry for obtaining the concentration of electro-active species on the electrode surface. It has been experimentally found in (Eckert, Kupper, and Hohmann 2014) that the characteristics of the surface of the concentration of the active material can be described as $m(t) = \mathcal{D}_t^{-0.5} i(t)$, where $i(t)$ denotes the electric current and the term $\mathcal{D}_t^{-0.5} i(t)$ is a half-integral of the current reactor (Eckert, Kupper, and Hohmann 2014). The same can be noted about the Randle's model (Randles 1947), which can also be considered for the battery modelling problem. This is due to a simplified resolution of the electrochemical diffusion equation (Randles 1947). The fractional-order behaviour of Randle's model is due to the fractional-order impedance $W(s)$. This impedance is also known as Warburg cell and is a fractional-order integrator of order $\alpha = 0.5$.

The derivation of the SRIVCF and RIVCF methods is presented in this chapter. In fact, the derivation of the proposed methods is similar to the derivation of the ordinary refined/simplified refined instrumental variable methods. The statistical performance of the SRIVCF and RIVCF methods is then evaluated in a numerical example.

The main outcome of this chapter is the fractional-order model identification for 1D solid diffusion system model of the lithium-ion cell from collected input-output data. The order of fractional-order transfer function is selected based on the estimated Bode plot while the parameters are estimated using SRIVCF method.

This chapter is organised as follows: The problem description for a linear system is defined in Section 3.2 and the SRIVCF method is stated in Section 3.3. The RIVCF method derivation is addressed in Section 3.4. A numerical example is given in Section 3.5. The Li-ion solid state diffusion mathematical model is introduced in Section 3.6. In Section 3.7,

there is an illustration of frequency domain comparison of fractional-order modelling approach with finite volume method. A numerical example, showing the diffusion model identification, is given in Section 3.8. Finally, the chapter ends with brief conclusions in Section 3.9.

3.2 Problem description for a linear system

A fractional-order differential equation can describe a fractional-order continuous-time linear time-invariant model in the following manner:

$$\begin{aligned} &a_0 \mathcal{D}^{\alpha_n} x(t) + a_1 \mathcal{D}^{\alpha_{n-1}} x(t) + \ldots + a_n \mathcal{D}^{\alpha_0} x(t) \\ &= b_0 \mathcal{D}^{\beta_m} u(t) + b_1 \mathcal{D}^{\beta_{m-1}} u(t) + \ldots + b_m \mathcal{D}^{\beta_0} u(t) \end{aligned} \tag{3.1}$$

where $x(t)$ and $u(t)$ represent the noise-free output and deterministic input of the model, respectively. The coefficients $a_j \ (j = 0,1,\ldots n)$ and $b_j \ (j = 0,1,2,\ldots m)$ are real and constants and the orders, $\alpha_j \ (j = n, n-1,\ldots 0)$, $\beta_j \ (j = m, m-1,\ldots 0) \in \mathbb{R}^+$, $\alpha_n > \alpha_{n-1} \ldots > \alpha_0$ and $\beta_m > \beta_{m-1} \ldots > \beta_0$.

It is assumed that the orders of the fractional-order derivative terms are a priori known for instance by knowing the model from physical laws (Das 2011). It is assumed that the fractional-order derivative terms are given by $\mathcal{D}^{\alpha_i} x(t) = \dfrac{d^{\alpha_i} x(t)}{dt^{\alpha_i}}$ in (3.1) and their orders are commensurate. In this work, the indices α_0 and β_0 are always taken to be zero, and this interpreted as:

$$\begin{aligned} \mathcal{D}^{\alpha_0} x(t) &= x(t) \\ \mathcal{D}^{\beta_0} u(t) &= u(t) \end{aligned}$$

Thus (3.1) can be expressed in fractional-order derivative polynomial form as:

$$x(t) = \frac{B(\mathcal{D}^{\beta})}{A(\mathcal{D}^{\alpha})} u(t) \tag{3.2}$$

where $A\left(\mathcal{D}^{\alpha}\right)$ and $B\left(\mathcal{D}^{\beta}\right)$ are, respectively, the output and input fractional-order polynomials and described as:

$$\begin{aligned} A\left(\mathcal{D}^{\alpha}\right) &= a_0\mathcal{D}^{\alpha_n} + a_1\mathcal{D}^{\alpha_{n-1}} + \ldots + a_{n-1}\mathcal{D}^{\alpha_1} + a_n \\ B\left(\mathcal{D}^{\beta}\right) &= b_0\mathcal{D}^{\beta_m} + b_1\mathcal{D}^{\beta_{m-1}} + \ldots + b_{m-1}\mathcal{D}^{\beta_1} + b_m \end{aligned} \tag{3.3}$$

$x(t)$ and $u(t)$ are uniformly sampled with a sampling interval T_s seconds (s). It yields a discrete instant $t_k = kT_s$ for $k = 1,2,\ldots N$, where N is the total number of the samples, so that samples of continuous signals $x(t)$ and $u(t)$ are given by $x(t_k)$ and $u(t_k)$, respectively. The noisy output, denoted $y(t)$, is generated by corrupting the noise-free output $x(t)$ by an additive, white or coloured noise. Equivalently, the same applies to the sampled case where $y(t_k)$ represents the noisy sampled output. In this work, three different structures are assumed, and these are described in the following subsections.

3.2.1 Hybrid fractional-order and integer-order model

This model is a hybrid of the fractional-order continuous-time and integer-order discrete-time models. It is described by two structures, known as Box-Jenkins (BJ) and output error (OE) models. The fractional-order BJ structure is obtained by corrupting the fractional-order continuous-time noise-free output in (3.1) by an integer-order discrete-time autoregressive moving-average (ARMA) process and expressed as:

$$\begin{aligned} A\left(\mathcal{D}^{\alpha}\right)x(t) &= B\left(\mathcal{D}^{\beta}\right)u(t) \\ y(t_k) &= x(t_k) + \frac{D\left(q^{-1}\right)}{C\left(q^{-1}\right)}e(t_k) \end{aligned} \tag{3.4}$$

where $y(t_k)$ denotes as the sampled noisy output at kT_s.In this particular structure, the noise model polynomials are represented in discrete-time and given by:

$$C\left(q^{-1}\right)=1+c_1q^{-1}+\cdots+c_pq^{-p}$$
$$D\left(q^{-1}\right)=1+d_1q^{-1}+\cdots+d_vq^{-v} \tag{3.5}$$

where q^{-1} is a backward shift operator. While the fractional-order OE model is similar to the fractional-order BJ model when $C\left(q^{-1}\right)=D\left(q^{-1}\right)=1$, and expressed as:

$$y(t_k)=x(t_k)+e\left(t_k\right) \tag{3.6}$$

where $e\left(t_k\right)$ in both (3.5) and (3.6), is a discrete additive white (zero mean) Gaussian noise with σ^2 variance.

3.2.2 Fractional-order ARX

The fractional-order ARX model is the abbreviation of the fractional-order continuous-time autoregressive with external input model. It is expressed as:

$$A\left(\mathcal{D}^{\alpha}\right)y(t)=B\left(\mathcal{D}^{\beta}\right)u(t)+e(t) \tag{3.7}$$

where $y\left(t\right)$ represents the continuous noisy output signal and continuous $e\left(t\right)$ represents the white (zero mean) Gaussian noise with σ^2 variance.

3.3 SRIVCF method

The simplified refined instrumental variable method was firstly proposed by Young and Jakeman (1980). It was then extended to deal with fractional-order continuous-time systems and denoted by SRIVCF method by Malti in (2008). The error function of the fractional-order continuous-time model is the difference between the noisy output and the noise-free output, i.e. $y(t)-x(t)$, and expressed as:

$$\varepsilon(t)=y(t)-\frac{B\left(\mathcal{D}^{\beta}\right)}{A\left(\mathcal{D}^{\alpha}\right)}u(t) \tag{3.8}$$

For generating the higher fractional-order derivative terms, (3.8) is reformulated based on the property of linear filtering. Since (3.8) is linear, the derivation of the approach becomes clear in the Laplace transform domain. Take the Laplace transform of (3.8) and considering zero initial conditions leads to:

$$\mathrm{E}(s) = Y(s) - \frac{B(s^{\beta})}{A(s^{\alpha})} U(s) \tag{3.9}$$

where the input and output polynomials in the Laplace domain are described as $B(s^{\beta}) = b_0 s^{\beta_m} + b_1 s^{\beta_{m-1}} + \ldots + b_{m-1} s^{\beta_1} + b_m$ and $A(s^{\alpha}) = a_0 s^{\alpha_n} + a_1 s^{\alpha_{n-1}} + \ldots + a_{n-1} s^{\alpha_1} + a_n$, respectively and s is the Laplace variable.

The left-hand side of (3.9) can be retained as white noise and, as such, (3.9) can be presented in fractional-order ARX model form. This can exist by considering the commutative property of the linear systems in (3.9) and introducing the filter $\frac{1}{A(s^{\alpha})}$. To achieve this, (3.9) can be rearranged as:

$$\mathrm{E}(s) = A(s^{\alpha}) \frac{1}{A(s^{\alpha})} \mathrm{Y}(s) - B(s^{\beta}) \frac{1}{A(s^{\alpha})} U(s) \tag{3.10}$$

This can then be transformed back to the time-domain and expressed as:

$$\varepsilon(t) = A(\mathcal{D}^{\alpha}) \frac{1}{A(\mathcal{D}^{\alpha})} y(t) - B(\mathcal{D}^{\beta}) \frac{1}{A(\mathcal{D}^{\alpha})} u(t) \tag{3.11}$$

The introduced filter $\frac{1}{A(\mathcal{D}^{\alpha})}$ in (3.11) can be used as a source of the continuous-time higher linear fractional-order derivative terms of the filtered input and output. Therefore, the error function in (3.11) can be expressed in a filtered form as:

$$\varepsilon(t) = A(\mathcal{D}^{\alpha}) y_F(t) - B(\mathcal{D}^{\beta}) u_F(t) \tag{3.12}$$

where the filtered input and output are denoted by u_F and y_F, respectively, where the subscript F denotes that the signal is filtered, i.e. by $\frac{1}{A\left(\mathcal{D}^{\alpha}\right)}$. So that u_F and y_F are obtained, respectively, from:

$$\begin{aligned} u_F(t) &= \frac{1}{A\left(\mathcal{D}^{\alpha}\right)} u(t) \\ y_F(t) &= \frac{1}{A\left(\mathcal{D}^{\alpha}\right)} y(t) \end{aligned} \tag{3.13}$$

It can be observed from the error function in (3.12) that (3.12) has the fractional-order derivative polynomials $A\left(\mathcal{D}^{\alpha}\right)$ and $B\left(\mathcal{D}^{\beta}\right)$, required being identified. Now a direct method, such as least squares based method, can be used as an optimal estimator as the estimated quantity, denoted $\hat{A}\left(\mathcal{D}^{\alpha}\right)$, converges towards to the actual $A\left(\mathcal{D}^{\alpha}\right)$. To apply the least squares estimator, the error function in (3.12) must be reformulated in pseudo-linear regression form as:

$$\varepsilon(t_k) = \mathcal{D}^{\alpha_n} y_F(t_k) - \varphi_F^T(t_k)\theta_l \tag{3.14}$$

$$\varepsilon(t_k) = \mathcal{D}^{\alpha_n} y_F(t_k) - \mathcal{D}^{\alpha_n} \hat{y}_F\left(\hat{\theta}_l, t_k\right) \tag{3.15}$$

where $\hat{y}_F\left(\hat{\theta}_l, t_k\right)$ is the predictive sampled filtered output based on estimated parameter vector. The estimated parameter vector at iteration l is denoted $\hat{\theta}_l$ and the filtered regression vector is denoted φ_F^T. They are described, respectively, based on (3.12) as:

$$\theta_l = \left[a_1, \quad \cdots \quad a_n, \quad b_0 \quad \cdots \quad b_m\right]^T \tag{3.16}$$

$$\varphi_F^T(t_k) = [-\mathcal{D}^{\alpha_{n-1}} y_F(t_k) \quad \cdots \quad -y_F(t_k) \quad \mathcal{D}^{\beta_m} u_F(t_k) \quad \cdots \quad u_F(t_k)] \tag{3.17}$$

The higher fractional-order derivative terms of the filtered input and output can be obtained via a fractional-order transfer function when considering zero initial conditions or via a fractional-order state-space canonical form as:

$$\mathcal{D}^{\alpha_i} y_F(t) = y(t) * \mathcal{L}^{-1}\left\{\frac{s^{\alpha_i}}{A\left(s^{\alpha}\right)}\right\} \tag{3.18}$$

$$\underbrace{\begin{bmatrix} \mathcal{D}^{\alpha_n} y_F(t) \\ \mathcal{D}^{\alpha_{n-1}} y_F(t) \\ \vdots \\ \mathcal{D}^{\alpha_1} y_F(t) \end{bmatrix}}_{n\times 1} = \underbrace{\begin{bmatrix} -a_1 & -a_2 & \cdots & -a_n \\ 1 & 0 & \cdots & 0 \\ \vdots & \ddots & \ddots & \vdots \\ 0 & \cdots & 1 & 0 \end{bmatrix}}_{n\times n} \underbrace{\begin{bmatrix} \mathcal{D}^{\alpha_{n-1}} y_F(t) \\ \mathcal{D}^{\alpha_{n-2}} y_F(t) \\ \vdots \\ y_F(t) \end{bmatrix}}_{n\times 1} + \underbrace{\begin{bmatrix} 1 \\ 0 \\ \vdots \\ 0 \end{bmatrix}}_{n\times 1} y(t_k) \tag{3.19}$$

where $\beta_0 = \alpha_0 = 0, a_0 = 1$, $\mathcal{L}^{-1}$ and * are the inverse Laplace transform and the convolution operator, respectively. (3.19) can be implemented in the equivalent block diagram as illustrated in Figure 3-1. Figure 3-1 shows the fractional-order state variable filter configuration. It shows how the higher fractional-order derivative terms of the filtered input and output can be obtained from the sampled input and output data. In this way, the continuous-time input and output can be acquired at the sample instances via the fractional-order state variable filter from sampled data. On the other hand, the least squares estimators use the sampled-data, therefore, the filtered data $\mathcal{D}^{\alpha_i} y_F(t)$ can be sampled to generate $\mathcal{D}^{\alpha_i} y_F(t_k)$.

The two steps which summarise the SRIVCF are stated as:

Step one: The initial system parameters may be obtained via several techniques such as fractional-order least squares, fractional-order frequency analysis (Ghanbari and Mohammad 2011) or fractional-order state variable filter (Cois et al. 2001). In this thesis, a use is made of the simplified refined least squares method for continuous-time fractional-order model (SRLSCF) for initialisation as follows:

i. Set a fractional-order commensurate stable filter whose denominator has a similar order to the $A\left(\mathcal{D}^{\alpha}\right)$ polynomial:

$$F(\mathcal{D}^{\alpha}) = \frac{1}{\left(\mathcal{D}^{\alpha} + \lambda\right)^n} \tag{3.20}$$

ii. Filter $u(t_k)$ and $y(t_k)$ by using (3.20) for generating the filtered fractional-order derivative terms.

iii. Extract the parameters by applying the least squares algorithm, according to (3.14) and termed the simplified refined least square:

$$\hat{\theta}_1 = \left(\sum_{k=1}^{N} \varphi_F(t_k) \varphi_F^T(t_k) \right)^{-1} \sum_{k=1}^{N} \varphi_F(t_k) \mathcal{D}^{\alpha_n} y_F(t_k) \tag{3.21}$$

where φ_F^T is obtained from (3.17).

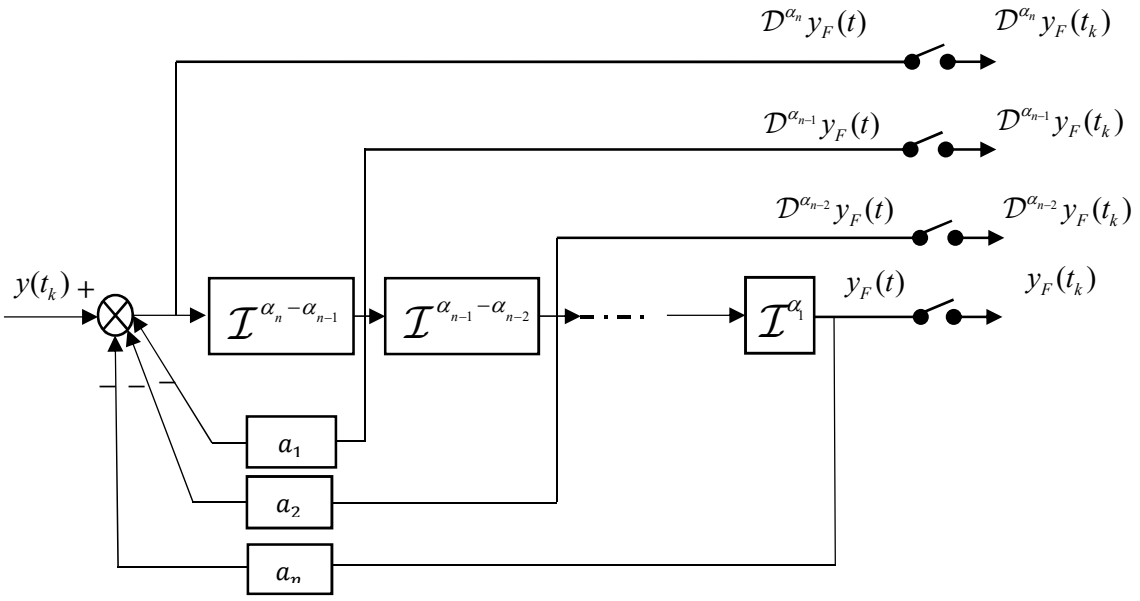

Figure 3-1: An equivalent block diagram of the state-space representation of the filter $\frac{1}{A(\mathcal{D}^{\alpha})}$ shows how to produce the higher fractional-order derivative terms of the filtered signal.

Step two: In this stage, the first estimated vector $\hat{\theta}_1$ is already obtained. This means that the estimated input $\hat{B}(\mathcal{D}^{\beta}, \hat{\theta}_{l-1})$ and output $\hat{A}(\mathcal{D}^{\alpha}, \hat{\theta}_{l-1})$ polynomials exist. Iteratively, the parameters are estimated and every new iteration is indicated by the subscript l, which represents the current iteration number. Iterative instrumental variable estimation is summarised as:

I. Regenerate the filtered input, output and their higher fractional-order derivative terms using the updated filter.

$$F(\mathcal{D}^{\alpha}) = \frac{1}{\hat{A}\left(\mathcal{D}^{\alpha}, \hat{\theta}_{l-1}\right)} \tag{3.22}$$

II. Simulate the output using the auxiliary model as:

$$\hat{x}(t) = \frac{\hat{B}\left(\mathcal{D}^{\beta}, \hat{\theta}_{l-1}\right)}{\hat{A}\left(\mathcal{D}^{\alpha}, \hat{\theta}_{l-1}\right)} u(t_k) \tag{3.23}$$

III. Filter the simulated output using (3.22) and using filtered signals to generate the filtered instrumental variable regression vector, expressed as:

$$\hat{\varphi}_F^T(t_k) = [-\mathcal{D}^{\alpha_{n-1}} \hat{x}_F(t_k) \quad \cdots \quad -\hat{x}_F(t_k) \quad \mathcal{D}^{\beta_m} u_F(t_k) \quad \cdots \quad u_F(t_k)] \tag{3.24}$$

IV. Obtain the estimates using:

$$\hat{\theta}_l = \left(\sum_{k=1}^{N} \hat{\varphi}_F(t_k) \varphi_F^T(t_k) \right)^{-1} \sum_{k=1}^{N} \hat{\varphi}_F(t_k) \mathcal{D}^{\alpha_n} y_F(t_k) \tag{3.25}$$

V. (I) to (IV) are repeated until the sum of the squares of the differences between $\hat{\theta}_i$ and $\hat{\theta}_{i-1}$ is less than a user-specific threshold limit which is selected to be 10^{-4} in the numerical example.

3.4 RIVCF method

A refined instrumental variable method for continuous-time fractional-order system is similar to the SRIVCF method when the noise process is coloured as illustrated model in (3.4). Iteratively, the parameters are estimated and every new iteration is identified by subscript l which represents the present iteration number. The initial $\hat{B}\left(\mathcal{D}^{\beta}, \hat{\theta}_{l-1}\right)$ and $\hat{A}\left(\mathcal{D}^{\alpha}, \hat{\theta}_{l-1}\right)$ are obtained by applying the SRIVCF method and then the estimates are refined as follows:

I. Simulate noise-free output $\hat{x}(t)$:

$$\hat{x}(t) = \frac{\hat{B}\left(\mathcal{D}^{\beta}, \hat{\theta}_{l-1}\right)}{\hat{A}\left(\mathcal{D}^{\alpha}, \hat{\theta}_{l-1}\right)} u(t_k) \tag{3.26}$$

II. Approximate the coloured disturbance processes using the noisy output and simulated output as:

$$\hat{\varepsilon}(t_k) = y(t_k) - \hat{x}(t_k) \tag{3.27}$$

On the left-hand side of (3.27), $\hat{\varepsilon}(t_k)$ is described by the integer-order discrete-time ARMA noise process. To achieve the optimal estimation, there is a need to filter $\hat{\varepsilon}(k)$ by the inverse of the ARMA process, in order to obtain white noise in the error function. Therefore, the ARMA must be estimated. This can be achieved by considering that the ARMA model in (3.4) can be approximated by a higher order AR process with a much larger order of $D\left(q^{-1}\right)$ denominator (Söderström, and Stoica 1989). Defining:

$$\frac{C\left(q^{-1}\right)}{D\left(q^{-1}\right)} e(k) \approx \frac{1}{\bar{D}\left(q^{-1}\right)} \hat{e}(k) \tag{3.28}$$

where the order of $\bar{D}\left(q^{-1}\right)$ is selected to be fifteen in the illustrative example.

III. Filter the input, noise-free output (simulated output) and noise output using the filter in (3.22)

IV. Filter the filtered input, simulated output and noisy output using the discrete filter obtained in (3.28).

$$\begin{aligned} u_{FD}(t_k) &= \bar{D}\left(q^{-1}\right) u_F(t_k) \\ \hat{x}_{FD}(t_k) &= \bar{D}\left(q^{-1}\right) \hat{x}_F(t_k) \\ y_{FD}(t_k) &= \bar{D}\left(q^{-1}\right) y_F(t_k) \end{aligned} \tag{3.29}$$

where the subscript D indicates that the signal is filtered by $\bar{D}\left(q^{-1}\right)$ and $\hat{x}_{FD}(t_k)$ is used as instrumental variables.

V. Reformulate (3.4) and (3.28) to obtain the white noise:

$$\hat{e}(t) = A\left(\mathcal{D}^{\alpha}\right) y_{FD}(t_k) - B\left(\mathcal{D}^{\beta}\right) u_{FD}(t_k) \tag{3.30}$$

VI. (3.30) illustrates that there is a need for estimating the parameters of the polynomial $\bar{D}\left(q^{-1}\right)$ which can be achieved from (3.28). Then the sampled filtered input $u_F(t_k)$ and output $y_F(t_k)$ can be passed through the estimated $\bar{D}\left(q^{-1}\right)$ filter in discrete-time. It is considered that $y_{FD}^{\alpha_n}(t_k)$ is an output of the model in (3.30). Therefore, (3.30) can be expressed in a regression form as:

$$\mathcal{D}^{\alpha_n} y_{FD}(t_k) = \varphi_{FD}^{T}(t_k)\theta + e(k) \tag{3.31}$$

where

$$\begin{aligned}\varphi_{FD}(t_k) = [&-\mathcal{D}^{\alpha_{n-1}} y_{FD}(t_k), -\mathcal{D}^{\alpha_{n-2}} y_{FD}(t_k), \ldots - y_{FD}(t_k), \\ &\mathcal{D}^{\beta_m} u_{FD}(t_k), \mathcal{D}^{\beta_{m-1}} u_{FD}(t_k), \ldots u_{FD}(t_k)]^{T}\end{aligned} \tag{3.32}$$

VII. Obtain the estimates based on (3.31) using:

$$\hat{\theta}_l = \left(\sum_{k=1}^{N} \hat{\varphi}_{FD}(t_k) \varphi_{FD}^{T}(t_k) \right)^{-1} \frac{1}{N} \sum_{k=1}^{N} \hat{\varphi}_{FD}(t_k) \mathcal{D}^{\alpha_n} y_{FD}(t_k) \tag{3.33}$$

where

$$\begin{aligned}\hat{\varphi}_{FD}(t_k) = [&-\mathcal{D}^{\alpha_{n-1}} \hat{x}_{FD}(t_k), -\mathcal{D}^{\alpha_{n-2}} \hat{x}_{FD}(t_k), \ldots - \hat{x}_{FD}(t_k), \\ &\mathcal{D}^{\beta_m} u_{FD}(t_k), \mathcal{D}^{\beta_{m-1}} u_{FD}(t_k), \ldots u_{FD}(t_k)]^{T}\end{aligned} \tag{3.34}$$

VIII. Repeat steps (I) to (VII) iteratively until the sum of the norm of the differences between $\hat{\theta}_l$ and $\hat{\theta}_{l-1}$ is very small, i.e. converges to within some pre-defined threshold which is selected to be 10^{-4} in the numerical example in this thesis.

3.5 Numerical example

A numerical example illustrates the performance of the RIVCF method for the parameter estimation of a hybrid fractional-order BJ model. The model is:

$$x(t)=\frac{2\mathcal{D}+\mathcal{D}^{0.5}+1}{\mathcal{D}^{1.5}+2\mathcal{D}+3}u(t)$$
$$y(t_k)=x(t_k)+\frac{1+0.2q^{-1}}{1-0.7q^{-1}}e(t_k) \quad (3.35)$$

where $y(t_k)$, $x(t)$and $u(t)$ are the noisy output, noise-free output and input, respectively. The input is selected to be a pseudo-random binary sequence with magnitude (-10, 10). The complete set of the input and output contains (1000, 2000, 3000) samples with sampling interval $T_s=5\times10^{-3}$s and $e(t_k)$ is a white noise sequence with zero mean and variance $\sigma^2=10^{-2}$. The parameter λ in (3.20) is selected to be 2.

Table 3-1: Illustrates means and standard deviations (std) of the five estimates of the numerical example using the SRLSCF algorithm where $a_0=1$.

	N=1000		*N=2000*		*N=3000*	
	mean(θ)	std(θ)	mean(θ)	std(θ)	mean(θ)	std(θ)
$a_1=2$	1.1915	0.0086	1.5305	0.0034	1.6149	0.0025
$a_2=3$	1.8737	0.0024	2.2835	0.0094	2.4215	0.0063
$b_0=2$	1.9609	0.0001	1.9721	0.0001	1.96751	0.0001
$b_1=1$	-0.1298	0.0173	0.3766	0.0063	0.4850	0.0049
$b_2=1$	1.8719	0.0026	0.8652	0.0007	0.8861	0.0005

3.5.1 Performance criteria

The SRIVCF and RIVCF algorithms are applied to (3.35) using Monte Carlo (MC) analysis for 100 runs. The mean values and standard deviation (std) of the obtained estimates of all MC runs are computed to evaluate the statistical performance of SRIVCF and RIVCF. The more efficient estimation occurres if the estimate provides a closer mean value to the value of the actual parameter with a smaller value of the std.

Table 3-2: Illustrates means and standard deviations of the five estimates of the numerical example using the RIVCF where $a_0=2$.

	N=1000		*N=2000*		*N=3000*	
	mean(θ)	std(θ)	mean(θ)	std(θ)	mean(θ)	std(θ)
$a_1=2$	2.0955	0.1274	2.0285	0.0105	2.0011	0.0091
$a_2=3$	3.1393	0.2420	3.0447	0.0402	2.9981	0.0206
$b_0=2$	2.0050	0.0006	1.0375	0.0001	2.0000	0.0001
$b_1=1$	1.1322	0.2407	1.0375	0.0297	1.0019	0.0170
$b_2=1$	1.0172	0.0072	1.0086	0.0020	0.9973	0.0019

3.5.2 Result and discussion

Table 3-1 illustrates that the SRLSCF method does not give accurate estimates, especially in b_s parameters when N=1000. However, it provides better estimates as the number of samples increases. In the case of the RIVCF algorithm, Performance criteria

The SRIVCF and RIVCF algorithms are applied to (3.35) using Monte Carlo (MC) analysis for 100 runs. The mean values and standard deviation (std) of the obtained estimates of all MC runs are computed to evaluate the statistical performance of SRIVCF and RIVCF. The more efficient estimation occurres if the estimate provides a closer mean value to the value of the actual parameter with a smaller value of the std.

Table 3-2 shows that much better estimates are obtained. The parameter estimation of the RIVCF algorithm improves as the number of the samples increases as well.

3.6 Li-ion solid state diffusion mathematical model

The current section presents a well-established solid-phase diffusion partial differential equation (Thomas et al. 2002), occurring in spherical particles as illustrated in Figure 3-2. The diffusion process follows the Fick's law and is presented in the spherical coordinates as follows:

$$\frac{\partial c}{\partial t} = \varepsilon \frac{1}{r^2} \frac{\partial}{\partial r}\left(r^2 \frac{\partial c}{\partial r} \right) \tag{3.36}$$

where the parameter c denotes the lithium concentration in the particles of solid, ε indicates the diffusion coefficient and R represents the particle radius. The concentration initial value for $0 \le r \le R$ at $t = 0$ is $c(t=0) = c_0$ while the boundaries are set to be:

$$\left. \frac{\partial c}{\partial r} \right|_{r=0} = 0 \tag{3.37}$$

$$-\varepsilon \left. \frac{\partial c}{\partial r} \right|_{r=R} = j(t) \tag{3.38}$$

where $j(t)$ refers to the boundary flux at time instance t.

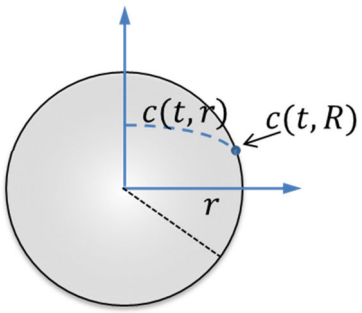

Figure 3-2: Solid state diffusion particle for Li-ion cell.

If the dimensionless form of the above model is considered, the diffusion coefficient and the radius R are assumed to be constants. The model in (3.36) is then represented as follows:

$$\frac{\partial \overline{c}}{\partial \tau} = \varepsilon \frac{1}{\overline{r}^2} \frac{\partial}{\partial \overline{r}}\left(\overline{r}^2 \frac{\partial \overline{c}}{\partial \overline{r}} \right) \tag{3.39}$$

where $\bar{c}(\tau=0)=\bar{c}_0$ and

$$\left.\frac{\partial \bar{c}}{\partial \bar{r}}\right|_{\bar{r}=0} = 0 \tag{3.40}$$

$$\left.\frac{\partial \bar{c}}{\partial r}\right|_{\bar{r}=R} = -\delta(\tau) \tag{3.41}$$

The following dimensionless variables are introduced $\bar{c}=c/c_{max}$ and $\tau=\varepsilon t/R^2$, where $c_{max}\left[\text{mol.m}^{-3}\right]$ denotes the maximum concentration of the lithium in the particle.

3.7 Frequency domain comparison of fractional-order modelling approach with finite volume method

The analytical solution to the 1D solid state diffusion equation, provided in (3.39) in form of a partial differential equation with $r=R=1$ and $\varepsilon=1$, is given by Jacobsen and West model (1995), i.e.

$$G(r,s)=\frac{\bar{c}(1,s)}{j(s)}=\frac{-\tanh\left(\sqrt{s}\right)}{\tanh\left(\sqrt{s}\right)-\sqrt{s}} \tag{3.42}$$

The Bode diagram of the analytical solution for (3.42) is shown in Figure 3-4 in a solid black line.

One of the common approaches to numerically solve (3.39) is to adopt the Finite Volume Method (FVM). In this method, the particle is divided into a number of control volumes (CVs). The Bode diagram of dimensional concentration on the surface of the particle using FVM for 10, 50, and 100 CVs is shown in Figure 3-4 as a plus, star and square symbols, respectively. It can be seen that the higher the number of control volumes the better the model fits to the analytic solution, especially at the high frequency.

For comparison, the following fractional-order model of the analytical solution (3.42) to the diffusion model in (3.39) has been identified:

$$\hat{G}(s)=\frac{\bar{c}(s)}{-j(s)}=\frac{\left(s^{0.5}+3\right)}{s} \tag{3.43}$$

where the fractional-order derivative term $s^{0.5}$ has been approximated by the Oustaloup method (Oustaloup et al. 2000) to be a 10th order linear transfer function. Thus, the fractional-order model in (3.43) has the same order as FVM with 10 CVs. The analytical solution and approximated Bode diagram of the fractional-order model in (3.43) are presented in Figure 3-4 as dots and triangles, respectively. Note, that although the approximated fractional-order model is simulated by the 10th order transfer function model, it outperforms the FVM with 100 CVs for high frequencies. This is why the fractional-order modelling approach can support the model order reduction techniques similarly to truncation based, projection based and data based methods.

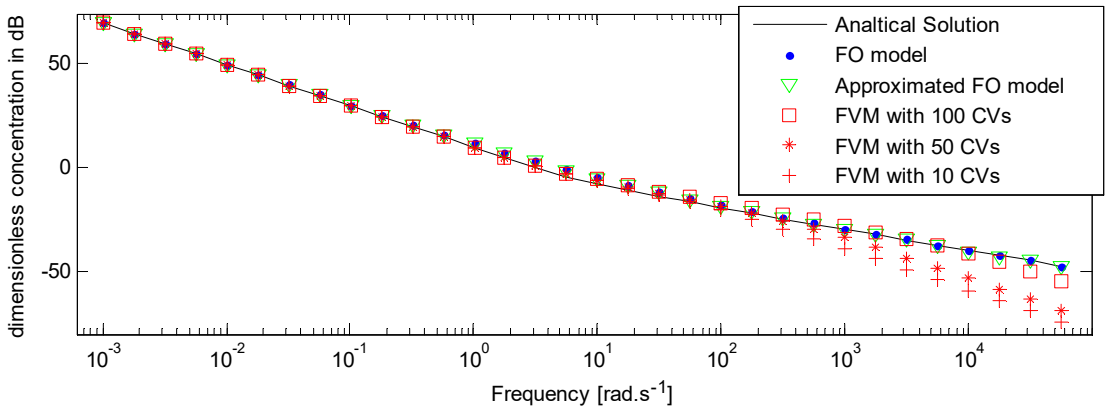

Figure 3-3: Demonstrates the Bode diagram of an analytic system, fractional-order model and it approximation, FVM with 100, 50, and 10CVs.

3.8 Numerical example: SRIVCF estimation

The partial differential equations (3.39), (3.40) and (3.41) are numerically solved by applying the FVM. The spatial domain is divided into 1000CVs with sampling interval10^{-6}s s. The fractional-order system is simulated using a higher integer-order transfer function, Oustaloup approximation method (Oustaloup et al. 2000).

3.8.1 Fractional-order selection and initial model parameter estimation

The orders of the fractional-order model can be identified based on an estimated Bode diagram of the system by using the empirical transfer function estimation (ETFE) or spectral analysis (SPA). Subsequently, asymptotic lines are fitted to the magnitude curve of the estimated Bode diagram (Ghanbari, and Haeri 2011). The orders can be approximated by the slopes of the asymptotic lines and pole locations can be determined from the intersection of these lines.

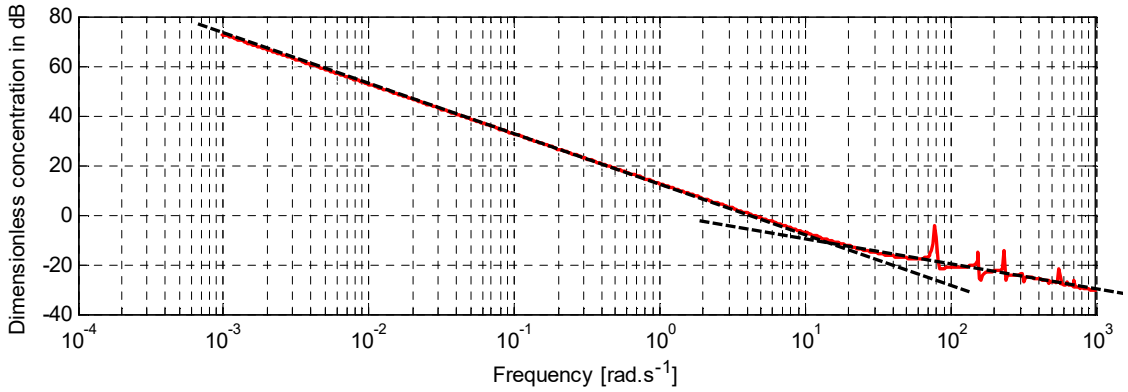

Figure 3-4: Estimated Bode diagram of the system. Solid line represents the SPA estimated Bode plot, while the dashed lines represent fitted asymptotic lines.

The SPA has been applied to estimate the magnitude Bode diagram of the system based on the simulated (measured) data. Figure 3-4 shows the SPA estimated Bode plot (solid red line) together with the fitted asymptotic lines (dashed lines). It can be noted, from Figure 3-4, that the first asymptotic line has a slope of -20dB/decade from which it can be deduced that the system has a single pole in the origin. Afterwards, the slope of the asymptotic line increases to -10dB/decade at a frequency of 20 rad/s. Therefore, the system zero is located at approximately -20. Moreover, the increase of slope by only 10dB/decade indicates a fractional order of 0.5. The initial transfer function becomes:

$$\hat{G}(s) = \frac{\overline{c}(s)}{-\delta(s)} = \frac{\left(s^{0.5} + 20\right)}{s} \tag{3.44}$$

3.8.2 SRIVCF estimation

The parameters of the fractional-order model with $s^{0.5}$ initially identified in Section 3.8.1, are estimated (refined) by the SRIVCF method. The model is stated as follows

$$\hat{G}(s)=\frac{\overline{c}(s)}{-\delta(s)}=\frac{\left(b_0 s^{0.5}+b_1\right)}{a_0 s} \tag{3.45}$$

where $\overline{c}(t_k)$ and $-\delta(t_k)$ are the output and input signals, respectively. The input is designed to be a pseudo-random binary sequence with magnitude ranging in the interval (-20, 20). The complete set of input and output data contains $\left(8\times10^6\right)$ samples.

The estimated model parameters are $a_0=1$, $b_0=0.9637$ and $b_1=1.3932$. Table 3-3 illustrates mean integral of absolute error between the FVM simulated and SRIVCF estimated $\overline{c}(t_k)$, abbreviated to IAE, for different order (NR) of integer-order transfer function, approximating the fractional-order transfer function. Table 3-3 shows that the smaller the order, the less accurate results are obtained. However, there is no further requirement to vary (or re-estimate) the model parameters. Overall, this leads to relatively simple model order reduction technique.

Table 3-3. The calculated IAE performance measure together with corresponding frequency ranges for different integer-order model orders of approximated fractional-order models.

Order of approximated integer-order of fractional-order $s^{0.}$	*IAE*	*Frequency range in* rad/s
NR =10	0.0301	[10^{-5}, 10^{7}]
NR =5	0.0924	[0.1, 14x10^{5}]
NR =3	0.2149	[1, 15x10^{5}]

3.9 Conclusions and further work

It has been shown that the identified fractional-order continuous-time transfer function model provides an efficient approximation of the diffusion process which occurs within a class of lithium ion batteries. The parameters of the identified fractional-order model have been estimated using the extended version of the simplified refined instrumental variable method, which uses sampled (measured) input-output signals. The identified fractional-order model can be subsequently used in model-based control designs and control-oriented system analysis, where notions such as transfer function form and phase lag are standard notions and tools of control engineering. Finally, it has been possible to obtain a reduced integer-order linear model directly from the fractional-order variable $s^{-\alpha n}$ based on constraints imposed on the system, e.g. the demanded frequency range of operation.

For further work, the nonlinear phenomena of diffusion equations can be more accurately and perhaps more conveniently approximated by a particular class of nonlinear fractional-order models.

Chapter 4: Parameter Estimation of the Fractional-order Hammerstein-Wiener Model Using RIVCF

This chapter proposes the direct parameter estimation of the stochastic single-input, single-output fractional-order continuous-time Hammerstein–Wiener Hybrid Box-Jenkins model by extending a well-known iterative method {refined/simplified refined instrumental variable} from observed input-output data with less constraints such as the output static nonlinearity must be invertible. Here the output static nonlinearity does not need to be invertible. The noise-free fractional-order Hammerstein–Wiener model is characterised by a cascade of nonlinear static functions and a fractional-order continuous-time linear model. The stochastic model is a hybrid of the fractional-order Hammerstein–Wiener model and a noise model which could be fractional-order continuous-time or integer-order discrete-time. The input and output static nonlinear functions are represented by a sum of the known basis functions. The proposed approach estimates the parameters of the fractional-order continuous-time linear subsystem and the input and output static nonlinear functions from the sampled input-output data by considering the system to have multi-input representing the input and output basis functions where the output basis functions are simulated according to the previous estimates of the fractional-order linear subsystem at every

iteration. In this chapter, Monte Carlo simulation analysis is applied for demonstrating the performance of the proposed approach to estimate the parameters of the fractional-order Hammerstein–Wiener hybrid Box-Jenkins model.

4.1 Introduction

There is considerable attention in developing approaches for nonlinear identification associated with the increasing use of nonlinear modelling to characterise complex systems in many fields (Nelles 2001). A class of these nonlinear models is the Hammerstein and Wiener continuous-time model which represents a class of the block-oriented nonlinear models. In the context of real applications, these models have been exploited for modelling many different physical systems. For example, these include radio frequency transmitters and power amplifiers (Taringou et al. 2010), electrical muscle stimulation in (Bai et al. 2009) and a magnetospheric and ionospheric system in (Palanthandalam-Madapusi, Ridley, and Bernstein 2005).

Advantages of the Hammerstein and Wiener continuous-time models associated with the advantages of the fractional-order continuous-time system, led to the introduction of the fractional-order continuous-time Hammerstein, Wiener and Hammerstein-Wiener (HFC, WFC and HWFC) models, respectively. Furthermore, the static nonlinear functions are assumed to be described by a sum of the known basis functions. Parameter estimation of those models is required when dealing with practical applications. Consequently, there is a proposition of the iterative methods, termed refined/simplified refined instrumental variable, for HFC, WFC and HWFC model parameter estimation and these are abbreviated as HRIVCF/HSRIVCF, WRIVCF/WSRIVCF and HWRIVCF/HWSRIVCF methods, respectively.

In this chapter, the derivation of the method is presented. In fact, the derivation of the proposed methods is similar to the derivation of the refined/simplified refined

instrumental variable methods for a multi-input single-output fractional-order continuous-time linear system. This approach basically reformulates the nonlinear HFC, WFC and HWFC models to be represented as multi-input single-output fractional-order continuous-time linear systems. The multi-input are the outputs of basis functions of the static nonlinear functions whose inputs are the actual input of the input static nonlinear function and the output of the estimated fractional-order continuous-time linear subsystem. The development of the algorithms in this chapter is necessarily repetitive since the same philosophy is applied as the development progresses.

This chapter is organised as follows: the problem description for a fractional-order Hammerstein–Wiener model is introduced in Section 4.2. In Section 4.3, there is an illustration of the problem reformulation based on a HFC model. The SRIVCF method is extended for a HFC model in Section 4.4. A numerical study of HFC model identification is presented in Section 4.5 while Sections 4.6 and 4.7 show the problem reformulation based on a WFC model and extending the SRIVCF method for a WFC model, respectively. A numerical study of WFC model identification is given in Section 4.8. Both the HFC and WFC models are coupled in one model in the problem reformulation based on a HWFC model in Section 4.9 and identified by applying HWSRIVCF in Section 4.10. The RIVCF method for a HWFC model is extended in Section 4.11 while a numerical study of HWFC model identification is presented in Section 4.12. Finally, the chapter ends with brief conclusions in Section 4.13.

4.2 Problem description for fractional-order Hammerstein–Wiener model

A Hammerstein–Wiener fractional-order continuous-time model has static (memoryless) nonlinear input and output functions, with an intermediate fractional-order continuous-

time model as illustrated in Figure 4-1. The HWFC model can be described by the input-output relationship in four equations as follows:

$$\begin{aligned} \bar{u}(t) &= f_u(u) \\ x(t) &= \frac{B(\mathcal{D}^\beta)}{A(\mathcal{D}^\alpha)}\bar{u}(t) \\ \bar{x}(t) &= g_x(x) \\ y(t_k) &= \bar{x}(t_k) + \frac{C(q^{-1})}{D(q^{-1})}e(t_k) \end{aligned} \tag{4.1}$$

where $u(t)$ and $\bar{u}(t)$ are the input and output of the input static nonlinear function $f_u(u)$. The output of the input static nonlinear function $\bar{u}(t)$ is the input of the fractional-order continuous-time linear model, while $x(t)$ is the output of the fractional-order continuous-time linear model and the input of the output static nonlinear function, denoted $g_x(x)$ which generates $\bar{x}(t)$. The sampled form of $\bar{x}(t)$ at instance k is denoted $\bar{x}(t_k)$ where $t = kT_s$ and T_s is the sampling time. Moreover, the last equation in (4.1) shows $y(t_k)$, produced by corrupting $\bar{x}(t_k)$, with discrete white (zero mean) noise $e(t_k)$, and this noise process is known as output error. The fractional-order continuous-time linear subsystem is described by input and output polynomials, denoted $B\left(\mathcal{D}^\beta\right)$ and $A\left(\mathcal{D}^\alpha\right)$, respectively, and given in (3.3). Furthermore, the noise process is described by, $C(q^{-1})$ and $D(q^{-1})$ discrete polynomials, given (3.5) If $C(q^{-1}) = D(q^{-1}) = 1$, it means the output of the output static nonlinear function is corrupted by white noise as in the case of the OE model in (3.6)

.

Finally, it is assumed that they are described by a sum of the basis functions and expressed as:

$$\begin{aligned} \bar{u}(t) &= \sum_{j=1}^{r} \bar{b}_j f_j(u) \\ \bar{x}(t) &= \sum_{i=1}^{l} \bar{a}_i g_i(x) \end{aligned} \tag{4.2}$$

where the coefficients $\{\overline{a}_i, \overline{b}_j\} \in \mathbb{R}$, $(i = 1,2,\cdots,l)$, $(j = 1,2,\cdots,r)$.

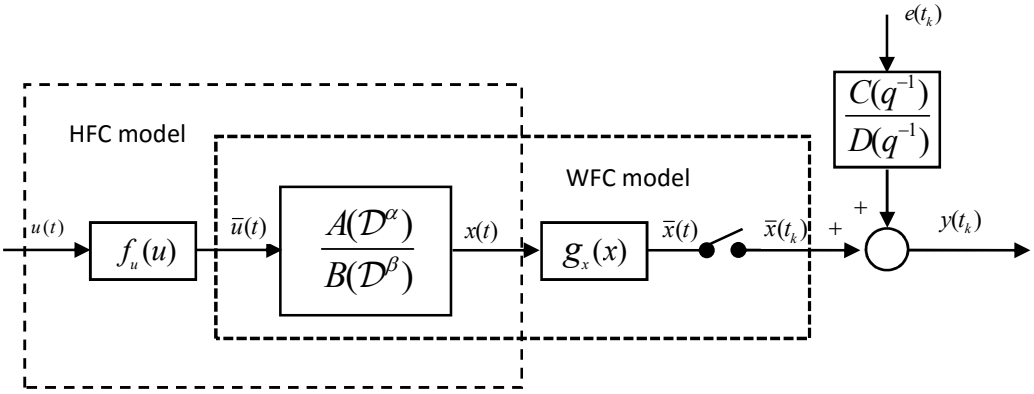

Figure 4-1: Block diagram of the Hammerstein-Wiener model processes.

4.3 Problem reformulation based on HFC model

In this section, the HWFC model is rearranged such that any linear estimation approach can be applied for extracting the parameters of the HWFC model. For the sake of simplicity, the output static nonlinearity is not involved in the linear dynamics. Therefore, the static nonlinear functions are individually treated as two different systems with a common linear subsystem. The HSRIVCF and WSRIVCF methods are then combined in a HWSRIVCF approach to identify the HWFC model as provided in Figure 4-1. Whilst it is well understood by practising engineers that a complex model is often costly to obtain, with its usage often being limited from a control systems design viewpoint, nonlinear models of the type studied here offer both complexity, in terms of modelling, and simplicity, in terms of control design. Consequently the Hammerstein-Wiener and bilinear models, adopted in this work, represent a valuable insight into a better understanding of complex phenomena. When extending this approach to fractional-order case, the range of applicability for modelling is significantly increased.

If the HFC subsystem in (4.1) is separately treated, the HFC model is a cascade of the input static nonlinear function and fractional-order-time continuous-time linear model as shown in the left-hand dotted box in Figure 4-1. It is assumed that the first parameter of

the input static nonlinear function is unity ($\bar{b}_1 = 1$). Since $f_i(u)$ and $u(t)$ are considered to be a *priori* known so $f_i(u)$ is assumed to be a time-dependent signal and denoted by $\bar{f}_i(t)$. Under these conditions, the HFC subsystem can be described as a multi-input single-output system:

$$x(t) = \frac{B(\mathcal{D}^\beta)}{A(\mathcal{D}^\alpha)}\left(\bar{f}_1(t) + \sum_{i=2}^{r} \bar{b}_i \bar{f}_i(t) \right) \tag{4.3}$$

where

$$\bar{f}_i(t) = f_i(u) \tag{4.4}$$

Both $B(\mathcal{D}^\beta)$ and the parameters of the input static nonlinear function can be coupled and it yields a vector of the over-parameterised input polynomial $\bar{B}_i(\mathcal{D}^\beta)$ where $\bar{B}_i(\mathcal{D}^\beta) = \bar{b}_i B(\mathcal{D}^\beta)$ and $\bar{B}_1(\mathcal{D}^\beta) = B(\mathcal{D}^\beta)$. Consequently (4.3) can be re-expressed in vector form as:

$$x(t) = \frac{1}{A(\mathcal{D}^\alpha)}\left[\bar{B}(\mathcal{D}^\beta)\bar{F}_B(t) \right] \tag{4.5}$$

Noted the subscript B indicates that $\bar{F}(t)$ is associated to the $B(\mathcal{D}^\beta)$ polynomial. The multi-input polynomial and multi-input vectors are:

$$\bar{B}(\mathcal{D}^\beta) = \left[\bar{B}_1(\mathcal{D}^\beta), \quad \bar{B}_2(\mathcal{D}^\beta), \quad \ldots, \quad \bar{B}_r(\mathcal{D}^\beta) \right] \tag{4.6}$$

$$\bar{F}_B(t) = \left[\bar{f}_1(t), \quad \cdots \quad , \bar{f}_r(t) \right]^T \tag{4.7}$$

The noise process can be introduced in (4.5) and expressed as:

$$y(t) = x(t) + \xi(t) \tag{4.8}$$

where $y(t)$ is the noisy output and $\xi(t)$ is the noise process such in (3.7), (3.6) and (3.4).

4.4 SRIVCF method for HFC model

If the noise process is structured as OE, the HFC model is re-expressed as the multi-input, single-output fractional-order continuous-time model. Hence, the error function in (4.5) can be expressed as:

$$\varepsilon_H(t) = y(t) - \frac{\overline{B}(\mathcal{D}^\beta)}{A(\mathcal{D}^\alpha)}\overline{F}_B(t) \tag{4.9}$$

The subscript *H* is an abbreviation for the Hammerstein. Therefore, the Laplace transform of (4.9) is:

$$\mathrm{E}_H(s) = Y(s) - \frac{\overline{B}(s^\beta)}{A(s^\alpha)}\overline{F}_B(s) \tag{4.10}$$

It is important to realise that, obtaining the higher fractional-order derivative terms of the input and output signals is not an easy task, especially from the stochastic observed input-output data. However, for identification purpose, this can be equivalently achieved by introducing a filter $\frac{1}{A(\mathcal{D}^\alpha)}$ when considering the commutative property of linear filtering.

This filter can then be used as a generator of the filtered input and output signals and their higher fractional-order derivative terms. This leads to a restructure of the model in (4.10) to a fractional-order ARX model and forcing the error to be white noise if the noise process is originally modelled as OE:

$$\mathrm{E}_H(s) = A(s^\alpha)\frac{1}{A(s^\alpha)}Y(s) - \left(\overline{B}(s^\beta)\frac{1}{A(s^\alpha)}\overline{F}_B(s)\right) \tag{4.11}$$

Taking the inverse Laplace of (4.11) and considering the filtered multi-input and output signals give:

$$\varepsilon_H(t) = A(\mathcal{D}^\alpha)y_F(t) - \overline{B}(\mathcal{D}^\beta)\overline{F}_{F,B}(t) \tag{4.12}$$

where the filtered multi-input vector and output signals are $\bar{F}_{F,B}(t)$ and $y_F(t)$, respectively and subscript *F* is a representation of the filtered signal by $\frac{1}{A(\mathcal{D}^\alpha)}$ as before.

So:

$$\begin{aligned} \bar{F}_{F,B}(t) &= \frac{1}{A(\mathcal{D}^\alpha)} F_B(t_k) \\ y_F(t) &= \frac{1}{A(\mathcal{D}^\alpha)} y(t_k) \end{aligned} \tag{4.13}$$

Thus, the pseudo-linear regression form can be deduced from (4.12) and expressed as:

$$y_F(t_k) = \varphi_{F,H}^T(t_k)\theta_H + \varepsilon_H(t_k) \tag{4.14}$$

where $a_n = 1$ and

$$\theta_H = \left[a_0, \ \cdots \ a_{n-1}, \ \bar{b}_1 b_0, \ \cdots \ \bar{b}_1 b_m, \ \bar{b}_2 b_0, \ \cdots \ \bar{b}_2 b_m, \ \cdots \ \bar{b}_r b_0, \ \cdots \ \bar{b}_r b_m \right]^T \tag{4.15}$$

$$\begin{aligned} \varphi_{F,H}^T(t_k) = [& -\mathcal{D}^{\alpha_n} y_F(t_k), \ \cdots \ -\mathcal{D}^{\alpha_1} y_F(t_k), \ \mathcal{D}^{\beta_m} \bar{F}_{F,1}(t_k), \ \cdots \ \bar{F}_{F,1}(t_k), \\ & \mathcal{D}^{\beta_m} \bar{F}_{F,2}(t_k), \ \cdots \ \bar{F}_{F,2}(t_k), \ \cdots \ \mathcal{D}^{\beta_m} \bar{F}_{F,r}(t_k), \ \cdots \ \bar{F}_{F,r}(t_k)] \end{aligned} \tag{4.16}$$

There are two steps which summarise the HSRIVCF as partially illustrated in Figure 4-2 which are:

Step one: This step is to find the output polynomial $\hat{A}(\mathcal{D}^\alpha)$ whose structure is known. The first step is to implement the simplified refined least squares method for the HFC model as follows:

I. Obtain the multi-input vector $\bar{F}_B(t_k)$ by using input static nonlinear function.

II. Filter $\bar{F}_B(t_k)$, $y(t_k)$ for generating the filtered required data for estimation, using:

$$F(\mathcal{D}^\alpha) = \frac{1}{\left(\mathcal{D}^\alpha + \lambda\right)^n} \tag{4.17}$$

III. Estimate the parameters using the Hammerstein simplified refined least squares algorithm based on (4.14):

$$\hat{\theta}_{l,H} = \left(\sum_{k=1}^{N} \varphi_{F,H}(t_k) \varphi_{F,H}^{T}(t_k) \right)^{-1} \sum_{k=1}^{N} \varphi_{F,H}(t_k) y_F(t_k) \tag{4.18}$$

where $\varphi_{F,H}^{T}$ is deduced from (4.16).

Step two: This part refines $\theta_{H,1}$, obtained in step one. Iteratively, the parameters are estimated and every new iteration is indicated by the subscript l, which represents the present iteration number. The iterative instrumental variable estimation is shown in Figure 4-2 and summarised as:

I. Generate the instrumental variable $\hat{x}(t)$ using the estimated auxiliary model as:

$$\hat{x}(t) = \frac{\hat{\bar{B}}(\mathcal{D}^{\beta}, \hat{\theta}_{l-1,H})}{\hat{A}\left(\mathcal{D}^{\alpha}, \hat{\theta}_{l-1,H}\right)} \bar{F}_B(t_k) \tag{4.19}$$

II. Filter $\bar{F}_B(t_k)$, $\hat{x}(t_k)$ and $y(t_k)$ using the updated filter:

$$F(\mathcal{D}^{\alpha}) = \frac{1}{\hat{A}\left(\mathcal{D}^{\alpha}, \hat{\theta}_{l-1,H}\right)} \tag{4.20}$$

III. Rearrange the filtered instrumental variable regression vector for HFC as:

$$\begin{aligned} \hat{\varphi}_{F,H}^{T}(t_k) = [& -\mathcal{D}^{\alpha_{n-1}} x_F(t_k) \quad \cdots \quad -\mathcal{D}^{\alpha_1} x_F(t_k) \quad \mathcal{D}^{\beta_m} \bar{F}_1(t_k) \quad \cdots \quad \bar{F}_1(t_k) \\ & \mathcal{D}^{\beta_m} \bar{F}_2(t_k) \quad \cdots \quad \bar{F}_2(t_k) \quad \cdots \quad \mathcal{D}^{\beta_m} \bar{F}_r(t_k) \quad \cdots \quad \bar{F}_r(t_k)] \end{aligned} \tag{4.21}$$

IV. Apply the instrumental variable least square algorithm based on regression vector in (4.16) and instrumental variable regression vector in (4.21) for obtaining the estimates:

$$\hat{\theta}_{l,H} = \left(\sum_{k=1}^{N} \hat{\varphi}_{F,H}(t_k) \varphi_{F,H}^{T}(t_k) \right)^{-1} \sum_{k=1}^{N} \hat{\varphi}_{F,H}(t_k) y_F(t_k) \tag{4.22}$$

V. Repeat (I) to (IV) until the sum of the squares of the differences between $\hat{\theta}_{l,H}$ and $\hat{\theta}_{l-1,H}$ is less than a user-specific threshold limit which is selected to be 10^{-4} in the numerical examples.

However, there is an issue associated with the estimates of the over-parameterised $\overline{B}(\mathcal{D}^{\beta})$ in (4.15), which is $\overline{b}_s$ and b_s are combined into one vector. Nevertheless, in (Laurain et al. 2008), it presents how $\overline{b}_s$ can be directly obtained from (4.15):

$$\overline{b}_i = \frac{1}{m+1}\sum_{k=0}^{m}\frac{\hat{b}_{i,k}}{\hat{b}_{1,k}} \tag{4.23}$$

where $\hat{b}_{i,k}$ is the estimated form of $b_{i,k} = \overline{b}_i b_k$, given in (4.15).

Comments

I. The parameter values of the input static nonlinearity must not cause a huge difference between the input and output of the input static nonlinearity function. This can be observed in physical systems, for instance, heating ventilation and air conditioning (HVAC) (Zajic 2013). For example, $\overline{u}(t) = u(t) + 0.02u(t)^2 + 0.25u(t)^3$ and illustrated in Figure 4-3.

II. The input must be selected to create some difference between the basis functions of the static input nonlinearity function to increase the estimation convergence and avoiding numerical issues due to the strong correlations. For example, in the case of the exponential polynomial when $u(t) = 1$ it follows that $u(t) = u(t)^2 = u(t)^3$.

4.5 Numerical study of HFC model identification

This section presents a numerical example to evaluate and highlight the performance of the proposed HSRIVCF method for parameter estimation of the HFC model. For this

example, the input nonlinear block has a basis function selected as $f_j(u) = u(t)^j$, which is originally defined in (4.2). The input in Figure 4-4 is used in the example and generated by square wave signal with random amplitude.

The HFC system is simulated for 100s with fixed sampling time 10^{-3}s. The selected Simulink solver is ode4 (Runge-Kutta). The fractional-order integral block is provided by FOMCON Simulink library with frequency range [0.001rad.s^{-1}; 1000 rad.s^{-1}] and 25 approximation order.

The fractional-order linear subsystem of the HFC model is given as:

$$\begin{aligned} x(t) &= \frac{\mathcal{D}^{0.5} + 0.2}{0.1667\mathcal{D}^{1.5} + \mathcal{D}^{1} + 1.8333\mathcal{D}^{0.5} + 1}\bar{u}(t) \\ y(t_k) &= x(t) + e(t_k) \end{aligned} \tag{4.24}$$

where $e(t_k)$ is white Gaussian noise whose variance is selected based on the signal to noise ratio (*SNR*) which is defined as:

$$SNR = 10\log_{10}\left[\frac{\sigma_x^2}{\sigma_e^2}\right] \tag{4.25}$$

where σ_x^2 and σ_e^2 are the variance of the noise-free output and the noise. The noise, added at the output, is selected such that it gives the *SNR* of 30*dB* and 60*dB.* The sampled noisy output $y(t_k)$ of the linear subsystem is shown in Figure 4-5 where *SNR*=30*dB*.

The input nonlinear function is represented by a static polynomial function:

$$\bar{u}(t) = u(t) + 0.02u^2(t) + 0.25u^3(t) \tag{4.26}$$

The model, considered for estimation using HSRIVCF method, is multi-input single-output and expressed in the following three equations:

$$\begin{aligned} \bar{f}_i(t) &= u^i(t) \\ x(t) &= \sum_{i=1}^{3} \frac{b_0\mathcal{D}^{0.5} + b_1}{a_0\mathcal{D}^{1.5} + a_1\mathcal{D}^{1} + a_2\mathcal{D}^{0.5} + a_3}\bar{b}_i\bar{f}_i(t) \\ y(t_k) &= x(t_k) + e(t_k) \end{aligned} \tag{4.27}$$

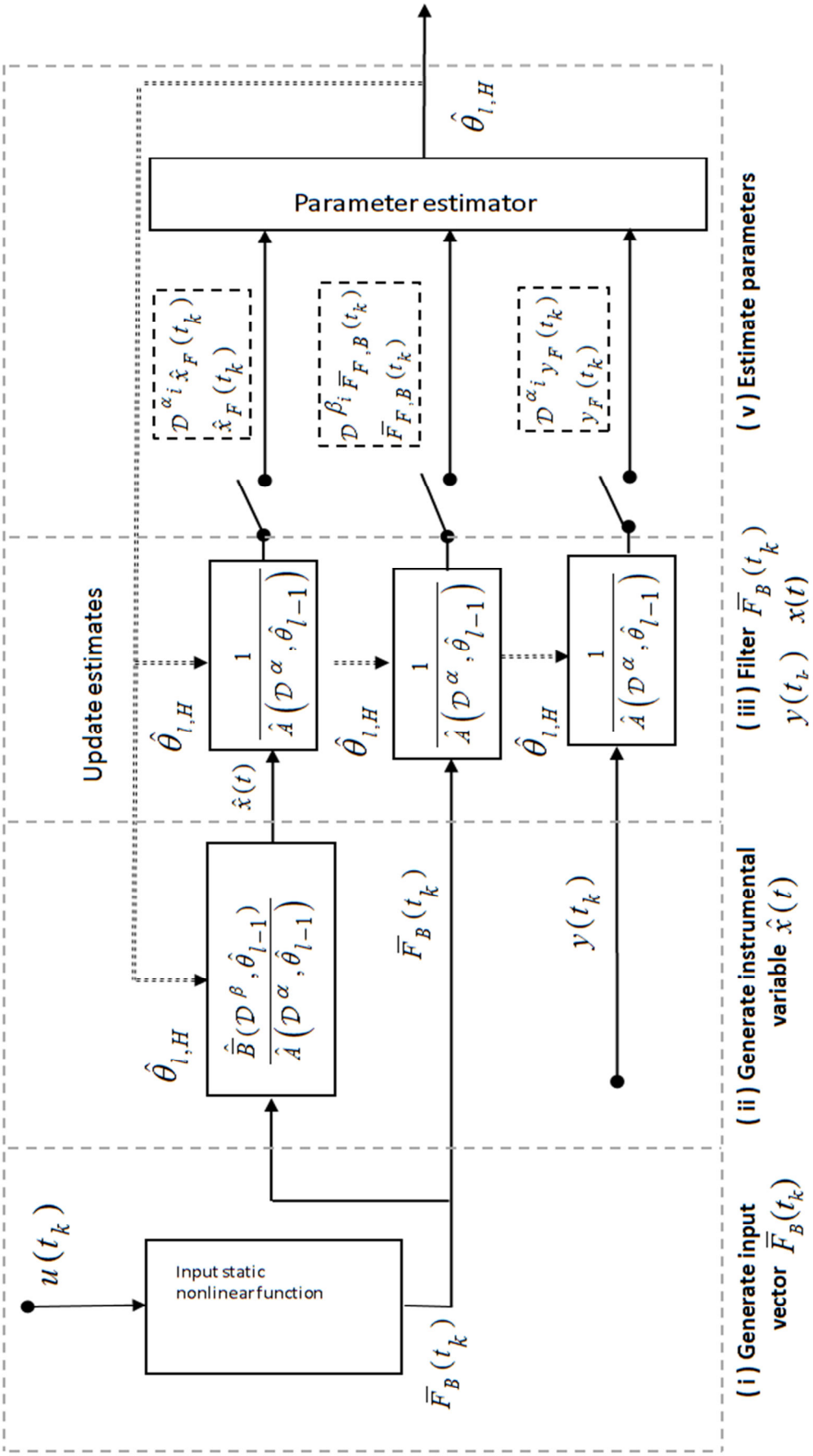

Figure 4-2: Iterative HSRIVCF method processes.

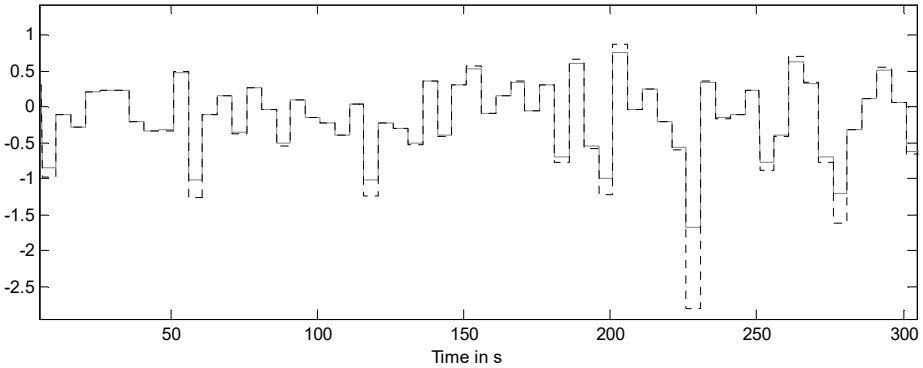

Figure 4-3: Input $u(t)$ and output $\overline{u}(t)$ of input static nonlinear function are represented in black-solid and black-doted lines, respectively, when $\overline{u}(t) = u(t) + 0.02u(t)^2 + 0.25u(t)^3$.

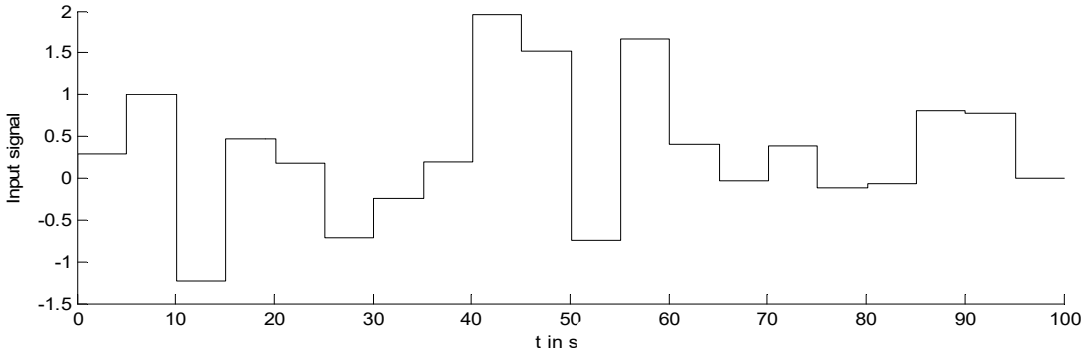

Figure 4-4: The input signal.

4.5.1 Performance criteria

To evaluate the statistical performance of the proposed approach, a Monte Carlo (MC) simulation is repeated for 50 runs with fixed input and rearranged noise for different levels of the a randomly selected Gaussian white noise for each realisation. The mean values and standard deviation (std) of the obtained estimates of all MC runs are computed to evaluate the statistical performance of proposed approaches in this chapter. The more efficient estimation occurred if the estimate provides a closer mean value to value of the actual parameter with a smaller value of the std.

4.5.2 Results and discussion

The MC results presented in Table 4-1, show that the model parameters are estimated accurately. Furthermore, as *SNR* increases, the mean value of the estimates converges to

the true value and the std decreases. Thus, *SNR* significantly affects the convergence of the parameters toward true values. To sum up, the statistical results indicate a robust performance of the proposed method for a given noise scenario.

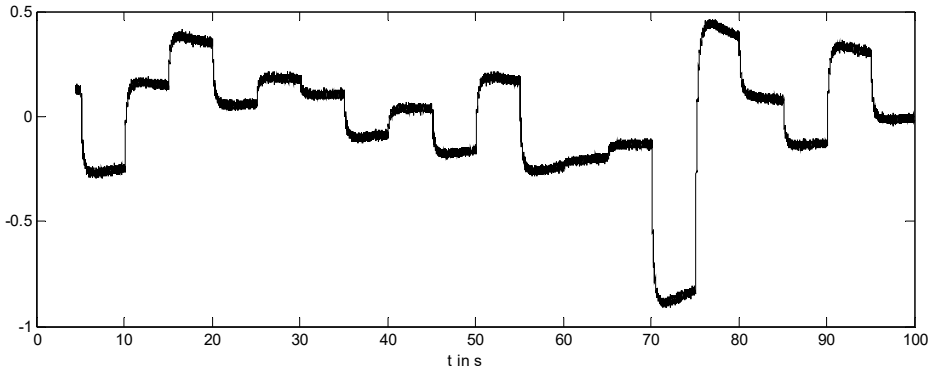

Figure 4-5: The noisy-output of HFC, used in the identification.

Table 4-1: Monte Carlo simulation results of parameter estimation of the HCF system where $a_3 = b_1 = 1$.

SNR	*True values*	$a_0=0.1667$	$a_1=1$	$a_2=1.8333$	$b_0=1$	$b_1=0.20$	$\bar{b}_2=0.02$	$\bar{b}_3=0.25$
30dB	mean	0.1665	0.9997	1.8325	0.9995	0.2000	0.0200	0.2500
	std	0.0016	0.0025	0.0110	0.0046	0.0006	0.0003	0.0007
60dB	mean	0.1667	1.0000	1.8333	1.0000	0.2000	0.0200	0.2500
	std	0.03E-3	0.04E-3	0.25E-3	0.10E-3	0.0006	0.01E-3	0.01E-3

4.6 Problem reformulation based on WFC model

This section illustrates how the WFC subsystem of the HWFC system in (4.1) is rearranged such that any linear estimator can be used. If the WFC subsystem of (4.1) is separately considered, i.e. it is a cascade of the fractional-order continuous-time linear model and the output static nonlinear function, as shown in the right-hand dotted box in Figure 4-1.

The parameter estimation is based on the collected input-output data. In this section, the input of the linear fractional-order continuous-time model is accessible but the output of linear model is not accessible. It is assumed that the first basis function of the static output

nonlinear (4.2) is linear, therefore, the static output nonlinear function in (4.2) can be re-described as:

$$\bar{x}(t) = x(t) + \sum_{i=2}^{l} \bar{a}_i g_i(x) \tag{4.28}$$

where $\bar{a}_1 = 1$. On the other hand, the other basis of the output static nonlinear functions $g_i(x)$ for $i = 2,3,\cdots l$ are *prior* known, therefore, they can be described by a function of time $\bar{g}_i(t) = g_i(x(t))$ if $x(t)$ is known. Thus, the $\bar{g}_i(t)$ functions can be considered to be additional input signals to the system. According to (4.1), (4.2) and (4.28), it is possible to characterise the WFC subsystem as a linear fractional-order continuous-time model with inputs $\bar{g}_i(t)$ and $\bar{u}(t)$ and single-output $\bar{x}(t)$ as:

$$\bar{x}(t) = \frac{B(\mathcal{D}^\beta)}{A(\mathcal{D}^\alpha)}\bar{u}(t) + \sum_{i=2}^{l} \bar{a}_i \bar{g}_i(t) \tag{4.29}$$

4.7 SRIVCF method for WFC model

If the noise process is structured as OE in (4.29), the WFC model is re-expressed as the multi-input, single-output fractional-order continuous-time model. Thus, the error function of (4.29) can be expressed as:

$$\varepsilon_W(t) = y(t) - \left(\frac{B(\mathcal{D}^\beta)}{A(\mathcal{D}^\alpha)}\bar{u}(t) + \sum_{i=2}^{l} \bar{a}_i \bar{g}_i(t) \right) \tag{4.30}$$

where the subscript *W* refers to Wiener. (4.30) is linear, therefore, the Laplace transform of (4.30), and considering zero initial conditions, is:

$$\mathrm{E}_W(s) = Y(s) - \left(\frac{B(s^\beta)}{A(s^\alpha)}\bar{U}(s) + \sum_{i=2}^{l} \bar{a}_i \bar{G}_i(s) \right) \tag{4.31}$$

where the input and output polynomials in the Laplace domain are described, respectively, as $B\left(s^\beta\right) = b_0 s^{\beta_m} + b_1 s^{\beta_{m-1}} + \ldots + b_m$ and $A\left(s^\alpha\right) = a_0 s^{\alpha_n} + a_1 s^{\alpha_{n-1}} + \ldots + a_n$.

For obtaining the higher filtered fractional-order derivative terms and retaining the left-hand side of (4.31) a white noise, a filter $\frac{1}{A\left(s^{\alpha}\right)}$ is introduced in the first term of (4.31).

This step leads to introduce an output polynomial $A\left(s^{\alpha}\right)$ in the first term of (4.31) as follows:

$$\mathrm{E}_{W}(s)=A\left(s^{\alpha}\right)\frac{1}{A\left(s^{\alpha}\right)}Y(s)-\left(B\left(s^{\beta}\right)\frac{1}{A\left(s^{\alpha}\right)}\bar{U}(s)+\sum_{i=2}^{l}\bar{a}_{i}\bar{G}_{i}(s)\right) \tag{4.32}$$

(4.32) can then be transformed to the time-domain and expressed as:

$$\varepsilon_{W}(t)=A(\mathcal{D}^{\alpha})\frac{1}{A(\mathcal{D}^{\alpha})}y(t)-\left(B(\mathcal{D}^{\beta})\frac{1}{A(\mathcal{D}^{\alpha})}\bar{u}(t)+\sum_{i=2}^{l}\bar{a}_{i}\bar{g}_{i}(t)\right) \tag{4.33}$$

It can be observed that $\bar{g}_{i}(t)$ is not filtered by $\frac{1}{A\left(\mathcal{D}^{\alpha}\right)}$. There is no need to filter $\bar{g}_{i}(t)$ because the $\bar{g}_{i}(t)$ signal is considered as an addition input with no derivative term. Thus, the error function in (4.33) is rearranged and described in a filtered form as:

$$\varepsilon_{W}(t)=A(\mathcal{D}^{\alpha})y_{F}(t)-\left(B(\mathcal{D}^{\beta})\bar{u}_{F}(t)+\sum_{i=2}^{l}\bar{a}_{i}\bar{g}_{i}(t)\right) \tag{4.34}$$

where the subscript *F* is an indication for a filtered signal by $\frac{1}{A\left(\mathcal{D}^{\alpha}\right)}$ and the filtered input and filtered noisy output are $\bar{u}_{F}(t)$ and $y_{F}(t)$, respectively, and obtained by:

$$\begin{aligned}\bar{u}_{F}(t)&=\frac{1}{A\left(\mathcal{D}^{\alpha}\right)}\bar{u}(t_{k})\\ y_{F}(t)&=\frac{1}{A\left(\mathcal{D}^{\alpha}\right)}y(t_{k})\end{aligned} \tag{4.35}$$

The pseudo-linear regression form can be obtained from the sampled form of (4.35) and expressed as:

$$y_{F}(t_{k})=\varphi_{F,\mathrm{W}}^{T}(t_{k})\theta_{W}+\varepsilon_{w}(t_{k}) \tag{4.36}$$

where $a_n = 1$ and

$$\theta_W = \left[a_0, \quad \cdots \quad a_{n-1}, \quad b_0, \quad b_1, \quad \cdots \quad b_m, \quad \bar{a}_2, \quad \cdots \quad \bar{a}_l\right]^T \tag{4.37}$$

$$\begin{aligned}\varphi_{F,W}^T(t_k) = [&-\mathcal{D}^{\alpha_n} y_F(t_k), \quad \cdots \quad -\mathcal{D}^{\alpha_1} y_F(t_k), \quad \mathcal{D}^{\beta_m} \bar{u}_F(t_k), \\ &\mathcal{D}^{\beta_{m-1}} \bar{u}_F(t_k), \quad \cdots \quad \bar{u}_F(t_k), \quad \bar{g}_2(t_k), \quad \cdots \quad \bar{g}_l(t_k)]\end{aligned} \tag{4.38}$$

There is an issue that the $\bar{g}_i(t_k)$ functions are not accessible, but, since $\bar{g}_i(t_k)$ is a function of $x(t_k)$, it can be simulated based on recent obtained estimates. The estimated $x(t_k)$ can be approximated according to the $\hat{B}(\mathcal{D}^\beta)$ and $\hat{A}(\mathcal{D}^\alpha)$ polynomials. In this thesis, the first $\hat{B}(\mathcal{D}^\beta, \hat{\theta}_{0,W})$ and $\hat{A}\left(\mathcal{D}^\alpha, \hat{\theta}_{0,HW}\right)$ polynomials are selected according to three main factors which are (i) considering the output steady state of the linear system, (ii) considering the type of the linear system whether it is underdamped or over-damped and (iii) cut-off frequency which can be selected according to the fractional-order state variable filter design (Cois et al. 2001). Similarly, the initial filter in (4.13) can be selected as $\frac{1}{\hat{A}\left(\mathcal{D}^\alpha, \hat{\theta}_{0,HW}\right)}$. The iterative WSRIVCF method is illustrated in Figure 4-6 and summarised as follows:

I. Simulate the noise-free output $\hat{x}(t)$ using:

$$\hat{x}(t) = \frac{\hat{B}\left(\mathcal{D}^\beta, \hat{\theta}_{l-1,W}\right)}{\hat{A}\left(\mathcal{D}^\alpha, \hat{\theta}_{l-1,W}\right)} \bar{u}(t_k) \tag{4.39}$$

where $\hat{x}(t)$ is used as the input to the static output nonlinear function and the instrumental variable and the subscript l indicates the current iteration number and $l-1$ indicates the previous iteration number.

II. Filter $\hat{x}(t)$, $y(t_k)$ and $\bar{u}(t_k)$ for generating their filtered form with their higher fractional-order derivatives, using:

$$F(D^{\alpha}) = \frac{1}{\hat{A}\left(\mathcal{D}^{\alpha}, \hat{\theta}_{l-1,W}\right)} \tag{4.40}$$

III. Generate $\hat{\bar{g}}_i(t_k)$ in (4.38) using $\hat{x}(t)$.

IV. Obtain the estimated parameters using the instrumental variable least square algorithm:

$$\hat{\theta}_{l,W} = \left(\sum_{k=1}^{N} \hat{\varphi}_{F,W}(t_k) \varphi_{F,W}^{T}(t_k) \right)^{-1} \sum_{k=1}^{N} \hat{\varphi}_{F,W}(t_k) y_F(t_k) \tag{4.41}$$

where $\varphi_{F,W}^{T}$ is defined in (4.38) and:

$$\begin{aligned} \hat{\varphi}_{F,\mathrm{W}}^{T}(t_k) = [&-\mathcal{D}^{\alpha_n} \hat{x}_F(t_k), \quad \cdots \quad -\mathcal{D}^{\alpha_1} \hat{x}_F(t_k), \quad \mathcal{D}^{\beta_m} \bar{u}_F(t_k), \\ &\mathcal{D}^{\beta_{m-1}} \bar{u}_F(t_k), \quad \cdots \quad \bar{u}_F(t_k), \quad \hat{\bar{g}}_2(t_k), \quad \cdots \quad \hat{\bar{g}}_l(t_k)] \end{aligned} \tag{4.42}$$

V. Iterate from (I) to (IV) until the sum of the squares of the differences between $\hat{\theta}_{l-1,W}$ and $\hat{\theta}_{l,W}$ is smaller than a threshold which is selected to be 10^{-4} in the numerical example.

Comments:

I. The parameter values of the static nonlinearity must not lead to a huge change between the input and output of the output static nonlinear function.

II. The simulated output of the WFC model can be used as the instrumental variable instead of the output of the linear part after the first iteration.

4.8 Numerical study of WFC model identification

The fractional-order linear subsystem of the WFC model is given as:

$$x(t) = \frac{\mathcal{D}^{0.5} + 0.5}{\mathcal{D}^{1.5} + 3\mathcal{D}^{1} + 1.9998\mathcal{D}^{0.5} + 1} \bar{u}(t) \tag{4.43}$$

The output nonlinear function is represented by a static polynomial function:

$$\begin{cases} \overline{x}(t) = x(t) + 0.2x^2(t) + 0.6x^3(t) \\ y(t_k) = \overline{x}(t) + e(t_k) \end{cases} \tag{4.44}$$

where $e(t_k)$ is white Gaussian noise whose variance is selected based on the *SNR*, defined in (4.25). The noise, added at the output, is selected such that it gives the *SNR* of 30*dB* and 60*dB*.

The model, considered for estimation using the WSRIVCF method, is of multi-input single-output form and expressed as:

$$\begin{aligned} \hat{x}(t) &= \frac{\hat{B}\left(\mathcal{D}^{\beta}, \hat{\theta}\right)}{\hat{A}\left(\mathcal{D}^{\alpha}, \hat{\theta}\right)} \overline{u}(t) \\ \hat{\overline{g}}_i(t) &= \hat{x}^i(t) \\ \overline{x}(t) &= \frac{\overline{a}_1 b_0 \mathcal{D}^{0.5} + \overline{a}_1 b_1}{a_0 \mathcal{D}^{1.5} + a_1 \mathcal{D}^{1} + a_2 \mathcal{D}^{0.5} + a_3} \overline{u}(t) + \overline{a}_2 \hat{\overline{g}}_2(t) + \overline{a}_3 \hat{\overline{g}}_3(t) \\ y(t_k) &= \overline{x}(t_k) + e(t_k) \end{aligned} \tag{4.45}$$

The same input signal, performance criteria and simulation environment in Section 4.4.1 are used in this example.

It can be seen from the MC results, provided in Table 4-2 that the estimated parameters are close to their true values. It can be also seen that when the *SNR* increases, the mean values of the estimated parameters converge toward the actual parameters with smaller std. In order words, the WSRIVCF method perform significantly to estimate the parameters of the WFC model.

4.9 Problem reformulation based on HWFC model

In this part, both the HFC and WFC models are coupled and reformulated to be adaptable to any linear estimator. Both the reformulated HFC model in (4.5) and WFC model in (4.29) are coupled by a fractional-order continuous-time linear system in one model, representing the noise-free HWFC model.

$$\bar{x}(t) = \frac{1}{A(\mathcal{D}^{\alpha})} B_i(\mathcal{D}^{\beta}, \theta_{bm,\bar{br}}) \bar{F}_B(t) + \sum_{i=2}^{l} \bar{a}_i \bar{g}_i(t) \tag{4.46}$$

where the over-parameterised polynomials $B_i(\mathcal{D}^{\beta}, \theta_{bm,\bar{br}})$ and $\bar{F}_B(t)$ are given in (4.7) and $\bar{g}_i(t) = g_i(x)$. The parameter estimation is implemented from measure data; therefore, the output of the model in (4.46) is corrupted by a noise process. Thus, the HWFC model in (4.46) can be re-expressed as:

$$y(t) = \bar{x}(t) + \xi(t) \tag{4.47}$$

where $y(t)$ is the noisy output and $\xi(t)$ represents process noise, such as in (3.4), (3.6) and (3.7).

Table 4-2: Monte Carlo simulation results of parameter estimation of the WCF system where $a_3 = \bar{a}_1 = 1$.

SNR	*True values*	a_0=1	a_1=3	a_2=1.9998	b_0=1	b_1=0.5	$\bar{a}_2$=0.2	$\bar{a}_3$=0.6
30dB	mean	1.0002	3.0004	2.0005	1.0003	0.5000	0.2000	0.5998
	std	0.0080	0.0116	0.0096	0.0064	0.0002	0.0002	0.0012
60dB	mean	0.9998	2.9997	1.9996	0.9999	0.5000	0.2000	0.6000
	std	0.0007	0.0010	0.0009	0.0006	0.0001	0.0001	0.0001

4.10 SRIVCF method for HWFC model

Considering $\bar{g}_i(t)$ and $\bar{F}_B(t)$ to be inputted to the HWFC model, the HWFC model can be described by a multi-input, single output fractional-order continuous-time model and the noise process is structured as OE. The error function of (4.47) can be expressed as:

$$\varepsilon_{HW}(t) = y(t) - \left(\frac{1}{A(\mathcal{D}^{\alpha})} \bar{B}(\mathcal{D}^{\beta}) \bar{F}_B(t) + \sum_{i=2}^{l} \bar{a}_i \bar{g}_i(t) \right) \tag{4.48}$$

The subscript *HW* refers to Hammerstein-Wiener. (4.48) is reformulated according to the properties of the linear filtering. With considering zero initial conditions, the Laplace transform of (4.48) is:

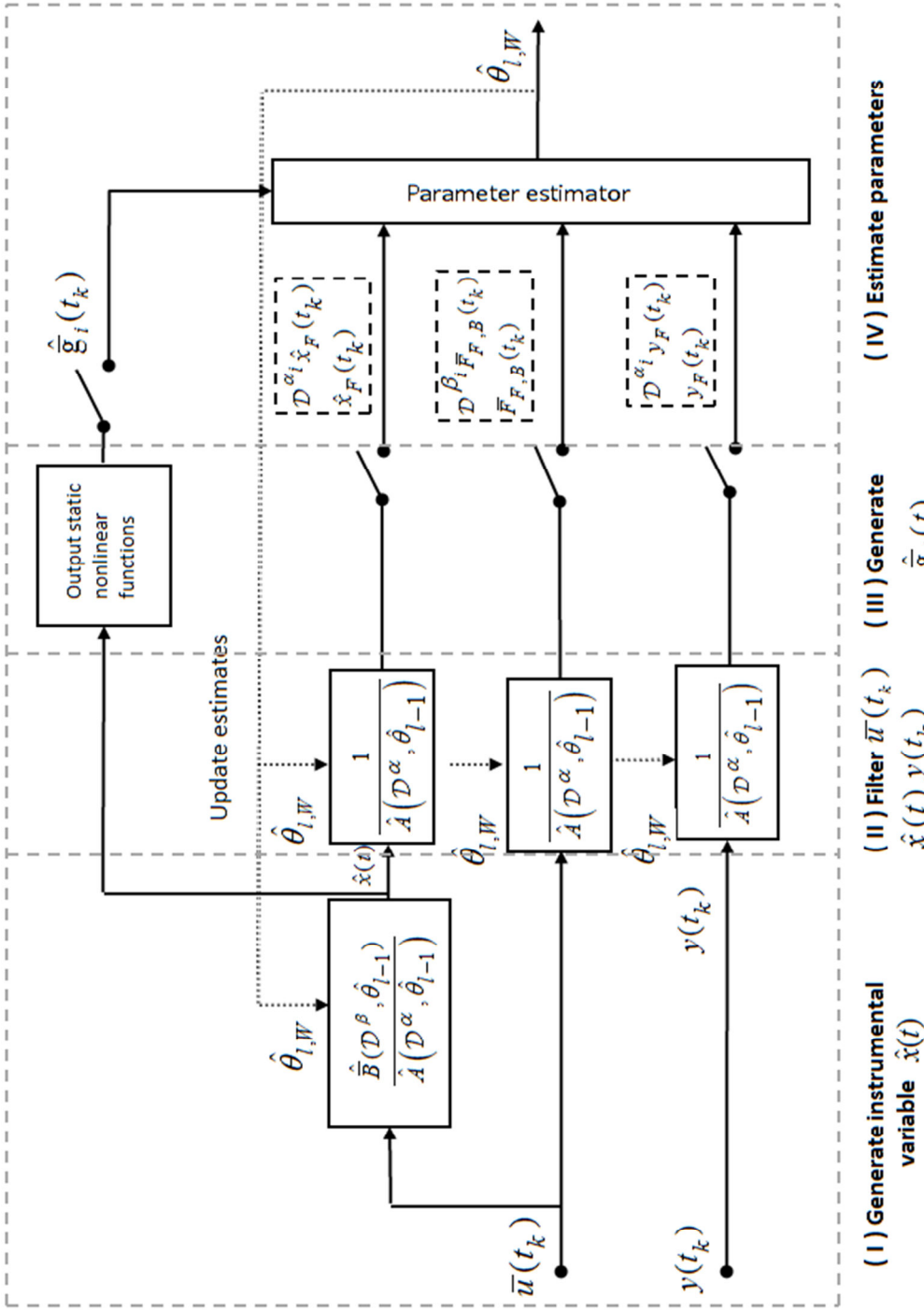

Figure 4-6: Iterative WSRIVCF method processes.

$$\mathrm{E}_{HW}(s) = Y(s) - \left(\frac{1}{A(s^{\alpha})} \overline{B}(s^{\beta}) \overline{F}_B(s) + \sum_{i=2}^{l} \overline{a}_i \overline{G}_i(s) \right) \tag{4.49}$$

The filter $\frac{1}{A(s^{\alpha})}$ is introduced in the first term on the right-hand side of (4.49), for generating the filtered output data, associated with retaining the ARX structure. Now, it is

possible to obtain reasonable higher fractional-order derivative terms of the filtered input and output data. Consequently, (4.49) can be expressed as:

$$\mathrm{E}_{HW}(s) = A\left(s^{\alpha}\right)\frac{1}{A\left(s^{\alpha}\right)}Y(s) - \left(\overline{B}(s^{\beta})\frac{1}{A\left(s^{\alpha}\right)}\overline{F}_{B}(s) + \sum_{i=2}^{l}\overline{a}_{i}\overline{G}_{i}(s)\right) \tag{4.50}$$

Taking the inverse Laplace of (4.50), leads to:

$$\varepsilon_{HW}(t) = A(\mathcal{D}^{\alpha})\frac{1}{A(\mathcal{D}^{\alpha})}y(t) - \left(\overline{B}(\mathcal{D}^{\beta})\frac{1}{A(\mathcal{D}^{\alpha})}\overline{F}_{B}(t) + \sum_{i=2}^{l}\overline{a}_{i}\overline{g}_{i}(t)\right) \tag{4.51}$$

(4.51) can be described by a model of the filtered multi-input filtered single-output and the error function in (4.51) is rearranged and described as:

$$\varepsilon_{HW}(t) = A(\mathcal{D}^{\alpha})y_{F}(t) - \left(\overline{B}(\mathcal{D}^{\beta})\overline{F}_{F,B}(t) + \sum_{i=2}^{l}\overline{a}_{i}\overline{g}_{i}(t)\right) \tag{4.52}$$

where the filtered output and the vector of the filtered inputs are denoted $\overline{F}_{F,B}(t)$ and $y_{F}(t)$, respectively, and the subscript *F* indicates that the signal is filtered by $\frac{1}{A(\mathcal{D}^{\alpha})}$.

Thus, the pseudo-linear regression form can be deduced based on sampled data of (4.52) and expressed as:

$$y_{F}(t_{k}) = \varphi_{F,HW}^{T}(t_{k})\theta_{HW} + \varepsilon_{HW}(t_{k}) \tag{4.53}$$

where

$$\begin{aligned}\theta_{HW} = [&a_{0}, \quad \cdots \quad a_{n-1}, \quad \overline{b}_{1}b_{0}, \quad \cdots \quad \overline{b}_{1}b_{m}, \quad \cdots \quad \overline{b}_{r}b_{0}, \quad \cdots, \quad \overline{b}_{r}b_{m-1}, \\ &\overline{b}_{r}b_{m}, \quad \overline{a}_{2}, \quad \cdots \quad \overline{a}_{l}]^{T}\end{aligned} \tag{4.54}$$

$$\begin{aligned}\varphi_{F,HW}^{T}(t_{k}) = [&-\mathcal{D}^{\alpha_{n-1}}y_{F}(t_{k}), \quad \cdots \quad -\mathcal{D}^{\alpha_{1}}y_{F}(t_{k}), \quad \mathcal{D}^{\beta_{m}}\overline{F}_{F,1}(t_{k}), \quad \cdots \quad \overline{F}_{F,1}(t_{k}), \\ &\cdots \mathcal{D}^{\beta_{m}}\overline{F}_{F,r}(t_{k}), \quad \cdots \quad \mathcal{D}^{\beta_{1}}\overline{F}_{F,r}(t_{k}), \quad \overline{F}_{F,r}(t_{k}), \quad \overline{g}_{2}(t_{k}), \quad \cdots \quad \overline{g}_{l}(t_{k})]\end{aligned} \tag{4.55}$$

Simulating $\overline{g}_{i}(t_{k})$ requires the $\hat{B}(\mathcal{D}^{\beta})$ and $\hat{A}(\mathcal{D}^{\alpha})$ polynomials and $\hat{\overline{b}}_{s}$. $\hat{\overline{b}}_{s}$ selection does not have a large influence on the estimation, for example in the numerical example in this chapter it is selected such as $\hat{\overline{b}}_{1} = \hat{\overline{b}}_{2} = \hat{\overline{b}}_{3} = 1$ while Section 4.7 shows how to initialise the

$\hat{B}(\mathcal{D}^{\beta},\hat{\theta}_{0,W})$ and $\hat{A}\left(\mathcal{D}^{\alpha},\hat{\theta}_{0,HW}\right)$ polynomials. The HWSRIVCF is iteratively implemented illustrated in Figure 4-7 and summarised as follows:

I. Compute the multi-input vector by using the input static nonlinear function.

II. Simulate the noise-free output $\hat{x}(t)$ using:

$$\hat{x}(t)=\frac{1}{\hat{A}(\mathcal{D}^{\alpha},\hat{\theta}_{l-1,HW})}\hat{\bar{B}}(\mathcal{D}^{\beta},\hat{\theta}_{l-1,HW})_i\bar{F}_B(t_k) \tag{4.56}$$

where $\hat{x}(t)$ is used as the input to the static output nonlinear function and the instrumental variable.

III. Filter $\hat{x}(t)$, $y(t_k)$ and $\bar{F}_B(t)$ for generating their filtered form with their higher fractional-order derivatives, using:

$$F(D^{\alpha})=\frac{1}{\hat{A}(\mathcal{D}^{\alpha},\hat{\theta}_{l-1,HW})} \tag{4.57}$$

IV. Generate $\hat{\bar{g}}_i(t_k)$ in (4.38) using $\hat{x}(t_k)$.

V. Obtain the estimated parameters using the instrumental variable least square algorithm:

$$\hat{\theta}_{l,HW}=\left(\sum_{k=1}^{N}\hat{\varphi}_{F,HW}(t_k)\varphi_{F,HW}^{T}(t_k)\right)^{-1}\sum_{k=1}^{N}\hat{\varphi}_{F,HW}(t_k)y_F(t_k) \tag{4.58}$$

where $\varphi_{F,HW}^{T}$ is obtained from (4.55) and $\hat{\varphi}_{F,W}(t_k)$ is defined as:

$$\begin{aligned}\hat{\varphi}_{F,HW}^{T}(t_k)=[&-\mathcal{D}^{\alpha_{n-1}}\hat{x}_F(t_k)\quad\cdots\quad-\mathcal{D}^{\alpha_1}\hat{x}_F(t_k)\quad\mathcal{D}^{\beta_m}\bar{F}_{F,1}(t_k)\quad\cdots\quad\mathcal{D}^{\beta_0}\bar{F}_{F,1}(t_k)\\&\cdots\quad\mathcal{D}^{\beta_m}\bar{F}_{F,r}(t_k)\quad\cdots\quad\mathcal{D}^{\beta_1}\bar{F}_{F,r}(t_k),\quad\mathcal{D}^{\beta_0}\bar{F}_{F,r}(t_k),\quad\hat{\bar{g}}_2(t_k),\quad\cdots\quad\hat{\bar{g}}_l(t_k)]\end{aligned} \tag{4.59}$$

VI. Stop iterating from (I) to (V) when the sum of the squares of the differences between $\hat{\theta}_{l-1,HW}$ and $\hat{\theta}_{l,HW}$ is smaller than a threshold which is selected to be 10^{-4} in the numerical example.

4.11 RIVCF method for the HWFC model

The HWFC method is derived by employing a similar approach for identifying the linear model such as in the integer-order continuous-time case (Young, Garnier, and Gilson 2006) and in fractional-order continuous-time (Allafi, and Burnham 2014). The HWSRIVCF model is not optimal when dealing with the coloured noise process $\xi(t)$ in the HWFC model in (4.48). For parameter estimation, this involves two iteratively adaptive filtering approaches. The first one is for the system model and the second one is for the ARMA noise model. They are iteratively coupled until a better estimate is obtained. According to (3.4) and (4.46), the error function of the HWFC model hybrid with ARMA process is:

$$\varepsilon_{HW}(t_k) = y(t_k) - \overline{x}(t_k) \tag{4.60}$$

where

$$\overline{x}(t) = \frac{1}{A(\mathcal{D}^{\alpha})}\overline{B}(\mathcal{D}^{\beta})\overline{F}_B(t) + \sum_{i=2}^{l}\overline{a}_i\overline{g}_i(t) \tag{4.61}$$

The initial parameters for simulating the noise-free output $\overline{x}(t)$ can be obtained by applying HWSRIVCF. The error function $\varepsilon_{HW}(t_k)$ is considered to be the ARMA process; therefore, the assumed white prediction error can be obtained as:

$$\hat{e}(t_k) = \frac{\hat{D}\left(q^{-1}\right)}{\hat{C}\left(q^{-1}\right)}\varepsilon_{HW}(t_k) \tag{4.62}$$

In fact, the noise polynomials $\hat{C}\left(q^{-1}\right)$ and $\hat{D}\left(q^{-1}\right)$ are not estimated. However, for simplicity, the integer-order discrete-time noise ARMA process in (4.1) can be

approximated by a higher order AR process with a much larger order of $D\left(q^{-1}\right)$ denominator (Söderström, and Stoica 1989). Defining:

$$\frac{C\left(q^{-1}\right)}{D\left(q^{-1}\right)}e(k)\approx\frac{1}{\bar{D}\left(q^{-1}\right)}\hat{e}(k) \tag{4.63}$$

where the order of $\bar{D}\left(q^{-1}\right)$ is selected to be fifteen in the illustrative example.

(4.63) leads to rearrange (4.62) such that:

$$\hat{e}(t_k)=\bar{D}\left(q^{-1}\right)\varepsilon_{HW}(t_k) \tag{4.64}$$

The parameters of the $\bar{D}\left(q^{-1}\right)$ polynomial are then estimated based on (4.64) by using the least squares algorithm. In order to force the coloured error function to be white error, the error function is described as a white prediction error by filtering (4.60) by $\bar{D}\left(q^{-1}\right)$:

$$\hat{e}(t_k)=\bar{D}\left(q^{-1}\right)\left(y(t_k)-\bar{x}(t_k)\right) \tag{4.65}$$

So both measured output and noise-free output are filtered by $\bar{D}\left(q^{-1}\right)$ in the discrete time-domain. This produces the filtered $y(t_k)$ and $\bar{x}(t_k)$ by $\bar{D}\left(q^{-1}\right)$ and termed as $y_D(t_k)$ and $\bar{x}_D(t_k)$, respectively where the subscript *D* indicates that the signal is filtered by $\bar{D}\left(q^{-1}\right)$. The filtered noise-free output model by $\bar{D}\left(q^{-1}\right)$ is described as:

$$\bar{x}_D(t)=\frac{1}{A(\mathcal{D}^{\alpha})}\bar{B}(\mathcal{D}^{\beta})\bar{F}_{DB}(t_k)+\sum_{i=2}^{l}\bar{a}_i\bar{g}_{D,i}(t_k) \tag{4.66}$$

where

$$\begin{aligned}\bar{F}_{DB}(t_k)&=\bar{D}\left(q^{-1}\right)\bar{F}_B(t_k)\\ \bar{g}_{D,i}(t_k)&=\bar{D}\left(q^{-1}\right)\bar{g}_i(t_k)\end{aligned} \tag{4.67}$$

This leads to obtaining parameters of the most optimal convergence of the multi-input, single-output model. By following a similar derivation of the HWSRIVCF, the pseudo-linear regression form can be obtained and expressed as:

$$y_{F,D}(t_k) = \varphi^T_{F,D,HW}(t_k)\theta_{HW} + \hat{e}_{HW}(t_k) \tag{4.68}$$

where θ_{HW} is illustrated in (4.54) and

$$\begin{aligned}&\varphi_{F,D,HW}(t_k) = \\ &[-\mathcal{D}^{\alpha_n} y_{F,D}(t_k), \quad \cdots \quad -\mathcal{D}^{\alpha_1} y_{F,D}(t_k), \quad \mathcal{D}^{\beta_m} \bar{F}_{F,D,1}(t_k), \quad \cdots \quad \bar{F}_{F,D,1}(t_k), \\ &\quad \cdots \mathcal{D}^{\beta_m} \bar{F}_{F,D,r}(t_k) \quad \cdots \quad \mathcal{D}^{\beta_1} \bar{F}_{F,D,r}(t_k), \quad \bar{F}_{F,D,r}(t_k), \quad \bar{g}_{D,2}(t_k), \quad \cdots \quad \bar{g}_{D,l}(t_k)]\end{aligned} \tag{4.69}$$

$$\begin{aligned}F_{F,D,i}(t) &= \frac{1}{A\left(\mathcal{D}^{\alpha}\right)} \bar{F}_{D,i} u(t_k) \\ y_{F,D}(t) &= \frac{1}{A\left(\mathcal{D}^{\alpha}\right)} y_D(t_k)\end{aligned} \tag{4.70}$$

$\bar{g}_i\left(t_k\right)$ can be simulated based on the estimated $\hat{\bar{B}}(\mathcal{D}^{\beta}, \hat{\theta}_{bm,\bar{b}r})$ and $\hat{A}(\mathcal{D}^{\alpha})$ polynomials. The required initial values are obtained using the HWSRIVCF method. Iterative estimation is then can be implemented as illustrated in Figure 4-8 and summarised as:

I. Obtain the multi-input vector $\bar{F}_B(t_k)$ by using the input static nonlinear function.

II. Compute the simulated noise-free output $\hat{x}(t)$ using:

$$\hat{x}(t) = \frac{1}{\hat{A}(\mathcal{D}^{\alpha}, \hat{\theta}_{l-1,HW})} \hat{\bar{B}}(\mathcal{D}^{\beta}, \hat{\theta}_{l-1,HW})_i \bar{F}_B(t_k) \tag{4.71}$$

where $\hat{x}(t)$ is used as the input to the static output nonlinear function and the instrumental variable.

III. Filter $\hat{x}(t)$, $y(t_k)$ and $\bar{F}_B(t)$ for generating their filtered form with their higher fractional-order derivatives, using:

$$F(D^{\alpha}) = \frac{1}{\hat{A}(\mathcal{D}^{\alpha}, \hat{\theta}_{l-1,HW})} \tag{4.72}$$

IV. Compute $\hat{\bar{g}}_i(t_k)$ using $\hat{x}(t)$.

V. Calculate $\hat{\bar{x}}(t_k)$ using (4.61).

VI. Compute $\hat{\varepsilon}_{HW}(t_k)$ using:

$$\hat{\varepsilon}_{HW}(t_k) = y(t_k) - \hat{\bar{x}}(t_k) \tag{4.73}$$

The discrete part of the model could be identified by using the higher order AR process with a much larger order of the $D\left(q^{-1}\right)$ denominator polynomial.

VII. Filter the instrumental variable $\hat{x}(t)$, $\bar{F}_{F,i}(t_k)$, $y_F(t_k)$ and $\bar{g}(t_k)$ are filtered by $\bar{D}\left(q^{-1}\right)$:

$$\begin{aligned}
\bar{F}_{F,D,i}(t_k) &= \bar{D}\left(q^{-1}\right)\bar{F}_{F,i}(t_k) \\
y_{F,D}(t_k) &= \bar{D}\left(q^{-1}\right)y_F(t_k) \\
\hat{x}_{F,D}(t_k) &= \bar{D}\left(q^{-1}\right)\hat{x}_F(t_k) \\
\bar{g}_D(t_k) &= \bar{D}\left(q^{-1}\right)\hat{\bar{g}}(t_k)
\end{aligned} \tag{4.74}$$

VIII. Obtain the estimated parameters using the instrumental variable least square algorithm:

$$\hat{\theta}_{l,HW} = \left(\sum_{k=1}^{N} \hat{\varphi}_{F,D,HW}(t_k)\varphi_{F,D,HW}(t_k) \right)^{-1} \sum_{k=1}^{N} \hat{\varphi}_{F,D,HW}(t_k) y_F(t_k) \tag{4.75}$$

where $\varphi_{F,HW}^T$ is obtained from (4.69) and $\hat{\varphi}_{F,W}(t_k)$ is defined as:

$$\begin{aligned}
\hat{\varphi}_{F,D,HW}^T(t_k) = [&-\mathcal{D}^{\alpha_n}\hat{x}_{F,D}(t_k), \quad \cdots \quad -\mathcal{D}^{\alpha_1}\hat{x}_{F,D}(t_k), \\
&\mathcal{D}^{\beta_m}\bar{F}_{F,D,1}(t_k), \quad \cdots \quad \mathcal{D}^{\beta_0}\bar{F}_{F,D,1}(t_k), \quad \cdots \quad \mathcal{D}^{\beta_m}\bar{F}_{F,D,r}(t_k) \\
&\cdots \quad \mathcal{D}^{\beta_1}\bar{F}_{F,D,r}(t_k), \quad \mathcal{D}^{\beta_0}\bar{F}_{F,D,r}(t_k), \quad \bar{g}_{D,2}(t_k), \quad \cdots \quad \bar{g}_{D,l}(t_k)]
\end{aligned} \tag{4.76}$$

IX. Stop iterating from (I) to (VIII) when the sum of the squares of the differences between $\hat{\theta}_{l-1,HW}$ and $\hat{\theta}_{l,HW}$ is smaller than a threshold which is selected to be 10^{-4} in the numerical example.

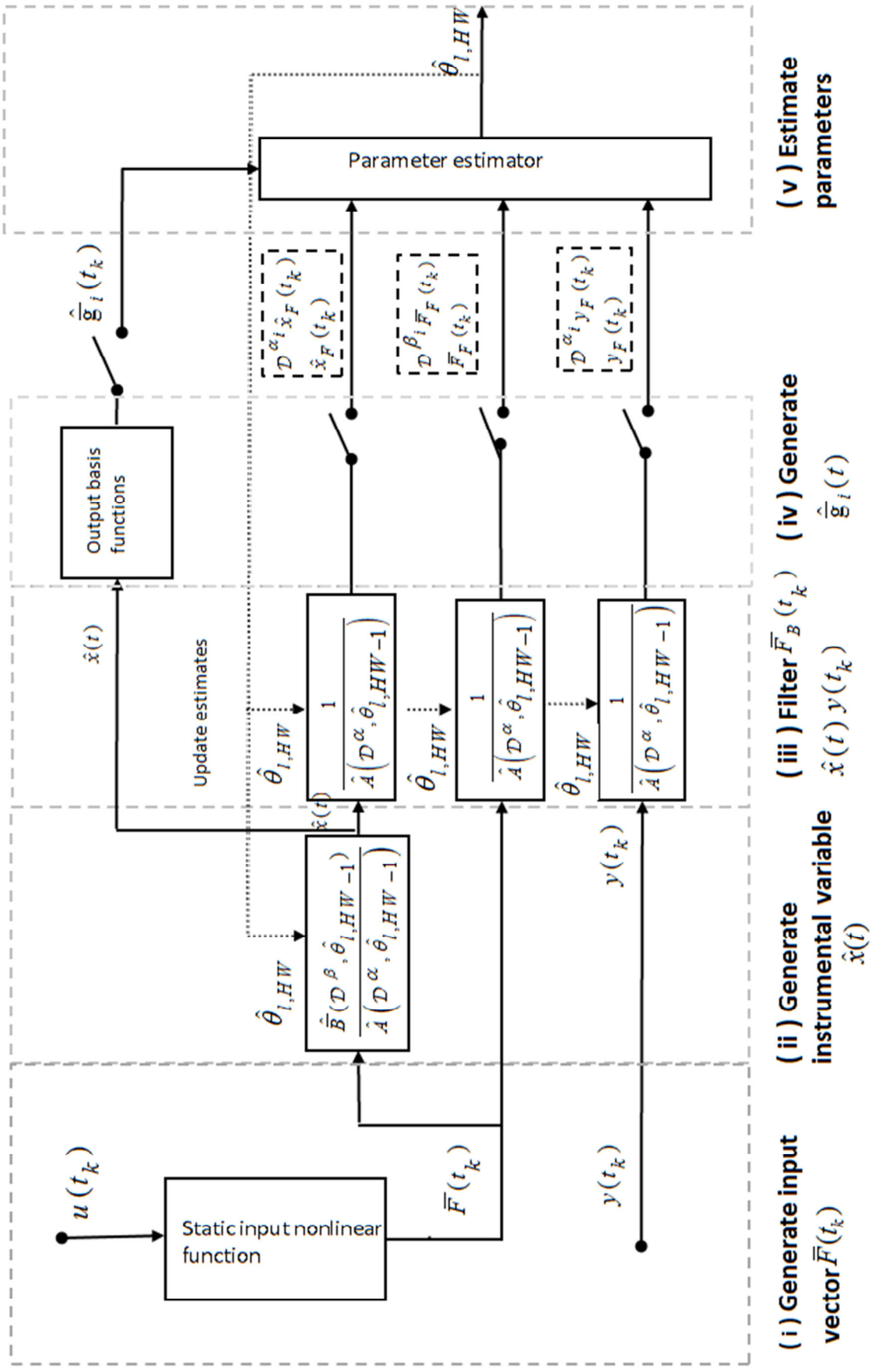

Figure 4-7: Iterative HWSRIVCF method processes.

Comment

I. All comments, considered in the previous HSIVCF, WSIVCF methods are very significant here as well.

II. The order of the continuous-time and discrete-time filtering is not significant because the system is considered to be linear. For convenience, in this chapter, the continuous-time filtering is done first and then the discrete-time and filtering follow iteratively.

4.12 Numerical study of HWFC model identification

A simple fractional-order linear subsystem of the HWFC model is given as:

$$x(t)=\frac{1}{0.5\mathcal{D}^{0.5}+1}\overline{u}(t) \tag{4.77}$$

The input and output nonlinear function are described by two static polynomial functions:

$$\begin{cases}\overline{u}(t)=u(t)+0.02u^2(t)+0.25u^3(t)\\ \overline{x}(t)=x(t)+0.01x^2(t)+0.3x^3(t)\end{cases} \tag{4.78}$$

The output of the output static nonlinear is corrupted by coloured noise process and give by:

$$y(t_k)=\overline{x}(t_k)+\frac{1+0.3q^{-1}}{1-0.6q^{-1}}e(t_k) \tag{4.79}$$

where $e(t_k)$ is white Gaussian noise whose variance is selected based on the *SNR*, given in (4.25). The noise, added at the output, is selected such that it gives the *SNR* of 30*dB* and 60*dB*.

The models, considered for estimation using HWSRIVCF and HWSRIVCF method, is multi-input, single-output and expressed, respectively, as:

$$HW_{HWSRIVCF}:\begin{cases}\overline{f}_i(t)=u^i(t)\\ \hat{x}(t)=\sum_{i=1}^{3}\dfrac{\hat{\overline{b}}_i\hat{b}_0}{\hat{a}_0\mathcal{D}^{0.5}+\hat{a}_1}\overline{f}_i(t)\\ \hat{\overline{g}}_i(t)=\hat{x}^i(t)\\ \overline{x}(t)=\sum_{i=1}^{3}\dfrac{\overline{b}_i b_0}{a_0\mathcal{D}^{0.5}+a_1}\overline{f}_i(t)+\overline{a}_2\hat{\overline{g}}_2(t)+\overline{a}_3\hat{\overline{g}}_3(t)\\ y(t_k)=\overline{x}(t_k)+e(t_k)\end{cases} \tag{4.80}$$

and

$$HW_{HWRIVCF}:\begin{cases}\overline{f}_i(t)=u^i(t)\\ \hat{x}(t)=\sum_{i=1}^{3}\dfrac{\hat{\overline{b}}_i\hat{b}_0}{\hat{a}_0\mathcal{D}^{0.5}+\hat{a}_1}\overline{f}_i(t)\\ \hat{\overline{g}}_i(t)=\hat{x}^i(t)\\ \overline{x}(t)=\sum_{i=1}^{3}\dfrac{\overline{b}_i b_0}{a_0\mathcal{D}^{0.5}+a_1}\overline{f}_i(t)+\overline{a}_2\hat{\overline{g}}_2(t)+\overline{a}_3\hat{\overline{g}}_3(t)\\ y(t_k)=\overline{x}(t_k)+\dfrac{1+0.3q^{-1}}{1-0.6q^{-1}}e(t_k)\end{cases} \tag{4.81}$$

The same simulation environment, used for identifying the HFC model, are used for identifying the HWFC model, is implemented but the input gained by 0.5 and for more details, see Section 4.4.1.

The results obtained from the Monte Carlo simulation analysis are presented in mean and standard deviations in Table 4-3. Table 4-3 demonstrates that the obtained results match the theory beyond the HWRIVCF and HWSRIVCF algorithm where they give similar, unbiased estimates of the HWFC model parameters.

Although the noise is rather high, at the level of 30dB, the proposed method converges. The standard deviations, obtained by HWSRIVCF are always larger than those obtained by HWSRIVCF but they are still within reasonable limits, as expected. This is caused by the HWSRIVCF method being designed for an OE model estimation scenario instead of BJ noise model scenario. This further increases the motivation of using HWSRIVCF method when used in practise.

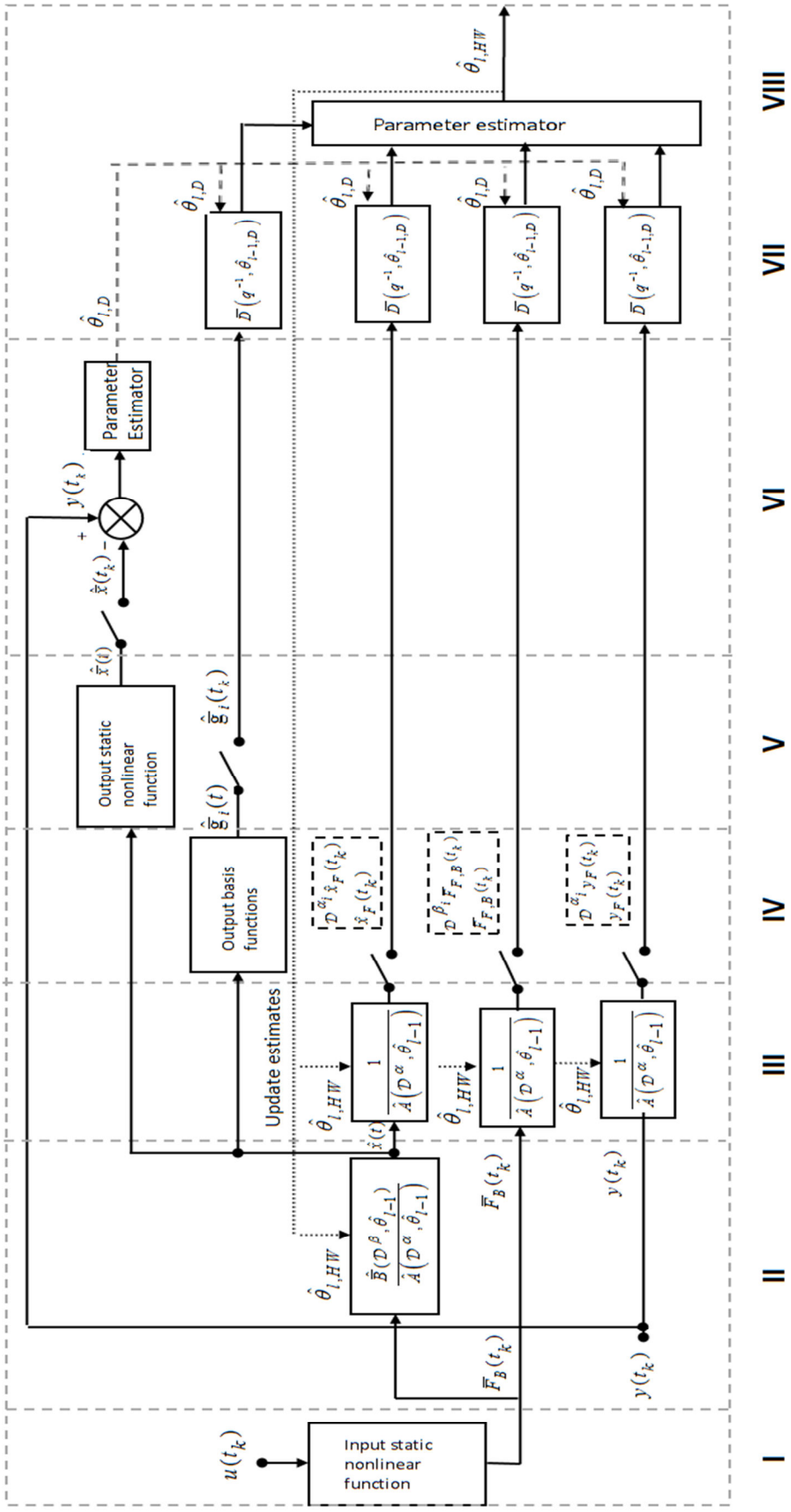

Figure 4-8: Iterative HWRIVCF method processes.

Table 4-3: Monte Carlo simulation results of parameter estimation of the HWCF system where $a_1=\bar{a}_1=b_1=1$.

SNR	*Method*		a_0=0.5	b_0=1	$\bar{a}_2$=0.01	$\bar{a}_3$ =0.3	$\bar{b}_2$=0.02	$\bar{b}_3$=0.25
30dB	HWSRIVCF	mean	0.4923	1.0102	0.0115	0.2912	0.0022	0.2602
		std	0.0070	0.0120	0.0012	0.0020	0.0009	0.0061
	HWRIVCF	mean	0.4975	1.0031	0.0108	0.2989	0.0021	0.2522
		std	0.0020	0.0080	0.0005	0.0012	0.0005	0.0029
60dB	HWSRIVCF	mean	0.4946	1.0088	0.0109	0.2974	0.0021	0.2531
		std	0.0038	0.0097	0.0007	0.0130	0.0005	0.0052
	HWRIVCF	mean	0.4992	1.0016	0.0102	0.2996	0.0021	0.2506
		std	0.0008	0.0053	0.0002	0.0040	1.0000	0.0012

4.13 Conclusions

The applications of the fractional-order models are widely extended to non-linear phenomena. Therefore, this chapter has proposed a new algorithm specifically developed for estimating the parameters of fractional-order nonlinear models in the form of the fractional-order continuous-time Wiener-Hammerstein model. The static nonlinear functions are represented by a combination of basis functions. The new algorithm is an extension of the refined instrumental variable approach developed by Peter Young for continuous-time integer-order Box-Jenkins models.

In a similar manner, the initialisation process involves a simplified version of the algorithm which does not assume measurement noise. This algorithm is used to establish the filter which is then implemented in the full hybrid algorithm.

Chapter 5: Delayed Fractional-order State Variable Filter Design for Nonlinear Parameter Estimation

This chapter presents a proposed delayed fractional-order state variable filter and its application for nonlinear parameter estimation. It illustrates how the delayed fractional-order state variable filter is designed so that its frequency response offers the maximally flat unity magnitude associated with a constant group-delay. The proposed filter is derived from equalising a proposed fractional-order Butterworth filter by integer-order all-pass filters. This equalisation is applied to achieve the required constant group-delay within a selected frequency range. In the proposed parameter estimation approach, all the required fractional-order derivative terms for identification are collected from the fractional-order Butterworth filter. Three different novel approaches for designing the delayed fractional-order state variable filter are addressed accordingly to the proposed fractional-order Butterworth. The first method is for designing the delayed fractional-order state variable filter which is able to generate only the delayed fractional-order derivative terms of 0.5 base-order. This is because the base-order of the proposed fractional-order Butterworth filter is 0.5. The second method is more generalised than the first method and capable of producing

the delayed fractional-order derivative terms with $\frac{1}{2^n}$ *base-order where* $n \in \mathbb{Z}$. *The third method is generalised and can generate the delayed fractional-order derivative terms with any arbitrary base-order. In this method, the proposed approach for designing the fractional-order Butterworth filter is termed here the compartmental fractional-order Butterworth design. The three methods use a similar all-pass filter equalisation, therefore, there is a more focus on describing the fractional-order Butterworth filter in this chapter.*

One of the applications of the delayed fractional-order state variable filter is for parameter estimation of a class of fractional-order nonlinear systems, described here as an input-output fractional-order continuous-time nonlinear model. The proposed filter is used as a source of the approximated delayed fractional-order nonlinear input and output and their higher linear and nonlinear fractional-order derivative terms from the collected input-output data. The more constant group-delay, achieved, leads to a better approximation. Therefore, more than two stages of the all-pass filter equaliser might be required according to the degree of the nonlinearity. The approximated terms are arranged based on the selected system structure and the parameters are then estimated by applying any linear estimator, such as an instrumental variable least squares estimator.

5.1 Introduction

Fractional-order calculus has been attractive to many researchers for the last two decades. This has encouraged researchers to extend a significant number of the classical theories and applications to fractional-order. However, fractional-order nonlinear system identification has not received major attention because of the complexity associated with it. For example, parameter estimation of the fractional-order continuous-time nonlinear systems is required fractional-order nonlinear derivative terms which are not accessible in a majority of systems. This leads to approximating them from collected data. In the

presence of noise, it is not an easy task to directly approximate the fractional-order nonlinear derivative terms.

In the fractional-order linear identification case, different publications have employed a commutative property between known recommended filters and the fractional-order continuous-time linear systems. This then produces filtered output, input and their higher fractional-order derivative terms. The filtered data is utilised for parameter estimation instead of the original data, for more details see (Garnier, Wang, and Young 2008 and Garnier 2015). Unfortunately, the commutative property of the recommended filters is not valid in the case of the fractional-order continuous-time nonlinear systems. Nonetheless, Kohr (1963) claimed that the delayed state variable filter and the nonlinear derivative terms could commute. He firstly introduced the delayed state variable filter in system identification field and demonstrated how it could be utilised to estimate the parameters of the continuous-time nonlinear system but with very simple nonlinearity (Kohr 1963). Then Tsang and Billing (1994) improved the filter to adopt higher nonlinearities. Due to advantages of the use of the delayed state variable filter and fractional-order system's properties, the delayed state variable filter is extended to the delayed fractional-order state variable filter.

In this chapter, the delayed fractional-order state variable filter is proposed to be directly applied for parameter estimation of the fractional-order continuous-time nonlinear system from collected input-output data. The process of parameter estimation, using a delayed fractional-order state variable filter, is denoted here by a delayed fractional-order state variable identification approach. In this approach, it is assumed that the system can be described by an input-output fractional-order nonlinear differential equation. There is also an illustration of how the proposed delayed fractional-order state variable filter is designed based on the proposed fractional-order Butterworth filter and an all-pass filter. In this thesis, the fractional-order Butterworth filter is defined as a filter which generates

fractional-order derivative terms of output whose frequency response gives the maximally flat magnitude. The numerical implementation of the delayed fractional-order state variable filter is achieved based on the fractional-order state-space representation.

This chapter is structured to cover the problem description and fractional-order identification argument in Sections 5.2 and 5.3, respectively. It is followed by an introduction to the design of the delayed fractional-order state variable filter in Section 5.4. In an individual section, the fractional-order Butterworth filter is designed and presented in Section 5.5. An introduction to the all-pass filter is given in Section 5.7. The numerical solution of the delayed fractional-order state variable filter appears in Section 5.7. Section 5.8 illustrates the influence of numerical process on the identification while Section 5.9 explains how to select the identification input properties. The summary of the proposed identification process and a numerical example are given in Sections 5.10 and 5.11, respectively. Section 5.12 provides the conclusions.

5.2 Problem description

A general single-input single-output fractional-order nonlinear system can be described by a fractional-order nonlinear ordinary differential equation as:

$$A\left(\mathcal{D}^{\alpha}\right)x(t)+\mathbf{N}\left(\mathcal{D}^{\kappa},x(t),u(t)\right)=B\left(\mathcal{D}^{\beta}\right)u(t) \tag{5.1}$$

where $u(t)$ and $x(t)$ denote input and output signals, respectively. $A\left(\mathcal{D}^{\alpha}\right)$ and $B\left(\mathcal{D}^{\beta}\right)$ are output and input fractional-order linear polynomials in $\mathcal{D}$ and expressed as:

$$\begin{aligned} A\left(\mathcal{D}^{\alpha}\right)&=a_0\mathcal{D}^{\alpha_n}+a_1\mathcal{D}^{\alpha_{n-1}}+\ldots+a_n \\ B\left(\mathcal{D}^{\beta}\right)&=b_0\mathcal{D}^{\beta_m}+b_1\mathcal{D}^{\beta_{m-1}}+\ldots+b_m \end{aligned} \tag{5.2}$$

where $\alpha_i<\alpha_{i+1}\le\alpha_n$, $\beta_i<\beta_{i+1}\le\beta_m$, $\alpha_i\in\mathbb{R}^+$, $\beta_i\in\mathbb{R}^+$ and $\alpha_n>\beta_m$. $\mathbf{N}(\cdot)$ is a known nonlinear mapping function of $u(t)$, $x(t)$ and the fractional-order derivative term $\mathcal{D}^{\kappa}$, and denoted in this chapter by the fractional-order polynomial nonlinear function where

$\kappa_i \in \mathbb{R}^+$, κ_p is the highest order of fractional-order polynomial nonlinear function, $\kappa_i \le \kappa_{i+1} \le \kappa_p$ and $\alpha_n > \kappa_p$. The fractional-order polynomial nonlinear function does not have a particular description. It is mainly a combination of the nonlinear terms which can have a general form as:

$$\mathbf{N}\left(\mathcal{D}^{\kappa}, x(t), u(t)\right) = \sum_{i=0}^{p} v_i N_i\left(\mathcal{D}^{\kappa_{p-i}}, x(t), u(t)\right) \tag{5.3}$$

where $v_i \in \mathbb{R}$ and $i = 0,1,2,\cdots,p$ are scalar weighting coefficients which signify the relative importance of the nonlinear functions N_i. The difference between the fractional-order polynomial nonlinear function in (5.3) and basis functions in (4.2) is that the basis function does not have derivative terms, i.e. it is a static function.

5.3 Identification argument

5.3.1 Linear considerations

In the linear case, the parameter estimation of the fractional-order continuous-time linear system depends on how to approximate the higher fractional-order derivative terms of the system. This can be achieved by approximating the higher fractional-order derivative terms of the filtered input and output. For example, if the fractional-order polynomial nonlinear function of (5.1) does not exist, (5.1) becomes a linear model. Consequently, it can be filtered by a linear fractional-order continuous-time filter $G\left(\mathcal{D}^{\gamma}\right)$. So the filter can commute with the linear polynomials as follows:

$$A\left(\mathcal{D}^{\alpha}\right)G\left(\mathcal{D}^{\gamma}\right)x(t) = B\left(\mathcal{D}^{\beta}\right)G\left(\mathcal{D}^{\gamma}\right)u(t) \tag{5.4}$$

This results a system with $A\left(\mathcal{D}^{\alpha}\right)$ and $B\left(\mathcal{D}^{\beta}\right)$ polynomials and filtered $x(t)$ and $u(t)$ by $G\left(\mathcal{D}^{\gamma}\right)$. Therefore, it is possible to estimate the parameters of the fractional-order $A\left(\mathcal{D}^{\alpha}\right)$ and $B\left(\mathcal{D}^{\beta}\right)$ polynomials using the filtered $x(t)$ and $u(t)$ values. There are several

methods to design the filter $G\left(\mathcal{D}^{\gamma}\right)$, such as the simplified refined instrumental variable method for fractional-order continuous-time models as illustrated in Chapter 3, and the fractional-order state variable filter approach, see (Cois et al. 2001).

5.3.2 Nonlinear considerations

In the case of nonlinear systems, the recommended filters in the linear case do not commute with the fractional-order polynomial nonlinear function in (5.1). However, the transport-delay filter can commute according to the fact, if a transport-delay, denoted *T* in s, is introduced in all terms in (5.1), it generates a transport-delay in all terms in (5.1):

$$A\left(\mathcal{D}^{\alpha}\right)x\left(t-T\right)+\mathbf{N}\left(\mathcal{D}^{\kappa},x\left(t-T\right),u\left(t-T\right)\right)=B\left(\mathcal{D}^{\beta}\right)u\left(t-T\right) \tag{5.5}$$

This is not enough to produce the delayed fractional linear and nonlinear derivative terms of the input and output, required for identification. This can be solved if the transport-delay is produced by a fractional filter. Only an ideal transport-delay filter $\Gamma(\mathcal{D}^{\eta})$ can generate the transport-delay in (5.5) where the fractional-order $\eta\in\mathbb{R}^{+}$ is to indicate the filter is fractional-order. Therefore, the filtered fractional-order nonlinear system can be re-expressed as:

$$A\left(\mathcal{D}^{\alpha}\right)\Gamma(\mathcal{D}^{\eta})x\left(t\right)+\mathbf{N}\left(\mathcal{D}^{\kappa},\Gamma(\mathcal{D}^{\eta})x\left(t\right),\Gamma(\mathcal{D}^{\eta})u\left(t\right)\right)=B\left(\mathcal{D}^{\beta}\right)\Gamma(\mathcal{D}^{\eta})u\left(t\right) \tag{5.6}$$

(5.6) can be rearranged and expressed in a filtered form as:

$$A\left(\mathcal{D}^{\alpha}\right)x_{\Gamma}\left(t\right)+\mathbf{N}\left(\mathcal{D}^{\kappa},x_{\Gamma}\left(t\right),u_{\Gamma}\left(t\right)\right)=B\left(\mathcal{D}^{\beta}\right)u_{\Gamma}\left(t\right) \tag{5.7}$$

where $x_{\Gamma}\left(t\right),u_{\Gamma}\left(t\right)$ are the filtered noise-free output and filtered input by the transport-delay filter $\Gamma(\mathcal{D}^{\eta})$. The higher fractional-order derivative terms of $x_{\Gamma}\left(t\right)$ and $u_{\Gamma}\left(t\right)$ are accessible by the transport-delay filter, hence, the parameters of $A\left(\mathcal{D}^{\alpha}\right)$, $B\left(\mathcal{D}^{\beta}\right)$ and $\mathbf{N}\left(\mathcal{D}^{\kappa},x_{\Gamma}\left(t\right),u_{\Gamma}\left(t\right)\right)$ can be estimated. The fractional-order polynomial nonlinear function

can be described as a linear combination of nonlinear terms by a similar approach, used in (5.3), so that the fractional-order nonlinear system is expressed in the filtered form as:

$$\begin{aligned} a_0\mathcal{D}^{\alpha_n}x_\Gamma(t)+a_1\mathcal{D}^{\alpha_{n-1}}x_\Gamma(t)+\ldots+a_nx_\Gamma(t)+\sum_{i=0}^{p}v_iN_i\left(\mathcal{D}^{\kappa_{p-i}},x_\Gamma(t),u_\Gamma(t)\right) \\ =b_0\mathcal{D}^{\beta_m}u_\Gamma(t)+b_1\mathcal{D}^{\beta_{m-1}}u_\Gamma(t)+\ldots+b_mu_\Gamma(t) \end{aligned} \tag{5.8}$$

Consequently, (5.8) can be reformulated into the following linear regression form:

$$x_\Gamma(t)=\varphi_\Gamma^T\theta \tag{5.9}$$

where it is assumed $a_n=1$ and

$$\begin{aligned} \varphi_{\Gamma(t)}^T=[&-\mathcal{D}^{\alpha_n}x_\Gamma(t),\ldots-\mathcal{D}^{\alpha_1}x_\Gamma(t)\ ,-N_0\left(\mathcal{D}^{\kappa_p},x_\Gamma(t),u_\Gamma(t)\right), \\ &,\ldots-N_p\left(\mathcal{D}^{\kappa_0},x(t),u(t)\right),\mathcal{D}^{\beta_m}u_\Gamma(t),\ldots u_\Gamma(t)\ ] \end{aligned}$$

$$\theta=\left[\ a_0,\ \ \ldots,\ \ a_{n-1},\ \ v_0,\ \ \ldots,\ \ v_p,\ \ b_0,\ \ \ldots,\ \ b_m\ \right]^T$$

$$x_\Gamma(t)=\Gamma(\mathcal{D}^\eta)x(t)$$

$$u_\Gamma(t)=\Gamma(\mathcal{D}^\eta)u(t)$$

The least squares algorithm needs the sampled data, hence, the filtered input-output data is uniformly collected and denoted by $u_\Gamma(t_k)$ and $x_\Gamma(t_k)$. They are then described as sampled data at a discrete instant $t_k=kT_s$ for $k=1,2,\ldots N$, where N is the total number of the samples. The estimates of the parameters and weighting coefficients of the single-input single-output fractional-order nonlinear ordinary differential equation in (5.1) can be extracted by using a linear least squares estimator according to (5.9) as:

$$\hat{\theta}=\left(\frac{1}{N}\sum_{k=1}^{N}\varphi_\Gamma(t_k)\varphi_\Gamma^T(t_k)\right)^{-1}\frac{1}{N}\sum_{k=1}^{N}\varphi_\Gamma(t_k)x_\Gamma(t_k) \tag{5.10}$$

In the development of the approach towards fractional-order identification of nonlinear systems, it is useful to review the existing literature which supports the properties for filter design. For completeness, a section of the Butterworth filter is also included.

5.4 Delayed fractional-order state variable filter

The ideal transport-delay filter is the filter which can generate a transport-delay for all fractional-order states for all angular frequencies ω. In other words, it is a filter whose gain frequency response is unity and the phase frequency response is denoted $\angle\Gamma(\omega j) = -\tau\omega$, for all ω where τ is a constant which is equal to the value of the transport-delay. This causes the transport-delay (which is the negative derivative of the phase with respect to frequencies ω) to be a constant and $T(\omega j) = \tau$ for all frequencies ω. Figure 5-1 illustrates the gain, phase and transport-delay axis of the transport-delay filter against ω, where phase and transport-delay axes are expressed in terms of τ.

Although there is no finite order filter that can generate an ideal transport-delay, by introducing some design constraints it is possible to approximate such a filter. Therefore, it is assumed that the ideal transport-delay filter can be designed within a selected range of the frequencies ω less than the cut-off frequency denoted ω_c. This generates a group-delay as illustrated in Figure 5-2, for more details about group-delay; see for example the text (Winder 2002). This filter is termed an ideal delayed fractional-order stated variable filter. The larger the frequency band of the system which is required to be identified, the higher the cut-off frequency must be considered. This leads to more computational effort, being required to design an appropriate delayed fractional-order state variable filter.

There are three essential requirements that must be considered when designing a delayed fractional-order state variable filter. These are (i) a unity gain, (ii) a constant group-delay and (iii) a stable filter. The design starts from selecting the most appropriate basic analogue filter, e.g. Bessel, Butterworth, or Chebyshev.

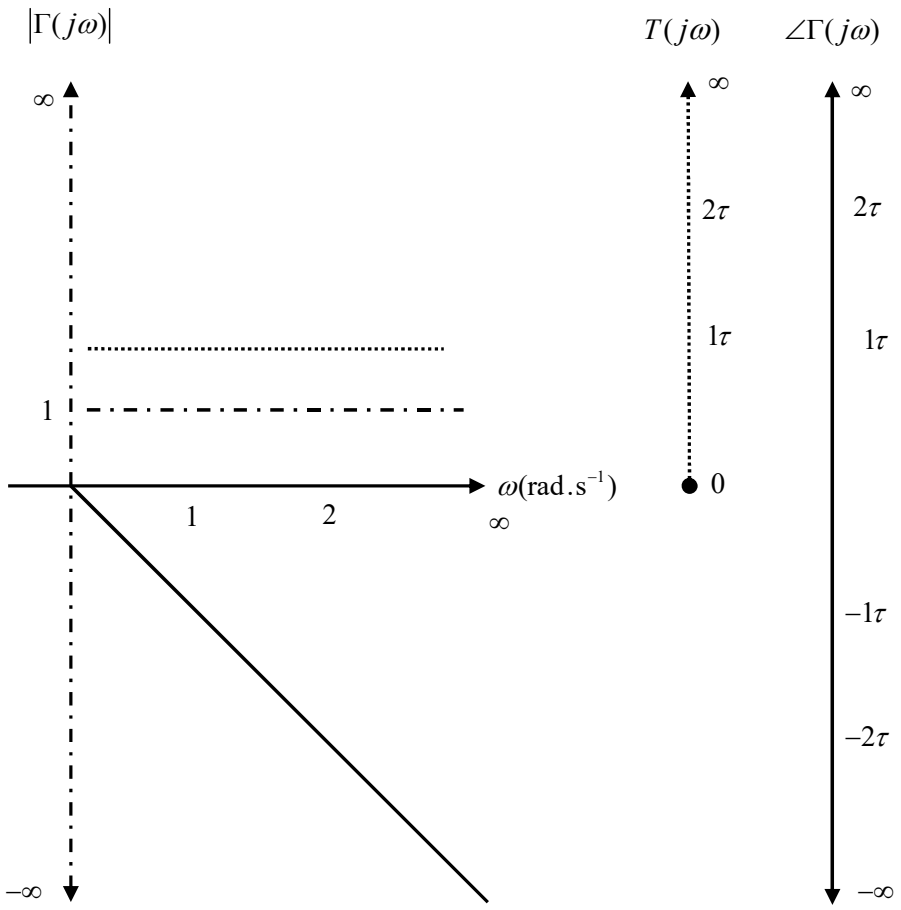

Figure 5-1: Gain, phase and transport-delay of $\Gamma(\omega j)$, expressed in dashed, solid and dotted lines, respectively.

Bessel filters have a constant group-delay because the phase change of the signals passing through them is proportional to the frequency but associated with insufficient attenuation at frequencies beyond the pass-band. This is because their frequency response has a gentle transition from pass-band to stop-band. If the Bessel filter gain is required to be improved this leads to loss of the constant group-delay (Blinchkoff, and Zverev 1976). On the other hand, the Butterworth filter gives a maximally flat gain but associated with a frequency dependent group-delay. In other words, there is a nonlinear phase shift and the rate of change of the phase generally increases as the filter's cut-off frequency is approached (Blinchkoff, and Zverev 1976). Nonetheless, this unwanted phase distortion and group-delay variation can be corrected and minimised to retain a maximally flat gain by the use of phase-equalising all-pass filters. All-pass filters can be designed to have a group-delay that is virtually complementary to a low-pass filter, so the two filters

connected in series produce an almost constant group-delay. Therefore, the Butterworth filter and all-pass filter are selected for designing the delayed fractional-order state variable filter, for more details about filters and their properties; see (Winder 2002 and Sedra, and Smith 2007).

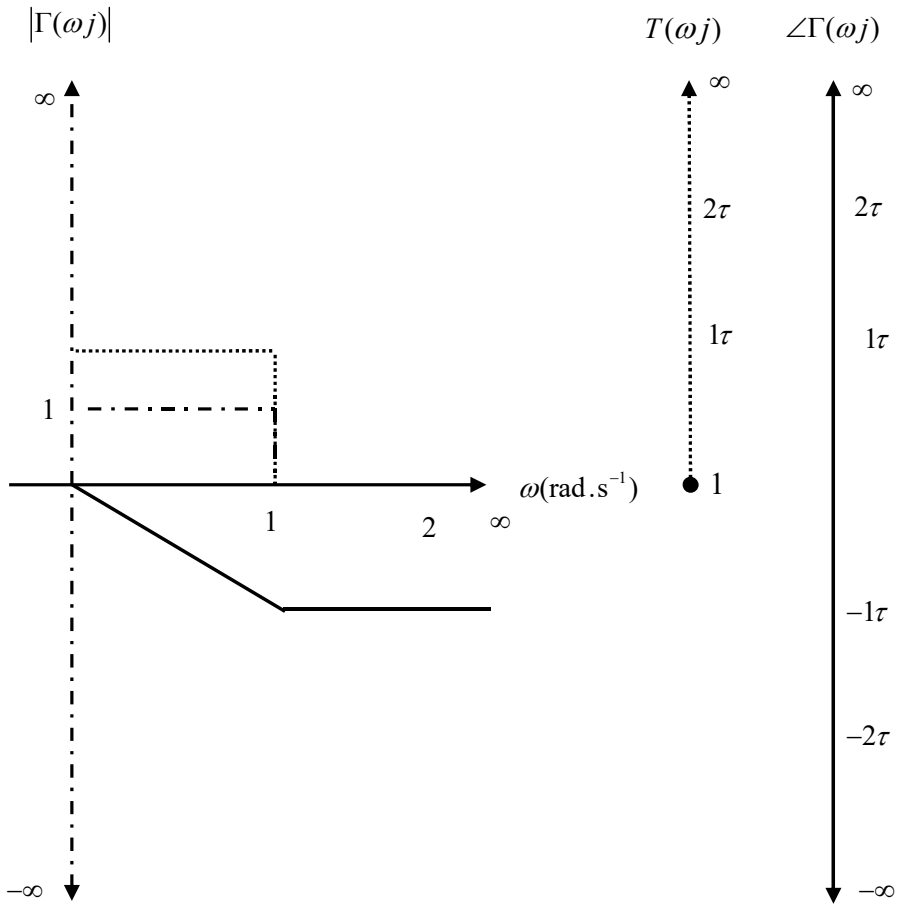

Figure 5-2: Gain, phase and group-delay of $\Gamma(\omega j)$, expressed in dashed, solid and dotted lines, respectively where ω_c=1.

Therefore, there is initially a need to obtain a maximally flat magnitude in pass-band and stop-band, with no attention paid to the phase and delay. Thus, the Butterworth filter is proposed to generate the desired magnitude response to eliminate the high-frequency response gain from the input signal. However, this filtering process causes a nonlinear phase-shift. This leads to introduce group-delay distortion near the cut-off frequency. This distortion could be removed by modifying the nonlinear phase to obtain a linear phase, in other words, a constant group-delay. This is achieved by equalising the approximated

Butterworth filter by an all-pass filter to produce a constant group–delay. By applying this, it produces a filter which has a maximally flat gain associated with an approximately constant group-delay within a selected frequency range.

5.5 Butterworth filter

The Butterworth filter is one of the most widely used filter because it provides a maximally flat frequency response gain. The low pass Butterworth filter is described as a filter which passes uniformly lower frequency (wanted frequency) signals whose frequencies are lower than the filter's cut-off frequency and rejects (unwanted frequency) higher frequency signals at frequencies above the filter's cut-off frequency (Butterworth 1930).

The filter approximates more the ideal Butterworth filter characteristics by increasing the filter's order. The degree of the pass-band flatness increases as the order N increases and the filter response becomes closer to the ideal 'brick-wall' type (Sedra, and Smith 2007). Thus, the complexity of the filter is determined by the filter's order.

It is also known that the roll-off rate, therefore, the width of the transition band, depends on upon the filter's order. For example, a 1st order classical integer-order Butterworth filter has a standard approximated roll-off rate of 20dB/decade. As the order increases by one, the approximated roll-off rate increases by 20dB/decade. The approximated filter will converge more towards, the ideal filter characterisation as the filter roll-off rate increases.

After this brief introduction to the Butterworth filter and the importance of the order selection, the following subsections describe how to approximate the transfer function of the fractional-order Butterworth filter and how to obtain its frequency response and group-delay.

5.5.1 Impractical generalised fractional-order Butterworth filter design

This section illustrates the issues, associated with the extension of generalised fractional-order Butterworth filter according to the generalised Butterworth magnitude squared function which leads to design a filter with a maximally flat gain frequency response. In this thesis, the approximated Butterworth filter is employed for the delayed fractional-order state variable design. Therefore, in this approximation, there is a consideration only to three parameters, which are (i) the number of energy-storage elements denoted N, (ii) base-order denoted α and (iii) cut-off angular frequency denoted ω_c, where $\alpha \in (0,1]$ and $N \in \mathbb{Z}$. The filter is assumed to be a commensurate-order filter whose order is αN.

The maximally flat squared gain function has been used to design the Butterworth filter whose base-order is unity, $\alpha = 1$. The squared magnitude function of the Butterworth filter, denoted $H(\omega)$, with cut-off frequency ω_c, was firstly proposed in (Butterworth 1930) and is expressed as:

$$\left|H(\omega)\right|^2 = \frac{1}{1+\mu^2\left(\frac{\omega}{\omega_c}\right)^{2N}} \tag{5.11}$$

where μ is a parameter responsible for determining the maximum variation band in pass-band transmission (Sedra and Smith 2007:1085). The flatness properties of the filter, which characterises equation (5.11), have been exploited by numerous authors; see for example (Schaumann, and Van Valkenburg 2001).

For simplicity, in this work μ is taken to be unity. The gain and phase frequency responses of the fractional-order systems are functions of ω^{α} not ω, as illustrated in Chapter 2. Therefore, the generalised integer-order Butterworth squared magnitude

function is extended to the generalised fractional-order Butterworth squared magnitude function by rescaling the ratio ω/ω_c in (5.11) by power of α and expressed as.

$$\left|H\left(\omega^{\alpha}\right)\right|^2 = \frac{1}{1+\left(\frac{\omega^{\alpha}}{\omega_c^{\alpha}}\right)^{2N}} \tag{5.12}$$

Figure 5-3 illustrates that the larger N the closer $\left|H(\omega^{\alpha})\right|^2$ is generated to the ideal squared magnitude.

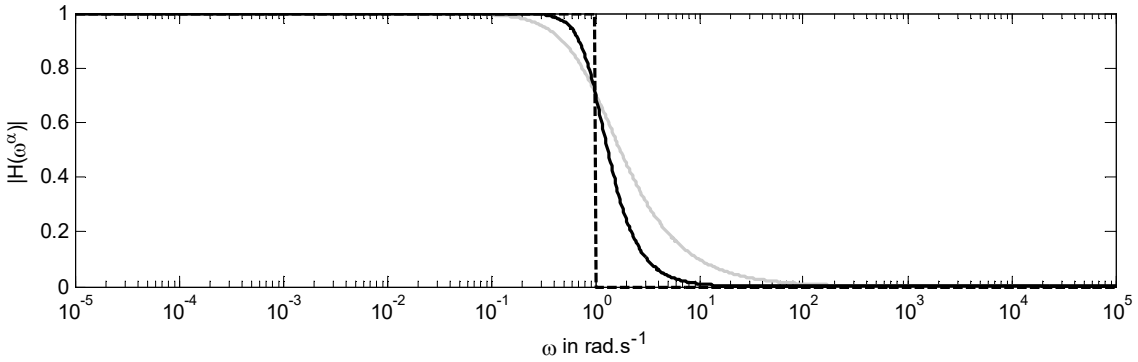

Figure 5-3: The ideal fractional-order Butterworth gain response is presented in black-dashed line and approximated fractional-order Butterworth gain $\left|H\left(\omega^{\alpha}\right)\right|$ in (5.12) when N=2 and 4, represented in solid-grey and solid- black, respectively where α=0.5 and ω_c=1.

Considering $\left|H\left(s^{\alpha}\right)H\left(-s^{\alpha}\right)\right|_{s^{\alpha}=(j\omega)^{\alpha}} = \left|H\left(\omega^{\alpha}\right)\right|^2$ and $\frac{s^{\alpha}|_{s=j\omega}}{j^{\alpha}} = \omega^{\alpha}$, the product of commensurate fractional-order transfer functions in the Laplace domain, which can generate the gain frequency response in (5.12), can be obtained and expressed as:

$$H\left(s^{\alpha}\right)H\left(-s^{\alpha}\right) = \frac{1}{1+\left(\frac{s^{\alpha}}{j^{\alpha}\omega_c^{\alpha}}\right)^{2N}} \tag{5.13}$$

The roots of the denominator in (5.13) can be determined according to the characteristic equation of (5.13) as follows:

$$1+\left(\frac{s^{\alpha}}{j^{\alpha}\omega_c^{\alpha}}\right)^{2N} = 0$$

$$\left(\frac{s^{2\alpha}}{j^{2\alpha}\omega_c^{2\alpha}}\right)^N = -1 = e^{j\pi} \tag{5.14}$$

Taking the N^{th} roots of both sides of (5.14) leads, where $k = 1,2,..,N$, to:

$$\frac{s^{2\alpha}}{j^{2\alpha}\omega_c^{2\alpha}} = e^{j\frac{(2k-1)\pi}{N}} \tag{5.15}$$

Now taking the square root of both sides of (5.15) and rearranging gives:

$$\begin{aligned} s_k &= \pm\omega_c^{\alpha} j^{\alpha} e^{j\frac{(2k-1)\pi}{2N}} \\ &= \pm\omega_c^{\alpha} e^{j\alpha\pi/2} e^{j(2k-1)\pi/2N} \end{aligned} \tag{5.16}$$

Since $j^{\alpha} = e^{j\alpha\pi/2}$, (5.16) can be expressed as:

$$s_k = \pm\omega_c^{\alpha} e^{j\alpha\pi/2} e^{j(2k-1)\pi/2N} \tag{5.17}$$

It then follows that:

$$s_k = \pm\omega_c^{\alpha}\left[\cos\left(\theta + \frac{(2k-1)\pi}{2N}\right) + j\sin\left(\theta + \frac{(2k-1)\pi}{2N}\right)\right] \tag{5.18}$$

where $\theta = \alpha\frac{\pi}{2}$, $s^{\alpha} = s_k$ is the k^{th} root of the denominators of both $H\left(s^{\alpha}\right)H\left(-s^{\alpha}\right)$ in (5.13) so that there are $2N$ roots in (5.18). In order to select the stable transfer function, there is a need to satisfy the stability condition of the commensurate form $\left|\arg(s_k)\right| > \frac{\alpha\pi}{2}$, see (Monje et al. 2010:22). Since, $0 < \alpha \le 1$, the phase of s_k in (5.18) is $\alpha\frac{\pi}{2} + \frac{(2k-1)\pi}{2N}$ and $0 < \frac{(2k-1)\pi}{2N} < \pi$, the positive complex number on the right-hand side of (5.18) always satisfies $\left|\arg(s_k)\right| > \frac{\alpha\pi}{2}$ so that it is selected to represent the roots. According to (5.13) and (5.18), the approximated fractional-order Butterworth transfer function can be described by a product of N root terms as:

$$H\left(s^{\alpha}\right) = \frac{1}{\prod_{k=1}^{N} s^{\alpha} - s_k} \tag{5.19}$$

where:

$$s_k = \omega_c^{\alpha}\left[\cos\left(\theta + \frac{(2k-1)\pi}{2N}\right) + j\sin\left(\theta + \frac{(2k-1)\pi}{2N}\right)\right] \tag{5.20}$$

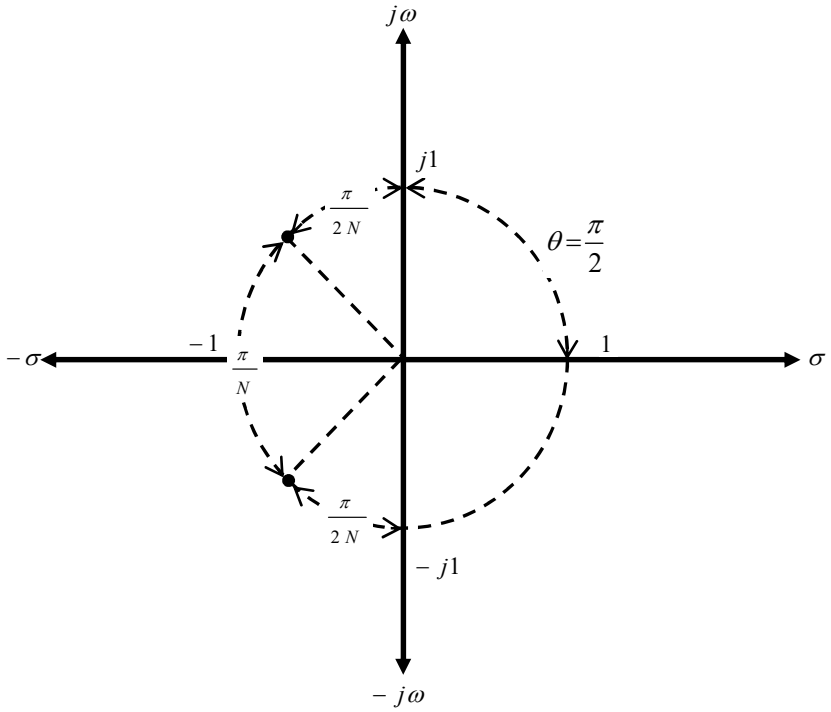

Figure 5-4: The bold dots represent locations of the poles of the approximated fractional-order Butterworth transfer function in the complex plane when α=1 and ω_c=1.

(5.20) shows that the roots are located on a circle of radius ω_c^{α}.

Figure 5-4 demonstrates that all roots of the denominator of the fractional-order Butterworth filter are located on the unit circle (i.e. for $\omega_c^{\alpha} = 1$). Furthermore, $\arg(s_1)$ on the complex plane is $\theta + \pi/2N$, while the phase of other roots $\arg(s_k) = \arg(s_{k-1}) + \pi/N$ where $k = 2,3\ldots N$. Therefore, it can be noted that the extension to the fractional-order Butterworth transfer function rotates all the roots of classical integer $\alpha = 1$ Butterworth transfer function by $(\alpha - 1)\frac{\pi}{2}$.

Figure 5-4 also illustrates when $\alpha \neq 1$, it leads to the complex roots that are not complex conjugate pairs. Consequently, it generates a polynomial containing complex coefficients in the denominator of (5.19). For instance, if $N = 2$ and $\alpha = 0.3$, (5.19) becomes:

$$\begin{aligned} H(s) &= \frac{1}{\left(s^{0.3} - (\ 0.3090 + 0.9511j)\right)\left(s^{0.3} - (-0.9511 + 0.3090j)\right)} \\ &= \frac{1}{s^{0.6} - (\ 0.642 - 1.26j)s^{0.3} - 0.588 - 0.809j} \end{aligned} \tag{5.21}$$

This cannot be numerically solved due to the nature of the complex coefficients. However, it does provide 'stepping' stone in the development of a practical realisation.

In this thesis, three different approaches are proposed for designing the maximally flat gain for any arbitrary selected real order. Two of the proposed approaches are derived from the integer-order Butterworth filter so that the frequency response and group-delay of proposed fractional-order Butterworth filter are the same as the integer-order Butterworth filter. The numerical implementations based on the state-space representation, phase and group-delay of integer-order Butterworth filter, are presented in the following subsections.

5.5.1.1 Numerical implementation of the integer-order Butterworth filter

There are several approaches used to express the ordinary differential equations. One of them is the state-space representation whose diagrammatic representation can be mapped into an equivalent block diagram as shown in Figure 5-5. The equivalent block diagram of an integer-order Butterworth filter can be consequently implemented in Simulink. It is then numerically solved at each sample by using one of the Simulink solvers such as the Euler or Runge-Kutta solver. Collecting the derivative terms of the signals becomes more obvious and simpler as demonstrated in Figure 5-5. Therefore, the focus in this section is on the state-space representation of an integer-order Butterworth filter and how it could be mapped into an equivalent block diagram.

In the case of the integer-order Butterworth filter, there is a need to determine the denominator coefficients of (5.19) when $\alpha = 1$. This is achieved by solving (5.19) or finding them in (Winder, 2002) and consequently, (5.19) becomes:

$$H_{BW}(s) = \frac{b_0}{s^N + a_1 s^{N-1} + \ldots + a_N} \tag{5.22}$$

where the subscript BW refers to Butterworth. (5.22) can be then converted to state-space form in the time-domain and expressed as:

$$\begin{bmatrix} \dot{x}_1 \\ \dot{x}_2 \\ \vdots \\ \dot{x}_{N-1} \\ \dot{x}_N \end{bmatrix} = \begin{bmatrix} 0 & 1 & 0 & \cdots & 0 \\ 0 & 0 & 1 & \ddots & 0 \\ \vdots & \vdots & \ddots & \ddots & 0 \\ 0 & 0 & \cdots & 0 & 1 \\ -a_N & -a_{N-1} & \cdots & -a_2 & -a_1 \end{bmatrix} \begin{bmatrix} x_1 \\ x_2 \\ \vdots \\ x_{N-1} \\ x_N \end{bmatrix} + \begin{bmatrix} 0 \\ 0 \\ \vdots \\ 0 \\ 1 \end{bmatrix} u(t) \tag{5.23}$$

$$v(t) = \begin{bmatrix} b_0, & 0, & \cdots & 0, & 0 \end{bmatrix} \begin{bmatrix} x_1 \\ x_2 \\ \vdots \\ x_{N-1} \\ x_N \end{bmatrix} \tag{5.24}$$

Consequently, the diagrammatic representation in the equivalent block diagram of (5.23) and (5.24) is provided in Figure 5-5. All blocks in Figure 5-5 are available in the Simulink library. Thus, the equivalent block diagram can be implemented in Simulink so that the derivative terms of the Butterworth output can be sampled and collected as shown in Figure 5-5.

5.5.1.2 Phase frequency response of the integer-order Butterworth filter

The phase frequency response of the system, whose transfer function is $H(s)$, is the sum of the phase frequency response curves of the zero terms minus the sum of the phase frequency response curves of the pole terms (Nise 2011). $H(s)$ is an all pole-filter (there are no zeros), this way the frequency response phase can be expressed as:

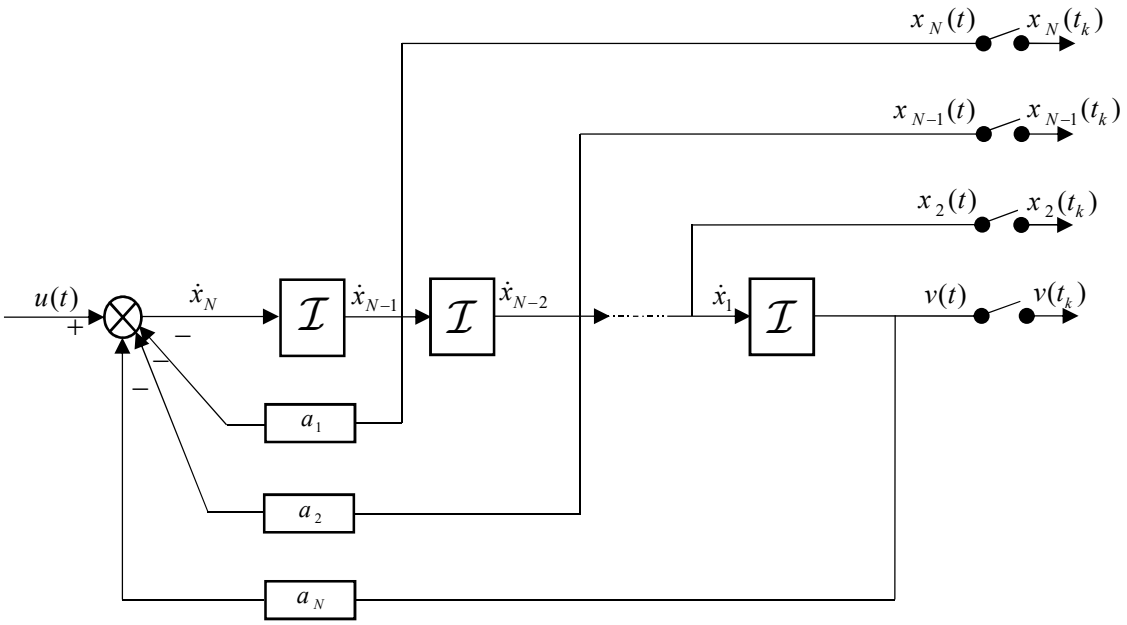

Figure 5-5: Equivalent block diagram to the state-space representation of the *N* order integer-order Butterworth filter in (5.23) and (5.24) where b_0=1.

$$\phi_{BW} = \angle H(j\omega) = -\sum_{k=1}^{N} \tan^{-1}\left(\frac{-\omega_c \sin\left(\frac{\pi}{2} + \frac{(2k-1)\pi}{2N}\right) + \omega}{-\omega_c \cos\left(\frac{\pi}{2} + \frac{(2k-1)\pi}{2N}\right)} \right) \tag{5.25}$$

where subscript BW refers to Butterworth. (5.25) shows that the phase response is not uniformly proportional to frequency and so that it leads to produce different delay times for different frequencies. Thus, it generates a non-constant group-delay.

5.5.1.3 Group-delay of the integer-order Butterworth filter

Group-delay is the term used for describing the time delay in the different frequency relationships of the transmitted signal. It is defined as the negative rate of change of the phase with respect to angular frequency. The term group-delay is very descriptive and is the delay seen by a group of frequencies, transmitted through a filter. A constant group-delay implies that all frequencies experience the same delay. A frequency dependent group-delay implies that some frequencies are delayed more than others (Windor 2002).

The group-delay of the integer-order Butterworth, $\alpha = 1$, is the time needed for each frequency to pass through the system and expressed as:

$$T_{BW}(\omega) = -\frac{d\phi_{BW}(\omega)}{d\omega} \tag{5.26}$$

$$T_{BW}(\omega) = \sum_{k=1}^{N} \frac{\omega_c \cos\left(\pi\frac{1}{2} + \pi\frac{2k-1}{2N}\right)}{\omega_c^2 - 2\omega_c\omega\sin\left(\pi\frac{1}{2} + \pi\frac{2k-1}{2N}\right) + \omega^2} \tag{5.27}$$

Figure 5-6 shows that the Butterworth filter has an almost flat group-delay in low and high frequencies with sharp group-delay around the cut-off frequency. The higher the order Butterworth filter generates the larger the difference in group-delay between low and high frequencies.

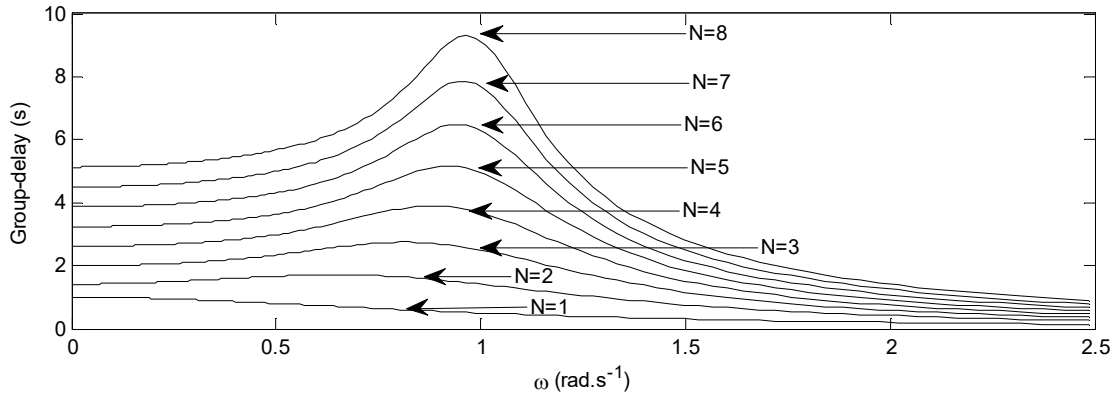

Figure 5-6: Group-delay in (s) of the integer-order Butterworth filter whose order *N*=1:8 and ω_c=1.

5.5.2 Practical approximated fractional-order Butterworth Transfer Function

Several authors have published how to extend the approximated integer-order to a fractional-order Butterworth filter. For example, (Soltan, Rawan, and Soliman 2011) has extended a two element Butterworth filter to a fractional-order in the case of the commensurate order. This is achieved by transforming the Butterworth filter to frequency-domain, and then the generated nonlinear equation is optimised to obtain the best flat gain with consideration given to the stability. It has then been extended to have two different non-equal base-orders for non-commensurate order in (Soltan, Rawan, and Soliman 2012). However, these are not straightforward solutions. Rather they depend on

knowledge and experience associated with the limited order. For two element circuit, it is relatively easy and it then becomes more complex as the number of elements increases.

If the target is to design the fractional-order Butterworth approximation for obtaining the maximally flat magnitude for any arbitrary $\alpha \in (0,1]$, it leads to a numerical issue as shown in (5.21). This is because the roots are not straightforward complex conjugates.

This section demonstrates how the maximally flat fractional-order Butterworth filter can be obtained with restricted a base-order $\alpha = 1/2^n$ where $n = 1,2,\ldots$. Although this is limited with restricted fractions, it is very helpful. This is because the most popular fractional-order is $\alpha = 1/2$. This can be seen in diffusion system, electrode-electrolyte interface impedance, battery dynamics, di-electric the capacitance impedance some examples of the electronics operational amplifier circuits, fractance circuit and more examples are illustrated in (Das 2011).

Nonetheless, the generalised fractional-order Butterworth filter is also proposed in compartmental fractional-order Butterworth filter form. It is obtained by considering a few properties of the fractional-order calculus for generating the fractional-order derivative terms of the Butterworth filter.

5.5.2.1 Fractional-order Butterworth filter of base-order $\alpha = 0.5$ design

The approximated fractional-order Butterworth filter should be designed with respect to simplicity and generalisation with avoiding the optimisation techniques as introduced in (Soltan, Rawan, and Soliman 2011). This section shows how the proposed fractional-order Butterworth filter with $\alpha = 0.5$ can be derived from the impractical Butterworth filter based on two observations:

I. The first observation: The frequency response of the fractional-order Laplace variable $s^{0.5}$ generates equal magnitudes of the imaginary and real numbers:

$$s^{0.5}\Big|_{s=j\omega} = \left(j\omega\right)^{0.5} = \left(0.7071 + j0.7071\right)\omega^{0.5} \tag{5.28}$$

II. The second observation: According to the fractional-order Butterworth filter of base-order $\alpha = 0.5$, derived from (5.20), the real and imaginary numbers of the complex roots when *k*=1*:N/*2 is equal to the imaginary and negative real of the complex roots when *k*=1*+N/*2*:N*, respectively. When $\omega_c^{0.5} = 1$, base-order $\alpha = 0.5$ and k is described by an arbitrary integer number $\psi \in \mathbb{Z}$ and $\psi = 1, 2, \cdots, N/2$, the fractional-order Butterworth filter roots for *k*=1*:N/*2 and *k*=1*+N/*2*:N* can be described as:

$$s_{k=\psi} = \cos\left(\frac{1}{4}\pi + \frac{(2\psi - 1)\pi}{2N}\right) + j\sin\left(\frac{1}{4}\pi + \frac{(2\psi - 1)\pi}{2N}\right) \tag{5.29}$$

and

$$s_{k=\psi+\frac{N}{2}} = \cos\left(\frac{1}{4}\pi + \frac{(2(\psi + \frac{N}{2}) - 1)\pi}{2N}\right) + j\sin\left(\frac{1}{4}\pi + \frac{(2(\psi + \frac{N}{2}) - 1)\pi}{2N}\right) \tag{5.30}$$

respectively. By considering $\cos\left(x\right) = -\sin\left(x + \frac{1}{2}\pi\right)$ and $\sin\left(x\right) = \cos\left(x + \frac{1}{2}\pi\right)$ in (5.30), (5.30) can be written as:

$$s_{k=\psi+\frac{N}{2}} = -\sin\left(\frac{1}{4}\pi + \frac{(2\psi - 1)\pi}{2N}\right) + j\cos\left(\frac{1}{4}\pi + \frac{(2\psi - 1)\pi}{2N}\right) \tag{5.31}$$

This satisfies the second observation.

It can be assumed that if $a_\psi = \sin\left(\frac{1}{4}\pi + \frac{(2\psi - 1)\pi}{2N}\right)$ and $b_\psi = \cos\left(\frac{1}{4}\pi + \frac{(2\psi - 1)\pi}{2N}\right)$ then (5.29) and (5.31) can be re-expressed as:

$$s_{k=\psi} = b_\psi + ja_\psi \tag{5.32}$$

and

$$s_{k=\psi+\frac{N}{2}} = -a_\psi + jb_\psi \tag{5.33}$$

The frequency gain response of the impractical fractional-order Butterworth filter with base-order $\alpha = 0.5$ according to (5.32) and (5.33) can be expressed as:

$$\left|H_{bw}(j^{0.5}\omega^{0.5})\right| = \prod_{k=1}^{N/2}\left[\left|\frac{1}{\omega^{0.5}\left(0.7071+j0.7071\right)-(b_k+ja_k)}\right| \left|\frac{1}{\omega^{0.5}\left(0.7071+j0.7071\right)-(-a_k+jb_k)}\right|\right] \tag{5.34}$$

By considering the two aforementioned observations (5.34) can be reformulated as:

$$\left|H_{bw}(j^{0.5}\omega^{0.5})\right| = \prod_{k=1}^{N/2}\left[\left|\frac{1}{\omega^{0.5}\left(0.7071+j0.7071\right)-(b_k+ja_k)}\right| \left|\frac{1}{\omega^{0.5}\left(0.7071+j0.7071\right)-(-b_k+ja_k)}\right|\right] \tag{5.35}$$

The fractional-order Butterworth filter in (5.35) is a practical filter because there are $N/2$ pairs of conjugates when $N>2$ and an even number. The first $1{:}N/2$ roots and their conjugates are selected not $1{+}N/2{:}\ N$ roots and their conjugates because they guarantee the stability. For example, when $N=2, \alpha=0.5$ in (5.20), there are two roots, represented the impractical generalised fractional-order Butterworth filter and its transfer function is:

$$H_{bw}(s^{0.5}) = \frac{1}{(s_1^{0.5}-(1j))((s_2^{0.5}-(-1)))} \tag{5.36}$$

It can be noted that, if the second complex root is reformatted by swapping the complex and imaginary, the resulting complex number is the conjugate of the first roots:

$$\begin{aligned}\left|H_{bw}(j^{0.5}\omega^{0.5})\right| &= \left|\frac{1}{(j\left(0.7071+j0.7071\right)\omega^{0.5}-(1j))(\left(0.7071+j0.7071\right)\omega^{0.5}-(-1))}\right| \\ &= \left|\frac{1}{j\left(0.7071+j0.7071\right)\omega^{0.5}-(1j)}\right|\left|\frac{1}{\left(0.7071+j0.7071\right)\omega^{0.5}-(-1)}\right|\end{aligned}$$

It can be seen that if the imaginary and real numbers of the second root are swapped, the gain frequency response of the Butterworth filter will not be affected.

$$\left|H_{bw}(j^{0.5}\omega^{0.5})\right| = \left|\frac{1}{(0.7071+j0.7071)\omega^{0.5}-(1j)}\right|\left|\frac{1}{(0.7071+j0.7071)\omega^{0.5}-(-1j)}\right| \tag{5.37}$$

As a result, only the first $N/2$ roots are selected and their conjugates are used to complete N roots. However when *N*=2, the fractional-order Butterworth filter as shown in (5.37) still have polynomials with complex coefficients if treated as two subsystems or it becomes an integer-order Butterworth filter if it is treated as one system as shown, respectively, in the following equations:

$$H_{bw}(s^{0.5}) = \left[\frac{1}{s^{0.5}-(1j)}\right]\left[\frac{1}{s^{0.5}-(-1j)}\right] \tag{5.38}$$

and

$$H_{bw}(s^{0.5}) = \frac{1}{s+1} \tag{5.39}$$

Therefore, *N* must be an even number and greater than 2, for example, when *N*=4 the fractional-order Butterworth filter can be described by two subsystems and expressed as:

$$\begin{aligned} H_{BW}(s^{0.5}) &= \frac{1}{(s^{0.5}-0.3827\pm j0.9239)(s^{0.5}+0.3827\pm j0.9239)} \\ &= \frac{1}{(s-0.7654s^{0.5}+1)}\frac{1}{(s+0.7654s^{0.5}+1)} \end{aligned} \tag{5.40}$$

The roots of the generalised fractional-order Butterworth filter with $\alpha = 0.5$ in (5.19) can be obtained as:

$$s_k = \omega_c^{0.5}\left[\cos\left(\frac{1}{4}\pi + \frac{(2k-1)\pi}{2N}\right) \pm j\sin\left(\frac{1}{4}\pi + \frac{(2k-1)\pi}{2N}\right)\right] \tag{5.41}$$

For $k = 1,2,...,N/2$ and N is restricted to be an even number and greater than 2 and the fractional-order Butterworth filter is described by two subsystems.

The development of the base-order $\alpha = 0.5$ Butterworth filter is a special case of the second design approach of the base-order $\alpha = \frac{1}{2^n}$, where *n* is a positive integer. Whilst the $\alpha = 0.5$, concluded here, is not taken further, it has provided an insight into the realisation

of fractional-order Butterworth filter design. In the next section, it will be shown that when *n*=1 both approaches here identical transfer functions.

5.5.2.2 Square root base design (base-order $\alpha = 1/2^n$ of the fractional-order Butterworth filter)

This section demonstrates how the maximally flat gain frequency response of fractional-order Butterworth filter can be obtained with a restricted order $\alpha = 1/2^n$ and $n = 1,2,\ldots$.

There are *N* root terms $\prod_{k=1}^{N} s^{\alpha} - s_k$ in (5.19). When $\alpha = 1$ and *N* is an even number, the roots s_k in (5.19) are given by *N*/2 complex numbers and their *N*/2 complex conjugates and denoted $\overline{s_k}$. Each root term is considered to be a quadratic function, described by a difference of two squares (s and s_k), and expressed in the standard quadratic form and factored form as:

$$\underbrace{s - s_k}_{\text{Standard quadractic form}} = \underbrace{(\sqrt{s} - \sqrt{s_k})(\sqrt{s} + \sqrt{s_k})}_{\text{Factored quadratic form}} \tag{5.42}$$

The factored quadratic form can be obtained by considering the square root of the complex number according to De Moivre's theorem:

$$\sqrt[q]{s_k} = \sqrt[q]{|s_k|}\left[\cos\left(\frac{\arg(s_k)}{q} + \frac{2\pi a}{q}\right) + j\sin\left(\frac{\arg(s_k)}{q} + \frac{2\pi a}{q}\right)\right] \tag{5.43}$$

where $a = 0,1$ and N is assumed to be an even number. From (5.42), it follows that each root term has two different complex roots $\sqrt{s} = \pm\sqrt{s_k}$. The same techniques are applied to the root term which contains the complex conjugate $\overline{s_k}$ so that the two different conjugate roots $\pm\sqrt{\overline{s_k}}$ are produced. For example, if $N = 2$, the integer-order Butterworth denominator of (5.19) is described as a product of two root terms as:

$$H_{BW}(s)=\frac{1}{(s-(-\sqrt{2}/2+j\sqrt{2}/2))(s-(-\sqrt{2}/2-j\sqrt{2}/2))} \tag{5.44}$$

where $\omega_c=1$. The factored form of the root term which contains one complex root and the root term which contains the conjugate root can be obtained from (5.42) and (5.43) as follows:

$$\begin{aligned}(s-(-\sqrt{2}/2+j\sqrt{2}/2))&=(s^{0.5}+(0.3827+j0.9239))(s^{0.5}-(0.3827+j0.9239))\\(s-(-\sqrt{2}/2-j\sqrt{2}/2))&=(s^{0.5}-(0.3827-j0.9239))(s^{0.5}+(0.3827-j0.9239))\end{aligned} \tag{5.45}$$

The fractional-order Butterworth transfer function of half-base order, derived from (5.44), is expressed as:

$$\begin{aligned}H_{BW}(s^{0.5})=\frac{1}{[&(s^{0.5}-0.3827+j0.9239)(s^{0.5}-0.3827-j0.9239)\\&(s^{0.5}+0.3827+j0.9239)(s^{0.5}+0.3827-j0.9239)]\end{aligned} \tag{5.46}$$

However, in order to avoid returning to the integer-order Butterworth transfer function, the fractional-order Butterworth transfer function must be described by two subsystems as following:

$$H_{BW}(s^{0.5})=\frac{1}{(s-0.7654s^{0.5}+1)}\frac{1}{(s+0.7654s^{0.5}+1)} \tag{5.47}$$

From (5.47), all the fractional-order derivative terms can be obtained, which can then be used in the identification process. From (5.40) and (5.47), it can be seen that the fractional-order Butterworth filter of base-order $\alpha=0.5$ design and square root base design give an identical fractional-order Butterworth filter.

This can then be factored into eight root terms of base-order 0.25, and it is expressed as:

$$\begin{aligned}H_{BW}(s^{0.25})=\frac{1}{[&(s^{0.25}-0.8315+j0.5556)(s^{0.25}-0.8315-j0.5556)\\&(s^{0.25}+0.5556+j0.8315)(s^{0.25}+0.5556-j0.8315)\\&(s^{0.25}+0.8315+j0.5556)(s^{0.25}+0.8315-j0.5556)\\&(s^{0.25}-0.5556+j0.8315)(s^{0.25}-0.5556-j0.8315)]\end{aligned} \tag{5.48}$$

The N root terms of the integer-order Butterworth transfer function produce $2^n N$ root terms of the fractional-order Butterworth filter of base-order $\alpha = 1/2^n$. For example, the first order Butterworth transfer function generates 2 root terms of a fractional-order Butterworth filter of base-order $\alpha = 0.5$.

The Butterworth filter of base-order $\alpha = 0.25$ in (5.48) can be described by two subsystems of first order s or two subsystems whose orders are 1.5 $s^{1.5}$ and 0.5 $s^{0.5}$, as shown in Figure 5-7, and, respectively, expressed as:

$$\begin{aligned} H_{BW}(s^{0.25}) &= \frac{1}{\left[(s+0.5518s^{0.75}+0.1522s^{0.5}+0.5518s^{0.25}+1)\right.} \\ &\quad \left.(s-0.5518s^{0.75}+0.1522s^{0.5}-0.5518s^{0.25}+1)\right] \\ &= \frac{1}{(s^{1.5}-1.6629s^{1.25}+1.7654s-1.2728s^{0.75}+} \\ &\quad 1.7645s^{0.5}-1.6629s^{0.25}+1)(s^{0.5}+1.6629s^{0.25}+1) \end{aligned} \tag{5.49}$$

The following algorithm can be used to directly generate the roots of the denominator of the fractional-order Butterworth filter of base-order $\alpha = 1/2^n$:

$r = 0$

for $k = 1:N$

$\theta = \pi\left(1/2 + (2k-1)/2N\right)$

for $a = 0:m-1$

$r = r+1$

$$s_r^{1/2^n} = \sqrt[m]{\omega_c}\left[e^{j\left(\theta/m + 2a\pi/m\right)}\right] \tag{5.50}$$

end

end

where $m = 2^n$, $M = mN$, $a = 0,1,...m-1$ and $k = 1,2,...,N$.

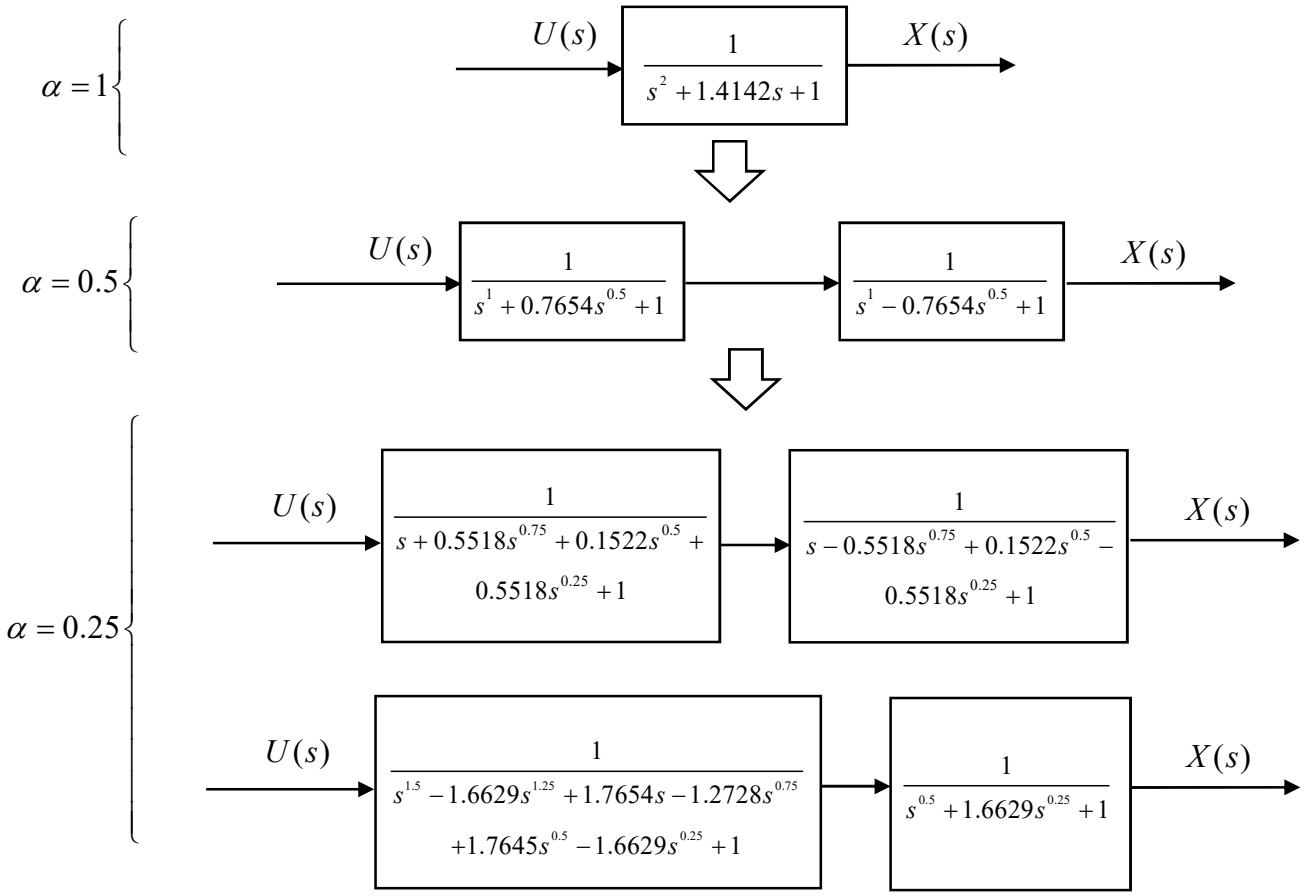

Figure 5-7: Fractional-order Butterworth filter of base-order α=0.5 and α=0.25 ω_c=1, derived from integer-order Butterworth filter where *U(s)* and *X(s)* are the input and output of Butterworth filter, respectively.

The proposed fractional-order Butterworth filter is derived from the integer-order Butterworth filter. Therefore, the frequency response and the group-delay are similar to the frequency response and the group-delay of the integer-order Butterworth filter. The group-delay of the integer-order Butterworth filter is shown in Figure 5-6. Furthermore, the proposed fractional-order filter is always stable because it is derived from a stable integer-order Butterworth filter.

Summary of the square root base design:

I. Design the classical integer-order Butterworth filter.

II. Obtain the factored quadratic form of each root term of the integer-order Butterworth transfer function by using the complex square roots in (5.43) for generating the root terms of the fractional-order Butterworth filter of base-

order $\alpha = 1/2$. The fractional-order Butterworth filter of base-order $\alpha = 1/4$ is then derived from the fractional-order Butterworth filter of base-order $\alpha = 1/2$ likewise, the fractional-order Butterworth filter of base-order $\alpha = 1/2^p$ is then derived from the fractional-order Butterworth filter of base-order $\alpha = 1/2^{p-1}$ until the targeted base-order is obtained. Furthermore, the roots of the denominator of the fractional-order Butterworth transfer function of the targeted base-order could be directly derived from the integer-order Butterworth transfer function by using (5.50).

5.5.2.3 Compartmental fractional-order Butterworth filter design

Building on the above development, the compartmental fractional-order Butterworth filter is also derived from the integer-order Butterworth filter. The goal of this approach is to approximate the higher fractional-order derivative terms of the fractional-order Butterworth output. The fractional-order Butterworth state-space representation can be given in a diagrammatic form. Every integer-order integral term is compartmentally divided into its equivalent fractional-order integral terms, based on the semigroup property of the fractional-order integral of the arbitrary order $\mathcal{I}^{\alpha}\,\mathcal{I}^{\beta} = \mathcal{I}^{\alpha+\beta}$ (Uchaikin 2013). Therefore, the integer-order integral block in equivalent block diagram form can be represented by sum of the fractional-order integral blocks. This is additional to the property of the fractional-order calculus, which is the fractional-order derivative term is the left inverse of the fractional-order integral term $\mathcal{D}^{\alpha}\,\mathcal{I}^{\alpha} = \mathrm{I}$, $\mathcal{I}^{\alpha}\,\mathcal{D}^{\alpha} \neq \mathrm{I}$, where I denotes the identity or unity. The fractional-order integral term is the left inverse of the fractional-order derivative term only with zero initial conditions, i.e. $\mathcal{I}^{\alpha}\,\mathcal{D}^{\alpha} = \mathrm{I}$ (Monje et al. 2010:11). Consequently, any fractional-order derivative term can be then obtained. This approach can be summarised into two steps as follows:

I. By taking advantage of the fact that when considering zero initial conditions the inverse operator of the fractional-order integral term is the left inverse of the fractional-order derivative term $\mathcal{I}^{\alpha}\mathcal{D}^{\alpha}=\mathrm{I}$. Therefore, any fractional-order derivative term can then be numerically approximated from the fractional-order integral as shown in Figure 5-8.

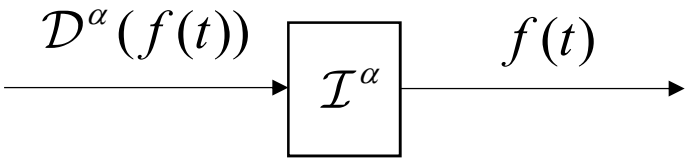

Figure 5-8: A block diagram of the fractional-order integral block.

II. Using semigroup property of the fractional-order integral of the arbitrary order $\mathcal{I}^{\alpha}\mathcal{I}^{\beta}=\mathcal{I}^{\alpha+\beta}$ leads to the first order integral block, shown in Figure 5-5, to be split up into compartmental form to produce the targeted order. For example, if there is a need to approximate the $\alpha=0.7$ derivative term of the output signal $v(t)$ of the Butterworth filter in Figure 5-5 whose order $N=1$, the first order integral block can be divided into the $\alpha=0.3$ and $\beta=0.7$ order integral blocks $\mathcal{I}^{0.3}\mathcal{I}^{0.7}=\mathcal{I}$, as shown in Figure 5-9.

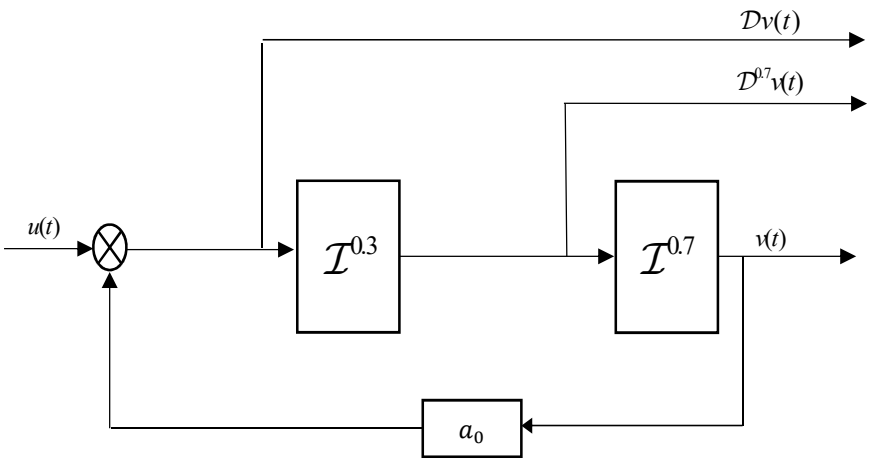

Figure 5-9: Compartmental fractional-order Butterworth filter of first order Butterworth filter for approximating the fractional-order derivative term $\mathcal{D}^{0.7}v(t)$.

5.5.2.4 Comparison of the proposed approaches

Three approaches for designing the fractional-order Butterworth filter have been developed in this thesis but only the square root base design and compartmental fractional-order Butterworth filter design are selected for comparison. This is because the Butterworth filter of base-order $\alpha = 0.5$ design is a subclass of the square root base design when the base-order is $\alpha = 0.5$ (i.e. n=1).

This comparison is for the selection of one approach to be used in approximating the higher fractional-order derivative terms of the output of the Butterworth filter. Accordingly, in this section, an illustrative example is used as a benchmark to evaluate the performance of the two proposal approaches. The second order classical Butterworth filter is used as a reference to validate both approaches and used for approximation of the higher fractional-order derivative terms. For instance, Butterworth output $v(t)$ and $\mathcal{D}^{0.25}v(t)$ are the collected targets. The square root base approach for the second order Butterworth filter is shown in

Figure 5-10. It can be observed that this approach has eight fractional-order integral blocks. This means more computational time is required, while the compartmental fractional-order Butterworth filter has only three fractional-order integral blocks as illustrated in Figure 5-11.

The simulation runs for 5 s by using Simulink and MATLAB®. The solver is selected to be Runge-Kutta with 0.001 sampling time. Fractional-order integral blocks are from The FOMCON Simulink block library where approximation order and frequency range are set to fifth order and [0.001; 100] rad.s^{-1}, respectively. The input is selected as a sum of the sinusoid signals within the range of the fractional-order integral blocks range as illustrated in Figure 5-12. The integral of the absolute error (IAE) between the output and higher fractional-order derivative terms, obtained from integer-order Butterworth filter,

are compared with those obtained by the compartmental and square root base fractional-order Butterworth filter.

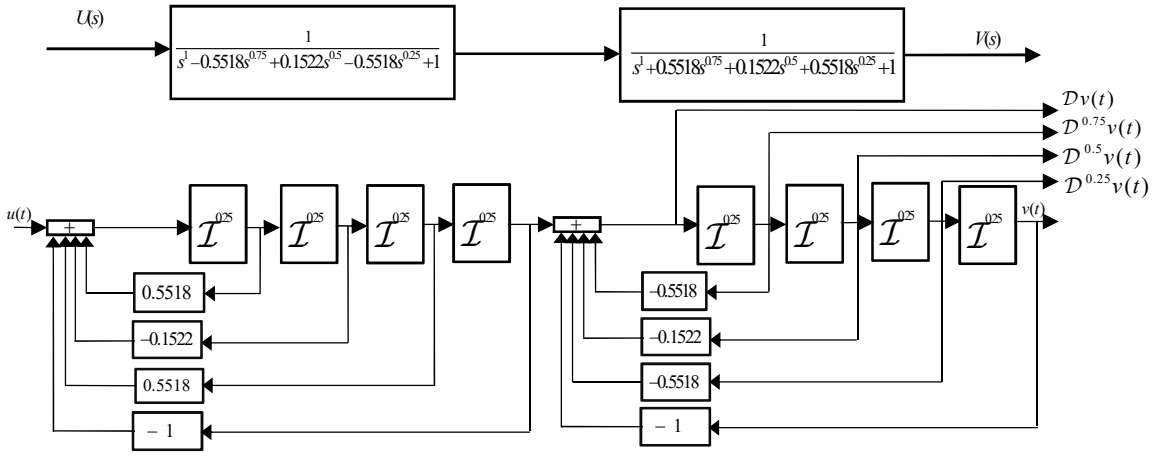

Figure 5-10: The upper part shows the transfer function of the two subsystems representing fractional-order-Butterworth filter and the equivalent block diagram by applying square root base for base-order $\alpha=1/2^n$ where $\alpha=1/4$ and $\omega_c=1$.

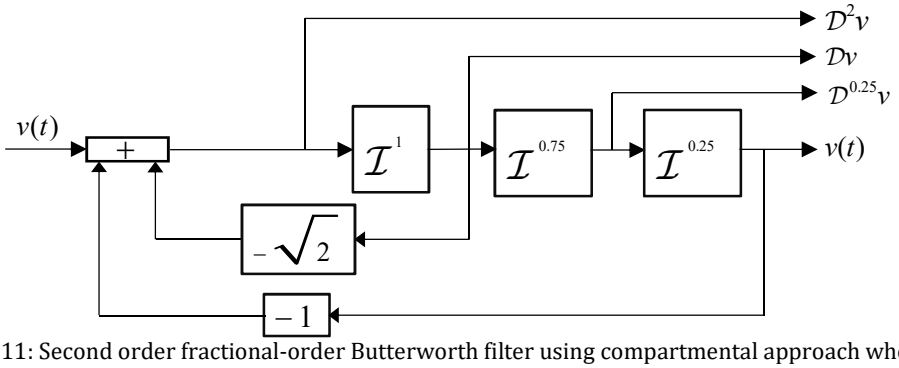

Figure 5-11: Second order fractional-order Butterworth filter using compartmental approach where $\omega_c=1$.

The Butterworth filter output, the $\mathcal{D}v(t)$ terms based on the three different designs and the $\mathcal{D}^{0.25}v(t)$ terms of both fractional-order filter designs are shown in Figure 5-13, Figure 5-14, Figure 5-15 and Table 5-1. From Table 5-1 it can be seen that compartmental fractional-order Butterworth filter provides a better approximation to the reference filter, i.e. classical Butterworth filter, as compared to square root base Butterworth filter in terms of IAE measure. This improved filtering performance of compartmental fractional-order Butterworth filter is further visible in Figure 5-13 and Figure 5-14, where it can be seen that the filtered signals are closer to their reference counterpart. This error occurs due to the numerical error associated with each fractional-order integral block.

Furthermore, this is because more fractional-order integral blocks are used for square root base Butterworth filter. The results, obtained from Figure 5-13 and Table 5-1, favour selection of the compartmental approach over the square root approach and are summarised as:

I. The design process of the compartmental approach is considerably simpler than square root base approach.

II. The compartmental approach can be applied to obtain any fractional-order, which is not the same case with the square root base approach once it is limited with base-order $\alpha = 1/2^n$.

III. A higher numerical accuracy is achieved by using compartmental approach than square root base approach for approximation of the same fractional-order derivative term.

IV. The computational time of the compartmental approach is rather smaller than the computational time of the square root approach.

V. The compartmental approach showed better ability in producing any arbitrary fractional-order derivative terms leads to this being the favourable method and increases the capability to adopt with non-commensurate systems.

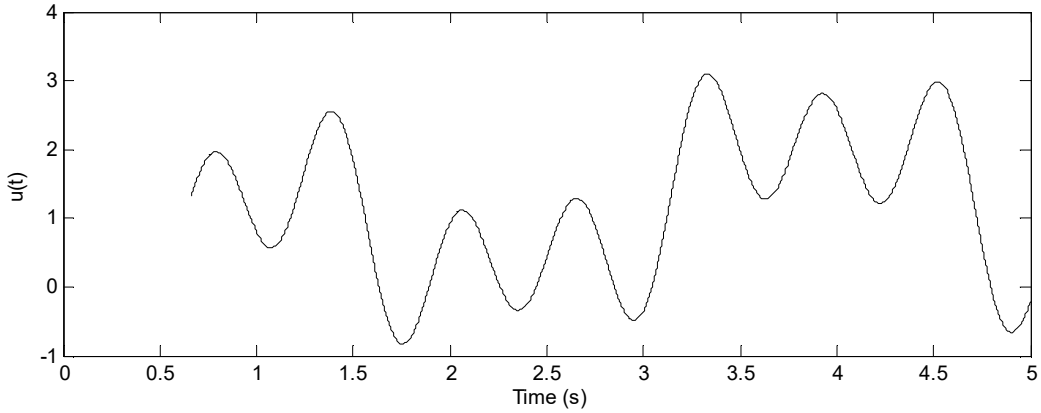

Figure 5-12: Input is used for simulation.

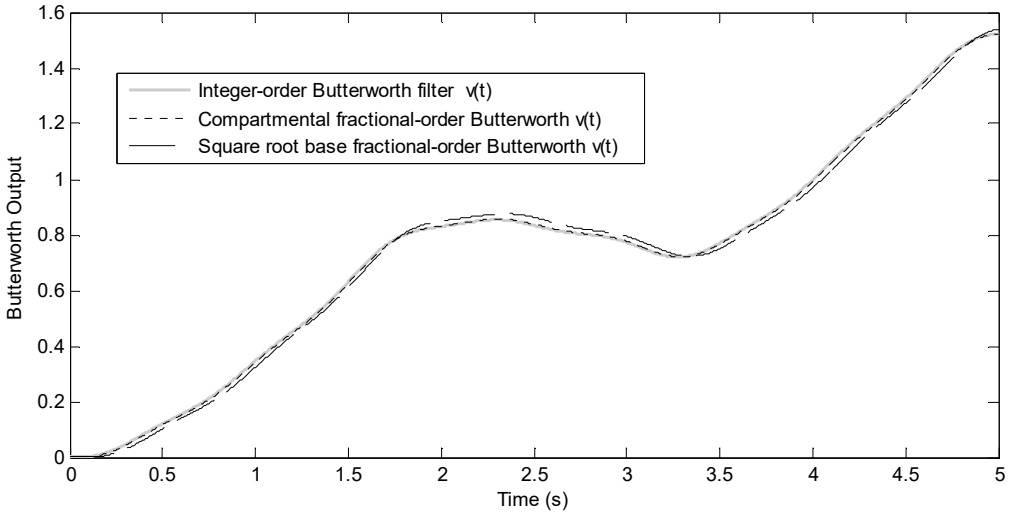

Figure 5-13: Bold grey solid-line is the integer-order Butterworth filter output $v(t)$, black doted-line and black dashed-line represent the compartmental fractional-order Butterworth output $v(t)$ and the square root base fractional-order Butterworth filter output $v(t)$, respectively.

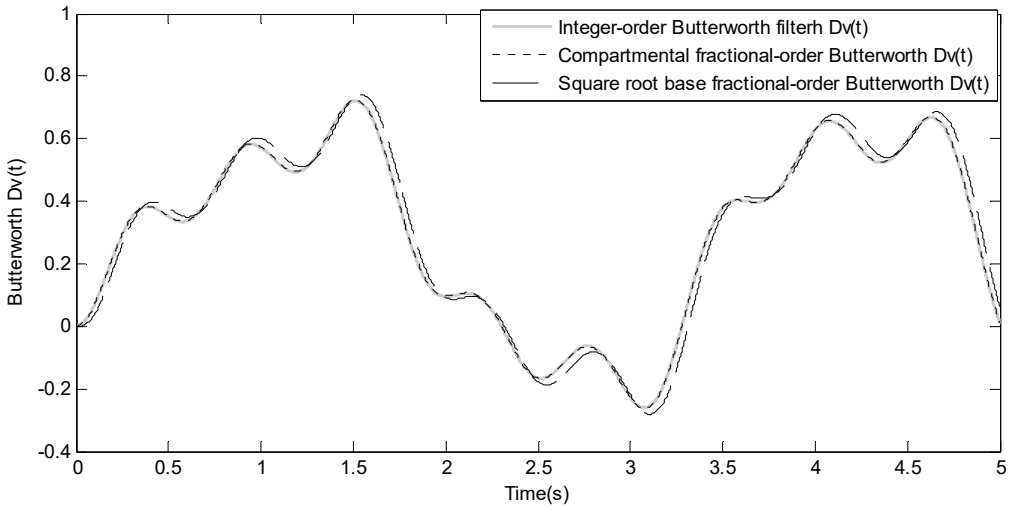

Figure 5-14: Bold grey solid-line is the derivative term $\mathcal{D}v(t)$ of the integer-order Butterworth filter and black doted-line and black dashed-line represent the derivative terms $\mathcal{D}v(t)$ of the compartmental fractional-order Butterworth and the square root base fractional-order Butterworth filter, respectively.

Table 5-1. The calculated IAE performance measure together with corresponding frequency ranges for different integer model orders of approximated fractional-order models.

	Integer-order Butterworth filter	*Compartmental fractional-order Butterworth filter*	*Square root base fractional-order Butterworth filter*
Computational time	0.4228s	0.9568s	1.0270s
$IAE(v)$	0	0.0036	0.0180
$IAE(D^1 v)$	0	0.0015	0.0262

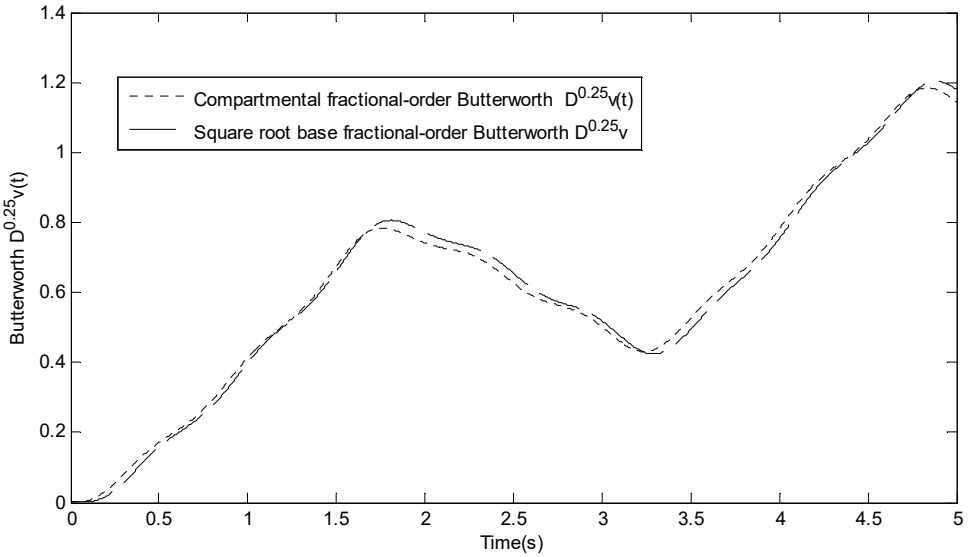

Figure 5-15: Black doted-line and black dashed-line represent the derivative terms $\mathcal{D}^{0.25}v(t)$ of the compartmental fractional-order Butterworth and the square root base fractional-order Butterworth filter, respectively.

5.6 All-pass filter

It is named as all-pass filter because it gives a constant magnitude ratio between numerator $\left|N(-j\omega)\right|$ and denominator $\left|D(j\omega)\right|$ for all frequencies and can be expressed as (Schaumann, and Van Valkenburg 2001):

$$\left|H(j\omega)\right| = \frac{\left|N(-j\omega)\right|}{\left|D(j\omega)\right|} = c \tag{5.51}$$

The second order all-pass transfer function can then be obtained from (5.51) and expressed as:

$$\left|H(s)\right| = \frac{\left|N(-s)\right|}{\left|D(s)\right|} \tag{5.52}$$

The constant gain is associated with nonlinear phase and inconstant group-delay for selected frequency band according to the filter design. This means, the phases and group-delay depend on frequency (ω), so that a signal with a particular frequency might be delayed differently than other signals have different frequencies. Accordingly, the all-pass filter can be used as a tool for modifying the phase or the group-delay of the signals

passing cross (Winder 2002). In another word, it varies the phase or the group-delay for the selected band of the frequencies with keeping the constant magnitude for all frequencies. The group-delay equalisation can approximate the aimed group-delay so that the selected signal frequencies are passed from the filter with the required delay (Winder 2002). Therefore, the all-pass filter is also called delay equaliser or phase linearizer (Su 2002). This is achieved by selecting the parameters of the all-pass filter whether it is a first, second or higher order.

Consider the first order all-pass filter, expressed as:

$$H_{1ap}(s)=\frac{s-a}{s+a}=1+\frac{-2a}{s+a} \tag{5.53}$$

where $a>0$ is for designing a stable filter. The phase response and group-delay of (5.53) are given, respectively, as:

$$\theta_{1ap}(j\omega)=-2tan^{-1}\left(\frac{\omega}{a}\right) \tag{5.54}$$

$$T_{1ap}(j\omega)=-\frac{d\theta_{1ap}}{d\omega}=\frac{2}{a}\frac{1}{1+\left(\omega/a\right)^2} \tag{5.55}$$

where subscript 1*ap* refers to the first order all-pass filter. The first derivative of (5.55) is deduced as:

$$\frac{dT_{1ap}(j\omega)}{d\omega}=-4\omega\Big/a\left(a+\left(\omega/a\right)^2\right)^2 \tag{5.56}$$

It can be noted that (5.56) is negative for all values of $\omega\geq 0$. Therefore, (5.55) monotonically decreases and the maximum value of (5.55) is $\frac{2}{a}$ when $\omega=0$ as shown in Figure 5-16. The bounded between 0 to ∞ the integral of (5.55) equals to π with regardless of the value of a, however, the smaller the a the higher the steepness of group-delay in (5.55), produced close to $\omega=0$. Thus, the a parameter only controls the maximum value of group-delay in (5.55) and its steepness is close to $\omega=0$.

However, in the majority cases, there is a need to modify the group-delay in a different range of frequencies. Thus, the second order all-pass filter is usually recommended because it has two parameters as it will be further illustrated in this section.

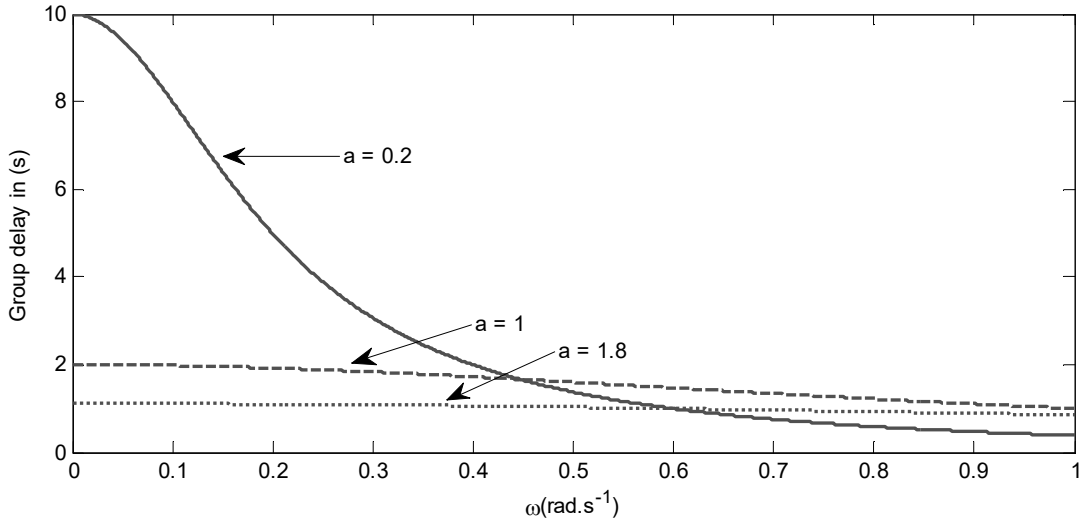

Figure 5-16: Group-delay of the first order all-pass filter of (5.55) for different values of *a*.

The second order transfer function of the all-pass filter can be expressed as:

$$H_{2ap}(s)=\frac{(s-a)^2+b^2}{(s+a)^2+b^2}=1-\frac{4as}{(s+a)^2+b^2} \tag{5.57}$$

where $a>0$ for producing a stable filter. The phase response and group-delay of (5.57) can be obtained, respectively, as:

$$\theta_{2ap}(j\omega)=-2tan^{-1}\left(\frac{2a\omega}{a^2+b^2-\omega^2}\right) \tag{5.58}$$

$$T_{2ap}(j\omega)=-\frac{d\theta_{2ap}}{d\omega}=\frac{4a\left(\omega^2+a^2+b^2\right)}{\left(a^2+b^2-\omega^2\right)^2+4a^2\omega^2} \tag{5.59}$$

where subscript 2*ap* refers to the second order all-pass filter. Figure 5-17 illustrates that the parameter selection of the second order all-pass filter is more flexible than the case of the first order all-pass filter. In addition, it shows that the parameter a has a larger effect on the value of the peak of the group-delay where the smaller the value of a the higher the peak value and the sharper the curve of the group-delay. While $|b|$ parameter has a

larger effect on locating the peak value on ω axis. For instance, if $b=0$ in (5.57), it produces two first order all-pass filters. Therefore, the produced group-delay is just twice the group-delay of the first order all-pass filter. More information about the parameter selecting impact on the group-delay of the second order all-pass filter can be found in (Schaumann, and Van Valkenburg 2001 and Su 2002).

5.6.1 State-space representation of all-pass filters

There are different approaches for mathematical descriptions of the filters to obtain the delayed states, in which the state variable form is widely used for simulations. The first order all-pass, second order all-pass and Butterworth transfer filter in (5.53), (5.57) and (5.19), respectively, can be converted to a state-space form in time-domain. The first order all-pass state-space representation, based on second part of (5.53), is expressed as:

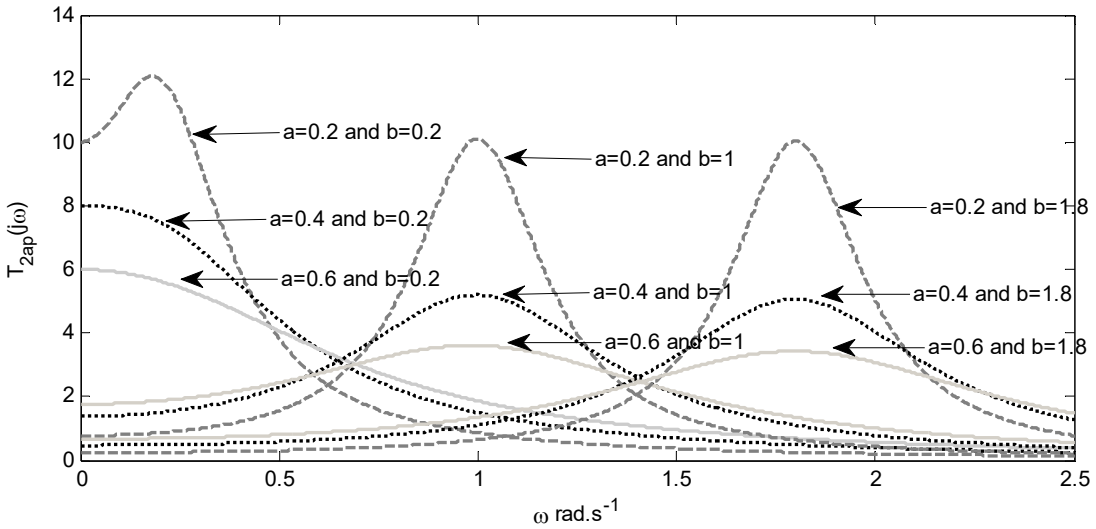

Figure 5-17: Group-delay of the one stage second order all-pass filter in (5.59) for different values of the parameters *a* and *b.*

$$\dot{x}_1 = -ax_1(t) + u(t) \tag{5.60}$$

$$v(t) = -2ax_1(t) + u(t) \tag{5.61}$$

where $\dot{x} = \frac{dx}{dt}$ and $u(t)$ and $v(t)$ denoted input and output of the filter. This can be represented in equivalent block diagram as shown in Figure 5-18.

The second order all-pass filter, whose transfer function is in (5.57), can be described by state-space representation as:

$$\begin{bmatrix} \dot{x}_1 \\ \dot{x}_2 \end{bmatrix} = \begin{bmatrix} 0 & 1 \\ -a^2b^2 & -2a \end{bmatrix} \begin{bmatrix} x_1 \\ x_2 \end{bmatrix} + \begin{bmatrix} 0 \\ 1 \end{bmatrix} u(t) \tag{5.62}$$

$$v(t) = \begin{bmatrix} 0 & -4a \end{bmatrix} \begin{bmatrix} x_1 \\ x_2 \end{bmatrix} + u(t) \tag{5.63}$$

This can be also represented in the equivalent block diagram as demonstrated in Figure 5-19.

5.6.2 Group-delay equalisation

The group-delay of the Butterworth filter gives sharper and higher peaks as its order increases, as shown in Figure 5-6. This means, a higher Butterworth order requires a higher equaliser order. However, an order higher than the second order of equaliser can be achieved by using a combination of the first and second order all-pass filters. For example, if an equaliser with the third order is required, then first and second order all-pass filters can be cascaded in series for achieving a decent constant group-delay. Thus, more parameters are required to be approximated as the order increases and the overall group-delay is the summation of the group-delay of all filters. This leads to solving a nonlinear function to obtain the parameters. For that, there are several methods that can be implemented to select all-pass filters parameters for achieving the most constant group-delay.

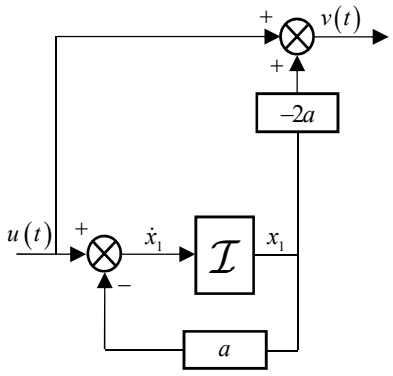

Figure 5-18: Equivalent block diagram of state-space representation for the first order all-pass filter in (5.60) and (5.61)

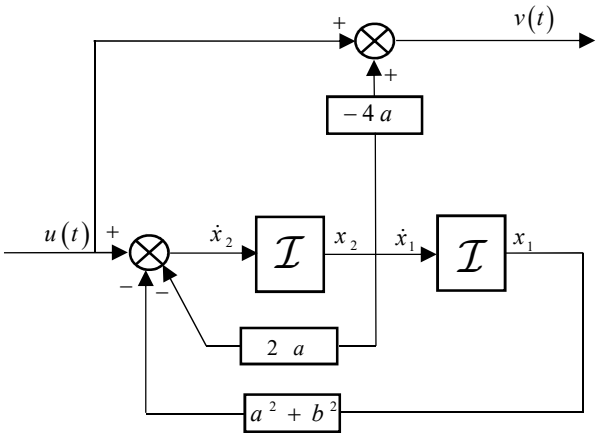

Figure 5-19: Equivalent block diagram of state-space representation for the second order all-pass filter in (5.62) and (5.63)

According to (Blinchkoff & Zverev 1976), the maximally flat, equiripple and least squares are broadly used for parameter selection. The maximally flat design provides much better correction at the lower part of the band, but very poor over the band edge. On the other hand, the equiripple method is good near the edge of the band but associated with a drawback of the poor response over the rest of the band. Nonetheless, the least squares design presents a better balance when compared to these two methods. That is why, in this thesis, the least squares algorithm is the method selected for obtaining the parameters.

In order to approximate a constant delay T_0, there is a need to equalise the Butterworth group-delay T_{BW} in (5.27) with T_{2ap} of second order all-pass function in (5.59) using the least squares algorithm from $\omega = 0$ to $\omega = \omega_{T_{\max}}$ where $\omega_{T_{\max}}$ is the value of ω in which T_{BW} reaches its maximum value. This can be expressed as:

$$\varepsilon = \int_0^{\omega_{T_{\max}}} \left[T_0 - T_{BW}(\omega) - T_{ap}(\omega) \right]^2 \tag{5.64}$$

where $T_{ap}(\omega)$ is the sum of the all-pass filter group-delays:

$$T_{ap}(\omega) = \sum_{k=1}^{m} T_{z(k)ap}(\omega) \tag{5.65}$$

where the subscript $z(k) \in \{1,2\}$ is one for the first order all-pass group-delay in (5.55) and two for the second order all-pass group-delay in (5.59). Furthermore, m represents the number of the all-pass filters or stages. Thus, there are a_s and b_s estimates from (5.55) and (5.59) associated with selecting T_0.

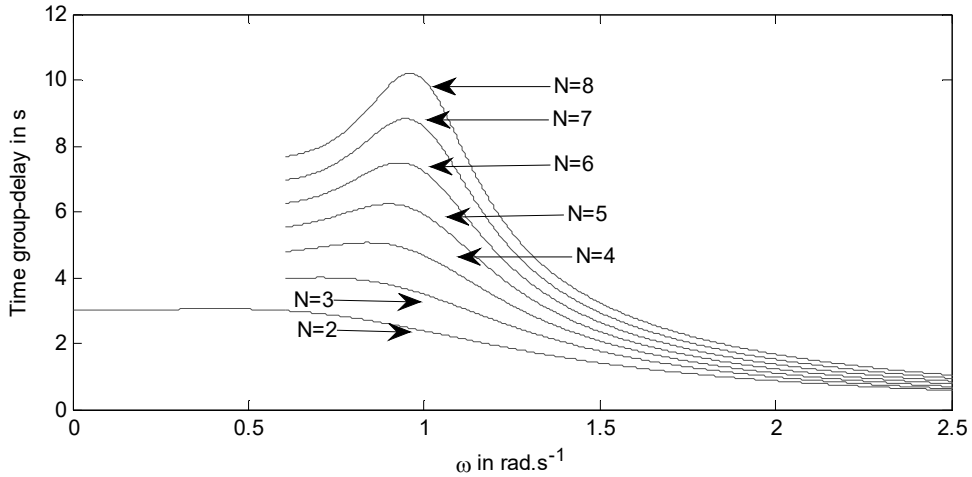

Figure 5-20: Equalisation Butterworth filter with the first order all-pass filter with *N=2:8* and ω_c=1.

In the case, there is only first order all-pass filter, a and T_0 estimates are varying based on the Butterworth order as described in Table 5-2. However, Figure 5-16 illustrates that it works less effective as Butterworth order is higher. Nonetheless, a better group-delay is achieved when second order all-pass filter is applied with the estimates in Table 5-3. But it

is less efficient when the Butterworth order is higher than 4 as shown in Figure 5-17. When two all-pass filters are used with the estimates in Table 5-4, it shows a significant group-delay for all Butterworth filters, especially with 5th and 6th orders. As a result, the selection of the number of the all-pass filter stages mainly depends on the Butterworth order.

Table 5-2: First order all-pass filter parameters that generate approximated group-delay with Butterworth filter with *N=2:8* and ω_c=1.

Butterworth filters Orders	*a*	*T0 in s*	*Wmaxin rad.s-1*
N=2	1.2543	3.0253	0.6436
N=3	0.9988	3.9662	0.8173
N=4	0.8381	4.8878	0.8879
N=5	0.7322	5.7799	0.9236
N=6	0.6571	6.6504	0.9443
N=7	0.6007	7.5055	0.9574
N=8	0.5563	8.3498	0.9663

Table 5-3: Second order all-pass filter parameters that generate group-delay with normalised Butterworth filter with *N=2:8*.

Butterworth filter Orders	*a*	*b*	T_0 *in s*
N=2	1.6247	0.000	3.8962
N=3	1.2011	0.3034	5.1147
N=4	0.7960	0.4167	6.5619
N=5	0.6534	0.4088	7.6891
N=6	0.5700	0.3974	8.7066
N=7	0.5137	0.3866	9.6637
N=8	0.4725	0.3768	10.5834

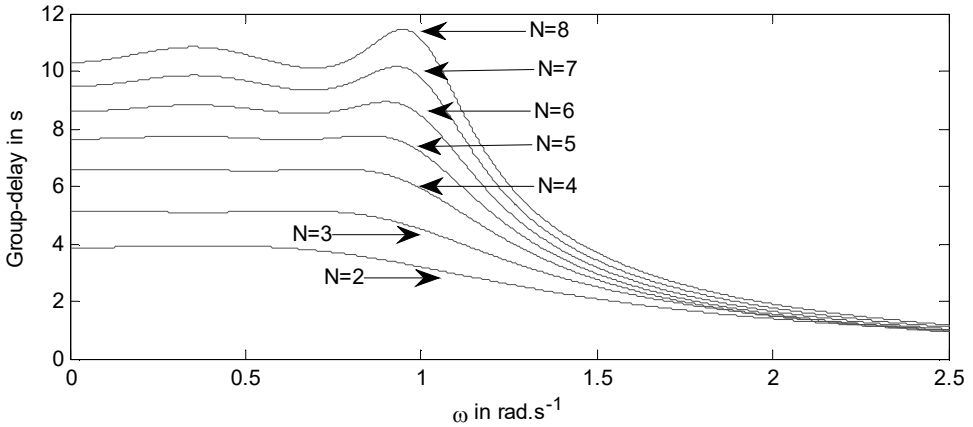

Figure 5-21: Equalisation Butterworth filter with the second order all-pass filter with *N=2:8* and ω_c=1.

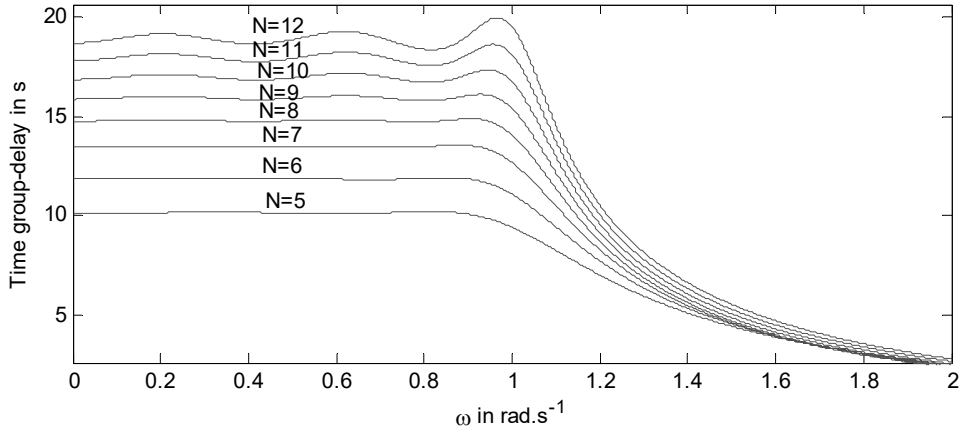

Figure 5-22: Equalisation normalised Butterworth filter with two second order all-pass filters with *N=5:12* and ω_c=1.

Table 5-4: Parameters of the second order all-pass filter in two stages cascaded with normalised Butterworth filter with *N=5:12* to generate the most constant group-delay of the delayed fractional-order filter.

Butterworth filter Orders	a_1	b_1	a_2	b_2	T_0 *in s*	W_{max} *in rad.s*$^{-1}$
N=5	0.7310	0.5594	1.1570	0.0000	10.1581	0.9236
N=6	0.5766	0.6269	0.8300	0.0000	11.8575	0.9443
N=7	0.4765	0.6723	0.5611	0.2198	13.4829	0.9574
N=8	0.4086	0.6747	0.4617	0.2245	14.7928	0.9663
N=9	0.3662	0.6675	0.4074	0.2219	15.9344	0.9726
N=10	0.3366	0.6559	0.3708	0.2185	16.9856	0.9772
N=11	0.3145	0.6504	0.3439	0.2152	17.9797	0.9807
N=12	0.2972	0.6422	0.3229	0.2121	18.9351	0.9835

5.7 Delayed fractional-order state variable filter implementation

The implementation and simulation of the delayed state variable filter are essential steps to proper parameter estimation. There are several approaches to express systems, such as the state-space representation. This approach allows collecting the derivatives of the signals in clearer and easier manner by implementing it in Simulink. It is then numerically solved at each sample by using one of the Simulink solvers such as the Euler or Runge-Kutta solver.

In previous sections, every filter is individually treated. However, all these filters can be combined in one filter called delayed fractional-order state variable filter for generating delayed fractional-order derivative terms whether they are linear or nonlinear.

Thus, the delayed state variable filter is simulated in two steps as illustrated in

Figure 5-23. The all-pass filters are firstly and individually cascaded and simulated in Simulink according to the equivalent block diagrams, shown in

Figure **5-18** and

Figure 5-19. The output of the cascaded all-pass filters is used as an input to simulate the fractional-order Butterworth filter in Simulink as shown in Figure 5-11. From fractional-order Butterworth filter, all the higher fractional-order derivative terms of the filtered signals can be obtained. For instance, an arbitrary signal $y(t)$ is passed through the delayed fractional-order state variable filter. Consequently, the filtered or delayed $y(t)$ is produced and denoted $y_{\Gamma}(t)$. Furthermore, all the higher fractional-order derivative terms

$\mathcal{D}^{\alpha_i} y_\Gamma = \frac{d^{\alpha_i} y_\Gamma(t)}{dt^{\alpha_i}}$ can be collected from fractional-order Butterworth as illustrated in Figure 5-11.

Figure 5-23 demonstrates the input and the outputs of the delayed fractional-order state variable filter where in later sections the input will be the signals, which are collected for identification. The system simulation and identification process steps are illustrated in Figure 5-24.

The design idea of the delayed state variable is based on the frequency response of the both all-pass and Butterworth filters. Thus, the next section will discuss the impact of the simulation on the frequency-response of delayed state variable filter in the following section.

5.8 Evaluation of the numerical delayed fractional-order state variable filter based on frequency response

This section shows how the ode solver in Simulink can participate in the accuracy of identification. The identification algorithm basically uses the frequency response of the delayed fractional-order state variable to add an approximated transport-delay within selected range of frequencies. Therefore, the accuracy is measured according to the frequency response of the simulated delayed fractional-order state variable filter.

In this section, the normalised delayed fractional-order state variable filter is represented by a first order all-pass filter, cascaded with a second order Butterworth filter, presented in Table 5-2. This filter is used as a benchmark to investigate the drawbacks of using the numerical solution in the frequency response. When $\alpha = 1$ and $\omega_c = 1$, the third order normalised delayed state variable transfer function, is expressed as:

$$R(s) = \frac{s - 1.2543}{s^3 + 2.6685s^2 + 2.7738s + 1.2543} \tag{5.66}$$

This system is used as a benchmark to observe the effect of the numerical solution on the frequency response of the delayed state variable filter. There are several methods to numerically solve the system in (5.66), such as Euler' method which is the simplest approach to solving the ordinary differential equation in Simulink. If this method shows a reasonable accuracy, it means that the other methods such as Hewn and Runge-Kutta, which generate less error, will give a better accuracy. This is because the other higher order methods provided by Simulink, such as Hewn and Runge-Kutta, are designed by the same approach with a higher order truncation error. The approximation of the first derivative of an arbitrary signal $x(t)$ can be obtained as:

$$\mathcal{D}x(t) \approx \frac{x(t+T_s)-x(t)}{T_s} \tag{5.67}$$

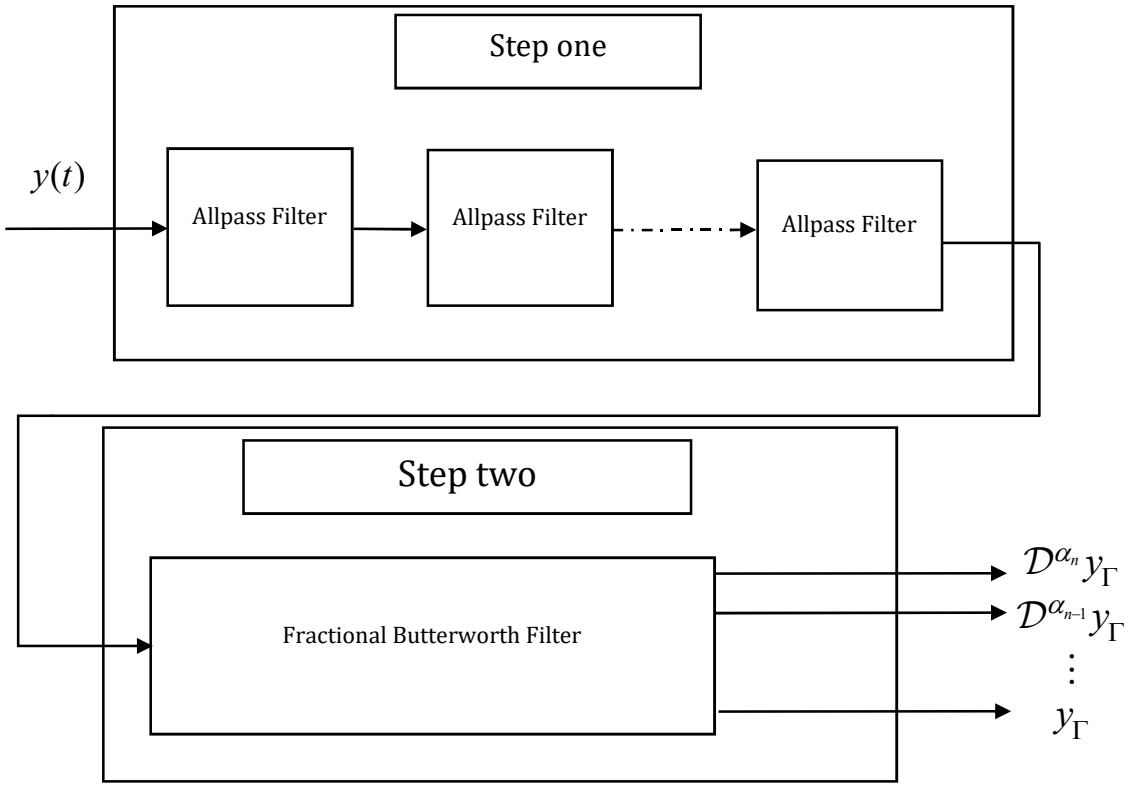

Figure 5-23: Block Diagram of the delayed state variable filter simulation.

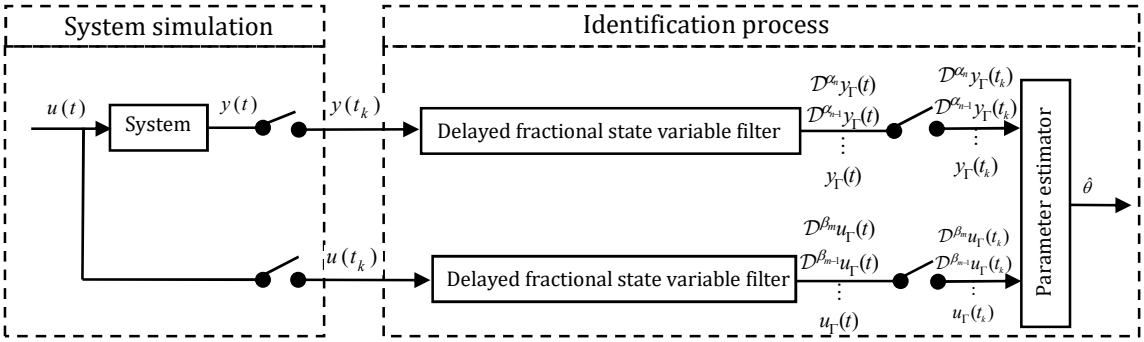

Figure 5-24: System simulation and identification process.

where T_s is the sampling time. With considering zero initial conditions, the Laplace transform can be applied on both sides of (5.67) and so that (5.67) can be expressed as:

$$sX(s) \approx \frac{e^{sT_s}-1}{T_s} X(s) \tag{5.68}$$

According to (5.68), the Euler approximated derivative term in Laplace-domain with considering zero initial conditions is expressed as:

$$s \approx \frac{e^{sT_s}-1}{T_s} \tag{5.69}$$

Substituting (5.69) into (5.66) it results the Euler numerical approximation for the delayed fractional-order state variable filter in the Laplace-domain. The frequency response is then obtained by replacing the s variable with $j\omega$.

Both gain and phase frequency responses of the delayed fractional-order state variable filter in (5.66) and numerical delayed fractional-order state variable filter, obtained by substituting (5.69) into (5.66), are calculated for a range of the frequencies [0.0001:0.01:100000] rad.s^{-1}. The difference in phase frequency response between the two filters is employed in order to evaluate the obtained phase frequency responses.

The obtained gain and difference in phase frequency responses are illustrated in Figure 5-25 and Figure 5-26, respectively. From these figures, it can be noted that the

smaller the sampling time, the further the gain and phase distortions more toward higher frequencies. All these issues associated with numerical solution can be eliminated by selecting the frequency of the input to be sufficiently low in order to avoid overlapping the distortion frequencies. Therefore, it is important to select an appropriate sampling time. Furthermore, the error can be reduced by using a higher order numerical method, such as Rouge-Kutta.

5.9 Input signal design

Input selection is very significant in system identification, especially for approaches using filtered data. In the delayed state variable identification approach, the sinusoid-based signals are expected to give better results. This is due to their capability to be effective within a selected frequency range, so that, it has zero gain in higher frequencies than the cut-off frequency. This is not the case for another signal where there may be infinite sinusoids, required to approximate these signals.

The second most important part is the maximum frequency selection. The maximum frequency of the sinusoid signal is recommended to be lower than the maximum frequency of the pass-band filter of the delayed fractional-order state variable filter. This can be simply identified by inspection of the gain frequency response of the delayed fractional-order state variable filter.

In the case of the delayed fractional-order state variable filter, represented in (5.66), its gain response is illustrated in Figure 5-27. By inspection, it can be observed that the maximum frequency of the pass-band is about 0.1 $rad.s^{-1}$. The selected two input signals are the sum of the sinusoids and chirp signal (Söderström, and Stoica 1989). More details about input signals can be found in (Söderström, and Stoica 1989).

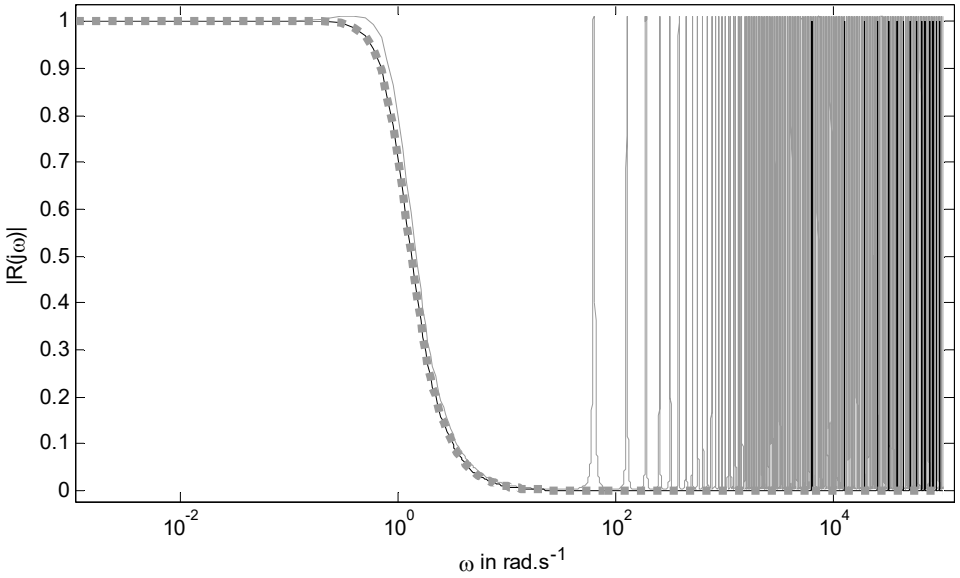

Figure 5-25: The gain frequency responses of the normalised delayed fractional-order state variable filter and the numerical delayed fractional-order state variable filter with Ts= 0.1 and 0.001s, presented in the bold dotted-grey, solid-grey and solid-black lines, respectively.

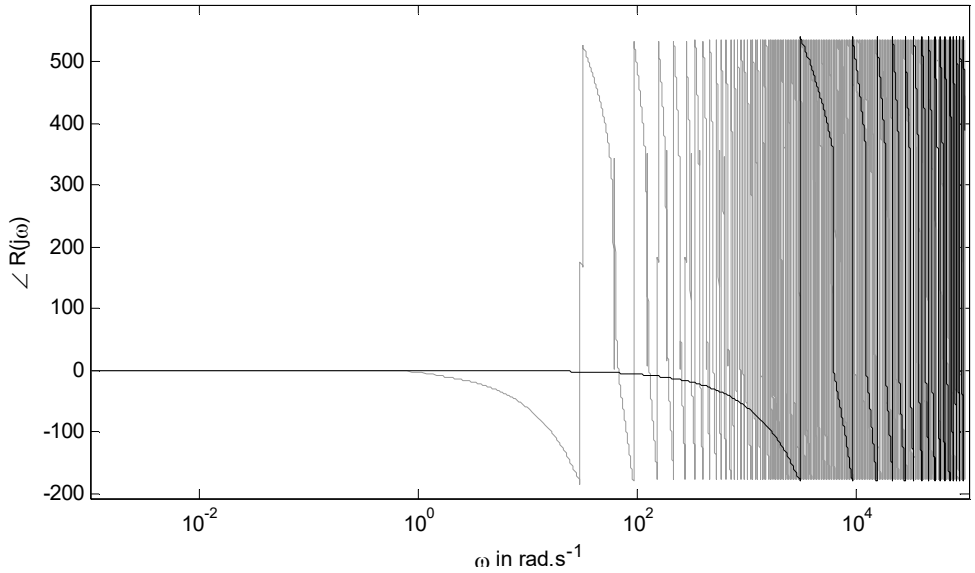

Figure 5-26: The phase difference between frequency responses of the normalised delayed fractional-order state variable filter and the numerical delayed fractional-order state variable filter with Ts= 0.1 and 0.001s, presented in the solid-grey and solid-black lines, respectively.

The sum of the sinusoids is described as:

$$u(t) = \sum_{k=1}^{m} a_k \sin(\omega_k t + \varphi_k) \tag{5.70}$$

where *m* is the number of the sine waves and a_k is amplitude and bounded based on the nonlinear system stability. $\omega_k < \omega_{k+1} < \omega_{k+2}$ is the frequency in rad. s^{-1} and φ_k is the phase in rad.

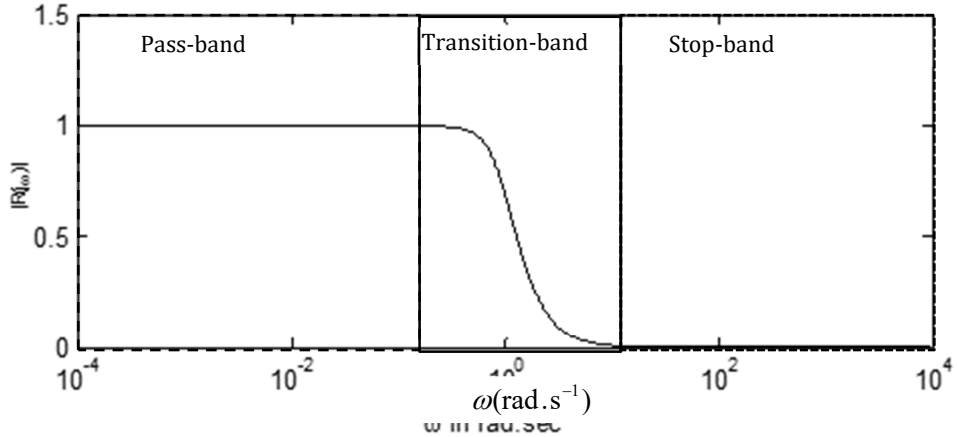

Figure 5-27: The gain response of the normalised delayed fractional-order state variable filter described in (5.66)

The chirp signal is also a sinusoid based function. The difference between these signals is that the chirp signal is a sequence of a gradually increase frequency sine wave signals and not a combination of them and expressed as:

$$u(t) = u_0 + a_k \sin(\omega_k t) \tag{5.71}$$

$$\omega_k = \omega_{\min} + \frac{k}{m}(\omega_{\max} - \omega_{\min}) \tag{5.72}$$

where u_0 is the offset. For nonlinear system, a_k should be repeated with different values. Moreover, the delayed fractional-order state variable filter is to be used as transport-delay, not as a filter. In addition, the more precisely the delayed fractional-order state variable filter approximates an ideal transport delay function, the more accurate the model parameter estimates and the model structure can be identified. Therefore, in order to achieve better identification, both signals in (5.70) and (5.71) might be filtered by a delayed state variable filter of the input design whose cut-off frequency is ten times lower than the cut-off frequency of the delayed state variable filter used in the identification

process. This may guarantee that all undesirable frequencies area eliminated. The filtered input is then used as an input to the system, required to be identified.

5.10 Parameter estimation summary

For simplification sake, the structure for the parameter estimation stage is considered to be known. From the time-domain sampled input/output data, the delayed fractional-order state variable identification approach can be surmised as follows:

I. Select the cut-off frequency of the delayed fractional-order state variable filter based on the property of the nonlinear system.

II. Design the delayed fractional-order state variable filter.

III. Design the input based on the selected cut-off frequency as described.

IV. Apply the designed input to the nonlinear system and then collect the sampled input and output data.

V. Use the delayed fractional-order state variable filter to produce the filtered input and output and their higher fractional-order derivative terms.

VI. Use the filtered data to obtain nonlinear terms.

VII. Use the instrumental variable least squares algorithm to estimate the parameters.

5.11 Numerical example

This section presents the performance of the application of the delayed fractional-order state variables for parameter estimation of fractional-order Duffing's oscillator which represents the fractional-order nonlinear system. More details about fractional-order Duffing's oscillator, please see (Petras 2011). In that example, the fractional-order

Duffing's system is described by the ordinary fractional-order differential equation in OE setup and ARX model given, respectively, as:

$$\varsigma_{OE}\begin{cases} a_0\mathcal{D}^{\alpha_2}x(t)+a_1\mathcal{D}^{\alpha_1}x(t)+a_2x(t)+v_0x^3(t)=b_0u(t) \\ y(t_k)=x(t_k)+e(t_k) \end{cases} \tag{5.73}$$

and

$$\varsigma_{ARX}:\ a_0\mathcal{D}^{\alpha_2}y(t)+a_1\mathcal{D}^{\alpha_1}y(t)+a_2y(t)+v_0y^3(t)=b_0u(t)+e(t) \tag{5.74}$$

where $y(t)$, $x(t)$ and $u(t)$ are the noisy output, noise-free output and input, respectively, while $e(t)$ is the white (zero mean) Gaussian noise with σ^2 variance, selected according to the *SNR* defined in (4.25). Furthermore, the subscripts OE and ARX of system ς represent OE and ARX models, respectively. The sampled form of these signals is denoted $y(t_k)$, $x(t_k)$, $u(t_k)$ and $e(t_k)$.

The goal is to estimate the system parameters a_i, b_i and v_i. To simulate the noise-free system in (5.73) can be expressed as:

$$\mathcal{D}^{\alpha_2}x(t)=-\frac{a_1}{a_0}\mathcal{D}^{\alpha_1}x(t)-\frac{a_2}{a_0}x(t)-\frac{v_0}{a_0}x^3(t)+\frac{b_0}{a_0}u(t) \tag{5.75}$$

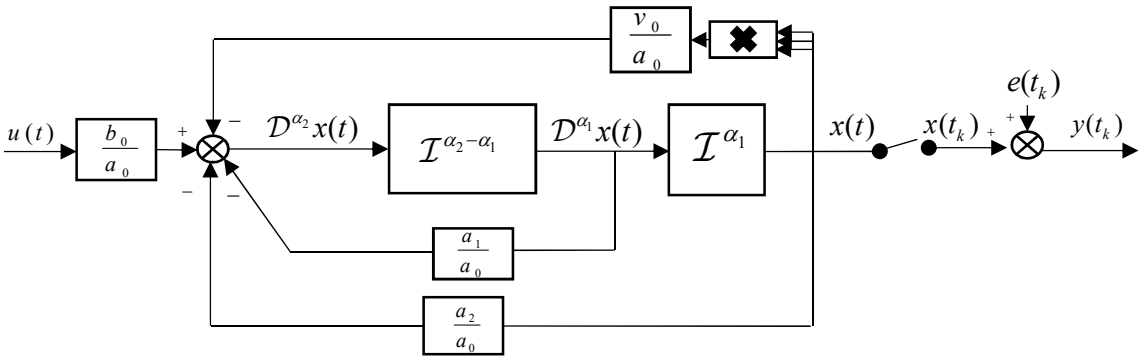

Figure 5-28: The equivalent block diagram of (5.75) with considering noise.

This can be simulated in Simulink by using equivalent block diagram as shown in Figure 5-28 considering the noise model in (5.73). The system in (5.74) is treated in the

same manner, but the continuous noise is added as a second input to the noise free system in (5.75), with gain $\frac{1}{a_0}$.

The input signal is selected to be a sum of the 10 sinusoids whose bandwidth is 1ω.rad^{-1}. This simulation has been run over a time period 50s with a time step T_s = 0.001s, using the selected Simulink solver ode4 (Runge-Kutta). The fractional-order integral block is provided by FOMCON Simulink library with frequency range [0.001rad.s^{-1}; 1000 rad.s^{-1}] and 25 approximation order. The input could be also another signal, such as a pseudorandom or Gaussian signal filtered by the delayed fractional-order state variable filter whose ω_c is smaller than the maximum frequency of pass-band of the delayed fractional-order state variable filter, used for identification. Thus it is recommended to delete the time delay caused by the filter due to the elimination caused by the input delayed filter in higher frequencies.

The delayed fractional-order state variable contains the eighth order fractional-order Butterworth and ten stages of the second order all-pass filter to achieve the better constant group-delay. Its cut-off is selected to be $\omega_c = 12$ rad.s^{-1}.

Figure 5-29 and Figure 5-31 show the performance of the selected delayed fractional-order state variable filter. The comparison of the input, output and fractional-order derivative terms and filtered output and fractional-order derivative terms in Figure 5-29 shows that a very good delay function has been obtained because the filtered signals are lagging behind the input by about 2.3s. The delayed fractional-order state variable filter is significantly efficient even though the level of *SNR* is high. The fractional-order derivative terms of the noisy output are also delayed but the higher fractional-order of the derivative term is more affected by the noise as shown in Figure 5-31. Therefore, the delayed fractional-order state variable filter commutes with the fractional-order derivative terms.

Monte Carlo simulation (MCs) of the 50 runs has been implemented with different random noise for each realisation. The mean and standard deviation of estimates are presented for comparing the statistical performance of the proposed approach. Noise added to the system is selected such that it corresponds to *SNR*=20, 10 *dB*.

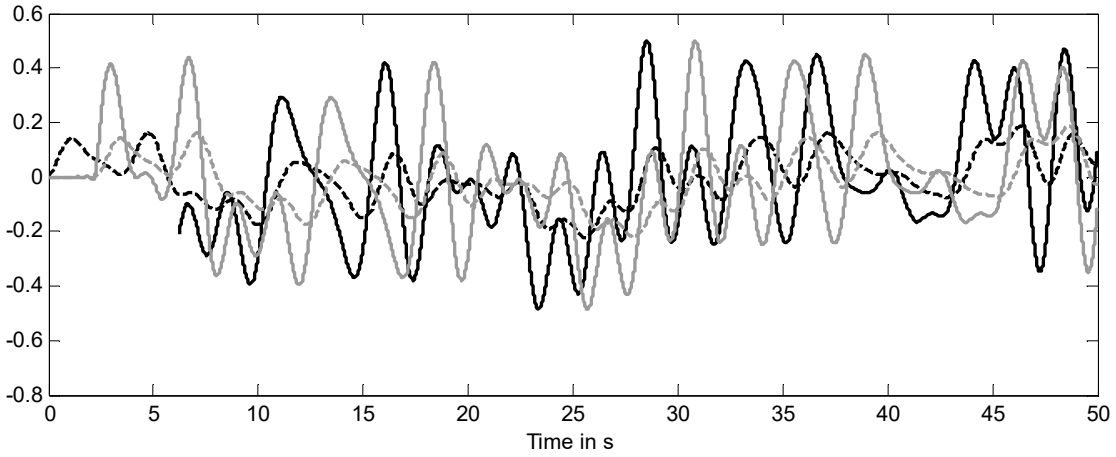

Figure 5-29: Input and filtered input are presented in solid-black and solid-grey, noise-free output $x(\mathrm{t})$ and filtered noisy output $y_{\Gamma}(\mathrm{t})$, shown in Figure 5-30 are presented in dotted-black and dotted-grey lines, respectively.

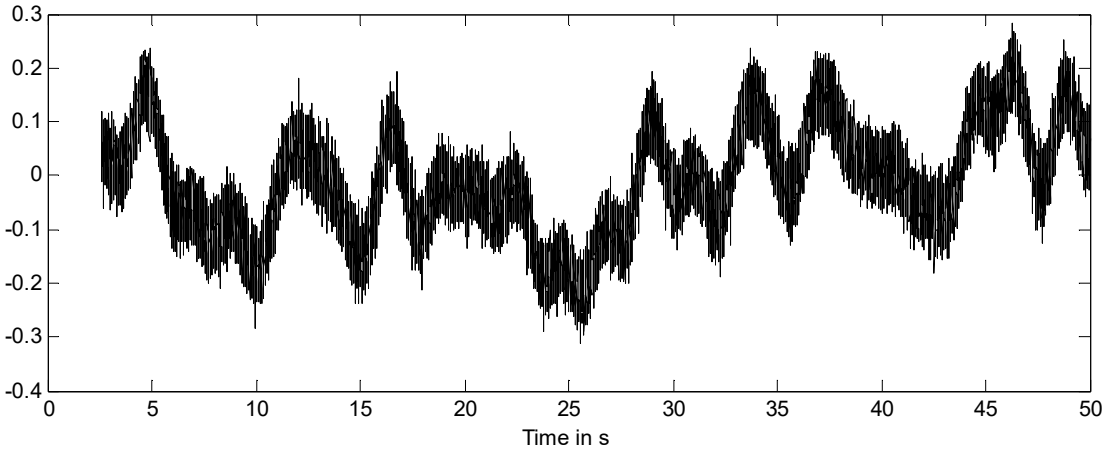

Figure 5-30: Noisy output $y(\mathrm{t})$ in (5.73) when *SNR*= 1.

In this example, the delayed fractional-order state variable identification approach has used the instrumental variable (IV) least squares estimator, see (3.25) where the filtered time derivatives are obtained by the proposed delayed fractional state variable filter. Additionally, in this example, the simulated output has been used as instrumental variable as the case in (3.25).

Table 5-5 shows that the IV least square estimator gives satisfactory result whether the model is OE or ARX. Furthermore, itTable 5-5 shows the high efficiency of the proposed approach to provide satisfactory estimates for commensurate and non-commensurate order. To sum up, the delayed fractional-order state variable identification approach works very efficiently with the selected noise.

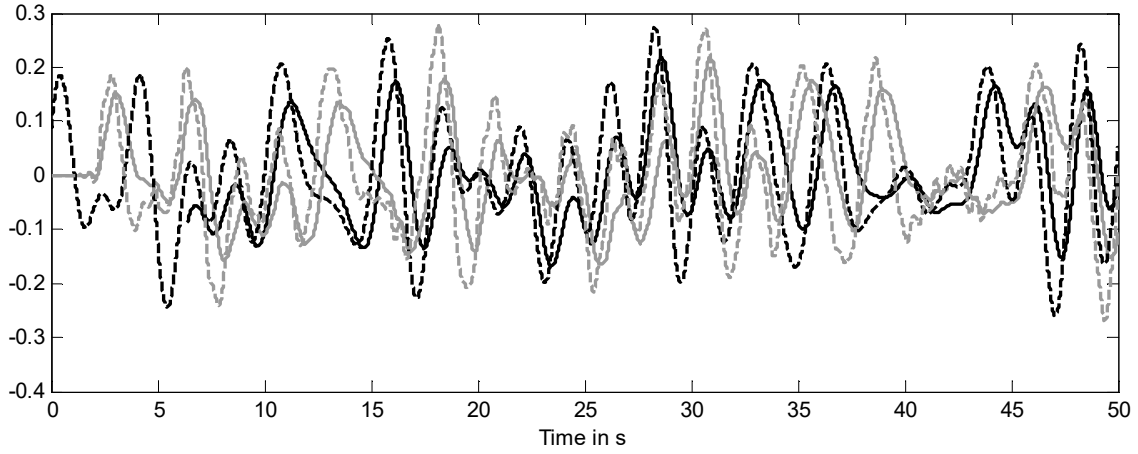

Figure 5-31: The fractional-order derivative terms $\mathcal{D}^{0.5}x(t)$, $\mathcal{D}\,x(t)$ and filtered derivative terms of the noisy output $\mathcal{D}^{0.5}y_{\Gamma}(t)$ and $\mathcal{D}\,y_{\Gamma}(t)$ are displayed in solid-black, dotted-black, solid-grey and dotted-grey, respectively.

5.12 Conclusions

In this chapter, the delayed state variable identification approach has been extended to fractional-order. This has been achieved by designing the delayed fractional-order state variable filter. The design of the delayed fractional-order state variable filter requires designing an approximate of the fractional-order Butterworth filter.

Three different methods are proposed for designing the fractional-order Butterworth filter and termed as fractional-order Butterworth of base-order $\alpha = 0.5$, square root base $\alpha = 1/2^n$ and compartmental fractional-order Butterworth designs. The compartmental fractional-order Butterworth filter showed better performance in the delayed fractional-order state variable identification approach over the fractional-order Butterworth of base

Table 5-5: The result of the MCs simulation of the fractional-order continuous-time nonlinear commensurate (α1 =0.5, α2 =1) and non-commensurate system (α1 =0.3, α2 =1), described in (5.73) and (5.74) where θ_j and θ_j^0 represent the actual parameters and the noise-free estimated parameters, respectively, a_2=1.

System	*SNR*	θ_j	a_0=1	a_1=1	a_3=0.6	b_0=1
		θ_j^0	1	1	0.6000	1
Commensurate	ς_{OE} 1	mean	1.0001	0.9994	0.5963	0.9998
		std	0.0081	0.0139	0.0859	0.0051
	ς_{OE} 2	mean	1.0000	0.9998	0.5988	0.9999
		std	0.0026	0.0044	0.0271	0.0016
	ς_{ARX} 1	mean	1.0002	0.9998	0.5987	0.9999
		std	0.0041	0.0064	0.0366	0.0024
	ς_{ARX} 2	mean	1.0001	0.9999	0.5996	1.0000
		std	0.0013	0.0020	0.0116	0.0008
Non-commensurate	ς_{OE} 1	mean	1.0003	0.9993	0.5973	0.9999
		std	0.0142	0.0178	0.0707	0.0043
	ς_{OE} 2	mean	1.0001	0.9998	0.5991	1.0000
		std	0.0045	0.0056	0.0223	0.0014
	ς_{ARX} 1	mean	1.0004	0.9996	0.5987	0.9999
		std	0.0072	0.0085	0.0324	0.0022
	ς_{ARX} 2	mean	1.0001	0.9999	0.5997	1.0000
		std	0.0023	0.0027	0.0102	0.0007

order $\alpha = 0.5$ and square root base $\alpha = 1/2^n$ filters in terms of simplicity and computational accuracy and computational time. The fractional-order Butterworth filter is

then equalised by all-pass filters to achieve the most constant group-delay. Furthermore, it was seen that the number of all-pass filters depends on the order of fractional-order Butterworth filter and selected cut-off frequency of the delayed fractional-order state variable filter. In addition, the input used for identification is recommended to be the sinusoid-based signals.

An illustrative example has shown how to simulate fractional nonlinear system and demonstrated that the performance of the proposed identification procedure is significantly efficient.

Chapter 6: BILINEAR FRACTIONAL-ORDER SYSTEM IDENTIFICATION

In this chapter, a bilinear system is extended to a bilinear fractional-order system. The introduced bilinear system is described by both an input-output model and a state-space representation. Applying the proposed delayed fractional-order state variable identification approach requires the system to be described by an input-output model. It also shows which state-space representation is realisable by the input-output model. Two numerical examples are presented to evaluate the performance of the proposed delayed fractional-order state variable identification approach for bilinear system identification.

This chapter also presents the structure detection, by using the error reduction ratio. The proposed delayed fractional-order state filter can generate from collected input-output data all the required linear and delayed nonlinear fractional-order derivative terms. This approximated data allows application of the error reduction ratio to rank the eligible fractional-order nonlinear derivative terms. The highest ranked terms are selected to describe the nonlinear model. The novelty of this approach is to show how the error reduction ratio can be applied when the system is described by the nonlinear fractional-order model. The delayed fractional-order state variable identification approach is then applied to the parameter estimation of the selected nonlinear fractional-order system.

6.1 Introduction

The majority of physical systems are considered to be nonlinear and continuous-time. The origina bilinear system models were initially defined in a continuous-time state-space form. The bilinear system is defined to be linear in system state and control input when considered independently, with the nonlinearity arising as a product of both state and control. Mohler (1973) has shown that bilinear systems arise in biology, engineering and socioeconomics. Bilinear system models are more efficient than linear system models to approximate nonlinear systems and less complex than many other nonlinear models. In a practical perspective, a general industrial plant could be characterised by a bilinear model and a controller designed considering the bilinearity as stated in (Dunoyer et al. 1996). Furthermore, a general heating, ventilation, and air conditioning system could be structured as a Hammerstein-bilinear model, and this model has offered improved capabilities and retained a close link to the well-understood linear models (Zajic 2013).

In the search for a more efficient modelling process, it is a significant task to devise a more convenient and accurate structure for modelling a practical nonlinear system. A better model structure generally leads to a better parameter estimation and validation. Of course, the efficiency/effectiveness of the estimated model reflects on the performance of the control design and model prediction. Optimisation techniques have been applied for the order detection of the linear fractional-order system, such as in (Zhou, Cao, and Chen 2013 and Wang et al. 2015). There are other approaches, considering the model structure such as a linear combination of fractional-order orthogonal basis functions (Aoun et al. 2007). Some methods are designed based on the linear model analysis in the frequency-domain, such as (Ghanbari and, Haeri 2011) in which the structure detection is based on fitting a piecewise linear approximating function to the estimated Bode diagram.

All those aforementioned methods are for order detection or linear structure model detection. In this thesis, an error reduction ratio (ERR) approach is used for detecting the

nonlinear fractional-order terms. It is achievable in this work because there is a capability to access the internal terms of the nonlinear fractional-order system by using a delayed fractional-order state variable filter, which is introduced in this thesis. Billings (1994) has claimed that ERR can be used for ranking the nonlinear terms of the nonlinear integer-order system regarding their importance and the selection of terms is thus based on the highest ERR.

Furthermore, the advantages, offered by the fractional-order systems combined with bilinear systems, greatly encouraged and prompted the extension of the linear to the bilinear fractional-order system models. This extension may assist to describe how the highest order bilinear integer-order model may more accurately be described by a much smaller bilinear fractional-order model. The model of the introduced bilinear fractional-order system is then identified. For parameter estimation, the delayed fractional-order state variable identification approach is considered.

This chapter is organised such that Section 6.2 introduces the notion of the bilinear fractional-order system and then highlights the definition of the bilinear fractional-order system, the equivalent bilinear fractional-order input-output model for the corresponding state-space model and bilinear fractional-order input-output model simulation. In Section 6.3, there is a brief description of how to use the error reduction ration for structure detection. Two numerical examples are presented in Section 6.4. The conclusions and further work are drawn in Section 6.5.

6.2 Bilinear fractional-order systems

Bilinear systems are considered to be significant in gaining a better understanding and insight and is yet is probably one of the simplest classes of nonlinear systems for which linear systems coexist as a special subclass, when setting the bilinear matrix coefficients to

zero. The system state and control input of a bilinear system are involved in generating the system nonlinearity that is modelled as multiplicative product terms.

In this section, the advantages of the bilinear systems associated with the advantages of fractional-order continuous-time systems led to the introduction of the bilinear fractional-order system. Two different representations of the bilinear fractional-order system are stated. Furthermore, the simulation and model identification are addressed for a selected class of the bilinear fractional-order systems.

6.2.1 Definition of bilinear fractional-order system

6.2.1.1 Fractional-order input-output model

A bilinear fractional-order commensurate input-out model can be described by the nonlinear fractional-order commensurate ordinary differential equation and expressed as:

$$\sum_{i=0}^{n} a_i \mathcal{D}^{\alpha_{n-i}} x(t) = \sum_{i=0}^{m} b_i \mathcal{D}^{\beta_{m-i}} u(t) + \sum_{i=1}^{n} \sum_{j=0}^{m} \mathcal{D}^{\alpha_{n-i}} x(t) \eta_{ij} \mathcal{D}^{\beta_{m-j}} u(t) \tag{6.1}$$

where $u(t)$ and $x(t)$ represent the input and noise-free output, respectively and η denotes the bilinear coefficients. The orders are assumed to be $\alpha_i, \beta_i \in \mathbb{R}^+$ where $\alpha_{i-1} \le \alpha_i \le \alpha_{i+1}$, $\beta_{i-1} \le \beta_i \le \beta_{i+1}$ and $\alpha_n > \beta_m$. The bilinear fractional-order system is assumed to be commensurate, therefore, $\alpha_i = i \times \alpha$, $\beta_i = i \times \alpha$ and the base-order $\alpha \in \mathbb{R}^+$. The bilinear part of (6.1) can also be expressed in the matrix form as:

$$\sum_{i=1}^{n} \sum_{j=0}^{m} \mathcal{D}^{\alpha_{n-i}} x(t) \eta_{ij} \mathcal{D}^{\beta_{m-j}} u(t) = \underbrace{\left[\mathcal{D}^{\alpha_{n-1}} x(t), \quad \mathcal{D}^{\alpha_{n-2}} x(t), \quad \cdots, \quad \mathcal{D}^{\alpha_0} x(t) \right]}_{n} \underbrace{\begin{bmatrix} \eta_{1,0} & \eta_{1,1} & \cdots & \eta_{1,m} \\ \eta_{2,0} & \eta_{2,1} & \cdots & \eta_{2,m} \\ \vdots & \vdots & \vdots & \vdots \\ \eta_{n,0} & \eta_{n,1} & \cdots & \eta_{n,m} \end{bmatrix}}_{n \times m+1} \underbrace{\begin{bmatrix} \mathcal{D}^{\beta_m} u(t) \\ \mathcal{D}^{\beta_{m-1}} u(t) \\ \vdots \\ \mathcal{D}^{\beta_0} u(t) \end{bmatrix}}_{m+1 \times 1} \tag{6.2}$$

6.2.1.2 Bilinear fractional-order state-space representation

The bilinear fractional-order commensurate system can also be described by a fractional-order state-space representation and expressed as:

$$D^{\alpha}\mathbf{x}(t) = A\mathbf{x}(t) + bu(t) + u(t)\mathrm{H}\mathbf{x}(t) \tag{6.3}$$

$$x(t) = c\mathbf{x}(t) \tag{6.4}$$

where $u(t)$ and $x(t)$ represent the (1×1) system input and noise-free output signals, respectively. A is the $(n\times n)$ matrix while b and c^T are the $(n\times1)$ input and output vectors, respectively where $n\in\mathbb{Z}$ and represents the number of states. Linear models coexist as a special subclass of bilinear models and can be obtained by setting the bilinear coefficients of the $(n\times n)$ matrix H to null. The vector $\mathbf{x}(t) = \left[x_1(t),\ldots,x_n(t)\right]^T$ denotes the $(n\times1)$ system state vector. The quantity $D^{\alpha}\mathbf{x}(t)$ vector denotes the fractional-order derivative state vector, whose order is commensurate with the base-order α. Therefore, the fractional-order commensurate derivative state vector can be expressed as:

$$D^{\alpha}\mathbf{x}(t) = \left[D^{\alpha}x_1(t), D^{\alpha}x_2(t)\ldots, D^{\alpha}x_n(t)\right]^T \tag{6.5}$$

Furthermore, (6.3) refers to the fractional-order state-space equation and (6.4) denotes the output equation. In this thesis, (6.3) and (6.4) are presented in phase variable canonical form and defined as:

$$\begin{aligned}
A &= \underbrace{\begin{pmatrix} 0 & 1 & 0 & \cdots & 0 \\ 0 & 0 & 1 & \ddots & 0 \\ 0 & 0 & 0 & \ddots & \vdots \\ 0 & 0 & 0 & \cdots & 1 \\ -a_n & -a_{n-1} & -a_{n-2} & \cdots & -a_1 \end{pmatrix}}_{n\times n}, \mathrm{H} = \begin{pmatrix} 0 & 0 & 0 & \cdots & 0 \\ 0 & 0 & 0 & \vdots & 0 \\ \vdots & \vdots & \vdots & \ddots & \vdots \\ 0 & 0 & 0 & \cdots & 0 \\ \eta_n & \eta_{n-1} & \eta_{n-2} & \cdots & \eta_1 \end{pmatrix} \\
b^T &= \underbrace{\begin{bmatrix} 0 & 0 & \cdots & 0 & 1 \end{bmatrix}}_{1\times n} \\
c &= \underbrace{\begin{bmatrix} b_0, & b_1, & \cdots, & b_m, & 0 \end{bmatrix}}_{1\times n}
\end{aligned} \tag{6.6}$$

where coefficients $a_i, b_i, \eta_i \in \mathbb{R}$.

The proposed identification algorithms are designed for nonlinear fractional-order input-output models. Therefore, the state-space equations in (6.3) and (6.4), is converted the equivalent bilinear fractional-order input-output model. In the case of bilinear integer-order systems, it has been shown in (Mullar et al. 2009 and Kotta et al. 2007) that not all bilinear input-output models are realisable by the bilinear state-space realisation. It is also the case for converting from the state-space to input-output model and this is demonstrated in the following subsections.

6.2.2 Equivalent bilinear fractional-order input-output model to the state-space model

Two scenarios are considered in this section because not all bilinear fractional-order state-space representations are realisable by bilinear fractional-order input-output models.

6.2.2.1 First case scenario

In this case, it is assumed that the output equation (6.4) depends only on the first state. Thus, the output equation is re-expressed as:

$$x(t) = \begin{bmatrix} b_0, & 0, & \cdots, & 0 \end{bmatrix} \begin{bmatrix} x_1 \\ x_2 \\ \vdots \\ x_n \end{bmatrix} \tag{6.7}$$

It is required to reformulate (6.3) based on the first state and writen as:

$$\begin{bmatrix} \mathcal{D}^{\alpha}x_1(t) \\ \mathcal{D}^{2\alpha}x_1(t) \\ \mathcal{D}^{3\alpha}x_1(t) \\ \vdots \\ \mathcal{D}^{\alpha\times n}x_1(t) \end{bmatrix} = \begin{pmatrix} 0 & 1 & 0 & \cdots & 0 \\ 0 & 0 & 1 & \ddots & 0 \\ \vdots & \vdots & \vdots & \ddots & \vdots \\ 0 & 0 & 0 & \cdots & 1 \\ -a_n+\eta_n u(t) & -a_{n-1}+\eta_{n-1}u(t) & -a_{n-2}+\eta_{n-2}u(t) & \cdots & -a_1+\eta_1 u(t) \end{pmatrix} \begin{bmatrix} x_1(t) \\ \mathcal{D}^{\alpha}x_1(t) \\ \mathcal{D}^{2\alpha}x_1(t) \\ \vdots \\ \mathcal{D}^{\alpha(n-1)}x_1(t) \end{bmatrix} + b_0 \begin{bmatrix} 0 \\ 0 \\ 0 \\ 1 \end{bmatrix} u(t) \tag{6.8}$$

Solving (6.7) leads to $x_1(t) = \frac{1}{b_0}x(t)$, and using this in (6.8) leads to:

$$\begin{bmatrix} \mathcal{D}^{\alpha}x(t) \\ \mathcal{D}^{2\alpha}x(t) \\ \mathcal{D}^{3\alpha}x(t) \\ \vdots \\ \mathcal{D}^{\alpha n}x(t) \end{bmatrix} = \begin{pmatrix} 0 & 1 & 0 & \cdots & 0 \\ 0 & 0 & 1 & \ddots & 0 \\ \vdots & \vdots & \vdots & \ddots & \vdots \\ 0 & 0 & 0 & \cdots & 1 \\ -a_n+\eta_n u(t) & -a_{n-1}+\eta_{n-1}u(t) & -a_{n-2}+\eta_{n-2}u(t) & \cdots & -a_1+\eta_1 u(t) \end{pmatrix} \begin{bmatrix} x(t) \\ \mathcal{D}^{\alpha}x(t) \\ \mathcal{D}^{2\alpha}x(t) \\ \vdots \\ \mathcal{D}^{\alpha(n-1)}x(t) \end{bmatrix} + b_0 \begin{bmatrix} 0 \\ 0 \\ 0 \\ 1 \end{bmatrix} u(t) \tag{6.9}$$

From this, the bilinear fractional-order input-output model can be obtained and expressed as:

$$\sum_{i=0}^{n} a_i \mathcal{D}^{\alpha\times(n-i)}x(t) = b_0 u(t) + \sum_{i=1}^{n} \mathcal{D}^{\alpha\times(n-i)}x(t)\eta_i u(t) \tag{6.10}$$

where $a_0 = 1$. The obtained bilinear fractional-order input-output model is a subclass of bilinear fractional-order input-output model in (6.1) when $m = 0$. This scenario has considered the case when the output only depends on the first state yielding in a relatively straightforward conversion, similarly to the linear system.

6.2.2.2 Second case scenario

In this scenario, the output depends on the second or higher state. By applying a similar approach, used in the first scenario, there is a need to use the fractional-order derivative of a two-function product $u(t)x_i(t)$. This is then solved by using the Leibniz product rule and it leads to a sum of infinite terms $\mathcal{D}^{\alpha}\left(u(t)x_i(t)\right)=\sum_{j=0}^{\infty}\binom{\alpha}{j}\left(\mathcal{D}^{\alpha-j}u(t)\right)\left(\mathcal{D}^{j}x_i(t)\right)$, see (Herrmann 2001:17). The finite sum only occurs in the case of the integer-order derivative when $\alpha\in\mathbb{Z}^{+}$. Therefore, this subsection only focuses on bilinear integer-order systems. Bear in mind that, the bilinear integer-order system is a subclass of bilinear fractional-order systems. If the output only depends on the second the state x_2 , then (6.7) can be re-expressed as:

$$x(t)=\begin{bmatrix}0, & b_1, & 0 & \cdots, & 0\end{bmatrix}\begin{bmatrix}x_1\\x_2\\x_3\\\vdots\\x_n\end{bmatrix} \tag{6.11}$$

Therefore, $x_2=\frac{1}{b_1}x(t)$ and $\alpha=1$ in (6.3). Taking the first derivative $\mathcal{D}$ of (6.8) enables the expression to be rewritten regarding x_1 and x_2 and results:

$$\begin{bmatrix}Dx_2(t)\\\mathcal{D}^2x_2(t)\\\mathcal{D}^3x_2(t)\\\vdots\\\mathcal{D}^nx_2(t)\end{bmatrix}=\begin{pmatrix}0&1&0&\cdots&0\\0&0&1&\ddots&0\\\vdots&\vdots&\vdots&\ddots&\vdots\\0&0&0&\cdots&1\\-a_n&-a_{n-1}&-a_{n-2}&\cdots&-a_1\end{pmatrix}\begin{bmatrix}x_2(t)\\\mathcal{D}x_2(t)\\\mathcal{D}^2x_2(t)\\\vdots\\\mathcal{D}^{n-1}x_2(t)\end{bmatrix}+$$
$$\begin{bmatrix}0\\0\\0\\\vdots\\1\end{bmatrix}\mathcal{D}u(t)+\begin{pmatrix}0&0&0&\cdots&0\\0&0&0&\ddots&0\\\vdots&\vdots&\vdots&\ddots&\vdots\\0&0&0&\cdots&0\\\eta_n&\eta_{n-1}&\eta_{n-2}&\cdots&\eta_1\end{pmatrix}\begin{bmatrix}\mathcal{D}\left(u(t)x_1(t)\right)\\\mathcal{D}\left(u(t)\mathcal{D}x_1(t)\right)\\\mathcal{D}\left(u(t)\mathcal{D}^2x_1(t)\right)\\\vdots\\\mathcal{D}\left(u(t)\mathcal{D}^{n-1}x_1(t)\right)\end{bmatrix} \tag{6.12}$$

It can be noted that the last term of (6.12) is the first derivative of a two function product and deduced as:

$$\begin{bmatrix} \mathcal{D}\left(u(t)x_1(t)\right) \\ \mathcal{D}\left(u(t)\mathcal{D}x_1(t)\right) \\ \mathcal{D}\left(u(t)\mathcal{D}^2x_1(t)\right) \\ \vdots \\ \mathcal{D}\left(u(t)\mathcal{D}^{n-1}x_1(t)\right) \end{bmatrix} = u(t)\begin{bmatrix} x_2(t) \\ \mathcal{D}x_2(t) \\ \mathcal{D}^2x_2(t) \\ \vdots \\ \mathcal{D}^{n-1}x_2(t) \end{bmatrix} + \mathcal{D}u(t)\begin{bmatrix} x_1(t) \\ x_2(t) \\ \mathcal{D}x_2(t) \\ \vdots \\ \mathcal{D}^{n-2}x_2(t) \end{bmatrix} \tag{6.13}$$

This derivative operation produces x_1. The existence of x_1 prevents conversion from state-space to input-output model. Considering $x_2 = \frac{1}{b_1}x(t)$, (6.12) and (6.13) can be express in terms of the input $u(t)$, output $x(t)$ and first state x_1 as described by the following equation:

$$\begin{aligned} \sum_{i=0}^{n} a_{n-i}\mathcal{D}^i x(t) = b_1\mathcal{D}u(t) + u(t)\sum_{i=1}^{n}\eta_i\mathcal{D}^{n-i}x(t) \\ + \mathcal{D}u(t)\left[\sum_{i=2}^{n}\eta_i\mathcal{D}^{n-i}x(t)\right] + b_1\mathcal{D}u(t)\eta_1 x_1 \end{aligned} \tag{6.14}$$

The last term of (6.14) contains the first state so that it is not the bilinear fractional-order input-output model, thus the conversion from bilinear fractional-order state-space representation to a bilinear fractional-order input-output model is not realisable in the second state-space scenario. Therefore, the proposed identification approach cannot be applied to identify the bilinear fractional-order state-space model unless the output depends on the first state as illustrated in the first case scenario.

6.2.3 Bilinear fractional-order input-output model simulation

In general, the simulation of a nonlinear system is a complex task, and it is even more complex when the system is of fractional-order. In the literature review, different approaches have been presented for approximating the fractional-order derivative-integral terms. The Simulink block, which approximates the fractional-order integral term,

has been already introduced in the FOMCON Simulink toolbox. Therefore, the bilinear fractional-order system is implemented using a Simulink-based approach. Essentially, the Simulink-based approach maps the state-space representation into Simulink. However, (as has been demonstrated) not all bilinear fractional-order input-output models are realised by bilinear fractional-order state-space and vice-versa. Hence, two different representations are considered in the following subsections:

6.2.3.1 Approach based on state-space

In this approach, the states are used to produce nonlinear operations of bilinear fractional-order state-space model. A diagrammatic representation of the bilinear fractional-order state-space model given by (6.3) and (6.4) and defined by matrices in (6.6) is provided in

Figure 6-1. Being able to express the input-output bilinear model in its state-space form provides a convenient way for the implementation of such a model in the MATLAB/Simulink software. However, the bilinear fractional-order input-output can also be directly implemented in Simulink as shown in Figure 6-2 because there are no fractional-order derivative terms associated with the input in (6.10).

6.2.3.2 Approach based on input-output model

The fractional-order input-output model, which can be expressed in the state-space, is only the case when there are no fractional-order derivative terms associated with the input terms as the first case scenario. The diagrammatic representation of the bilinear fractional-order input-output model in (6.10) is presented in Figure 6-2. The idea of the proposed approach in this thesis is to use the highest fractional-order derivative term of the input as an input to the Simulink model as shown in Figure 6-3. Therefore, the bilinear fractional-order input-output model, which contains the fractional-order derivative terms associated with the input terms, can be simulated when the input can be selected for the identification purpose in advance by the user. Three steps summarise this approach:

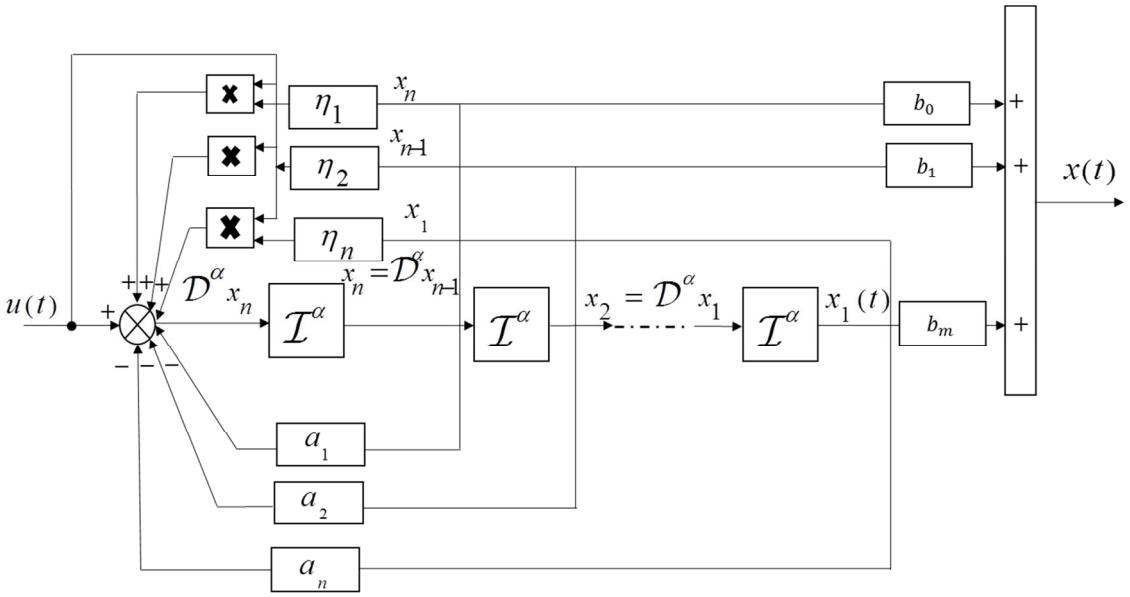

Figure 6-1: Equivalent block diagram for the generalised bilinear fractional-order commensurate state-space representation in (6.3), (6.4) and (6.6).

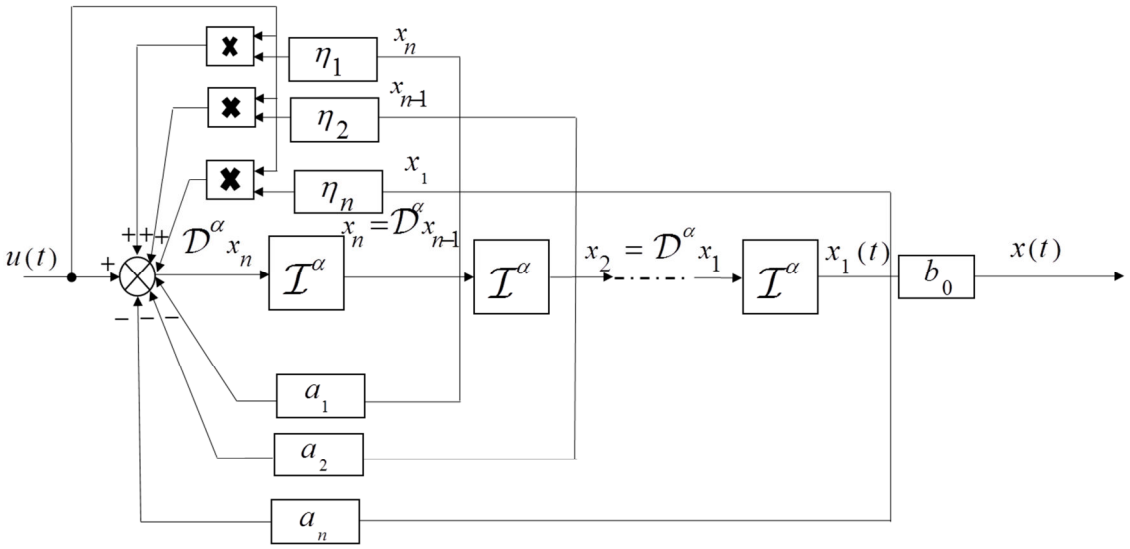

Figure 6-2: Equivalent block diagram for the bilinear fractional-order commensurate state-space representation in the first case scenario.

I. Design the input $u(t)$ according to the identification requirements.

II. Obtain the highest fractional-order derivative term of the input $\mathcal{D}^{\alpha m}u(t)$ based on the designed input signal. Therefore, the input and its higher fractional-order derivative term must be known in advance.

III. Use the selected input as an input $u(t)$ to the system, required to be identified, and the highest fractional-order derivative input term $\mathcal{D}^{\alpha m}u(t)$ as an input to the bilinear fractional-order input-output model as shown in Figure 6-3.

Since the highest fractional-order derivative input term is known, the generalised bilinear fractional-order commensurate input-output model, described in (6.1), can be diagrammatically represented as illustrated in Figure 6-3. By considering this, any generalised bilinear fractional-order commensurate input-output model can be realised in simulation using the Simulink.

6.3 Nonlinear structure detection

Leontaritis and Billings (1987) have firstly claimed that the ERR of each candidate term can show the importance of this term to the variance of the output. Since then, the ERR has been used to rank the importance of the candidate system's terms. The ERR of each candidate term is between 0 to 100% and the highest ERR means the candidate term contributes more to the output variance. The sum of the ERR of all terms of the actual system gives 100%. Therefore, selecting terms with the highest ERR leads to choosing the better nonlinear structure. The ERR is derived from the orthogonal least squares estimator and presented in (Tsang, and Billings 1994 and Billings 2013) as:

$$ERR_i = \frac{\frac{1}{N}\sum_{k=1}^{N} g_i^2 w_i^2(t_k)}{\frac{1}{N}\sum_{k=1}^{N} y^2(t_k)} \times 100 \tag{6.15}$$

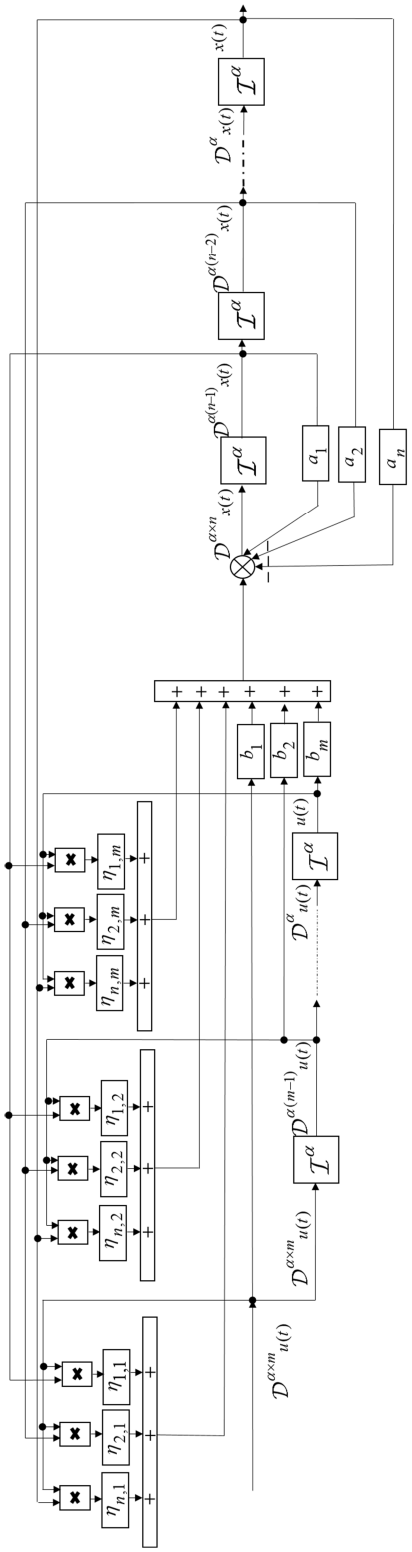

Figure 6-3: Equivalent block diagram for the generalised bilinear fractional-order commensurate input-output model in (6.1).

and

$$
\begin{aligned}
w_1(t_k) &= \varphi_1(t_k) \\
w_i(t_k) &= \varphi_i(t_k) - \sum_{j=1}^{i-1} \eta_{ji} w_j(t_k), \qquad i = 1,2,\cdots,M \\
\eta_{ji} &= \frac{\frac{1}{N}\sum_{k=1}^{N} w_j(t_k)\varphi_i(t_k)}{\frac{1}{N}\sum_{k=1}^{N} w_j^2(t_k)}, \qquad \begin{cases} j = 1,\cdots,\mathrm{i}-1 \\ i = 1,\cdots,M \end{cases} \\
\mathrm{g}_i &= \frac{\frac{1}{N}\sum_{k=1}^{N} y(t_k) w_i(t_k)}{\frac{1}{N}\sum_{k=1}^{N} w_i^2(t_k)}, \qquad i = 1,2,\cdots,M
\end{aligned}
\tag{6.16}
$$

where φ_i and g_i are the i^{th} elements in the classical regression and auxiliary vectors, respectively. N is the number of samples, collected. Furthermore, w_s are the orthogonal basis and related as

$$
\sum_{k=1}^{N} w_i(t_k) w_j(t_k) = \begin{cases} c_i, i = j \\ 0, i \neq j \end{cases}
\tag{6.17}
$$

A larger or smaller value of $\mathrm{ERR_i}$ indicates the significance or insufficiency of the candidate term to the variance of the output, respectively, for more details see (Billings 2013). The sum of the actual terms and the error function are equal to 100. This test is used in this work for selecting the better candidates for structuring the nonlinear fractional-order systems.

6.4 Numerical study on bilinear system identification

Two numerical examples are presented in this section for evaluating the empirical performance of the proposed identification approach for detecting the structure and estimating the parameters of bilinear fractional-order systems from collected input-output data. The selected bilinear structures are the bilinear fractional-order commensurate state-space model, addressed in the first scenario, and generalised bilinear fractional-order commensurate input-output model.

The system in (6.19) is simulated for 100s with fixed sampling time 10^{-3}s. The selected Simulink solver is ode4 (Runge-Kutta). The fractional-order integral block is provided by the FOMCON Simulink library with a frequency range [0.001rad.s^{-1}; 1000 rad.s^{-1}] and approximation order 25.

The input is selected based on two significant properties (i) it should be bounded by such small constraints because the stability of the bilinear fractional-order system is a function of the input, thus, it is quite sensitive to the input quantities and (ii) the frequency range, the input covers, should be less than a cut-off frequency of the delayed fractional-order state variable filter. Thus, the input is selected to be a sum of ten sine waves with different amplitudes and frequencies less than the cut-off frequency and then it is filtered by the delayed fractional-order state variable filter, which is a cascade of 6^{th} order Butterworth filter and three stages of 2^{nd} order of all-pass filter. The cut-off frequency is selected to be 6rad.s^{-1} and the generated delay is 3.0914s as shown in Figure 6-4. The delay is then eliminated from the input signal and then the input can be used for identification purposes.

The delayed fractional-order state variable filter, used for filtering the input and output signals in both examples, is designed using an 8^{th} order fractional-order Butterworth filter, equalised by five stages of 2^{nd} order all-pass filters. The cut-off frequency is selected to be 12rad.s^{-1} and the delay is 2.3960s as shown in Figure 6-4.

6.4.1 Performance criteria

For studying the statistical properties of the estimators, a Monte Carlo (MC) simulation of 100 runs is implemented with different noise realisations. To evaluate the statistical performance of the proposed approach, there is a need to compute the mean and standard deviations (std) of the estimates of bilinear fractional-order model parameters.

Furthermore, the empirical normalised root mean square error, denoted RMSE, is computed and defined as:

$$RMSE(\hat{\theta}_j) = \sqrt{\frac{1}{N_{MC}} \sum_{i=1}^{N_{MC}} \left(\frac{\theta_j - \hat{\theta}_j(i)}{\theta_j} \right)^2} \tag{6.18}$$

where θ_j and $\hat{\theta}_j$ denoted the j[th] element of the true and estimated parameters in parameter vector, respectively, and N_{MC} is the number of MC runs. The normalised mean square error between the estimated parameter vectors, obtained from the noise-free output and other estimated parameter vectors, is denoted RMSE[0].

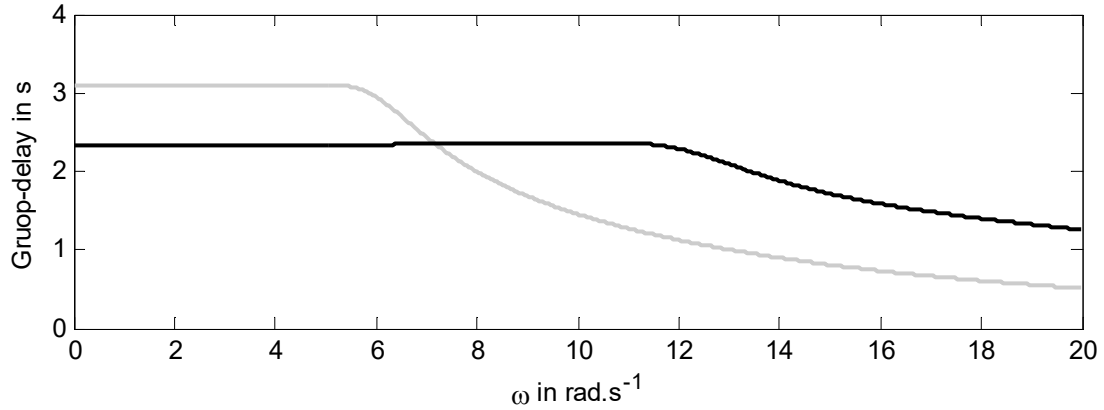

Figure 6-4: Equalisation 6[th] and 8[th] order Butterworth filters with three and five stages of second order all-pass filters, respectively and presented in solid-grey and solid-black, respectively.

6.4.2 First scenario example

A bilinear fractional-order commensurate state-space system, described in ARX and OE models, respectively, is expressed as:

$$\varsigma_{1,ARX}\begin{cases}\begin{bmatrix}\mathcal{D}^{0.5}x_1(t)\\ \mathcal{D}^{0.5}x_2(t)\\ \mathcal{D}^{0.5}x_3(t)\end{bmatrix}=\begin{pmatrix}0 & 1 & 0\\ 0 & 0 & 1\\ -0.75 & -2.75 & -3\end{pmatrix}\begin{bmatrix}x_1(t)\\ x_2(t)\\ x_3(t)\end{bmatrix}+\begin{pmatrix}0\\ 0\\ 1\end{pmatrix}u(t)\\ \qquad +u(t)\begin{pmatrix}0 & 0 & 0\\ 0 & 0 & 0\\ -0.2 & -0.5 & -1\end{pmatrix}\begin{bmatrix}x_1(t)\\ x_2(t)\\ x_3(t)\end{bmatrix}+\begin{pmatrix}0\\ 0\\ 1\end{pmatrix}e(t)\\ y(t)=\begin{bmatrix}1 & 0 & 0\end{bmatrix}\begin{bmatrix}x_1(t)\\ x_2(t)\\ x_3(t)\end{bmatrix}\end{cases} \tag{6.19}$$

$$\varsigma_{1,OE}\begin{cases}\begin{bmatrix}\mathcal{D}^{0.5}x_1(t)\\ \mathcal{D}^{0.5}x_2(t)\\ \mathcal{D}^{0.5}x_3(t)\end{bmatrix}=\begin{pmatrix}0 & 1 & 0\\ 0 & 0 & 1\\ -0.75 & -2.75 & -3\end{pmatrix}\begin{bmatrix}x_1(t)\\ x_2(t)\\ x_3(t)\end{bmatrix}+\begin{pmatrix}0\\ 0\\ 1\end{pmatrix}u(t)\\ \qquad +u(t)\begin{pmatrix}0 & 0 & 0\\ 0 & 0 & 0\\ -0.2 & -0.5 & -1\end{pmatrix}\begin{bmatrix}x_1(t)\\ x_2(t)\\ x_3(t)\end{bmatrix}\\ y(t)=\begin{bmatrix}1 & 0 & 0\end{bmatrix}\begin{bmatrix}x_1(t)\\ x_2(t)\\ x_3(t)\end{bmatrix}+e(t)\end{cases} \tag{6.20}$$

where $u(t)$, $x(t)$, $y(t)$ and $x_i(t)$ are the input, noise-free output, noisy output and the ith state of the system while $e(t)$ is a white noise signal with variance σ_e^2, and is selected based on the *SNR*, defined in (4.25).

Before starting the identification steps, the system which is required to be identified, must be represented in the input-output model form. The state-space representation can be converted to the input-output model form by following the equation from (6.7) to (6.10). Thus, the input-output models of (6.19) and (6.20), required to apply the delayed fractional-order state variable identification approach, are expressed, respectively:

$$\varsigma_{1,ARX}\begin{cases}\mathcal{D}^{1.5}y(t)+a_1\mathcal{D}y(t)+a_2\mathcal{D}^{0.5}y(t)+a_3y(t)=b_0u(t)\\ +u(t)\eta_3y(t)+u(t)\eta_2\mathcal{D}^{0.5}y(t)+u(t)\eta_1\mathcal{D}y(t)+e(t)\end{cases} \tag{6.21}$$

and

$$\varsigma_{1,\mathrm{OE}}\begin{cases}\mathcal{D}^{1.5}x(t)+a_1\mathcal{D}x(t)+a_2\mathcal{D}^{0.5}x(t)+a_3x(t)=b_0u(t)\\ +u(t)\eta_1\mathcal{D}x(t)+u(t)\eta_2\mathcal{D}^{0.5}x(t)+u(t)\eta_3x(t)\\ \\ y(t_k)=x(t_k)+e(t_k)\end{cases} \tag{6.22}$$

The performance of the selected delayed fractional-order state variable filter can be observed from the delay introduced in the input, output, derivative terms and nonlinear terms as illustrated in Figure 6-5, Figure 6-6, Figure 6-7, Figure 6-8, Figure 6-9, Figure 6-10, Figure 6-11 and Figure 6-12 where *SNR*=10dB. The comparison of the input and filtered input shows that a significant delay function has been obtained because the filtered input is lagging behind the input by approximately 2.3960s, as shown in Figure 6-5. The same delay appears in the filtered output, filtered fractional-order derivative terms of the noise-free output and the filtered bilinear terms as illustrated in Figure 6-6, Figure 6-7, Figure 6-8, Figure 6-9, Figure 6-10, Figure 6-11, Figure 6-12. Although, the *SNR*=10dB is a rather high noise level, the delayed fractional-order state variable filter is demonstrated to perform well. It results from the fact that the delayed fractional-order state variable filter commutes with the bilinear terms.

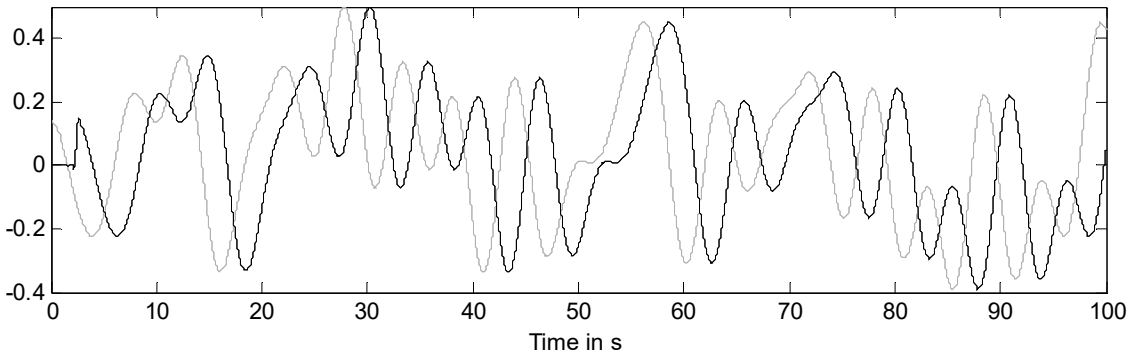

Figure 6-5: Input and filtered input are presented in black and grey, respectively.

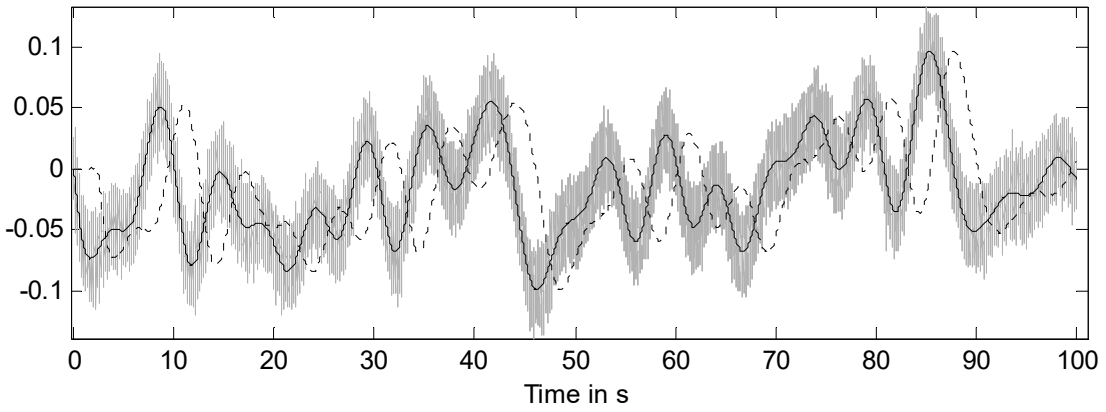

Figure 6-6: Noise-free output $x(t)$, noisy output $y(t)$ and filtered noisy output $y_{\Gamma}(t)$ are presented in solid-black, solid-grey and dotted-grey lines, respectively.

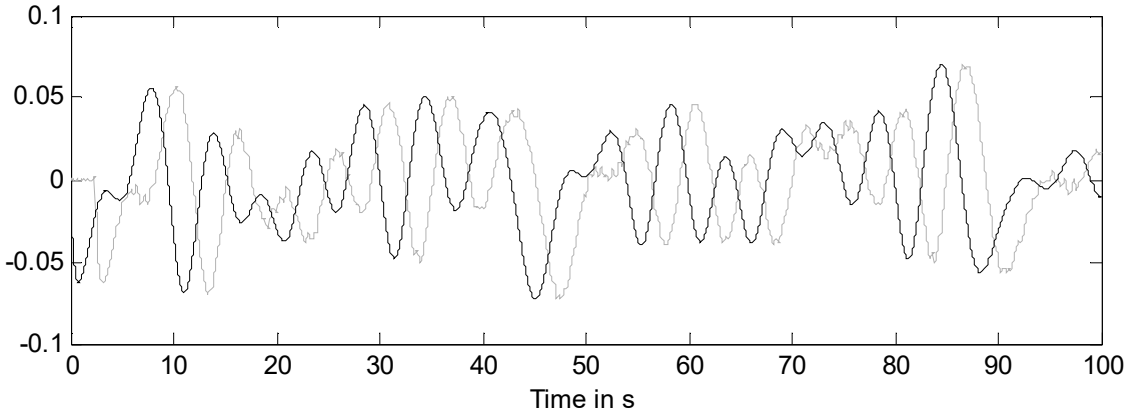

Figure 6-7: The noise-free 0.5 order derivative term of $\mathcal{D}^{0.5}x(t)$ and the filtered noisy 0.5 order derivative term $\mathcal{D}^{0.5}y_{\Gamma}(t)$ are in solid-black and solid-grey lines, respectively.

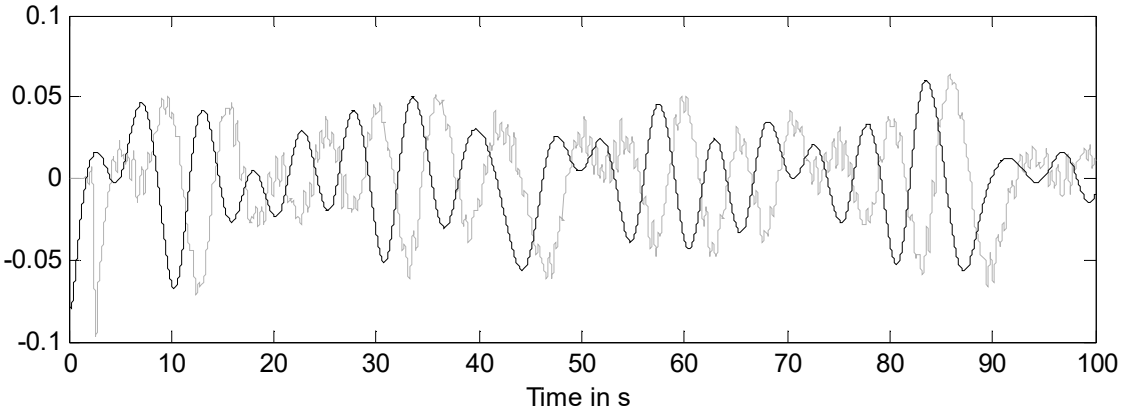

Figure 6-8: The noise-free first order derivative term of $\mathcal{D}x(t)$ and the filtered noisy first order derivative term $\mathcal{D}y_{\Gamma}(t)$ are in solid-black and solid-grey lines, respectively.

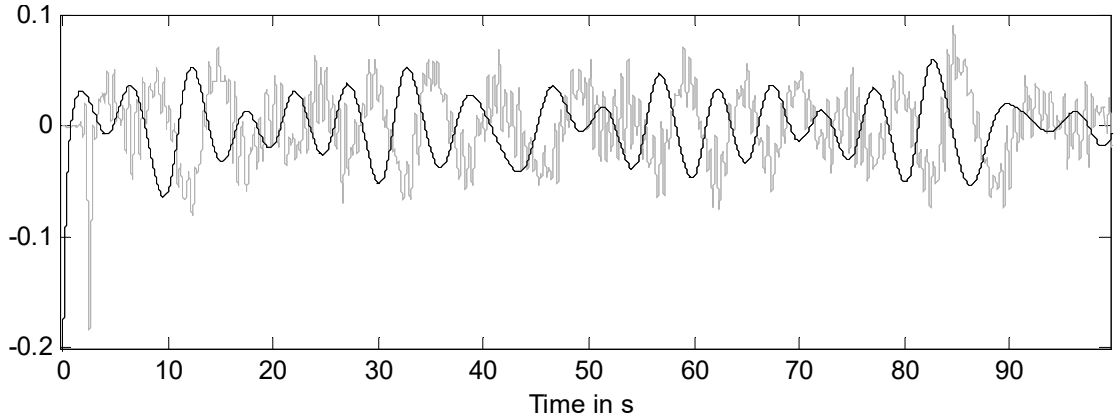

Figure 6-9: The noise-free 1.5 order derivative term of $\mathcal{D}^{1.5}x(t)$ and the filtered noisy 1.5 order derivative term $\mathcal{D}^{1.5}y_{\Gamma}(t)$ are in solid-black and solid-grey lines, respectively.

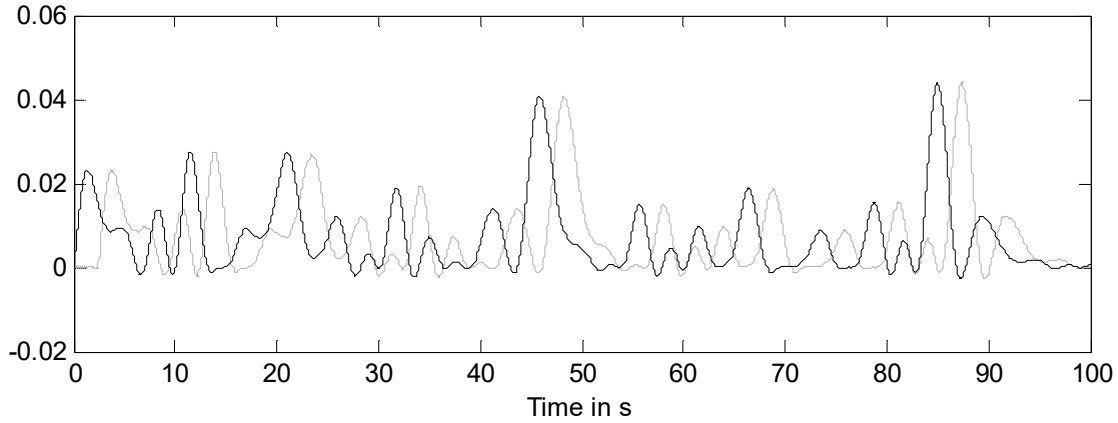

Figure 6-10: The noise-free bilinear fractional-order terms $u(t)\times x(t)$ and the filtered noisy bilinear fractional-order terms $u(t)\times y_{\Gamma}(t)$ are presented in solid-black and solid-grey lines, respectively.

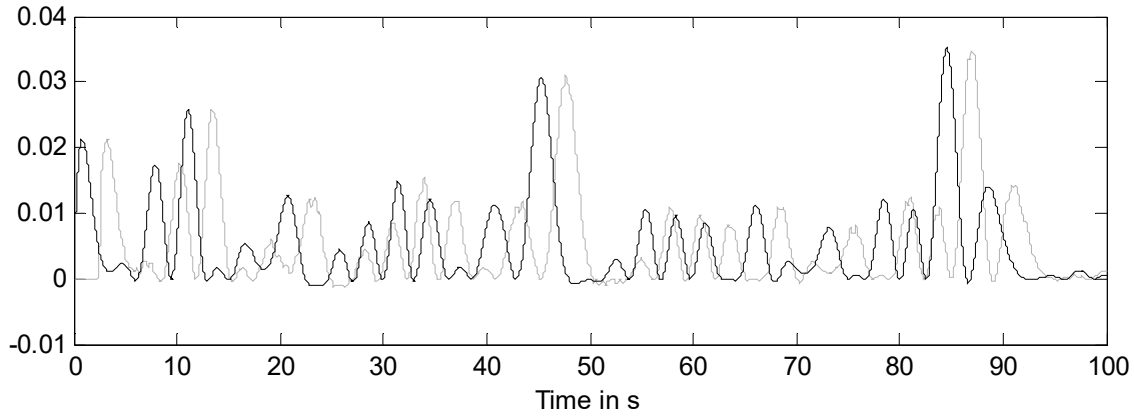

Figure 6-11: The noise-free bilinear fractional-order terms $u(t)\times\mathcal{D}^{0.5}x(t)$ and the filtered noisy bilinear fractional-order terms $u(t)\times\mathcal{D}^{0.5}y_{\Gamma}(t)$ are presented in solid-black and solid-grey lines, respectively.

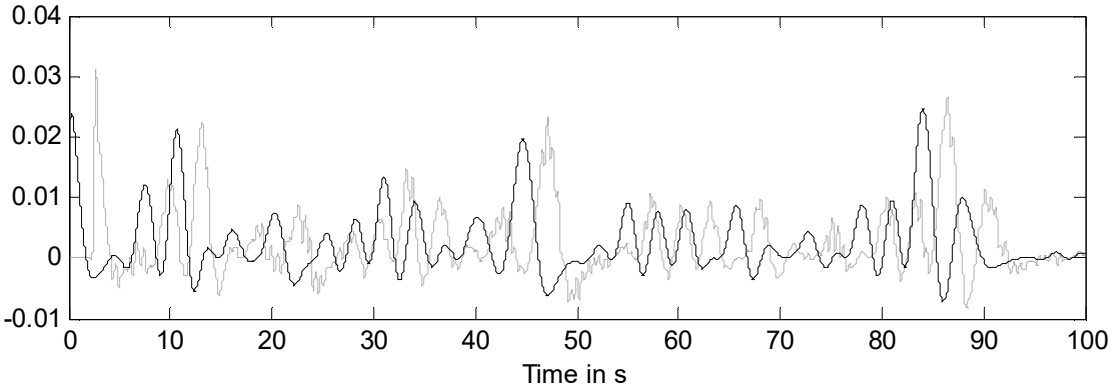

Figure 6-12: The noise-free bilinear fractional-order terms $u(t)\times\mathcal{D}x(t)$ and the filtered noisy bilinear fractional-order terms $u(t)\times\mathcal{D}y_{\Gamma}(t)$ are presented in solid-black and solid-grey lines, respectively.

6.4.2.1 Structure detection

This stage has crucial importance for the system identification process because the better-selected structure leads to a simpler parameter estimation stage. In this case, the initial specification contains twelve candidate terms to identify the structure of (6.21) (as presented in iteration 1 in Table 6-1. At each iteration, the most significant term, which has the highest ERR, is selected and removed from candidate term list where the selected terms are shown underlined in Table 6-1. This process is repeated until no significant terms exist in the candidate term list. It can be noted from Table 6-1 that the final selected structure matches the actual structure in (6.21) and (6.22).

Table 6-1: Process of term selection

Iteration	*Candidate term*	*ERR*

1	$\underline{u_\Gamma(t)}$	<u>49.0310</u>
	$\mathcal{D}^{0.5}y_\Gamma(t)$	28.0050
	$\mathcal{D}^{0.5}u_\Gamma^2(t)$	0.0310
	$\mathcal{D}y_\Gamma(t)$	14.9989
	$\mathcal{D}^{1.5}y_\Gamma(t)$	0.8002
	$u_\Gamma^2\mathcal{D}^{1.5}y_\Gamma(t)$	0.8002
	$u_\Gamma(t)\mathcal{D}y_\Gamma^2(t)$	6.3570
	$y_\Gamma^2(t)$	0.0002
	$u_\Gamma(t)y_\Gamma(t)$	0.0132
	$u_\Gamma(t)\mathcal{D}^{0.5}y_\Gamma(t)$	0.0071
	$u_\Gamma(t)\mathcal{D}y_\Gamma(t)$	0.0020
	$u_\Gamma^2(t)\mathcal{D}y_\Gamma^2(t)$	0.0013
2	$\underline{\mathcal{D}^{0.5}y_\Gamma(t)}$	<u>42.3120</u>
	$\mathcal{D}^{0.5}u_\Gamma^2(t)$	0.0241
	$\mathcal{D}y_\Gamma(t)$	0.0089
	$\mathcal{D}^{1.5}y_\Gamma(t)$	0.0014
	$u_\Gamma^2\mathcal{D}^{1.5}y_\Gamma(t)$	0.0003
	$u_\Gamma(t)\mathcal{D}y_\Gamma^2(t)$	0.0001
	$y_\Gamma^2(t)$	0.0002
	$u_\Gamma(t)y_\Gamma(t)$	5.0012
	$u_\Gamma(t)\mathcal{D}^{0.5}y_\Gamma(t)$	0.9010
	$u_\Gamma(t)\mathcal{D}y_\Gamma(t)$	0.0201
	$u_\Gamma^2(t)\mathcal{D}y_\Gamma^2(t)$	0.0001
3	$\mathcal{D}^{0.5}u_\Gamma^2(t)$	0.0241
	$\mathcal{D}y_\Gamma(t)$	1.2023
	$\mathcal{D}^{1.5}y_\Gamma(t)$	0.0801
	$u_\Gamma^2\mathcal{D}^{1.5}y_\Gamma(t)$	0.0003
	$u_\Gamma(t)\mathcal{D}y_\Gamma^2(t)$	0.0006
	$y_\Gamma^2(t)$	0.0020
	$\underline{u_\Gamma(t)y_\Gamma(t)}$	<u>12.7234</u>
	$u_\Gamma(t)\mathcal{D}^{0.5}y_\Gamma(t)$	0.0090
	$u_\Gamma(t)\mathcal{D}y_\Gamma(t)$	0.0012
	$u_\Gamma^2(t)\mathcal{D}y_\Gamma^2(t)$	0.0001

4	$\mathcal{D}^{0.5}u_\Gamma^2(t)$	0.0241
	$\underline{\mathcal{D}y_\Gamma(t)}$	<u>3.1001</u>
	$\mathcal{D}^{1.5}y_\Gamma(t)$	0.0061
	$u_\Gamma^2\mathcal{D}^{1.5}y_\Gamma(t)$	0.0003
	$u_\Gamma(t)\mathcal{D}y_\Gamma^2(t)$	0.0001
	$y_\Gamma^2(t)$	0.06E-2
	$u_\Gamma(t)\mathcal{D}^{0.5}y_\Gamma(t)$	0.8080
	$u_\Gamma(t)\mathcal{D}y_\Gamma(t)$	0.0012
	$u_\Gamma^2(t)\mathcal{D}y_\Gamma^2(t)$	0.001E-2
5	$\mathcal{D}^{0.5}u_\Gamma^2(t)$	0.07E-3
	$\mathcal{D}^{1.5}y_\Gamma(t)$	0.0061
	$u_\Gamma^2\mathcal{D}^{1.5}y_\Gamma(t)$	0.0003
	$u_\Gamma(t)\mathcal{D}y_\Gamma^2(t)$	0.02E-3
	$y_\Gamma^2(t)$	0.09E-4
	$\underline{u_\Gamma(t)\mathcal{D}^{0.5}y_\Gamma(t)}$	<u>0.7256</u>
	$u_\Gamma(t)\mathcal{D}y_\Gamma(t)$	0.0002
	$u_\Gamma^2(t)\mathcal{D}y_\Gamma^2(t)$	0.008E-3
6	$\mathcal{D}^{0.5}u_\Gamma^2(t)$	0.01E-5
	$\underline{\mathcal{D}^{1.5}y_\Gamma(t)}$	<u>0.0805</u>
	$u_\Gamma^2\mathcal{D}^{1.5}y_\Gamma(t)$	0.09E-4
	$u_\Gamma(t)\mathcal{D}y_\Gamma^2(t)$	0.08E-5
	$y_\Gamma^2(t)$	0.01E-4
	$u_\Gamma(t)\mathcal{D}y_\Gamma(t)$	0.0012
	$u_\Gamma^2(t)\mathcal{D}y_\Gamma^2(t)$	0.006E-4
7	$\mathcal{D}^{0.5}u_\Gamma^2(t)$	0.01E-6
	$u_\Gamma^2\mathcal{D}^{1.5}y_\Gamma(t)$	0.09E-5
	$u_\Gamma(t)\mathcal{D}y_\Gamma^2(t)$	0.03E-5
	$y_\Gamma^2(t)$	0.09E-5
	$\underline{u_\Gamma(t)\mathcal{D}y_\Gamma(t)}$	<u>0.0091</u>
	$u_\Gamma^2(t)\mathcal{D}y_\Gamma^2(t)$	0.006E-4

6.4.2.2 Parameter estimation

The results obtained from the MC simulation analysis are presented in Table 6-2, where mean values, standard deviations, RMSE and RMSE^0 performance criteria, introduced in (6.18), are shown. Due to the fact that the delay is approximated by the filter and seven

parameters are required to be estimated, the noise-free estimated parameters do not equal to the actual parameters and are provided in Table 6-2. The average value of $RMSE^0$ is less than RMSE because the estimates converge towards the estimates of the noise-free system. The estimation of the higher derivative terms of the output are less accurate because the filter higher derivative terms are more effected by the noise, as shown in Figure 6-7, Figure 6-8 and Figure 6-9. Therefore, similar observations can be seen in the estimated bilinear parameters because they are obtained using the higher output derivative terms additional to the bilinear influence on the estimation. Although the noise type in the second system seems rather high, the proposed approach, which uses the instrumental variables, appears to be robust.

Table 6-2: Monte Carlo simulation results of parameter estimation of the bilinear fractional-order state-space model with a different number of runs where a_0= 1 and SNR =20, 40dB for ARX and OE model respectively.

System	N_{MC}	θ_j	a_3=0.75	a_2=2.75	a_1=3	b_0=1	η_1=-1	η_2=-0.5	η_3=-0.2
		θ_j^0	0.7501	2.7501	3.0001	1.0000	-1.0012	-0.5000	-0.2001
$\varsigma_{1,ARX}$	50	mean	0.7430	2.7452	2.9912	0.9973	-0.9835	-0.5131	-0.1960
		std	0.0504	0.0651	0.0858	0.0281	0.1534	0.0732	0.0235
		RMSE	0.0125	0.0006	0.0010	0.0027	0.0165	0.0525	0.1008
		$RMSE^0$	0.0127	0.0006	0.0010	0.0027	0.0177	0.0525	0.1032
$\varsigma_{1,ARX}$	100	mean	0.7521	2.7538	3.0040	1.0013	-1.0133	-0.5015	-0.2005
		std	0.0467	0.0598	0.0785	0.0257	0.1573	0.0785	0.0233
		RMSE	0.0037	0.0005	0.0004	0.0013	0.0133	0.0059	0.0126
		$RMSE^0$	0.0036	0.0005	0.0004	0.0013	0.0121	0.0059	0.0101
$\varsigma_{2,OE}$	50	mean	0.7473	2.7481	2.9965	0.9989	-0.9945	-0.5054	-0.1984
		std	0.0213	0.0259	0.0353	0.0115	0.0657	0.0314	0.0100
		RMSE	0.0048	0.0003	0.0004	0.00011	0.0055	0.0216	0.0410
		$RMSE^0$	0.0050	0.0003	0.0004	0.0011	0.0067	0.0216	0.0435
$\varsigma_{2,OE}$	100	mean	0.7511	2.7515	3.0017	1.0006	-1.0078	-0.5000	-0.2002
		std	0.0200	0.0242	0.0328	0.0107	0.0658	0.0343	0.0106

RMSE	0.0019	0.0002	0.0002	0.0006	0.0078	0.0001	0.0051
$RMSE^0$	0.0017	0.0002	0.0002	0.0006	0.0066	0.0001	0.0026

6.4.3 Bilinear fractional-order with input derivative term example

The issue associated with the generalised bilinear fractional-order commensurate input-output model is that it is not an easy task to simulate the system when the system requires any derivative input term. For evaluating the proposed approach for simulating this kind of system, the systems in (6.21) and (6.22) are re-described by including fractional-order input derivative terms, and re-expressed, respectively, as:

$$\varsigma_{2,ARX}\begin{cases}\mathcal{D}^{1.5}y(t)+0.75\mathcal{D}y(t)+2.75\mathcal{D}^{0.5}y(t)+3y(t)=0.2\mathcal{D}u(t)+0.8\mathcal{D}^{0.5}u(t)\\ +u(t)-u(t)\mathcal{D}y(t)-0.5u(t_k)\mathcal{D}^{0.5}y(t)-0.2u(t)y(t)+e(t)\end{cases} \tag{6.23}$$

and

$$\varsigma_{2,OE}\begin{cases}\mathcal{D}^{1.5}x(t)+0.75\mathcal{D}x(t)+2.75\mathcal{D}^{0.5}x(t)+3x(t)=0.2\mathcal{D}u(t)+0.8\mathcal{D}^{0.5}u(t)\\ +u(t)-u(t)\mathcal{D}x(t)-0.5u(t)\mathcal{D}^{0.5}x(t)-0.2u(t)x(t)\\ \\ y(t_k)=x(t_k)+e(t_k)\end{cases} \tag{6.24}$$

where $u(t)$, $x(t)$, $y(t)$ and $x_i(t)$ are the input, noise-free output, noisy output and the i^{th} state of the system while $e(t)$ is a white noise signal with variance, selected based on the *SNR* in (4.25).

Representations (6.23) and (6.24) are in input-output model form, therefore, the delayed fractional-order state variable identification approach can be directly applied to estimate the parameters of (6.23) and (6.24). In this part, the simulation has used $\mathcal{D}u(t)$ instead of $u(t)$ to generate all the required data for identification.

6.4.3.1 Parameter estimation

The results obtained from the MC simulation analysis are presented in mean and standard deviations in Table 6-3. Furthermore, the noise-free estimated parameters are obtained

and presented in Table 6-3. Table 6-3 demonstrates that the proposed approach gives unbiased estimates of the bilinear fractional-order model parameters. Although, the noise type in the second system is high, the proposed approach, using the instrumental variables, would again appear to be robust. RMSE^0 and RMSE in (6.18) show that the estimates tend to converge towards the estimates of the noise-free system.

Table 6-3: Monte Carlo simulation results of parameter estimation of the bilinear fractional-order state-space model with a different number of MC runs where a_0= 1 and *SNR* =30,50 dB for ARX and OE model respectively.

		θ_j	a_3=0.75	a_2=2.75	a_1=3	b_0=0.2	b_1=0.8	b_2=1	η_1=-1	η_2=-0.5	η_3=-0.2
System	N_{MC}	θ_j^0	0. 7483	2.7527	2.9994	0.1994	0.8009	0.9998	-1.0007	-0.5004	-0.2000
$\varsigma_{1,ARX}$	50	mean	0.7783	2.6978	3.0507	0.2091	0.7814	1.0168	-0.9968	-0.5014	-0.2031
		std	0.1550	0.2518	0.1939	0.0568	0.0867	0.0644	0.0270	0.0273	0.0122
		RMSE	0.0502	0.0069	0.0056	0.2264	0.0291	0.0168	0.0049	0.0058	0.0769
		RMSE^0	0.0535	0.0073	0.0057	0.2428	0.0304	0.0170	0.0056	0.0042	0.0769
$\varsigma_{1,ARX}$	100	mean	0.7875	2.6909	3.0281	0.2133	0.7797	1.0093	-0.9968	-0.4981	-0.2017
		std	0.1673	0.2758	0.1979	0.0612	0.0951	0.0657	0.0267	0.0274	0.0126
		RMSE	0.0667	0.0078	0.0031	0.3314	0.0317	0.0093	0.0032	0.0077	0.0430
		RMSE^0	0.0700	0.0082	0.0032	0.3485	0.0330	0.0095	0.0039	0.0093	0.0430
$\varsigma_{2,OE}$	50	mean	0.7692	2.7224	3.0145	0.2066	0.7905	1.0048	-0.9998	-0.4993	-0.2009
		std	0.0669	0.1031	0.0690	0.0248	0.0351	0.0229	0.0105	0.0116	0.0044
		RMSE	0.0341	0.0037	0.0016	0.1650	0.0149	0.0048	0.0016	0.0027	0.0234
		RMSE^0	0.0373	0.0040	0.0017	0.1811	0.0162	0.0050	0.0023	0.0043	0.0234
$\varsigma_{2,OE}$	100	mean	0.7666	2.7273	3.0052	0.2060	0.7924	1.0017	-0.9998	-0.4986	-0.2004
		std	0.0726	0.1153	0.0739	0.0267	0.0395	0.0246	0.0109	0.0114	0.0047
		RMSE	0.0295	0.0030	0.0006	0.1502	0.0119	0.0017	0.0002	0.056	0.0094
		RMSE^0	0.0327	0.0033	0.0006	0.1662	0.0133	0.0019	0.0009	0.0072	0.0094

6.5 Conclusions and further work

In this chapter, the bilinear fractional-order system has been introduced. It has been demonstrated that not all bilinear fractional-order state-space representations are realised by the bilinear fractional-order input-output model. It has been shown that the only realisable bilinear fractional-order state-space model corresponds to an input-output model is when the output equation depends only on the first state.

For simulating the bilinear fractional-order input-output model, there is a need to have the state-space representation of the system. In the case where the bilinear fractional-order input-output model has any input derivative terms, obtaining the state-space realisation could be a difficult step or may even not be realisable. However, this stimulating issue has been solved by considering the highest fractional-order derivative input term, so long as this it know a priori, and treated as an input to the model. This is an interesting observation, and one whereby even if the highest power were not known a priori, it could be estimated in an iterative manner as part of an extended model structure identifications scheme.

The main goal of this chapter was to identify the bilinear fractional-order system from collected input data. This chapter has outlined how the error reduction ratio can be used as an elegant tool for detecting the system structure. After the system structure has been selected, the delayed fractional-order state variable identification approach has been applied to the simulated bilinear system with different noise types. The parameters of the bilinear fractional-order model have been estimated.

Note that the identification process is implemented regardless of the stability of the bilinear fractional-order system. It would be useful if the stability of bilinear fractional-order system could be considered in future work.

The proposed approach works well with bilinear systems when it is possible to describe the system in input-output model. It is recommended in that further work should consider the state-space representations, which have been covered in this chapter, and where natural extensions of the procedure have been alluded.

Chapter 7: CONCLUSIONS AND FURTHER RESEARCH DIRECTIONS

7.1 Conclusions

This section presents a comprehensive summary of the key outcomes and main contributions that have arisen in this research in the order of their considered importance.

7.1.1 Design of delayed fractional-order state variable filter for nonlinear model parameter estimation

In Chapter Five, an extension to the delayed state variable identification approach to handle fractional-order nonlinear systems has been proposed. This extension is considered to be the key algorithmic outcome of this thesis. The delayed state variable identification approach is based on a Butterworth filter in a series connection with an all-pass filter resulting in filtered signals having a constant group-delay. The design of the delayed fractional-order state variable filter requires the fractional-order implementation of the Butterworth filter. Three methods are proposed, termed: fractional-order Butterworth filter of base-order $\alpha = 0.5$ design, the square root base design for base-order $\alpha = 1/2^n$ and the compartmental fractional-order Butterworth filter design. The

compartmental fractional-order Butterworth filter showed the best performance when generating the delayed fractional-order state variables. Subsequently, the state variables are equalised by an all-pass filter to achieve constant group-delay. The number of all-pass filters depends on the order of the fractional-order Butterworth filter and the selected cut-off frequency of the delayed fractional-order state variable filter.

7.1.2 Parameter estimation of continuous-time fractional-order Hammerstein (HFC), Wiener (WFC), and Hammerstein-Wiener (HWFC) models

In Chapter Four, motivated by historical applications of integer-order Hammerstein-Wiener models, the WFC and HWFC model structures are introduced. The HFC model has already been published by other authors in the past. The HWFC model structure is characterised by a cascade connection of nonlinear static functions transforming the input and output signals of a fractional-order continuous-time dynamic model. The input and output static nonlinear functions are represented by a sum of a *priori* known basis functions. The HWFC model is also considered in a stochastic setting, where the noise model is described by a discrete-time auto-regressive moving-average (ARMA) filter resulting in a hybrid model structure (combination of continuous and discrete-time models). It has been shown that it is possible to model real-world physical phenomena sufficiently well, while retaining relatively simple WFC and HWFC model structures. It is believed that this further enhances the applicability of the presented research and generates a basis for the concept of a so-called fractional-order Hammerstein–Wiener approach for the modelling and control of real-world systems.

The second key outcome of this research is the solution to the parameter estimation problem of the proposed nonlinear model structures. In Chapter Four, it has been shown how to formulate the HFC, WFC and HWFC model structures in a multi-input single-

output, bilinear in the parameters, regression form. Subsequently, refined and simplified refined instrumental variable parameter estimation methods have been extended to accommodate for the fractional-order case, subject to output error and ARMA output noise scenarios. The proposed fractional-order continuous-time refined and simplified instrumental variable parameter estimation methods (RIVCF/SRIVCF), extended to the HFC, WFC and HWFC model cases, are abbreviated HRIVCF/HSRIVCF, WRIVCF/WSRIVCF and HWRIVCF/HWSRIVCF, respectively. Note, that the proposed HWRIVCF/HWSRIVCF methods include the estimation of HFC and WFC model structures as a special case and that these differ only in the type of assumed noise model. The advantage of the proposed parameter estimation methods resides in the relaxed need for the output static nonlinearity (Wiener model case) to be invertible.

7.1.3 Bilinear fractional-order system model identification

In Chapter 6, the bilinear fractional-order system model has been introduced. It has been shown that not all bilinear fractional-order state-space model representations are realisable in input-output model form (required by the proposed parameter estimation methods). However, for simulation purposes the bilinear fractional-order input-output model needs to be in the state-space form. Therefore, it has been proposed to consider only a certain class of bilinear system models in this thesis.

The main outcome of Chapter 6 was the identification of the bilinear fractional-order system from sampled input-output data. It was also outlined how the error reduction ratio can be used as an elegant tool for detection of the system structure. After the system structure had been selected, the delayed fractional-order state variable identification approach was applied to the simulated bilinear system under different output noise scenarios.

7.1.4 Identification of 1D solid diffusion process in lithium ion cell

In Chapter Three, motivated by the diffusion phenomena occurring in a lithium ion cell system, a fractional-order continuous-time transfer function model of a 1D linear solid diffusion system has been identified. The structure of a fractional-order transfer function model has been detected using the estimated Bode plot of the diffusion model from collected input-output data. The model parameters have been estimated using the extended version of the simplified refined instrumental variable method, which uses sampled (measured) input-output signals.

It has been shown that the identified fractional-order continuous-time transfer function model offers an accurate approximation of the diffusion process which occurs within a class of lithium ion batteries. It has also been possible to obtain a reduced order integer-order linear model directly from the fractional-order derivative term based on constraints imposed on the system model, e.g. the demanded frequency range of approximation.

Finally, note, that the flexibility of the identified fractional-order transfer function model allows adequate models of physical phenomena to be obtained across a wide range of real-world systems (natural and manmade). This further increases the applicability of the research into areas such as model based control design and control oriented system analysis.

7.2 Further research directions

This section presents the further research directions and potential research topics, directly connected and motivated by the conducted research in this thesis.

7.2.1 Coupling the HWFC and bilinear fractional-order models

This thesis has outlined the importance of HWFC and bilinear fractional-order models. According to this and the simplicity associated with HWFC and bilinear fractional-order models, it could be motivational to couple these models in to a single model class. In the integer-order case, there are such models and these have shown superior performance with higher efficacy than the linear models, i.e. the coupled Hammerstein-bilinear model for identifying the heating ventilation and air conditioning system, see (Zajic 2013). Coupling the HWFC and bilinear fractional-order models is by extending the linear fractional-order continuous-time subsystem in HWFC model to the bilinear fractional-order continuous-time subsystem.

7.2.2 Extended delayed fractional-order state variable identification approach for generalised state-space

It might be a significant step to investigate further extensions of the fractional-order state variable identification approach when the system must be described by a fractional-order nonlinear state-space model. This extension allows identifying a large range of complex nonlinear systems. It is expected, that such extensions may lead to further increase the applicability of the presented research for a wider class of real-world problems, while retaining a well-structured mathematical framework for nonlinear control system design. This extension might be achieved by restructuring the Butterworth filter according to the structure of the system, required to be identified. Restructuring the Butterworth filter must be considering during the design of the Butterworth filter.

7.2.3 Coupling the HWRIVCF method and delayed fractional-order state variable identification approach

There are some systems which can be described by models resulting from coupling for instance the HWFC and bilinear fractional-order model due to the advantages of both models as aforementioned. This might promote the coupling of the HWRIVCF method and delayed fractional-order state variable identification approach into one combined approach.

7.2.4 The battery state of charge nonlinear model identification

State of charge estimation is considered to be a fundamental requirement for the battery management system. In the smart grid and electric vehicle, it is assumed that the battery is the most significant energy storage. Regarding those applications, the state of charge estimation algorithm is expected to be accurate and easy to implement. This is not an easy task if considering the complexity associated with the governing equations, modelling the battery system. However, the results obtained in Chapter Three, which has dealt with the fractional-order model identification for a 1D solid diffusion system model of lithium ion cell, might support the identification of a bilinear fractional-order input-output model for describing the state of charge. The more significant structure might be detected by using the error reduction ratio. The parameters of the selected structure of a bilinear fractional-order input-output model might be then estimated using the delayed fractional-order state variable filter.

7.2.5 Analysing the stability of bilinear systems

In this thesis, the identification process is implemented regardless of the stability of the bilinear fractional-order system. It would be useful if the stability of bilinear fractional-order system could be considered in future work. The existing generalized Mittag–Leffler

stability and the (generalized) fractional Lyapunov direct method might lead to a simple approach which is limited to analysis the bilinear fractional-order system.

REFERENCES

Akcay, H. (ed.) (2008) *Decision and Control, 2008. CDC 2008. 47th IEEE Conference on*. 'Synthesis of Complete Orthonormal Fractional Bases'

Allafi, W., Zajic, I., and Burnham, K. J. (2015a) Delayed Half-Base Order State Variable Filter for Fractional-order Nonlinear Parameter Estimation. in 24th Int. Conf. on Systems Engineering, Coventry, UK

Allafi, W., Zajic, I., and Burnham, K. J. (2015b) 'Identification of Fractional Order Models: Application to 1D Solid Diffusion System Model of Lithium Ion Cell'. in *Progress in Systems Engineering: Proceedings of the Twenty-Third International Conference on Systems Engineering*. ed. by Selvaraj, H., Zydek, D., and Chmaj, G. Cham: Springer International Publishing, 63-68

Allafi, W. and Burnham, K. J. (2014) 'Identification of Fractional-order Continuous-Time Hybrid Box-Jenkins Models using Refined Instrumental Variable Continuous-Time Fractional-order Method'. in *Advances in Systems Science: Proceedings of the International Conference on Systems Science 2013 (ICSS 2013).* ed. by Swiatek, J., Grzech, A., Swiatek, P., and Tomczak, M. J. Cham: Springer International Publishing, 785-794

Allafi, W. and Burnham, K. J. (2013). Fractional-order systems: a tutorial and overview. In proceeding of 13th Polish-British Workshop, 6-9 June, Wroclaw, Poland, [Abstract]

Almeida, L., B. (1994) 'The Fractional Fourier Transform and Time-Frequency Representations'*. IEEE Transactions on Signal Processing* 42 (11), 3084-3091

Aoun, M., Malti, R., Levron, F., and Oustaloup, A. (2007) 'Synthesis of Fractional Laguerre Basis for System Approximation'*. Automatica* 43 (9), 1640-1648

Bai, E., Cai, Z., Dudley-Javorosk, S., and Shields, R. K. (2009) 'Identification of a Modified Wiener–Hammerstein System and its Application in Electrically Stimulated Paralyzed Skeletal Muscle Modeling'*. Automatica* 45 (3), 736-743

Bernardi, D., Pawlikowski, E., and Newman, J. (1985) 'A General Energy Balance for Battery Systems'*. Journal of the Electrochemical Society* 132 (1), 5-12

Billings, S. and Zhu, Q. (1994) 'A Structure Detection Algorithm for Nonlinear Dynamic Rational Models'*. International Journal of Control* 59 (6), 1439-1463

Billings, S. and Fakhouri, S. (1978) 'Identification of a Class of Nonlinear Systems using Correlation Analysis'*. Electrical Engineers, Proceedings of the Institution of* 125 (7), 691-697

Blinchikoff, H. J. and Zverev, A. I. (1986) *Filtering in the Time and Frequency Domains*.: John Wiley & Sons, Inc.

Botte, G. G., Subramanian, V. R., and White, R. E. (2000) 'Mathematical Modeling of Secondary Lithium Batteries'. *Electrochimica Acta* 45 (15), 2595-2609

Butterworth, S. (1930) 'On the Theory of Filter Amplifiers'. *Wireless Engineer* 7 (6), 536-541

Candan, C., Kutay, M., A., and Ozaktas, H., M. (2000) 'The Discrete Fractional Fourier Transform'. *IEEE Transactions on Signal Processing* 48 (5), 1329-1337

Carlson, G. and Halijak, C. (1964) 'Approximation of Fractional Capacitors $(1/s)^{1/n}$ by a Regular Newton Process'. *IEEE Transactions on Circuit Theory* 11 (2), 210-213

Chen, H., Hwang, S., and Chang, C. (2009) 'Iterative Identification of Continuous-Time Hammerstein and Wiener Systems using a Two-Stage Estimation Algorithm'. *Industrial & Engineering Chemistry Research* 48 (3), 1495-1510

Cheng, B. and Hsu, N. (1982) 'Analysis and Parameter Estimation of Bilinear Systems Via Block-Pulse Functions'. *International Journal of Control* 36 (1), 53-65

Chetoui, M., Thomassin, M., Malti, R., Aoun, M., Najar, S., Abdelkrim, M. N., and Oustaloup, A. (2013) 'New Consistent Methods for Order and Coefficient Estimation of Continuous-Time Errors-in-Variables Fractional Models'. *Computers & Mathematics with Applications* 66 (5), 860-872

Cois, O., Oustaloup, A., Poinot, T., and Battaglia, J., L (eds.) (2001) *Control Conference (ECC), 2001 European*. 'Fractional State Variable Filter for System Identification by Fractional Model'

Daniel-Berhe, S. and Unbehauen, H. (1998) 'Bilinear Continuous-Time Systems Identification Via Hartley-Based Modulating Functions'. *Automatica* 34 (4), 499-503

Das, S. and Pan, I. (2011) *Fractional Order Signal Processing: Introductory Concepts and Applications*.: Springer Science & Business Media

Das, S. (2011) *Functional Fractional Calculus*.: Springer-Verlag Berlin Heidelberg

Doyle, C. M. (2010) 'Design and Simulation of Lithium Rechargeable Batteries'. *Lawrence Berkeley National Laboratory*

Doyle, M., Fuller, T. F., and Newman, J. (1993) 'Modeling of Galvanostatic Charge and Discharge of the lithium/polymer/insertion Cell'. *Journal of the Electrochemical Society* 140 (6), 1526-1533

Dunoyer, A., Burnham, K., J, and McAlpine, T. S. (eds.) (1996) *Adaptive Controllers in Practice - Part Two (Digest no: 1996/060), IEE Colloquium on*. 'Comparison of Bilinear and PID Control on a Test Furnace at British Steel'

Eckert, M., Kupper, M., and Hohmann, S. (2014) 'Functional Fractional Calculus for System Identification of Battery Cells'. *At–automatisierungstechnik* 62 (4), 272-281

Gabano, J. D., Poinot, T., and Kanoun, H. (2011) 'Identification of a Thermal System using Continuous Linear Parameter-Varying Fractional Modelling'. *IET Control Theory & Applications* 5 (7), 889-899

Garnier, H. and Wang, L. (eds.) (2008) *Identification of Continuous-Time Models from Sampled Data.*: Springer-Verlag London

Garnier, H. (2015) 'Direct Continuous-Time Approaches to System Identification. Overview and Benefits for Practical Applications'*. European Journal of Control* 24, 50-62

Ghanbari, M. and Haeri, M. (2010) 'Parametric Identification of Fractional-Order Systems using a Fractional Legendre Basis'*. Proceedings of the Institution of Mechanical Engineers, Part I: Journal of Systems and Control Engineering* 224 (3), 261-274

Ghanbari, M. and Haeri, M. (2011) 'Order and Pole Locator Estimation in Fractional Order Systems using Bode Diagram'*. Signal Processing* 91 (2), 191-202

Greblicki, W. and Pawlak, M. (2008) *Nonparametric System Identification*.: Cambridge University Press Cambridge

Hosseini, M., Johansen, T. A., and Fatehi, A. (2011) 'Comparison of Nonlinearity Measures Based on Time Series Analysis for Nonlinearity Detection'*. Modeling, Identification and Control* 32 (4), 123-140

Hsiao, C. and Wang, W. (2000) 'State Analysis and Parameter Estimation of Bilinear Systems Via Haar Wavelets'*. Circuits and Systems I: Fundamental Theory and Applications, IEEE Transactions on* 47 (2), 246-250

Huang, Y., Guo, F., Li, Y., and Liu, Y. (2015) 'Parameter Estimation of Fractional-Order Chaotic Systems by using Quantum Parallel Particle Swarm Optimization Algorithm'*. PloS One* 10 (1), 1-14

Hwang, C. and Chen, M. (1986) 'Analysis and Parameter Identification of Bilinear Systems Via Shifted Legendre Polynomials'*. International Journal of Control* 44 (2), 351-362

Ichise, M., Nagayanagi, Y., and Kojima, T. (1971) 'An Analog Simulation of Non-Integer Order Transfer Functions for Analysis of Electrode Processes'*. Journal of Electroanalytical Chemistry and Interfacial Electrochemistry* [online] 33 (2), 253-265.

Jacobsen, T. and West, K. (1995) 'Diffusion Impedance in Planar, Cylindrical and Spherical Symmetry'*. Electrochimica Acta* 40 (2), 255-262

Juang, J. (2012) 'Generalized Bilinear System Identification with Coupling Force Variables'. in *Modeling, Simulation and Optimization of Complex Processes*. ed. by Anon: Springer, 169-182

Juang, J. and Lee, C. (2012) 'Continuous-Time Bilinear System Identification using Single Experiment with Multiple Pulses'*. Nonlinear Dynamics* 69 (3), 1009-1021

Juang, J. (2009) 'Generalized Bilinear System Identification'*. The Journal of the Astronautical Sciences* 57 (1-2), 261-273

Juang, J. (2005) 'Continuous-Time Bilinear System Identification'*. Nonlinear Dynamics* 39 (1-2), 79-94

Karanam, V., Frick, P., and Mohler, R. (1978) 'Bilinear System Identification by Walsh Functions'. *Automatic Control, IEEE Transactions on* 23 (4), 709-713

Kerschen, G., Worden, K., Vakakis, A. F., and Golinval, J. (2006) 'Past, Present and Future of Nonlinear System Identification in Structural Dynamics'. *Mechanical Systems and Signal Processing* 20 (3), 505-592

Kohr, R. H. (1963) 'A Method for the Determination of a Differential Equation Model for Simple Nonlinear Systems'. *Electronic Computers, IEEE Transactions on* (4), 394-400

Kotta, Ü., Mullari, T., Zinober, A., and Kotta, P. (2007) 'State Space Realization of Bilinear Continuous-Time input–output Equations'. *International Journal of Control* 80 (10), 1607-1615

Lanusse, P., Malti, R., and Melchior, P. (2013) 'CRONE Control System Design Toolbox for the Control Engineering Community: Tutorial and Case Study'. *Philosophical Transactions.Series A, Mathematical, Physical, and Engineering Sciences* 371 (1990)

Laurain, V., Gilson, M., Garnier, H., and Young, P., C (eds.) (2008) *Decision and Control, 2008. CDC 2008. 47th IEEE Conference on*. 'Refined Instrumental Variable Methods for Identification of Hammerstein Continuous-Time Box-Jenkins Models'

Lee, C. and Juang, J. (2012) 'Nonlinear System identification—a Continuous-Time Bilinear State Space Approach'. *The Journal of the Astronautical Sciences* 59 (1-2), 398-420

Leontaritis, I. and Billings, S. (1987) 'Model Selection and Validation Methods for Non-Linear Systems'. *International Journal of Control* 45 (1), 311-341

Liu, C. and Shih, Y. (1984) 'Analysis and Parameter Estimation of Bilinear Systems Via Chebyshev Polynomials'. *Journal of the Franklin Institute* 317 (6), 373-382

Liu, D., Y, Laleg-Kirati, T., M, Gibaru, O., and Perruquetti, W. (eds.) (2013) *2013 American Control Conference*. 'Identification of Fractional Order Systems using Modulating Functions Method'

Liu, X., Wang, J., and Zheng, W. (2011) 'Convergence Analysis of Refined Instrumental Variable Method for Continuous-Time System Identification'. *IET Control Theory & Applications* 5 (7), 868-877

Maachou, A., Malti, R., Melchior, P., Battaglia, J., Oustaloup, A., and Hay, B. (eds.) (2010) *4rd IFAC Workshop on Fractional Differentiation and its Applications (FDA)*. 'Thermal System Identification for Large Temperature Variations using Fractional Volterra Series'

Maachou, A., Malti, R., Melchior, P., Battaglia, J., Oustaloup, A., and Hay, B. (2014) 'Nonlinear Thermal System Identification using Fractional Volterra Series'. *Control Engineering Practice* 29, 50-60

Majji, M., Juang, J., and Junkins, J. L. (2009) 'Continuous-Time Bilinear System Identification using Repeated Experiments'. *Advances in the Astronautical Sciences* 135 (2), 1065-1084

Malti, R., Aoun, M., and Oustaloup, A. (eds.) (2004) *Control, Communications and Signal Processing, 2004. First International Symposium on*. 'Synthesis of Fractional Kautz-Like Basis with Two Periodically Repeating Complex Conjugate Modes'

Malti, R., Aoun, M., Battaglia, J., Oustaloup, A., and Madami, K. (eds.) (2003) *13th IFAC Symposium on System Identification, Rotterdam, the Netherlands*. 'Fractional Multimodels-Application to Heat Transfert Modelling'

Malti, R., Victor, S., Oustaloup, A., and Garnier, H. (eds.) (2008) *Proceeding of 17th IFAC World Congress*. 'An Optimal Instrumental Variable Method for Continuous-Time Fractional Model Identification'

Manabe, S. (1961) 'The Non-Integer Integral and its Application to Control Systems'. *ETJ of Jaban* 16 (3-4), 83-87

Mathieu, B., Melchior, P., Oustaloup, A., and Ceyral, C. (2003) 'Fractional Differentiation for Edge Detection'. *Signal Processing* 83 (11), 2421-2432

Matignon, D. (ed.) (1998) *Proceedings of the Colloquium Fractional Differential Systems: Models, Methods and Applications,*. 'Stability Results for Fractional Differential Equations with Applications to Control Processing' at Paris: Lille France

Matsuda, K. and Fujii, H. (1993) 'H∞ optimized Wave-Absorbing Control-Analytical and Experimental Results'. *Journal of Guidance, Control, and Dynamics* 16 (6), 1146-1153

Mohler, R., R (1973) *Bilinear Control Processes: With Applications to Engineering, Ecology and Medicine*.: Academic Press

Momani, S. and Hadid, S. (2004) 'Lyapunov Stability Solutions of Fractional Integrodifferential Equations'. *International Journal of Mathematics and Mathematical Sciences* 2004 (47), 2503-2507

Monje, C. A., Chen, Y., Vinagre, B. M., Xue, D., and Feliu-Batlle, V. (2010) *Fractional-Order Systems and Controls: Fundamentals and Applications*.: Springer-Verlag London

Mu, B. and Chen, H. (2014) 'Recursive Identification of Errors-in-Variables Wiener–Hammerstein Systems'. *European Journal of Control* 20 (1), 14-23

Mullaria, T., Kottaa, U., Kottaa, P., Tonsoa, M., and Zinoberb, A. S. (2009) 'Removing the Input Derivatives in the Generalized Bilinear State Equations'. *Proceedings of the Estonian Academy of Sciences* 58 (2), 98-107

Mzyk, G. (2014) *Combined Parametric-Nonparametric Identification of Block-Oriented Systems*.: Springer

Mzyk, G. (2010) 'Wiener-Hammerstein System Identification with Non-Gaussian Input'. *IFAC Proceedings Volumes* 43 (10), 106-111

Nagarajan, G. S., Van Zee, J., and Spotnitz, R. (1998) 'A Mathematical Model for Intercalation Electrode Behavior I. Effect of Particle-Size Distribution on Discharge Capacity'. *Journal of the Electrochemical Society* 145 (3), 771-779

Nelles, O. (2001) *Nonlinear System Identification: From Classical Approaches to Neural Networks and Fuzzy Models*.: Springer-Verlag Berlin Heidelberg

Newman, J. and Thomas-Alyea, K. E. (2012) *Electrochemical Systems*.: John Wiley & Sons

Ni, B., Gilson, M., and Garnier, H. (2013) 'Refined Instrumental Variable Method for Hammerstein-Wiener Continuous-Time Model Identification'*. Control Theory & Applications, IET* 7 (9), 1276-1286

Nise, N. S. (2011) *Control Systems Engineering, Sixth*.: Wiley Global Education

Oldham, K. and Spanier, J. (1974) *The Fractional Calculus Theory and Applications of Differentiation and Integration to Arbitrary Order*. 1st edn: Elsevier

Ortigueira, M. D. (2011) *Fractional Calculus for Scientists and Engineers*.: Springer Netherlands

Palanthandalam-Madapusi, H., J, Ridley, A., J, and Bernstein, D., S (eds.) (2005) *Proceedings of the 2005, American Control Conference, 2005.* 'Identification and Prediction of Ionospheric Dynamics using a Hammerstein-Wiener Model with Radial Basis Functions'

Petras, I. (2011) *Fractional-Order Nonlinear Systems: Modeling, Analysis and Simulation*.: Springer Science & Business Media

Podlubny, I. (1999) 'Fractional-Order Systems and $PI^{\lambda} D^{\mu}$ controllers'*. IEEE Transactions on Automatic Control* 44 (1), 208-214

Podlubny, I. (ed.) *Advances in Difference Equations: Proceedings of the Second International Conference on Difference Equations*. 'Numerical Solution of Ordinary Fractional Differential Equations by the Fractional Difference Method'. held 1997 at Amsterdam: CRC Press

Podlubny, I. (1998) *Fractional Differential Equations*. 1st edn: Academic press

Randles, J. E. B. (1947) 'Kinetics of Rapid Electrode Reactions'*. Discussions of the Faraday Society* 1 (0), 11-19

Rao, G., P and Unbehauen, H. (2006) 'Identification of Continuous-Time Systems'*. IEE Proceedings - Control Theory and Applications* 153 (2), 185-220

Sabatier, J., Lanusse, P., Melchior, P., and Oustaloup, A. (2015) *Fractional Order Differentiation and Robust Control Design*.: Springer Netherlands

Sabatier, J., Aoun, M., Oustaloup, A., Grégoire, G., Ragot, F., and Roy, P. (2006) 'Fractional System Identification for Lead Acid Battery State of Charge Estimation'*. Signal Processing* 86 (10), 2645-2657

Schäfer, I. and Krüger, K. (2008) 'Modelling of Lossy Coils using Fractional Derivatives'*. Journal of Physics D: Applied Physics* 41 (4), 045001

Schaumann, R. . and Van Valkenburg, M. (2001) *Design of Analog Filters*.: Oxford University Press

Schiff, J. L. (1999) *The Laplace Transform*.: Springer-Verlag New York

Sedra, A. S. and Smith, K. C. (2007) 'Microelectronic Circuits Revised Edition'

Söderström, T. and Stoica, P. (1988) *System Identification*.: Prentice-Hall, Inc.

Soltan, A., Radwan, A., and Soliman, A., M (eds.) (2011) *Microelectronics (ICM), 2011 International Conference on*. 'Butterworth Passive Filter in the Fractional-Order': IEEE

Soltan, A., Radwan, A. G., and Soliman, A. M. (2012) 'Fractional Order Filter with Two Fractional Elements of Dependant Orders'*. Microelectronics Journal* 43 (11), 818-827

Stanisławski, R., Latawiec, K., J, Hunek, W., P, and Łukaniszyn, M. (eds.) (2013) *Methods and Models in Automation and Robotics (MMAR), 2013 18th International Conference on*. 'Laguerre-Based Modeling of Fractional-Order LTI SISO Systems'

Su, K. L. (2002) *Analog Filters*.: Springer Science & Business Media

Tang, Y., Zhang, X., Hua, C., Li, L., and Yang, Y. (2012) 'Parameter Identification of Commensurate Fractional-Order Chaotic System Via Differential Evolution'*. Physics Letters A* 376 (4), 457-464

Taringou, F., Hammi, O., Srinivasan, B., Malhame, R., and Ghannouchi, F. M. (2010) 'Behaviour Modelling of Wideband RF Transmitters using Hammerstein-Wienermodels'*. IET Circuits, Devices & Systems* 4 (4), 282-290

Tepljakov, A., Petlenkov, E., and Belikov, J. (eds.) (2011) *Mixed Design of Integrated Circuits and Systems (MIXDES), 2011 Proceedings of the 18th International Conference*. 'FOMCON: Fractional-Order Modeling and Control Toolbox for MATLAB'

Thomas, K. E., Newman, J., and Darling, R. M. (2002) 'Mathematical Modeling of Lithium Batteries'. in *Advances in Lithium-Ion Batteries*. ed. by van Schalkwijk, W. A. and Scrosati, B. Boston, MA: Springer US, 345-392

Tsang, K., M. and Billings, S., A. (1994) 'Identification of Continuous Time Nonlinear Systems using Delayed State Variable Filters'*. International Journal of Control* 60 (2), 159-180

Uchaikin, V. V. (2013) *Fractional Derivatives for Physicists and Engineers*.: Springer-Verlag Berlin Heidelberg

Valerio, D. (2005) 'Ninteger v. 2.3 Fractional Control Toolbox for Matlab'*. Universidade Técnica De Lisboa*

Victor, S., Malti, R., Melchior, P., and Oustaloup, A. (2011) 'Instrumental Variable Identification of Hybrid Fractional Box-Jenkins Models'*. IFAC Proceedings Volumes* 44 (1), 4314-4319

Vinagre, B., Podlubny, I., Hernandez, A., and Feliu, V. (2000) 'Some Approximations of Fractional Order Operators used in Control Theory and Applications'*. Fractional Calculus and Applied Analysis* 3 (3), 231-248

Vörös, J. (2007) 'Parameter Identification of Wiener Systems with Multisegment Piecewise-Linear Nonlinearities'. *Systems & Control Letters* 56 (2), 99-105

Vörös, J. (2004) 'An Iterative Method for Hammerstein-Wiener Systems Parameter Identification'. *Journal of Electrical Engineering* 55 (11-12), 328-331

Wang, B., Li, S. E., Peng, H., and Liu, Z. (2015) 'Fractional-Order Modeling and Parameter Identification for Lithium-Ion Batteries'. *Journal of Power Sources* 293, 151-161

Wang, D. and Ding, F. (2011) 'Least Squares Based and Gradient Based Iterative Identification for Wiener Nonlinear Systems'. *Signal Processing* 91 (5), 1182-1189

Wang, M., Chang, R., Yeu, and YANG, S., Yien (1987) 'Analysis and Parameter Estimation of Bilinear Systems Via Generalized Orthogonal Polynomials'. *International Journal of Control* 46 (2), 719-729

Winder, S. (2002) *Analog and Digital Filter Design*. Second edition edn: Newnes

Xue, D., Chen, Y., and Atherton, D. (2007) *Linear Feedback Control - Analysis and Design with MATLAB*.: Society for Industrial and Applied Mathematics

Young, P. and Jakeman, A. (1980) 'Refined Instrumental Variable Methods of Recursive Time-Series Analysis Part III. Extensions'. *International Journal of Control* 31 (4), 741-764

Young, P. C. (ed.) (2002) *15th Triennial IFAC World Congress on Automatic Control*. 'Optimal IV Identification and Estimation of Continuous-Time TF Models' at Barcelona

Young, P., Garnier, H., and Gilson, M. (2006) 'An Optimal Instrumental Variable Approach for Identifying Hybrid Continuous-Time Box-Jenkins Models'. *IFAC Proceedings Volumes* 39 (1), 225-230

Yuan, X., Song, C., Wang, H., and Zhang, J. (2010) *Electrochemical Impedance Spectroscopy in PEM Fuel Cells*.: Springer-Verlag London

Zajic, I. (2013) *A Hammerstein-Bilinear Approach with Application to Heating Ventilation and Air Conditioning Systems*. [online] PhD thesis or dissertation. Coventry: Coventry University

Žecová, M. and Terpák, J. (2015) 'Heat Conduction Modeling by using Fractional-Order Derivatives'. *Applied Mathematics and Computation* 257, 365-373

Zhang, B. and Billings, S. (2015) 'Identification of Continuous-Time Nonlinear Systems: The Nonlinear Difference Equation with Moving Average Noise (NDEMA) Framework'. *Mechanical Systems and Signal Processing* 60, 810-835

Zhou, L., Li, X., and Pan, F. (2013) 'Least-Squares-Based Iterative Identification Algorithm for Wiener Nonlinear Systems'. *Journal of Applied Mathematics* 2013

Zhou, S., Cao, J., and Chen, Y. (2013) 'Genetic Algorithm-Based Identification of Fractional-Order Systems'. *Entropy* 15 (5), 1624-1642

Zhu, Q., Wang, Y., Zhao, D., Li, S., and Billings, S. A. (2015) 'Review of Rational (Total) Nonlinear Dynamic System Modelling, Identification, and Control'. *International Journal of Systems Science* 46 (12), 2122-2133

APPENDIX A

Fractional-order integral and derivatives definitions

The most known definition of fractional-order integral and derivatives are summarised in Table A.1 and Table.2, respectively.

Table A. 1: Fractional-order integral definitions where $\alpha \in \mathbb{R}^+$ (Ortigueira 2011).

Designation	*Definition*
Liouville integral	$\mathcal{I}^{\alpha} f(t) = \frac{1}{(-1)^{\alpha}\Gamma(\alpha)} \int_0^{+\infty} f(t+\tau)\tau^{\alpha-1} d\tau$
Riemann integral	$\mathcal{I}^{\alpha} f(t) = \frac{1}{\Gamma(\alpha)} \int_0^{t} f(\tau)(t-\tau)^{\alpha-1} d\tau, t > 0$
Left side Riemann–Liouville integral	$\mathcal{I}^{\alpha} f(t) = \frac{1}{\Gamma(\alpha)} \int_a^{t} f(\tau)(t-\tau)^{\alpha-1} d\tau, t > a$
Right side Riemann–Liouville integral	$\mathcal{I}^{\alpha} f(t) = \frac{1}{\Gamma(\alpha)} \int_t^{b} f(\tau)(\tau-t)^{\alpha-1} d\tau, t < b$
Left side Weyl integral	$\mathcal{I}^{\alpha} f(t) = \frac{1}{\Gamma(\alpha)} \int_{-\infty}^{t} f(\tau)(t-\tau)^{\alpha-1} d\tau$
Right side Weyl integral	$\mathcal{I}^{\alpha} f(t) = \frac{1}{\Gamma(\alpha)} \int_t^{-\infty} f(\tau)(\tau-t)^{\alpha-1} d\tau$

Table A. 2: Fractional-order derivative definitions where T_s is the time interval, $\alpha \in \mathbb{R}^+$, $n-1 \le \alpha < n \in \mathbb{Z}^+$ and subscript (n) means $H^{(n)}(t) = \dfrac{d^n H(t)}{dt^n}$, (Ortigueira 2011).

Designation	*Definition*
Left side Riemann–Liouville derivative	$${}_a\mathcal{D}_t^{\alpha} f(t) = \frac{1}{\Gamma(n-\alpha)} \mathcal{D}^n \left(\int_a^t f(\tau)(t-\tau)^{n-\alpha-1} d\tau \right)$$
Right side Riemann–Liouville derivative	$${}_t\mathcal{D}_b^{\alpha} f(t) = \frac{(-1)^n}{\Gamma(n-\alpha)} \mathcal{D}^n \left(\int_t^b f(\tau)(\tau-t)^{n-\alpha-1} d\tau \right)$$
Left side Caputo derivative	$$\mathcal{D}^{\alpha} f(t) = \frac{1}{\Gamma(n-\alpha)} \left(\int_0^t f^{(n)}(\tau)(t-\tau)^{m-\alpha-1} d\tau \right), t > 0$$
Right side Caputo derivative	$$\mathcal{D}^{\alpha} f(t) = \frac{1}{\Gamma(n-\alpha)} \left(\int_t^{+\infty} f^{(n)}(\tau)(\tau-t)^{m-\alpha-1} d\tau \right)$$
Generalised function	$$\mathcal{D}^{\alpha} f(t) = \frac{1}{\Gamma(-\alpha)} \int_{-\infty}^t f(\tau)(t-\tau)^{-\alpha-1} d\tau$$
Left Grünwald–Letnikov	$$\mathcal{D}_-^{\alpha} f(t)\Big\|_{t=KT_s} = \lim_{T_S \to 0+} \frac{1}{T_s^{\alpha}} \sum_{k=0}^{\infty} (-1)^k \binom{\alpha}{k} f((K-k)T_s)$$
Right Grünwald–Letnikov	$$\mathcal{D}_+^{\alpha} f(t)\Big\|_{t=KT_s} = \lim_{T_S \to 0+} \frac{1}{T_s^{\alpha}} \sum_{k=0}^{\infty} (-1)^k \binom{\alpha}{k} f((K+k)T_s)$$